Special purpose quantum information processing with atoms in optical lattices

Alexander Klein
Keble College, Oxford

A thesis submitted to the Mathematical and Physical Sciences Division
for the degree of Doctor of Philosophy in the University of Oxford

Michealmas Term, 2007

Atomic and Laser Physics,
University of Oxford

Special purpose quantum information processing with atoms in optical lattices

Alexander Klein, Keble College, Oxford
Michaelmas Term 2007

Abstract

Atoms in optical lattices are promising candidates to implement quantum information processing. Their behaviour is well understood on a microscopic level, they exhibit excellent coherence properties, and they can be easily manipulated using external fields. In very deep optical lattices, each atom is restricted to a single lattice site and can be used as a qubit. If the lattice is shallow enough such that the atoms can move, their properties can be used to simulate certain condensed matter phenomena such as superconductivity.

In this thesis, we show how technical problems of optical lattices such as restricted decoherence times, or fundamental shortcomings such as the lack of phonons or strong spin interactions, can be overcome by using current or near-future experimental techniques. We introduce a scheme that makes it possible to simulate model Hamiltonians known from high-temperature superconductivity. For this purpose, previous simulation schemes to realise the spin interaction terms are extended. We especially overcome the condition of a filling factor of exactly one, which otherwise would restrict the phase of the simulated system to a Mott-insulator. This scheme makes a large range of parameters accessible, which is difficult to cover with a condensed matter setup.

We also investigate the properties of optical lattices submerged into a Bose-Einstein condensate (BEC). A weak-coupling expansion in the BEC-impurity interaction strength is used to derive a model that describes the lattice atoms in terms of polarons, i.e. atoms dressed by Bogoliubov phonons. This is analogous to the description of electrons in solids, and we observe similar effects such as a crossover from coherent to incoherent transport for increasing temperatures. Moreover, the condensate mediates an attractive off-site interaction, which leads to macroscopic clusters at experimentally realistic parameters. Since the atoms in the lattice can also be used as a quantum register with the BEC mediating a two-qubit gate, we derive a quantum master equation to examine the coherence properties of the atomic qubits. We show that the system exhibits sub- and superdecoherence and that a fast implementation of the two-qubit gate competes with dephasing.

Finally, we show how to realise the encoding of qubits in a decoherence-free subspace (DFS) using optical lattices. We develop methods for implementing robust gate operations on qubits encoded in a DFS exploiting collisional interactions between the atoms. We also give a detailed analysis of the performance and stability of the gate operations and show that a robust implementation of quantum repeaters can be achieved using our setup. We compare the robust repeater scheme to one that makes use of conventional qubits only, and show the conditions under which one outperforms the other.

Contents

Chapter 1

Introduction

1.1 Quantum computation and simulation

Computers are nowadays a standard tool in science. They have eased the life of experimentalists when acquiring and processing data, and of theorists in solving complex problems both analytically and numerically. Furthermore, for the last four decades the number of transistors on a reasonably-priced integrated chip has doubled every 18 to 24 months, allowing for faster processors and bigger memories. By extrapolating this behaviour, which is known as Moore's law [1], one can see that the size of a transistor will soon approach a few atoms, and unless new technologies are developed this trend will stop due to physical limitations. Apart from this, and despite the improvement seen over the last decades, the performance of computers is still insufficient for a large class of physical problems. This becomes especially apparent in quantum mechanics [2], where numerical simulations are often necessary to gain a deeper understanding of the underlying physics. In general, the dimensionality of the Hilbert space describing the quantum system growths exponentially with the number of particles involved. This leads to memory requirements easily surpassing the storage capacity of even the most powerful available computers, and calculation times that can exceed months. Although many efforts are currently underway in order to devise algorithms for an approximate description of quantum systems, only a very restricted class of such systems can be simulated so far [3–9]. Even for seemingly simple systems known from condensed matter physics, such as a few tens of electrons in a two-dimensional crystal, an exact simulation is at the moment far beyond the accessible regime.

Due to these problems, R. Feynman made the ingenious suggestion that, in order to calculate the behaviour of a quantum system, one should simply use another quantum system [10]. There are two principal ways to achieve this goal. One is to tailor a quantum system for the special purpose of simulating a more complicated one or a model Hamiltonian of interest. The other way is to build a universal quantum computer, which in many ways would behave like a universal Turing machine for classical computing [11]. This idea was proposed by D. Deutsch [12] and has led to a range of new algorithms for quantum computers, which often

offer a considerable speed-up compared to the best-known classical algorithms [13]. These new quantum algorithms include Grover's search algorithm in an unsorted database [14], the algorithm by Deutsch and Jozsa to determine whether a function is balanced or constant [15], and Shor's number factorisation algorithm [16]. They make use of the fact that the information is not encoded in strings of zeros and ones as for a classical computer, but instead in a set of quantum bits or qubits, which can be in a coherent superposition of different states and might exhibit entanglement. Maintaining this coherence makes an experimental implementation extremely difficult, since the quantum systems representing the qubits typically couple to their environment [2].

Although a universal quantum computer would lead to many opportunities, the experimental difficulties involved with its implementation have not yet been overcome. It is thus worthwhile to concentrate on the other principal way of quantum simulations, namely to specially tailor a quantum system for studying model Hamiltonians of interest. The simulating system is chosen to be one that can be easily manipulated and which exhibits the desired Hamiltonian. Such a quantum simulator would then serve as a computer that has been devised to perform an exactly defined task.

1.2 Atoms in optical lattices: Simulators and registers

A suitable and promising candidate for implementing special purpose quantum simulators for condensed matter physics is given by ultracold atoms in optical lattices [17–20]. In general, for a given solid most of the parameters, such as the electron hopping and their interaction, are not easy to control. This is different for ultracold fermionic atoms trapped in an optical lattice, which are described by the Hubbard model.[1] Within the tight-binding approximation, the atoms can hop from one lattice site to a neighbouring one and density-density interactions between two atoms only take place if they occupy the same lattice site. By changing the intensities of the lasers that create the lattice potential, it is possible to drive the atoms from a superfluid state, where the hopping of the atoms is large compared to the interatomic interaction and they are delocalised over the lattice, to a Mott insulator, where the hopping of the atoms is small compared to the interaction, leading to a localisation of the atoms in their lattice sites. This phase transition, which also occurs for bosons [21], was first demonstrated in a milestone experiment by M. Greiner et al. [22], showing the wide range of parameter regimes that can be covered in a single experiment.

[1] It has been shown in Ref. [17] that ultracold bosonic atoms in optical lattices are described by the Bose-Hubbard model. The derivation for fermionic atoms is similar.

Since then, there has been tremendous success in this field. On the theory side it was shown that atoms in optical lattices can simulate a wide range of different condensed matter Hamiltonians [20] such as the Hubbard Hamiltonian [18] or spin-spin interactions [23, 24]. It is also possible to simulate effective magnetic fields in these systems, for example by Raman-assisted hopping [25], by applying oscillating quadrupole fields [26] or by using light with orbital angular momentum [27, 28]. On the experimental side progress has been made in the manipulation of ultracold atoms in optical lattices. Higher order correlations between fermions in a lattice have been measured, a technique which allows to experimentally investigate models of high-temperature superconductivity with this setup [29]. Moreover, Bloch oscillations, originally predicted for electrons in a crystal [30], were observed using atoms in tilted optical lattices [31, 32], showing the excellent coherence properties of this setup. The admixture of fermions to bosonic atoms in the lattice changes their coherence properties considerably as demonstrated in [33, 34].

Atoms in optical lattices are not only useful to simulate condensed matter systems, they also provide a first step towards the long-term goal of universal quantum computing. The atoms in the lattice can be used as a quantum register [35], a device to store qubits analogous to a classical register. For manipulation of the atoms they have to be addressed individually, which in an optical lattice requires special techniques due to the small distance between the atoms. Several methods have been proposed, such as using marker atoms [36], or by employing additional external fields [37, 38]. In experiments, the addressability problem has been circumvented by leaving empty sites between the atoms [39, 40] or by using infrared lattices [41], where the distance between the atoms is larger than in lattices with optical wave lengths. It is also possible to move these atoms from one lattice site to another using a setup known as an optical conveyor belt [42, 43]. Entanglement between the atoms can be created by spin-dependent optical lattices, where state-dependent collisional phases between the atoms are created [44]. This idea has been realised in recent experiments [45, 46], again underlining the excellent coherence properties of this setup.

However, atoms in optical lattices still exhibit some shortcomings. Although the coherence properties in the above experiments are very good, they are currently not sufficient for schemes which require long storage times of the order of a few tens of milliseconds. Such storage times can occur for example in quantum repeaters [47–49]. The qubits have to wait for operations on other qubits to be performed and during this period coherence has to be maintained. Due to their architecture, even a weak decoherence has a detrimental effect on the performance of quantum repeaters [50], and ways have to be found to enhance the coherence properties of the used registers.

Limitations also exist when it comes to the simulation of condensed matter phenomena. In a crystal, the electrons couple to the lattice phonons of the solid, which affects their properties considerably [51, 52]. The coupling to the phonons

changes the transport behaviour of the electrons from a coherent, wavelike motion to an incoherent, diffusive process. Also, the electrons are typically surrounded by phonon clouds and the resulting quasi-particles, known as polarons, can exchange phonons thus leading to bound polaron pairs, or bi-polarons, which are used to explain high-temperature superconductivity [53]. Since in typical experiments optical lattices are produced using intense laser beams which create conservative potentials, such phonons do not exist in a standard setup, thus restricting the number of models that can be simulated.

Another problem encountered in optical lattices is the fact that the off-site interaction, which might depend on the internal state of the atoms and thus resemble a nearest-neighbour spin interaction, cannot be changed easily and is typically very weak. However, some of the models discussed in high-temperature superconductivity include a spin-spin interaction term between the electrons whose strength is on the order of the electron hopping and the on-site electron interaction [54, 55]. Although an appreciable nearest-neighbour interaction can be achieved by using a very weak optical lattice, typically these lattices become too weak to justify the description of the atoms by a single band tight-binding Hamiltonian which is assumed to be correct for the electrons.

1.3 Thesis overview

In this thesis, we will show how the shortcomings of optical lattices in both simulating condensed matter systems and using them as quantum registers in quantum repeaters, might be overcome with current or near-future experimental techniques. The lack of phonons is remedied by submerging the optical lattice setup into a Bose-Einstein condensate which naturally exhibits Bogoliubov phonons. Spin-spin interactions between atoms in neighbouring lattice sites are introduced by exploiting spin-dependent optical lattices. The reliability of atoms used as quantum registers is enhanced by encoding the qubits in so-called decoherence-free subspaces [56–59]. In more detail, this thesis is structured as follows.

- In chapter 2 we review some of the essential preliminaries which are used throughout this thesis. After a brief overview of the cooling techniques we describe the basic mechanisms which lead to the trapping of atoms in an optical dipole potential. We then illustrate that for the low collision energies in a BEC the interaction of atoms depends on a single parameter only, namely the s-wave scattering length. This allows us to use a delta-like pseudo-potential in the Hamiltonian which simplifies the interaction term considerably. The dynamics of a weakly interacting BEC is described by a mean-field approach, the so-called Gross-Pitaevskii equation. This ansatz is extended by the Bogoliubov approximation, in which the effects of small quantum fluctuations are included. We then review the properties of ultra-cold bosonic atoms in

optical lattices. We show that for low enough temperatures the atoms realise the tight-binding model and are described by the Bose-Hubbard Hamiltonian. This model exhibits a phase transition between a superfluid and a Mott insulator as is shown by a mean-field ansatz. We conclude the chapter by discussing loss mechanisms for the atoms in the lattice which lead to a non-unitary evolution.

- In chapter 3 we show that certain model Hamiltonians applied in high-temperature superconductivity can be simulated using fermionic atoms in optical lattices. We especially focus on the simulation of the so-called t-J-U model [54, 55]. The spin-spin interaction J and the conventional Hubbard Hamiltonian (the t and U terms) are simulated independently from each other and combined by experimentally performing a Trotter-Suzuki expansion, thereby realising the full model Hamiltonian. The simulation of the spin interaction makes use of spin-dependent optical lattices to create state-dependent collisional phases. The proposed method can be implemented with current experimental techniques and we give estimates of the reliability of our scheme.

- In chapter 4 we investigate the properties of atoms in an optical lattice which are submerged into a Bose-Einstein condensate. We show that this system is accurately described by the Hubbard-Holstein Hamiltonian known from condensed matter physics. The atoms in the lattice couple to the Bogoliubov phonons of the condensate, which allows a description of the system in terms of polarons. By using a generalised master equation we show that the transport properties of the atoms change from coherent, or wavelike, to incoherent, or diffusive, depending on the coupling strength to the phonons and the temperature of the BEC. We also demonstrate that an attractive off-site interaction is mediated by the condensate, leading to a clustering of the atoms in the lattice. All of these effects can be observed at experimentally realistic parameters.

- In chapter 5 we extend the studies of chapter 4 by using a quantum master equation (QME). This allows also the investigation of the off-diagonal matrix elements which was not possible with the generalised master equation used in chapter 4. With this we show that the coupling to the BEC leads to sub- and superdecoherence which has severe consequences if the setup is to be used as a quantum register. We also extend the studies of clustering of the lattice atoms and show that for sufficiently low temperatures and strong couplings the atoms aggregate in an single large cluster, which breaks up for increasing temperature. The limits of the QME are demonstrated for atoms in a tilted lattice. Since the QME does not include terms which cause dissipation, it leads to incorrect results since in the tilted setup this dissipation is essential for a correct description.

- In chapter 6 and the following two chapters we will shift our emphasis to quantum repeaters and decoherence free subspaces. We begin with an overview in chapter 6 and explain why currently used asymmetric cryptosystems cannot guarantee security and that a new way of secure cryptography has to be implemented. We describe the basic protocols of quantum cryptography and that by using the current techniques the distance between the two communicating parties is restricted. This restriction was overcome by the introduction of quantum repeaters, which we will discuss in some more detail. We then give an introduction to decoherence and a method to overcome its effects, namely decoherence free subspaces (DFSs).

- In chapter 7 a robust implementation of a quantum repeater scheme is discussed. For this purpose, we combine the ideas of DFSs and conventional repeater schemes. The DFS is realised by encoding one logical qubit into four atoms stored in an array of optical dipole traps such as an optical lattice. Since an implementation of a controlled phase gate between two DFS-qubits involves complicated many-body interacitons, we employ an auxiliary atom that mediates the gate between the two qubits. This atom is subject to dephasing and the influence of this noise on the performance of the gate is investigated.

- In chapter 8 we extend the investigations of the preceding chapter. We calculate in detail the influence the decoherence of the auxiliary atom has on the entanglement swapping and purification. The performance of the whole repeater scheme using DFS qubits is investigated and compared to a repeater which makes use of conventional qubits, i.e. qubits that are subject to decoherence. We find that for short distances between the two communicating parties the conventional scheme can do better, however the robust implementation using DFSs is favourable for large distances between the two communicating parties.

- We conclude in chapter 9 and give an outlook on the further direction of our work.

Apart from the research presented in this thesis, I have also contributed to other work related to quantum information theory and Bose-Einstein condensation. In Ref. [60], we investigated the behaviour of mirror-inverting spin chains that are subject to noise. These spin chains can be used in order to transport a qubit or to entangle two qubits which are initially located at the two ends of the chain. However, these properties are impaired by the unavoidable coupling to the environment. We have modeled this coupling by independent local noise and numerically calculated the thresholds for which the spin chain still maintains its properties. I have also contributed to the investigation of the dynamics of vortices

in weakly interacting Bose-Einstein condensates [61]. We used the Ritz method in order to calculate the vortex wave functions for the weakly interacting case and deduced the vortex dynamics from these functions. The results were compared to numerical solutions of the Gross-Pitaevskii equation and are in excellent agreement with the analytical predictions.

Chapter 2

Ultracold degenerate quantum gases

In this chapter, we review some of the techniques and results which are essential for the remainder of this thesis. We start with a short overview of the cooling techniques [62–66], which eventually have led to Bose-Einstein condensation [67, 68]. We then focus on the theoretical description of a Bose-Einstein condensate (BEC). Due to the low collision energies in the interatomic scattering processes, the interaction potential can be replaced by an effective contact interaction, which only contains a single parameter, namely the s-wave scattering length [69]. This allows to simplify the Hamiltonian considerably. However, further approximations are necessary for an analytical description, and we therefore review the Bogoliubov approximation for a weakly interacting BEC [70, 71]. The condensate is described by a classical function, also known as the order parameter, and quantum fluctuations, which are the so-called Bogoliubov phonons. These phonons are an important part of our investigations carried out in chapters 4 and 5. After introducing this approximation, we give a short overview of the physics of ultracold atoms in optical lattices [17–19]. The main approximations involved when deriving the Bose-Hubbard Hamiltonian [21] are given and the existence of different phases, namely the Mott insulator and the superfluid phase, are briefly discussed. We finally give some details on spin-dependent optical lattices [44–46]. In these lattices, the atoms can be displaced depending on their internal state leading to state-dependent collisional phases, which will be exploited in chapter 3.

2.1 Cooling and trapping of atoms in optical traps

The extremely low temperatures that are necessary to attain Bose-Einstein condensation can only be achieved with special techniques involving laser fields. Atoms are typically evaporated from an oven and need to be slowed down. One of the first proposals for slowing down atoms using lasers came up in 1975 by T. Hänsch and A. Schawlow [62] and the experimental realisation [63–66] of the slowing techniques led in 1997 to Nobel Prizes for C. Cohen-Tannoudji, S. Chu and W. Phillips.

The working principle of these slowing techniques is to transfer the photon momentum of the laser beam to the atoms [62, 72]. The atoms, which are evaporated from an oven, are collimated into an atom beam, propagating in x-direction. This beam is irradiated with a counter-propagating laser. The frequency ω of the laser light is chosen to correspond to a transition line of the atom ω_0, such that the atoms can absorb the light and get a momentum kick in $-x$-direction. Typically after the lifetime $\tau = \Gamma^{-1}$ of the upper level the atom will emit a photon into a random direction, provided that stimulated emission can be neglected. It can be shown [72] that the average scattering force acting on the atom beam in $-x$-direction is given by

$$F_{\text{scatt}} = \hbar k \frac{\Gamma}{2} \frac{I/I_{\text{sat}}}{1 + I/I_{\text{sat}} + 4\delta^2/\Gamma^2} \,. \tag{2.1}$$

Here, I is the intensity of the laser beam, I_{sat} is the saturation intensity with $I/I_{\text{sat}} = 2\Omega^2/\Gamma^2$ and Ω the Rabi frequency. The detuning $\delta = \omega - \omega_0 + kv$ takes the Doppler shift into account, which is given by the velocity of the atoms v and the wave vector $k = 2\pi/\lambda = \omega/c$ of the laser beam, with c the speed of light. For high intensities I, this leads to a maximum decelerating force of $F_{\text{max}} = \hbar k\Gamma/2$. As an example [72], sodium atoms with an initial velocity of $v_0 = 1000\text{m/s}$, which is a typical value when the oven is operated at a temperature $T = 900\text{K}$, can be slowed down using their $\lambda = 589\text{nm}$ transition line which has a life time of $\tau = 16\text{ns}$. The required stopping distance at half of the maximum deceleration is then given by 1.1m. This is a typical stopping length for most of the alkaline metals.

During the slowing down of the atom beam the decreasing velocity of the atoms causes a change in the Doppler shift kv, which can reduce the efficiency of the cooling process considerably at lower intensities. To compensate for this effect, different methods have been devised. One way is to use the Zeeman effect to balance the changing Doppler shift [63–65]. The atomic beam is propagated along the x-axis through a varying field solenoid whose magnetic field $B(x)$ is chosen such that it fulfils the condition [72] $\omega_0 + \mu_{\text{B}} B(x)/\hbar = \omega + kv$, where μ_{B} is the Bohr magneton. An alternative way is to directly change the laser frequency during the slowing process [66, 73]. This method is known as a frequency chirp and can be achieved by using electro-optic modulators [73] or by directly scanning the frequency of infra-red semiconductor lasers [72].

Once the atoms are sufficiently slow they can be cooled down using an "optical molasses". An optical molasses is a setup which consists of three orthogonal pairs of counter-propagating laser beams. By a suitable choice of the detunings, the atoms can be cooled down by the same principle as described above. Due to the random emissions during that process the momentum of the atom behaves as a random walk when the deterministic slowing down caused by the absorption is subtracted. This random walk leads to a finite variance of the momentum and thus to a finite temperature. One can show [72] that the minimum temperature one expects to be achievable with this optical molasses is given by $k_{\text{B}} T_{\text{D}} = \hbar\Gamma/2$. This temperature

is also known as the Doppler cooling limit. For sodium, it is given by $T_{\mathrm{D}} = 240\mu\mathrm{K}$. With more sophisticated schemes taking more internal states of the atoms into account, temperatures below the Doppler limit can be reached, for example by applying the Sisyphus cooling technique [74]. Once the atoms are cooled down to sufficiently low temperatures, they can be trapped in a magneto-optical trap (MOT) or an optical dipole trap. Since the latter one plays a more important role for the implementations considered in this thesis, especially in the special case of optical lattices, we will focus mainly on the theory of dipole traps.

Dipole traps confine the atoms by exploiting the dipolar force acting on an atom subject to an electric field. Let us for simplicity assume a single atom of mass m with two internal states in one spatial dimension. The internal ground state $|g\rangle$ and the excited state $|e\rangle$ of the atom shall be separated by an energy $\hbar\omega_0$. The atom is then described by the Hamiltonian

$$\hat{H}_{\mathrm{a}} = \frac{\hat{p}^2}{2m} + \frac{\hbar\omega_0}{2}(\mathbf{1} + \hat{\sigma}_3)\,, \tag{2.2}$$

where $\mathbf{1} = |e\rangle\langle e| + |g\rangle\langle g|$ is the unity operator, $\hat{\sigma}_3 = |e\rangle\langle e| - |g\rangle\langle g|$, and $\hat{p}$ the momentum operator of the atom in x direction. We furthermore define the raising and lowering operators $\hat{\sigma}_+ = |e\rangle\langle g|$ and $\hat{\sigma}_- = |g\rangle\langle e|$. If the wavelength of the electric field $\mathbf{E}$ is larger than the orbit of the electrons, and the strength of the field is smaller than the electric field of the nucleus which binds the electrons to the atom, the interaction between the atom and the electric field is well described by the dipole approximation $\hat{H}_{\mathrm{dp}} = -e_0\hat{\mathbf{r}}\cdot\hat{\mathbf{E}}$, where e_0 is the charge of the electron [75].

For an electric field which is dominated by a single mode, e.g. a laser beam or if the atom is stored in a single-mode cavity, the field is described by

$$\hat{\mathbf{E}}(x) = \mathbf{e}\sqrt{\frac{\hbar\omega}{2\varepsilon_0 L}}\,(\hat{a}W(x) + \hat{a}^\dagger W^*(x))\,, \tag{2.3}$$

where $W(x)$ is the mode function describing the field, $\hbar\omega$ is the energy of this mode, $\hat{a}^\dagger$ and $\hat{a}$ are creation and annihilation operators of the mode, $\mathbf{e}$ its polarisation vector, L is the quantisation volume, and ε_0 is the free space permittivity. The dynamics of the electric field itself is described by the simple harmonic oscillator Hamiltonian [76] $\hat{H}_{\mathrm{f}} = \hbar\omega(\hat{a}^\dagger\hat{a}+1/2)$. With the expansion $\mathbf{r} = \sum_{i,j=g,e}|i\rangle\langle i|\,\mathbf{r}\,|j\rangle\langle j|$ and the assumption that the dipole matrix elements $\mathbf{d} = e_0\langle e|\,\mathbf{r}\,|g\rangle = e_0\langle g|\,\mathbf{r}\,|e\rangle$ are real[1], the total Hamiltonian describing the atom, the electric field, and the atom-field interaction, is given by

$$\hat{H} = \hat{H}_{\mathrm{a}} + \hat{H}_{\mathrm{f}} + \hbar g(\hat{\sigma}_+ + \hat{\sigma}_-)(\hat{a}^\dagger W^*(x) + \hat{a}W(x))\,, \tag{2.4}$$

[1]This can always be achieved by multiplying the wave functions of the internal states with a suitable phase factor.

where we have defined the coupling constant

$$g = -\frac{\mathbf{d}\cdot\mathbf{e}}{\hbar}\sqrt{\frac{\hbar\omega}{2\varepsilon_0 L}}\,. \tag{2.5}$$

This Hamiltonian contains terms which apparently violate the conservation of energy: They allow for the creation of a photon and the excitation of the atom at the same time as well as the relaxation of the atom and the annihilation of a photon. An understanding of this phenomenon is given when we change to the interaction picture via the unitary operator $\hat{U}(t) = \exp(\mathrm{i}\omega_0\hat{\sigma}_3 t/2 + \mathrm{i}\omega\hat{a}^\dagger\hat{a})$. This yields

$$\hat{H}_{\mathrm{IA}} = \hat{U}(t)\hat{H}\hat{U}^\dagger(t) = \frac{\hat{p}^2}{2m} + \hbar g(\hat{\sigma}_+ \mathrm{e}^{\mathrm{i}\omega_0 t} + \hat{\sigma}_- \mathrm{e}^{-\mathrm{i}\omega_0 t})(\hat{a}^\dagger \mathrm{e}^{\mathrm{i}\omega t} W^*(x) + \hat{a}\mathrm{e}^{-\mathrm{i}\omega t} W(x))\,. \tag{2.6}$$

In order to trap the atom the detuning $\Delta = \omega - \omega_0$ is chosen to fulfill the condition $\Delta \ll \omega_0$. In this case, the rapidly rotating terms containing the expression $\omega + \omega_0$ average to zero for typical time scales and can be dropped. This is known as the rotating wave approximation [75]. The non-energy preserving terms are interpreted as quantum fluctuations, which have no impact on the energy conservation when long time scales are considered. After another transformation $\hat{U} = \exp(-\mathrm{i}\Delta\hat{\sigma}_3 t/2)$ we arrive at

$$\hat{H}_{\mathrm{JC}} = \frac{\hat{p}^2}{2m} + \hbar g(\hat{\sigma}_+\hat{a}W(x) + \hat{\sigma}_-\hat{a}^\dagger W^*(x)) + \frac{\hbar\Delta}{2}(\mathbf{1} + \hat{\sigma}_3)\,, \tag{2.7}$$

which is known as the Jaynes-Cummings Hamiltonian containing the momentum operator of the atom [76]. Without the momentum operator this Hamiltonian is often used to describe the dynamics of a fixed atom held in a single-mode cavity. The exchange of excitations between the atom and the cavity mode is well described by this model, coupling states of the form $|g, n+1\rangle$ with $|e, n\rangle$, where $n \geq 0$ is the number of photons.

Here, however, we are not interested in this dynamics but concentrate on the atom. If we assume that the detuning fulfils $\hbar\Delta \gg \hbar g\sqrt{n}$ and $W(x)$ being on the order of one, we can treat the coupling term as a perturbation, which yields in first order

$$|g, n+1\rangle \to |g, n+1\rangle - \frac{g\sqrt{n+1}\,W(x)}{\Delta}\,|e, n\rangle\ . \tag{2.8}$$

This means that the ground state of the dressed atom has only a very small contribution from the excited state and the probability of finding the atom in its internal ground state is given by $P_g = \Delta^2/[\Delta^2 + (g\sqrt{n+1}W(x))^2] \approx 1$. This allows us to adiabatically eliminate the excited state of the atom and to derive an effective Hamiltonian by using the projection method [77, 78]

$$\hat{H}_{\mathrm{eff}} = \lim_{\varepsilon\to 0} \mathcal{P}\hat{H}_{\mathrm{JC}}\mathcal{P} - \mathcal{P}\hat{H}_{\mathrm{JC}}\mathcal{Q}(\mathcal{Q}\hat{H}_{\mathrm{JC}}\mathcal{Q} + \varepsilon\mathbf{1})^{-1}\mathcal{Q}\hat{H}_{\mathrm{JC}}\mathcal{P}\,. \tag{2.9}$$

In our case, the projector $\mathcal{P}$ onto the desired internal states is given by $\mathcal{P} = \sum_n |g,n\rangle \langle g,n|$, whereas the eliminated internal states are given by the projector $\mathcal{Q} = \sum_n |e,n\rangle \langle e,n|$ and $\mathbf{1} = \mathcal{P} + \mathcal{Q}$. This treatment is equivalent to perturbation theory, where the unperturbed Hamiltonian is assumed to be $\mathcal{P}\hat{H}_{\mathrm{JC}}\mathcal{P}$ and the perturbation is given by $\mathcal{P}\hat{H}_{\mathrm{JC}}\mathcal{Q} + \mathcal{Q}\hat{H}_{\mathrm{JC}}\mathcal{Q} + \mathcal{Q}\hat{H}_{\mathrm{JC}}\mathcal{P}$ [77]. Note that the motional states of the atom commute with the projectors and are hence not affected. After some algebra, equation (2.9) gives

$$\hat{H}'_{\mathrm{eff}} = \frac{\hat{p}^2}{2m} - \frac{\hbar g^2 |W(x)|^2}{\Delta}\, \hat{a}^\dagger \hat{a}\,. \tag{2.10}$$

The last term of this Hamiltonian represents the ac Stark shift, a force which an atom experiences when it is subject to an electric field, and still contains the mode operators $\hat{a}$. When this shift is used to trap atoms, one uses laser fields which are described by a coherent state [75]

$$|\alpha\rangle = \mathrm{e}^{-|\alpha|^2/2} \sum_{n=0}^{\infty} \frac{\alpha^n}{\sqrt{n!}} |n\rangle\ , \tag{2.11}$$

such that the average photon number fulfils $\langle \hat{n} \rangle = |\alpha|^2 \gg 1$. To achieve a sufficiently deep trap the laser intensity is typically so large that $|\alpha|^2 \gg 1$ and quantum fluctuations (which are on the order of $\sqrt{|\alpha|^2}$) can be neglected. Hence, taking the expectation value of the effective Hamiltonian with respect to this state is a good approximation and gives

$$\hat{H}_{\mathrm{eff}} = \frac{\hat{p}^2}{2m} - \frac{\hbar |\Omega(x)|^2}{4\Delta}\,, \tag{2.12}$$

where we have introduced the spatially dependent Rabi frequency $\Omega(x) = 2W(x)\mathbf{d}\cdot\mathbf{e}\sqrt{\hbar\omega\langle n\rangle/2\varepsilon_0 L} = \Omega_0 W(x)$. The optical potential depends on the intensity of the laser beam and on the detuning Δ. For a red-detuned laser, that means $\Delta > 0$, the atoms occupy regions with a high laser intensity to minimise their energy, whereas for a blue-detuned lattice ($\Delta < 0$) the atoms seek regions with a low intensity. One of the simplest ways to confine atoms with such traps is a focused, red-detuned laser beam. The atoms will gather in the focal point of the beam provided that their initial temperature is low enough. The depth of this optical potential is typically on the order of a few 100μK and hence on the order of the Doppler cooling limit [72]. If the temperature of the atoms is well below the depth of the optical potential, the laser beam provides a trap which is accurately described by an asymmetric harmonic oscillator.

Another important type of potential is created when a standing wave laser field with wave vector $k = 2\pi/\lambda$ is used, which is created by two counter-propagating laser beams. This leads to a trapping potential $V_0(x) = (\Omega_0^2/4\Delta^2)\sin^2(kx)$. Such a potential is known as an optical lattice. Its impact on the dynamics of the atoms will be discussed in Section 2.3.

2.2 Bose-Einstein condensates

The first work on Bose-Einstein condensation was done by A. Einstein some 80 years ago [79]. He expanded an earlier analysis of S. Bose [80] on the statistics of photons. Einstein predicted a phase transition of a non-interacting atomic gas at very low temperatures, where all atoms aggregate in the ground state. Since there were no experimental techniques to verify Einstein's prediction, his theory remained controversial. Only after the discovery of superfluid Helium [81] the interest in Einstein's theory sparked again when F. London speculated whether there was a connection between superfluidity and Bose-Einstein condensation [82, 83]. Later, N. Bogoliubov developed the first microscopic theory of interacting Bose gases that made use of Einstein's concepts [70]. This was followed by further theories which made connections between Bose-Einstein condensation and superfluidity [84].

An experimental proof of Bose-Einstein condensation was only possible after cooling methods as described in Section 2.1 had been developed. Efforts culminated in the direct experimental observation of Bose-Einstein condensates in 1995 [67, 68], which led to Nobel Prizes for E. Cornell, W. Ketterle, and C. Wieman in 2001. These experiments have opened the way to new fascinating developments in both theory and experiment. Especially the experimental realisation [22] of the Mott-insulator to superfluid transition [21] with ultracold atoms in optical lattices [17] has led to an increased interest in the Bose-Hubbard and related models due to their close connection to condensed matter physics [20]. In section 2.3 we will go into more detail. Here, we will concentrate on some aspects of Bose-Einstein condensation, especially interactions and the Bogoliubov theory.

2.2.1 Interactions between ultracold atoms

The interaction between the atoms plays an important role in Bose-Einstein condensation and can change the properties of a condensate considerably. Normally, the interaction potentials between atoms are rather complicated and are often not known precisely. As we will show in this section the low temperatures and hence low collision energies of the atoms in a Bose-Einstein condensate (BEC) enable us to use a simplified model interaction potential. In our presentation we will follow the theory given in [69]. A more detailed discussion can be found in [85].

We assume two particles of mass m_j, which interact via a potential V_{ia}. The potential should fulfil the condition $\lim_{r\to\infty} rV_{\mathrm{ia}}(r) = 0$, which is a reasonable assumption for an interatomic potential. The Hamiltonian describing this system is given by

$$\hat{H} = \frac{\hat{\mathbf{p}}^2}{2m_{\mathrm{red}}} + V_{\mathrm{ia}}(\mathbf{r})\,, \tag{2.13}$$

where $\mathbf{r} = \mathbf{r}_1 - \mathbf{r}_2$ is the relative coordinate of the two particles, $\hat{\mathbf{p}}$ the canonical conjugated momentum operator, and $m_{\mathrm{red}} = m_1 m_2/(m_1 + m_2)$ is the reduced

mass of the two atoms. We are only interested in the unbound solutions $\psi_{\mathrm{S}}(\mathbf{r})$ of the Schrödinger equation and assume for the moment that any coupling to bound (metastable) states is suppressed. The unbound states have a positive energy E and hence we make the ansatz $E = \hbar^2 k^2 / 2m_{\mathrm{red}}$. Putting this into the Schrödinger equation gives after some algebra

$$(\nabla^2 + k^2)\psi_{\mathrm{S}}(\mathbf{r}) = \frac{2m_{\mathrm{red}}}{\hbar^2} \int \mathrm{d}\mathbf{r}'\, V_{\mathrm{ia}}(\mathbf{r}')\psi_{\mathrm{S}}(\mathbf{r}')\delta(\mathbf{r} - \mathbf{r}')\,, \tag{2.14}$$

where the Dirac delta function δ has been formally introduced to get the integral expression. This equation is equivalent to a single particle scattered at a central potential. From the theory of Green's functions we know that the differential equation $(\nabla^2 + k^2)G(\mathbf{r} - \mathbf{r}') = \delta(\mathbf{r} - \mathbf{r}')$ is solved by $G(\mathbf{r} - \mathbf{r}') = -\exp(\mathrm{i}k|\mathbf{r} - \mathbf{r}'|)/4\pi|\mathbf{r} - \mathbf{r}'|$. This yields for the scattering state

$$\psi_{\mathrm{S}}(\mathbf{r}) = \psi_{\mathrm{S},0}(\mathbf{r}) - \frac{2m_{\mathrm{red}}}{4\pi\hbar^2} \int \mathrm{d}\mathbf{r}'\, \frac{\mathrm{e}^{\mathrm{i}k|\mathbf{r}-\mathbf{r}'|}}{|\mathbf{r} - \mathbf{r}'|} V_{\mathrm{ia}}(\mathbf{r}')\psi_{\mathrm{S}}(\mathbf{r}')\,. \tag{2.15}$$

The wave function $\psi_{\mathrm{S},0}(\mathbf{r})$ is a solution of the homogenous Helmholtz equation $(\nabla^2 + k^2)\psi_{\mathrm{S},0}(\mathbf{r}) = 0$. Since it is interpreted as an incoming wave it is reasonable to assume a plain wave as its solution, $\psi_{\mathrm{S},0}(\mathbf{r}) = \exp(\mathrm{i}\mathbf{k} \cdot \mathbf{r})$ with $|\mathbf{k}| = k$. The integral equation (2.15) is still not solvable for the general case. We hence apply the Born approximation to first order, which means that in the integral we replace the full wave function $\psi_{\mathrm{S}}(\mathbf{r}')$ by the incoming one $\psi_{\mathrm{S},0}(\mathbf{r}')$. This corresponds to an expansion of $\psi_{\mathrm{S}}(\mathbf{r}')$ to zeroth order in V_{ia} and is reasonable for the low interaction energies considered in the atomic context [69]. Since typical interatomic potentials fall off very rapidly we can furthermore approximate the denominator of the Green function as $|\mathbf{r} - \mathbf{r}'| \approx |\mathbf{r}| = r$. However, the phase factor in the numerator is more crucial, and therefore needs to be expanded in first order as $|\mathbf{r} - \mathbf{r}'| \approx r - \mathbf{r}' \cdot \mathbf{r}/r$. Together, we find for the Green function $G(\mathbf{r} - \mathbf{r}') \approx -\exp(\mathrm{i}k(r - \mathbf{r}' \cdot \mathbf{r}/r))/4\pi r$, which yields for the scattered state $\psi_{\mathrm{S}}(\mathbf{r}) = \psi_{\mathrm{S},0}(\mathbf{r}) + f_{\mathbf{k}}(\mathbf{n}) \exp(ikr)/r + \mathcal{O}(1/r^2)$, where $\mathbf{n} = \mathbf{r}/r$. The scattering amplitude

$$f_{\mathbf{k}}(\mathbf{n}) = -\frac{2m_{\mathrm{red}}}{4\pi\hbar^2} \int \mathrm{d}\mathbf{r}'\, \mathrm{e}^{-ik\mathbf{n}\cdot\mathbf{r}'} V_{\mathrm{ia}}(\mathbf{r}')\psi_{\mathrm{S},0}(\mathbf{r}') \tag{2.16}$$

does no longer depend on the distance r of the two atoms and contains the full information about the scattered state for large distances. Due to the low temperatures in the condensate the momentum k is so small that the condition $kr \ll 1$ holds for distances r for which the potential $V_{\mathrm{ia}}(r)$ is appreciable. We thus can neglect the phase factor in the integral of the scattering amplitude, which also eliminates the dependence of $f_{\mathbf{k}}$ from the scattering direction $\mathbf{n}$. The scattered state is spherically symmetric, which means that the scattering process only happens in the s wave. Moreover, in a BEC the average distance between the atoms is

typically larger than the range where the interaction potential differs significantly from zero. This means that only the long-range behaviour of the scattering process is important to describe the interactions in a BEC. We thus can replace the full interaction potential $V_{\mathrm{ia}}(r)$ by an effective one which reproduces the same asymptotic scattering behaviour for $k \to 0$. One of the simplest model potentials is the contact interaction described by $g\delta(\mathbf{r})$, with the coupling constant $g = 4\pi\hbar^2 a/2m_{\mathrm{red}}$. Here, the s-wave scattering length a is given by the limit $-a = \lim_{k\to 0} f_{\mathbf{k}}(\mathbf{n})$, yielding the correct asymptotic behaviour. In the context of BECs, it is the only parameter describing the interaction potential and typically deduced from experimental data [86].

2.2.2 Feshbach resonances

As shown in the previous section the only relevant parameter of the interatomic interaction in the cold atom context is the s-wave scattering length a. The scattering length does not only depend on the element, but also on the isotope of the atom and varies considerably as for example for Potassium [87]. Despite this big choice it would be desirable to have more freedom in changing the interaction strength. For example, for the production of molecules in optical lattices a dynamical change of the scattering length is necessary [88].

One way of achieving this is to make use of a Feshbach resonance. They were first investigated in the context of atomic nuclei [89, 90], but the theory is also applicable for the interatomic interaction. For a detailed discussion we refer the reader to the literature [86, 88], here we only state the main idea. Interatomic interaction potentials exhibit many excited states, which are bound and whose energies lie within the scattering continuum. If the energy E_{in} of an incoming, scattering particle coincides with the energy of a bound state E_{bs} of the interatomic potential, the two particles can virtually occupy this state and a Breit-Wigner-like resonance occurs [91]. This resonance strongly enhances the scattering length a. The scattering energy E_{in} is given by the temperature of the atomic gas and is normally close to zero. A dynamical variation of this energy is hence not practical. By using a magnetic field B, however, the energy level of the bound states E_{bs} can be shifted due to the Zeeman effect. One can show [86] that the scattering length a close to a Feshbach resonance is given by

$$a = a_{\mathrm{bg}}\left(1 + \frac{\Delta B}{B - B_0}\right), \tag{2.17}$$

where a_{bg} is the scattering length far away from the resonance, ΔB is the width of the resonance and B_0 is the magnetic field strength at the resonance. Typical values for the resonance are on the order of several mT and allow for changing the scattering length from large negative to positive values or even to zero [92, 93]. The possibility of tuning the value of the interaction strength dynamically has led

to ground-breaking experiments such as the creation of a molecular BEC [94, 95] or measurements on a degenerate quantum gas in the BEC-BCS crossover regime [96].

2.2.3 The Bogoliubov approximation for weakly interacting BECs

In this section we will illustrate the Bogoliubov formalism, which is used to describe the main properties of a BEC. Our starting point is the Hamiltonian of a system of identical Bosons described by a field operator $\hat{\psi}$ and trapped in a potential V_{ext}. Typically, the number density n of a BEC ranges between $10^{15}/\text{m}^3$ and $10^{22}/\text{m}^3$ [97], whereas the scattering length a is for the alkali atoms on the order of a few nanometers. Thus $na^3 \ll 1$, which means that the average distance between the atoms is so large that only the asymptotic behaviour of the scattering process is important. We furthermore note that higher partial waves than the s-wave with an angular momentum $\hbar l > 0$ are suppressed by a factor of $(k_{\text{B}}T/E_c)^l$, where E_c is the characteristic energy of the centrifugal barrier, which for alkali atoms is on the order of $E_c/k_{\text{B}} \approx 1\text{mK}$ [91, 97]. Since the critical temperature for achieving Bose-Einstein condensation is on the order of a few 100nK, only s-wave scattering is important and the real atomic potential can be replaced by the model potential $g\delta(\mathbf{r})$ introduced in Section 2.2.1. The Hamiltonian is then given by

$$\hat{H}_{\text{B}} = \int \mathrm{d}\mathbf{r}\, \hat{\psi}^\dagger(\mathbf{r}) \left(-\frac{\hbar^2\nabla^2}{2m_{\text{B}}} + V_{\text{ext}}(\mathbf{r}) - \mu \right) \hat{\psi}(\mathbf{r}) + \frac{g}{2} \int \mathrm{d}\mathbf{r}\, \hat{\psi}^\dagger(\mathbf{r})\hat{\psi}^\dagger(\mathbf{r})\hat{\psi}(\mathbf{r})\hat{\psi}(\mathbf{r})\,, \tag{2.18}$$

where μ is the chemical potential of the Bosons and m_{B} their mass. A negative interaction constant $g < 0$ means that the Bosons attract each other, which can lead to a collapse of the BEC when the density is above criticality [69]. In what follows we therefore restrict ourselves to the repulsive case $g > 0$.

In a BEC the ground state is macroscopically occupied for weak interactions and temperatures well below the critical temperature T_c. Hence, the condensate is well described by a classical wave function $\psi_0(\mathbf{r})$ and quantum fluctuations $\hat{\xi}(\mathbf{r})$, i.e., $\hat{\psi}(\mathbf{r}) = \psi_0(\mathbf{r}) + \hat{\xi}(\mathbf{r})$.[2] If we put this ansatz into the Heisenberg equation of motion and neglect all terms containing the fluctuations $\hat{\xi}$, we get

$$\left(-\frac{\hbar^2\nabla^2}{2m_{\text{B}}} + V_{\text{ext}}(\mathbf{r}) - \mu + g\,|\psi_0(\mathbf{r})|^2 \right) \psi_0(\mathbf{r}) = 0\,. \tag{2.19}$$

This is the well-know Gross-Pitaevskii equation (GPE), which was found independently from each other by E. Gross and L. Pitaevskii [100, 101]. A mathematically

[2]The method described in the following is not particle-number conserving. An alternative method, which conserves the number of particles, has been devised in Ref. [98, 99].

rigorous derivation of this equation was recently given by E. Lieb and coworkers [102].

Since the ground state of the BEC is macroscopically occupied, we have $\psi_0 \sim \sqrt{N}$, with N the number of condensate atoms, whereas the expectation value of the fluctuations fulfil $\langle\hat{\xi}\rangle \sim 1$. This means that when we put the ansatz $\hat{\psi}(\mathbf{r}) = \psi_0(\mathbf{r}) + \hat{\xi}(\mathbf{r})$ into the Hamiltonian equation (2.18), we can neglect higher orders of $\hat{\xi}$ yielding

$$\hat{H}_\mathrm{B} \approx H_\mathrm{B}^0 + \int \mathrm{d}\mathbf{r} \left\{ \hat{\xi}^\dagger(\mathbf{r}) \left(-\frac{\hbar^2}{2m_\mathrm{B}}\nabla^2 + V_\mathrm{ext}(\mathbf{r}) - \mu \right) \hat{\xi}(\mathbf{r}) \right. \\ \left. + \frac{g}{2} \left(4\left|\psi_0(\mathbf{r})\right|^2 \hat{\xi}^\dagger(\mathbf{r})\hat{\xi}(\mathbf{r}) + \psi_0^2(\mathbf{r})\hat{\xi}^\dagger(\mathbf{r})\hat{\xi}^\dagger(\mathbf{r}) + {\psi_0^*}^2(\mathbf{r})\hat{\xi}(\mathbf{r})\hat{\xi}(\mathbf{r}) \right) \right\}. \tag{2.20}$$

The expression H_B^0 does not involve quantum terms and is hence not important for the following. Furthermore, we have made use of the fact that all terms linear in $\hat{\xi}$ sum up to zero due to the Gross-Pitaevskii equation. The resulting Hamiltonian is bi-linear in the operators $\hat{\xi}$ and thus allows for a diagonalisation using the Bogoliubov transformation. This transformation was first applied by N. Bogoliubov for a homogenous condensate [70] and was later generalised by P. de Gennes [103]. The quantum fluctuations are expanded as $\hat{\xi}(\mathbf{r}) = \sum_\nu{}' u_\nu(\mathbf{r})\hat{b}_\nu - v_\nu^*(\mathbf{r})\hat{b}_\nu^\dagger$. The ground state is excluded from this summation, which is indicated by the prime at the sum symbol. The operators $\hat{b}_\nu^\dagger$ and $\hat{b}_\nu$ are bosonic creation and annihilation operators, respectively, which represent elementary excitations of the condensate, the so-called Bogoliubov phonons. If the classical functions u_ν and v_ν satisfy the Bogoliubov-de Gennes equations [104]

$$\left(-\frac{\hbar^2\nabla^2}{2m_\mathrm{B}} + V_\mathrm{ext}(\mathbf{r}) - \mu \right) u_\nu(\mathbf{r}) + g\left|\psi_0(\mathbf{r})\right|^2 \left(2u_\nu(\mathbf{r}) - v_\nu(\mathbf{r})\right) = E_\nu u_\nu(\mathbf{r}), \tag{2.21}$$

$$\left(-\frac{\hbar^2\nabla^2}{2m_\mathrm{B}} + V_\mathrm{ext}(\mathbf{r}) - \mu \right) v_\nu(\mathbf{r}) + g\left|\psi_0(\mathbf{r})\right|^2 \left(2v_\nu(\mathbf{r}) - u_\nu(\mathbf{r})\right) = -E_\nu v_\nu(\mathbf{r}), \tag{2.22}$$

the Hamiltonian describing the condensate simplifies to

$$\hat{H}_\mathrm{B} = H_\mathrm{B}^0 - \sum_\nu{}' E_\nu \int \left|v_\nu(\mathbf{r})\right|^2 \mathrm{d}\mathbf{r} + \sum_\nu{}' E_\nu \hat{b}_\nu^\dagger \hat{b}_\nu . \tag{2.23}$$

For this derivation we have assumed that the condensate wave function can be chosen to be real. For a condensate in its ground state this is always possible as was first supposed by R. Feynman [105] and later shown by O. Penrose and L. Onsager [84]. The Hamiltonian in equation (2.23) has a very simple form. Apart from the constant terms, which are normally neglected, it contains only the number operators $\hat{b}_\nu^\dagger\hat{b}_\nu$ of the Bogoliubov phonons. They behave as Bosons and for

a finite temperature $T \ll T_c$ the occupation number is given by the Bose statistics, $\langle \hat{b}_\nu^\dagger \hat{b}_\nu \rangle = 1/(\exp(\beta E_\nu) - 1)$ with $\beta = 1/k_B T$.

By using the above ansatz we find that the expectation value of the field operator with respect to a thermal state is no longer 0, but has a finite value $\langle \hat{\psi}(\mathbf{r}) \rangle = \psi_0(\mathbf{r})$. This mathematical artefact is know as breaking the $U(1)$-symmetry of the condensate, since its phase is explicitly fixed. It does not spoil the validity of the results used in this thesis. As a consequence of fixing the phase, the particle number of the condensate is no longer conserved. Methods which work without this symmetry breaking have been developed in Refs. [98, 99].

For illustration and since they are used later in this thesis we present the solutions of the Bogoliubov-de Gennes equations for a homogenous condensate. The wave function of the BEC is then simply given by the square root of the condensate density n_0, $\psi_0(\mathbf{r}) = \sqrt{n_0}$. From the GPE, equation (2.19), we find for the chemical potential $\mu = g n_0$, which means that the chemical potential simply reflects the interaction energy within the condensate. Using this we can rewrite the Bogoliubov-de Gennes equations in the form

$$-\frac{\hbar^2 \nabla^2}{2m_B} f_\nu^+(\mathbf{r}) = E_\nu f_\nu^-(\mathbf{r}) \,, \tag{2.24}$$

$$-\frac{\hbar^2 \nabla^2}{2m_B} f_\nu^-(\mathbf{r}) + 2g n_0 f_\nu^-(\mathbf{r}) = E_\nu f_\nu^+(\mathbf{r}) \,, \tag{2.25}$$

where we have defined $f_\nu^\pm(\mathbf{r}) = u_\nu(\mathbf{r}) \pm v_\nu(\mathbf{r})$. The solutions of these equations are given by

$$f_{\mathbf{k}}^\pm(\mathbf{r}) = \frac{1}{\sqrt{V}} \left(\sqrt{\frac{E_{\mathbf{k}}}{\varepsilon_{\mathbf{k}}^0}} \right)^{\pm 1} \mathrm{e}^{i\mathbf{k}\cdot\mathbf{r}} \,, \tag{2.26}$$

where V is the quantisation volume, $\varepsilon_{\mathbf{k}}^0 = \hbar^2 k^2 / 2m_B$ is the energy of a free particle with momentum $\mathbf{k}$, and $E_{\mathbf{k}} = \sqrt{\varepsilon_{\mathbf{k}}^0 (\varepsilon_{\mathbf{k}}^0 + 2g n_0)}$ is the energy of a Bogoliubov phonon.

2.3 Ultracold atoms in optical lattices and the Bose-Hubbard Model

An optical lattice is a dipole trap which creates a potential with a regular periodic pattern. One of the simplest lattice structures in three dimensions is created by three orthogonal pairs of counter-propagating laser beams which result in a potential of the form

$$V(\mathbf{r}) = V_{0,x} \sin^2(kx) + V_{0,y} \sin^2(ky) + V_{0,z} \sin^2(kz) \,. \tag{2.27}$$

Here, $k = 2\pi/\lambda$ is the wave vector of the laser creating the optical lattice in a certain direction and we have chosen k to be the same in all three directions. $V_{0,\alpha}$ is the depth of the optical lattice in direction $\alpha = x, y, z$. The above lattice is known as a simple cubic lattice in three dimensions. More exotic lattice geometries [106] such as a hexagonal lattice [24] or a Kagomé lattice [107] have also been proposed, here we however focus on the simple cubic case.

One of the main features of optical lattices is the unique control one has over the lattice depths $V_{0,\alpha}$. By tuning the laser intensity, depths up to several 100kHz can be achieved in times which are short compared to the typical time scale given by the evolution of the atoms in the lattice [108]. Since the lattice is created by light, it is essentially defect free in contrast to solid crystals and it also does not exhibit lattice phonons as long as quantum effects at low intensities can be neglected [109]. This property leads to the fact that phonons have to be introduced to the system by other means when the behaviour of electrons in solids is to be simulated, as will be discussed in chapter 4. It is furthermore possible to apply additional laser beams in order to change the periodicity of the lattice [110] or to apply pseudo-random potentials [111]. By choosing very deep lattices in one or two directions the tunnelling of the atoms through the potential barriers is essentially prohibited and quasi-two and one dimensional geometries can be created [18, 19]. In the one-dimensional case for example the atoms are restricted to single tubes, in which they are still subject to the lattice in the third, weak direction.

The depth of the optical lattice is typically given in units of the recoil energy $E_\mathrm{R} = (2\pi\hbar)^2/2m\lambda^2$, with m the mass of the atoms. In the following we assume that the lattice is appreciably deep, $V_0 \gg E_\mathrm{R}$. In this case, the bottom of each lattice well can be approximated by a harmonic oscillator potential $V_\mathrm{ho}(x) = m\omega_\mathrm{tr}x^2/2$ over the size of the ground state. The trapping frequency is given by $\omega_\mathrm{tr} = 2\sqrt{V_0 E_\mathrm{R}}/\hbar$. The state of an atom at the bottom of a single well in one spatial dimension can then be estimated by the ground state of the harmonic oscillator $\psi_\mathrm{ho} = \exp(-x^2/2a_\mathrm{ho}^2)/\sqrt{\sqrt{\pi}a_\mathrm{ho}}$ with the length of the harmonic oscillator given by $a_\mathrm{ho} = \sqrt{\hbar/m\omega_\mathrm{tr}}$ [18]. Estimating the wave function in this way leads to simple analytic results for the parameters U and J of the Bose-Hubbard model, see section 2.3.2.

Before we proceed with the properties of atoms confined to optical lattices we need to discuss the validity of the approximations done to derive the optical dipole potential. As was shown in Section 2.1, there exists a finite probability that an atom trapped by a dipole potential is in an excited state. Since this state has only a finite lifetime the atom can emit a photon and hence the dynamics would no longer be coherent. The rate of this spontaneous photon emission Γ_eff is given by the probability of finding the atom in the excited level times the lifetime of this upper state [18]. For a blue detuned optical lattice where the atoms are repelled by the intensity maxima, the emission rate is given by $\Gamma_\mathrm{eff} \approx -\Gamma\omega_\mathrm{t}/4\Delta$. In contrast, if the lattice is red detuned, the atoms are attracted by the intensity maxima

and $\Gamma_{\text{eff}} \approx \Gamma V_0/\hbar\Delta$. In both cases, Δ is the detuning of the laser introduced in Section 2.1. Since we require a sufficiently deep lattice we find $V_0 > \hbar\omega_{\text{tr}}$ and hence that the spontaneous emission for a blue detuned dipole trap is always lower than for a red detuned one (provided the absolute value of the detuning is the same). To be concrete let us assume a typical blue-detuned lattice with $\lambda = 514$nm for ^{23}Na, which uses the $S_{1/2} \to P_{3/2}$ transition at $\lambda_{\text{t}} = 589$nm with $\Gamma = 2\pi \times 10$MHz. The recoil energy is $E_{\text{R}}/\hbar \approx 2\pi \times 33$kHz and the detuning $\hbar\Delta \approx -2.3 \times 10^9 E_{\text{R}}$. For a lattice with $V_0 = 25E_{\text{R}}$ corresponding to $\hbar\omega_{\text{tr}} = 10E_{\text{R}}$ this leads to an emission rate of $\Gamma_{\text{eff}} = 10^{-2}$/s [18], whilst experiments are typically conducted in times shorter than one second. For a typical red-detuned lattice as done with ^{87}Rb in a $\lambda = 852$nm lattice operated at the $S_{1/2} \to P_{1/2}$ transition with $\lambda_{\text{t}} = 795$nm and $\Gamma = 2\pi\times 6$MHz we find $E_{\text{R}} \approx 2\pi\times 3.1$kHz and a detuning of $\hbar\Delta \approx 8.0\times 10^9 E_{\text{R}}$. For a lattice with $V_0 = 25E_{\text{R}}$ this leads to an effective emission rate of $\Gamma_{\text{eff}} = 0.2 \times 10^{-2}$/s [112]. In conclusion, for typical experimental setups the spontaneous emission can be neglected and the evolution of the atoms is coherent as was impressively confirmed by experiments [22, 113].

2.3.1 A single atom in an optical lattice

After a detailed discussion of the trapping properties we now illustrate the effect an optical lattice has on the dynamics of a single atom. For simplicity, we always assume a quasi one-dimensional setup, where two of the trap depths, say $V_{0,y} = V_{0,z} = V_{0,\perp}$, are so deep that the atom is effectively restricted to one tube of the lattice. The dynamics perpendicular to the tube is frozen out if the energy of the atom is smaller than the excitation energy $\hbar\omega_{\text{tr},\perp} = 2\sqrt{V_{0,\perp}E_{\text{R}}}$ in that direction, and the atom is described by the Hamiltonian

$$\hat{H}_{\text{1D}} = \frac{\hat{p}^2}{2m} + V_0 \sin^2(kx)\,, \tag{2.28}$$

where $\hat{p} = -\mathrm{i}\hbar\nabla$. In the third direction, here the x-direction, the atom is subject to a periodic potential with period $a = \lambda/2$. The periodicity of the lattice allows us to apply Bloch's theorem [52], which is well-known from condensed matter physics. It states that the eigenstates $\psi_q(x)$ of the Hamiltonian equation (2.28) have the form $\psi_q(x) = \exp(\mathrm{i}qx)u_q(x)$ with periodic functions $u_q(x) = u_q(x + a)$. The wave differs from the free wave of the atom only by a periodic modulation [51]. The so-called quasi-momentum q behaves in many ways similar to a free-space momentum, however it is only defined modulo a reciprocal lattice vector $K = 2\pi/a$. This means that when discussing the properties of the wave functions one can restrict themselves to quasi-momenta in the first Brillouin zone $-\pi/a < q \leq \pi/a$.

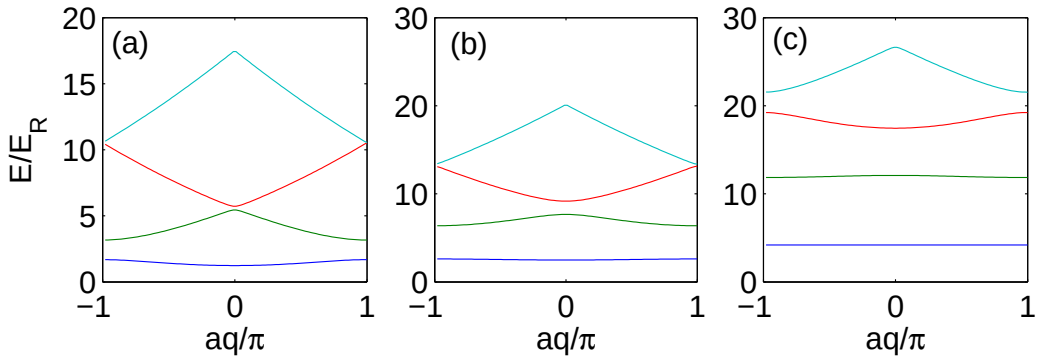

Figure 2.1. Energy levels $E = E_{q,n}$ for a single atom in an optical lattice. Shown are the first four Bloch bands for (a) $V_0 = 3E_\mathrm{R}$, (b) $V_0 = 8E_\mathrm{R}$, and (c) $V_0 = 20E_\mathrm{R}$. The energy levels have been calculated by using the central equation (2.30).

If we put the wave function into the Schrödinger equation we find

$$\mathrm{e}^{\mathrm{i}qx} E_q u_q(x) = \hat{H}_{1\mathrm{D}} \psi_q(x) = \mathrm{e}^{\mathrm{i}qx} \left(\frac{(\hat{p} + \hbar q)^2}{2m} u_q(x) + V_0 \sin^2(kx) u_q(x) \right) . \qquad (2.29)$$

Since $u_q(x)$ fulfils periodic boundary conditions on a finite spatial regime $0 \leq x < a$, we expect for fixed q a discrete energy spectrum for the solutions of this equation. The corresponding quantum number n is known as the band index of the respective wave function. For each index n, the energies $E_{q,n}$ form a quasi-continuum with respect to the quasi-momentum q, which is known as the band structure. Numerical solutions of the band structure can be obtained by solving the equivalent algebraic equation

$$\left(\frac{\hbar^2 q^2}{2m} - E_{q,n} \right) C_q + \sum_l U_l C(q - 2\pi l/a) = 0 \,, \qquad (2.30)$$

which is also known as the central equation [51]. Here, the constants are given by $\psi(x) = \sum_l C(2\pi l/L) \exp(\mathrm{i}2\pi lx/L)$, with L the length of the quantisation volume, and $V(x) = \sum_l U_l \exp(\mathrm{i}2\pi lx/a)$. The algebraic equation seems to be quite impractical to solve at the first glance, since a very large number of constants C needs to be determined. However, experience shows that in practice a small number often suffices [51]. The band structure for different lattice depths is shown in figure 2.1. We observe that for deeper optical lattices the energy gap between the lowest and the first excited band gets larger and that the lowest band gets also flatter. For a lattice depth of $V_0 = 3E_\mathrm{R}$ the height of the lowest band is $0.45E_\mathrm{R}$ with an energy gap to the next band of $E_g = 1.5E_\mathrm{R}$, whereas for a lattice depth of $V_0 = 20E_\mathrm{R}$ the hight of the lowest band is reduced to $0.01E_\mathrm{R}$, whereas the gap is increased to

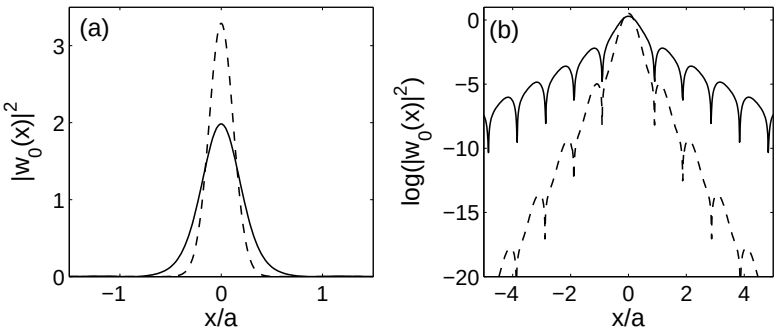

Figure 2.2. (a) Square of the absolute value of two different lowest band Wannier functions localised at lattice site 0. (b) Logarithm thereof. The solid line shows the Wannier function for a lattice depth of $V_0 = 3E_\mathrm{R}$, the dashed one for $V_0 = 15E_\mathrm{R}$.

$E_g = 7.6E_\mathrm{R}$. This shows that for low atom energies and deep optical lattices it is valid to ignore the higher bands, which is typically done in the Bose-Hubbard model. We note that for our special case $V(x) = V_0 \sin^2(kx)$ the band structure can also be solved analytically since the Schrödinger equation becomes equivalent to the Mathieu equation [114].

Due to their periodicity, the Bloch functions are delocalised, that means they spread over the whole lattice. Intuitively, one would expect that their Fourier transforms are localised functions. Indeed, one can show that the Fourier transform

$$w_n(\mathbf{R}_j, \mathbf{r}) = \frac{1}{v_0} \int \mathrm{d}\mathbf{k}\, \mathrm{e}^{-\mathrm{i}\mathbf{R}_j \cdot \mathbf{k}} \psi_{n,\mathbf{k}}(\mathbf{r}) \tag{2.31}$$

is essentially restricted to a single lattice site for small band indices n provided that the energy gap between adjacent bands is large [52].[3] This requires the lattice to be deep enough, $V_{0,x} \gg E_\mathrm{R}$ for the lowest band. The Fourier transform is also known as a Wannier function, localised at lattice site $\mathbf{R}_j = j\mathbf{a}$. In higher dimensions, this vector corresponds to a Bravais lattice vector. Examples of Wannier functions are shown in figure 2.2. The exponential localisation of the Wannier functions is clearly visible, and even for a comparatively weak lattice with $V_0 = 3E_\mathrm{R}$ the localisation is sufficiently strong. At this point we shall note that for more complicated periodic structures than our simple sinusodial potential the correct choice of a complete set of localised functions becomes a delicate issue. For more information we refer the reader to [115] and, for a recent treatment in the field of optical lattices, to [110].

The Wannier functions only depend on the distance between $\mathbf{R}_j$ and $\mathbf{r}$ as is

[3] We note that the details of the localisation also depend on the phases chosen for the Bloch functions [110].

evident from their definition and Bloch's theorem[4]. They fulfil the orthonormality condition $\int \mathrm{d}\mathbf{r}\, w_n(\mathbf{r}-\mathbf{R}_j)w^*_{n'}(\mathbf{r}-\mathbf{R}_{j'}) = \delta_{n,n'}\delta_{j,j'}$ and are a complete set of functions [52]. As indicated above for a sufficiently deep lattice the Wannier function of the lowest band $n = 0$ can be estimated by a Gaussian

$$w_{n=0}(\mathbf{r}-\mathbf{R}_j) \approx \frac{1}{\sqrt{\sqrt{\pi}\sigma}}\, \mathrm{e}^{-\frac{(\mathbf{r}-\mathbf{R}_j)^2}{2\sigma^2}} \tag{2.32}$$

with a width $\sigma = (E_\mathrm{R}/V_0)^{1/4}a/\pi$.

Since the Wannier functions form a complete orthonormal set we can expand the field operator of the bosons as

$$\hat{\psi}(\mathbf{r}) = \sum_{n,j} w_n(\mathbf{r}-\mathbf{R}_j)\hat{a}_{j,n}\,, \tag{2.33}$$

where $\hat{a}_{j,n}$ are bosonic annihilation operators with the canonical commutation relations $[\hat{a}_{j,n}, \hat{a}^\dagger_{j',n'}] = \delta_{j,j'}\delta_{n,n'}$ and $[\hat{a}_{j,n}, \hat{a}_{j',n'}] = 0$. With this, we can rewrite the Hamiltonian $\hat{H}_\mathrm{1D}$ from equation (2.28) in second quantisation yielding

$$\hat{H} = \sum_{j,j',n,n'} J_{n,n'}(j,j')\hat{a}^\dagger_{j',n'}\hat{a}_{j,n}\,. \tag{2.34}$$

The amplitude of the transition process from state (j,n) to (j',n') is given by $J_{n,n'}(j,j') = \int \mathrm{d}\mathbf{r}\, w_n(\mathbf{r}-\mathbf{R}_j)\hat{H}_\mathrm{1D}w^*_{n'}(\mathbf{r}-\mathbf{R}_{j'})$. When we use the definition of the Wannier functions equation (2.31) and the fact that $\hat{H}_\mathrm{1D}\psi_{n,q} = E_{n,q}\psi_{n,q}$ we find that $J_{n,n'}(j,j')$ equals zero whenever $n \neq n'$. This means that the atom cannot change from one energy band to another. Furthermore, the hopping amplitude only depends on the difference $j-j'$ and we find $J_n(j-j') = \int_\mathrm{BZ}\mathrm{d}q\, \exp(\mathrm{i}q(j-j')a)E_{q,n}/v_\mathrm{BZ}$, where the integral is taken over the first Brillouin zone and v_BZ is the volume of that zone in reciprocal space. Hence the hopping amplitude is simply the Fourier transform of the energy bands, which does not depend on the localisation properties of the Wannier functions.

When the energy of the single atom is smaller than the gap between the lowest and first excited band, a regime which can be achieved with current experiments, it is justified to assume that the atom only occupies the lowest band and the other bands are no longer important for the dynamics. For deep enough optical lattices with $V_0 \gg E_\mathrm{R}$, it is furthermore possible to neglect all amplitudes $J_0(j-j')$ which are beyond nearest neighbours, that means for which $|j-j'| > 1$, since they are typically one order of magnitude smaller than the amplitude for $|j-j'| = 1$ [17]. This remaining hopping amplitude only couples neighbouring lattice sites, i.e. the atom can only hop from one lattice well to an adjacent one. This model is also known as the single band tight binding model, described by

[4]Note that $\mathbf{R}_j$ can only be shifted by a multiple of the lattice periodicity a.

the Hamiltonian $\hat{H}_{\mathrm{tb}} = -\sum_{\langle i,j\rangle} J\hat{a}_i^\dagger \hat{a}_j$, where the symbol $\langle i,j\rangle$ denotes that only nearest neighbour lattice sites are included in the sum. Using Wannier functions approximated by Gaussians as in equation (2.32), the hopping amplitude is given by $J = -J_0(\pm 1) = -(4/\sqrt{\pi})E_{\mathrm{R}}(V_0/E_{\mathrm{R}})^{3/4}\exp(-2\sqrt{V_0/E_{\mathrm{R}}})$ [114]. The coupling decreases exponentially for an increasing lattice depth V_0.

2.3.2 Interactions between atoms in an optical lattice

So far we only considered the dynamics of a single atom and did not take the interactions between atoms into account. As discussed in section 2.2.1 the interaction between the atoms can be described by a model potential, which simplifies the interaction Hamiltonian of identical Bosons to

$$\hat{H}_{\mathrm{int}} = \frac{g}{2}\int \mathrm{d}\mathbf{r}\, \hat{\psi}^\dagger(\mathbf{r})\hat{\psi}^\dagger(\mathbf{r})\hat{\psi}(\mathbf{r})\hat{\psi}(\mathbf{r})\,. \tag{2.35}$$

As in the previous section, this Hamiltonian will be expanded in terms of Wannier functions. If we neglect higher bands and all off-site terms, that means terms which involve Wannier functions from different sites, the interaction Hamiltonian simplifies to [17]

$$\hat{H}_{\mathrm{int}} = \frac{U}{2}\sum_j \hat{n}_j(\hat{n}_j - 1)\,, \tag{2.36}$$

where $\hat{n}_j = \hat{a}_j^\dagger \hat{a}_j$ counts the number of bosons in lattice site j. The interaction constant is given by $U = 4\pi a_s \hbar^2 \int \mathrm{d}^3\mathbf{r}\,|w(\mathbf{r})|^4/m$. By approximating the Wannier function by the harmonic oscillator ground state given in equation (2.32) we get for one spatial dimension $U \approx 2\hbar\omega_{\mathrm{tr}}(a_s/a_{\mathrm{ho}})/\sqrt{2\pi} = \sqrt{2\pi}(g/\lambda)(V/E_{\mathrm{R}})^{1/4}$ [17, 114].

The above assumption of neglecting off-site terms is justified for deep enough optical lattices $V_0 \gg E_{\mathrm{R}}$. For neglecting higher bands we estimate the band gap between the lowest band and the first excited one by the harmonic oscillator energy $\hbar\omega_{\mathrm{tr}}$. In this case, the assumption is consistent with the above interaction term if $Un_j(n_j-1)/2 \ll \hbar\omega_{\mathrm{tr}}$, where n_j is the average number of atoms in lattice site j. For using the simplified model potential we furthermore need that the scattering length a_s fulfils the condition $a_s \ll a_{\mathrm{ho}} \ll \lambda/2$ [17].

When we combine the hopping and interaction contributions and also include a slowly-varying, weak trapping potential $V_{\mathrm{T}}(\mathbf{r})$ in addition to the optical lattice, we get the well-known Bose-Hubbard Hamiltonian

$$\hat{H}_{\mathrm{BH}} = -J\sum_{\langle i,j\rangle}\hat{a}_i^\dagger\hat{a}_j + \frac{U}{2}\sum_j \hat{n}_j(\hat{n}_j-1) + \sum_j \varepsilon_j\hat{n}_j\,. \tag{2.37}$$

The terms taking the additional trap into account are give by $\varepsilon_j = \int \mathrm{d}^3\mathbf{r}|w_0(\mathbf{r} - \mathbf{R}_j)|^2 V_{\mathrm{T}}(\mathbf{r}) \approx V_{\mathrm{T}}(\mathbf{R}_j)$, which is the average of the trapping potential on a site.

2.3.3 Properties of the Bose-Hubbard Hamiltonian

For Fermions, the Hubbard model was originally introduced to investigate the interaction of electrons in a narrow energy band and the magnetic properties of those electrons [116]. The main characteristics of the model are that electrons in the solid can hop from one atom to another and that the interaction between the electrons is restricted to the case where electrons occupy the same atom. Later, J. Hubbard extended the model and discussed a crossover between two regimes, one in which there are no interactions between the electrons and one in which the band width is zero, which corresponds to a vanishing hopping and whence to an insulating phase [117]. Various extensions of the model have been devised to include off-site spin-spin interaction between the electrons and these models are currently studied in order to explain high-temperature superconductivity [54, 118–120].

For Bosons, extensive theoretical investigations have been done in [21], where a transition from a superfluid phase to a Mott-insulator has been discussed. The latter phase is characterised by an integer filling of the lattice sites, by an excitation gap and zero compressibility. The model was originally compared to experimental studies of ^{4}He atoms adsorbed on porous materials [121]. The advent of optical lattices has allowed for a clean realisation of the model and to tune its parameters over a wide range from the superfluid to the insulating case in a single experiment. This has eventually led to the experimental observation of the superfluid to Mott-insulator transition [22].

To discuss the two limiting cases of vanishing hopping and vanishing interaction between the bosonic atoms we assume that there is no additional weak trapping and the atoms are described by the Hamiltonian

$$\hat{H}_{\mathrm{BH}} = -J \sum_{\langle i,j \rangle} \hat{a}_i^\dagger \hat{a}_j + \frac{U}{2} \sum_j \hat{n}_j(\hat{n}_j - 1) - \mu \sum_j \hat{n}_j \,, \tag{2.38}$$

with μ the chemical potential. For simplicity of notation we again assume a one-dimensional lattice with M lattice sites and periodic boundary conditions, the extension to the simple cubic case in three dimensions is straightforward. The lattice sites shall be denoted by their index j and the vector pointing to that lattice site shall be $\mathbf{R}_j$. We first assume $U = 0$, that means a vanishing interaction. We define the transformation

$$\hat{c}_{\mathbf{q}} = \frac{1}{\sqrt{M}} \sum_j \hat{a}_j \mathrm{e}^{-\mathrm{i}\mathbf{q}\cdot\mathbf{R}_j} \,, \tag{2.39}$$

where $\mathbf{q}$ is a vector in the first Brillouin zone, $\mathbf{q} \in (-\pi/2, \pi/2]$. Using this transformation the Bose-Hubbard Hamiltonian is diagonalised as $\hat{H}_{\mathrm{BH}} = \sum_{\mathbf{q}} (E_{\mathbf{q}} - \mu) \hat{c}_{\mathbf{q}}^\dagger \hat{c}_{\mathbf{q}}$ with the energies $E_{\mathbf{q}} = -2J\cos(\mathbf{q}a)$. From this we deduce that the ground state

of the system is given when all N atoms are in the $\mathbf{q} = 0$ mode, that means

$$|\psi_{\mathrm{gs},U=0}\rangle = \frac{\hat{c}^\dagger_{\mathbf{q}=0}}{\sqrt{N!}}\,|\mathrm{vac}\rangle = \frac{1}{\sqrt{N!}}\left(\frac{1}{\sqrt{M}}\sum_{j=1}^{M}\hat{a}^\dagger_j\right)^N|\mathrm{vac}\rangle\ . \tag{2.40}$$

The atoms in this state are delocalised over the whole lattice and exhibit an off-diagonal long range order [18]. Since all particles occupy the ground state it furthermore describes a Bose-condensed superfluid state [18, 91]. The energy spectrum for this case is gapless in the thermodynamic limit where the quasi-momenta $\mathbf{q}$ become continuous.

The situation changes in the opposite limit where $J = 0$ and the interaction has a finite value. If the number of atoms N is not a multiple of the number of lattice sites M, the ground state will be degenerate, that means there will be several states which all have the same ground state energy. We therefore restrict our considerations to a commensurate filling where $N = \gamma M$ with integer $\gamma \geq 0$. In this case, the ground state is given by a Fock state with

$$|\psi_{\mathrm{gs},J=0}\rangle = \prod_{j=1}^{M}\frac{\left(\hat{c}^\dagger_j\right)^\gamma}{\sqrt{\gamma!}}\,|\mathrm{vac}\rangle\ , \tag{2.41}$$

where the value of γ depends on the chemical potential and is chosen to minimise the energy of the state, $E_\gamma = MU\gamma(\gamma-1)/2-\mu\gamma M$. This state is also known as the Mott insulator state. Excitations of this state consist for instance of taking an atom out of one lattice site and putting it into a different one leading to an excitation energy of U, or by adding or removing a single particle [122, 123]. The latter states also exhibit an excitation gap apart from the cases where the ratio μ/U is an integer number. These cases are known as degeneracy points and the Mott insulator is compressible for these points, whereas its compressibility $\partial\langle\hat{N}\rangle/\partial\mu$ vanishes for all other chemical potentials, i.e. the number of atoms (and hence the density) stays constant for varying chemical potential μ [21]. Here, $\hat{N} = \sum_j \hat{n}_j$ is the operator counting the total number of particles. In contrast to the superfluid state where $U = 0$, the atoms in the Mott insulator state are localised in their lattice sites and do not exhibit any off-diagonal long range order.

The regime in between those two limiting cases, where both U and J have finite values, is not currently accessible with exact analytical methods. Instead, approximations are used to get an insight into the involved physics. We employ a consistent mean-field theory [124, 125], which changes the hopping operator to

$$\hat{a}^\dagger_i\hat{a}_j \to \langle\hat{a}^\dagger_i\rangle\hat{a}_j + \hat{a}^\dagger_i\langle\hat{a}_j\rangle - \langle\hat{a}^\dagger_i\rangle\langle\hat{a}_j\rangle = \psi(\hat{a}^\dagger_i + \hat{a}_j) - \psi^2\,, \tag{2.42}$$

where $\psi = \langle\hat{a}_j\rangle = \langle\hat{a}^\dagger_j\rangle$ is the (real) superfluid order parameter. Putting this into

the Bose-Hubbard Hamiltonian yields

$$\hat{H}_{\mathrm{MF}} = -zJ\psi \sum_j (\hat{a}_j^\dagger + \hat{a}_j) + zJ\psi^2 M + \frac{U}{2}\sum_j \hat{n}_j(\hat{n}_j - 1) - \mu \sum_j \hat{n}_j \,, \tag{2.43}$$

where z is the number of nearest neighbours. This Hamiltonian does not involve any hopping terms anymore and is thus block diagonal in terms of the lattice sites. We thus only consider the Hamiltonian for one lattice site and drop the site index. This leads to $\hat{H}_{1\mathrm{MF}} = \hat{H}_0 + \psi\hat{V}$, where $\hat{H}_0 = \tilde{U}\hat{n}(\hat{n}-1)/2 - \tilde{\mu}\hat{n} + \psi^2$, $\hat{V} = -(\hat{a}^\dagger + \hat{a})$ and the constants have been renormalised to $\tilde{U} = U/zJ$, $\tilde{\mu} = \mu/zJ$. The ground state energy of this Hamiltonian is calculated using perturbation theory [126]. For the unperturbed Hamiltonian $\hat{H}_0$ we get

$$E_g^{(0)} = \begin{cases} \psi^2 & \text{if} \quad \tilde{\mu} < 0 \\ \tilde{U}\gamma(\gamma-1)/2 - \tilde{\mu}\gamma + \psi^2 & \text{if} \quad \tilde{U}(\gamma-1) < \tilde{\mu} < \tilde{U}\gamma \,. \end{cases} \tag{2.44}$$

The first order perturbation in the energy vanishes, whereas the second order is given by

$$E_g^{(2)} = \psi^2 \left(\frac{\gamma}{\tilde{U}(\gamma-1) - \tilde{\mu}} + \frac{\gamma+1}{\tilde{\mu} - \tilde{U}\gamma} \right) . \tag{2.45}$$

We now apply the Landau criterion in order to determine the second order phase transition [85]. If we expand the ground state energy as

$$E_g(\psi) = c_0(\gamma, \tilde{U}, \tilde{\mu}) + c_2(\gamma, \tilde{U}, \tilde{\mu})\psi^2 + \mathcal{O}(\psi^4) \tag{2.46}$$

and neglect the higher orders in ψ we see that for $c_2 > 0$ the energy is minimised only if $\psi = 0$, which means that there is no superfluid density present. For $c_2 < 0$, however, the minimum occurs at a $\psi \neq 0$. This means that the boundary between the Mott insulating and the superfluid phase is given by $c_2 = 0$, which yields [124]

$$\tilde{\mu}_\pm = \frac{1}{2}[\tilde{U}(2\gamma - 1) - 1] \pm \frac{1}{2}\sqrt{\tilde{U}^2 - 2\tilde{U}(2\gamma+1) + 1} \,. \tag{2.47}$$

The two possible values for $\mu_\pm$ mark the two boundaries of a Mott insulating phase space region with a filling of γ particles per lattice site. The minimum value of $\tilde{U}$, where the Mott insulator still exists, is given by $\mu_+ = \mu_-$, which yields

$$\tilde{U}_c = 2\gamma + 1 + \sqrt{(2\gamma+1)^2 - 1} \,, \tag{2.48}$$

and especially for $\gamma = 1$ we find $\tilde{U} \approx 5.83$. The resulting phase diagram for the Bose-Hubbard model is shown in figure 2.3. The results of the mean-field theory are exact for $z \to \infty$. For three spatial dimensions ($z = 6$) the shown boundaries are still fairly accurate [122], whereas for one spatial dimension ($z = 2$) the results found with the density matrix renormalisation group (DMRG) method deviate

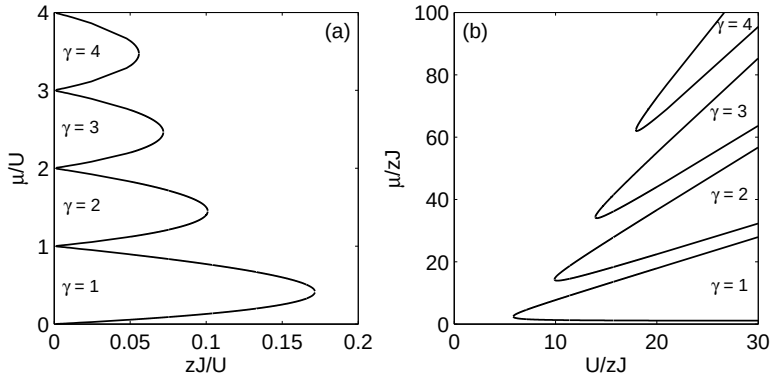

Figure 2.3. Phase diagram of the Bose-Hubbard model. Shown are the phase boundaries for the first four insulating lobes with integer filling γ. The results are derived from mean-field theory, equation (2.47). Outside the lobes the lattice gas is superfluid and exhibits in general a non-integer filling.

considerably at the tips of the lobes, which in the numerical calculations bend downwards and have a sharp kink [127].

2.3.4 Numerical exact solutions of the Bose-Hubbard model

In later parts of this thesis we will tailor the constants of the Bose-Hubbard model in such a way that the atoms can be used, for example, to store quantum information in a reliable way. For this we need to solve the dynamics of the Bose-Hubbard Hamiltonian $\hat{H}_{\mathrm{BH}}$ exactly. Given that the Hamiltonian is time-independent, the dynamics of the state $\psi(t)$ can be solved formally by

$$\psi(t) = \exp(-\mathrm{i}\hat{H}_{\mathrm{BH}}t/\hbar)\psi(0)\,. \tag{2.49}$$

Since $\hat{H}_{\mathrm{BH}}$ is a linear operator on a finite-dimensional Hilbert space, it can be represented by a matrix and the exponentiation of this matrix should be easy. This is certainly true as long as the Hilbert space is small. However, for an optical lattice with M lattice sites filled with N bosons, the dimension $\mathcal{D}$ of the Hilbert space is given by

$$\mathcal{D}(M,N) = \binom{N+M-1}{N} = \frac{(M+N-1)!}{(M-1)!N!}\,. \tag{2.50}$$

By using the asymptotic behaviour of the central binomial coefficient, $\binom{2M}{M} \sim \sqrt{2/\pi}4^M/\sqrt{2M+1}$, one can show that for large $M = N \gg 1$ the dimensionality of the Hilbert space behaves as $\mathcal{D}(M,M) \sim 4^M/\sqrt{2\pi(2M+1)}$, which means an

exponential growth of the Hilbert space dimension. From this it is evident that we have to restrict ourselves to small systems when we solve the Schrödinger equation exactly. For example, the Hilbert space dimension for $N = 8$ atoms in $M = 8$ lattice sites is given by $\mathcal{D}(8, 8) = 6435$. Storing a non-sparse[5] 7000×7000 matrix with double precision needs about 400MB of RAM. A typical workstation at the time of writing this thesis has 1GB of RAM. Hence we see that the above example is about the maximum that can be solved exactly with present standard office equipment.

We should note at this point that alternative methods have been developed to solve the Bose-Hubbard model in an approximate way. These include quantum Monte Carlo methods [128, 129], the density matrix renormalisation group (DMRG) [3–6], and time-evolving block decimation (TEBD) [7–9]. The first method is a stochastic one, which approximates the process by random variables that converge to the desired state. The latter two methods truncate the Hilbert space in such a way that the essential properties of the states or density matrices are conserved. Although we compare some of our results to ones obtained with TEBD, a description of these methods is beyond the scope of this thesis and we refer the reader to the literature [7–9].

2.3.5 State-dependent and selectively moving lattices

So far we have only considered simple optical lattices where the potential does not depend on the internal state of the trapped atoms. By a suitable choice of the laser beams and atomic species it is possible to make the potential dependent on the internal state of the atoms and to move them selectively according to their state. Since this method is heavily used in chapter 3, in the following we briefly sketch its main ideas.

Two counterpropagating linearly polarised laser beams with the same wavelength, intensity and polarisation plane create a standing wave field. If the two polarisation planes are tilted by an angle 2ϑ the resulting field can be described as two standing waves with $\sigma^{\pm}$-polarisation, given by the electric field

$$\mathbf{E}(\mathbf{r}, t) = E_0 \left[\cos(kx - \vartheta)\mathbf{e}_- - \cos(kx + \vartheta)\mathbf{e}_+\right] , \tag{2.51}$$

where we have assumed that the laser fields are propagating in x-direction and the polarisation vectors are given by $\mathbf{e}_\pm = \mathbf{e}_y \pm \mathrm{i}\mathbf{e}_z$, with $\mathbf{e}_y$, $\mathbf{e}_z$ unit vectors in y- and z-direction, respectively [18]. As we will see below, for certain cases the optical dipole potential depends on the polarisation vector of the laser light which results in the two dipole potentials $V_\pm(x) \propto \cos^2(kx \pm \vartheta)$.

[5] Although the Hamiltonian $\hat{H}_{\mathrm{BH}}$ can be represented as a sparse matrix, that means a matrix which mainly contains zeros, the unitary $\exp(-\mathrm{i}\hat{H}_{\mathrm{BH}}t/\hbar)$ describing the time evolution is typically non-sparse.

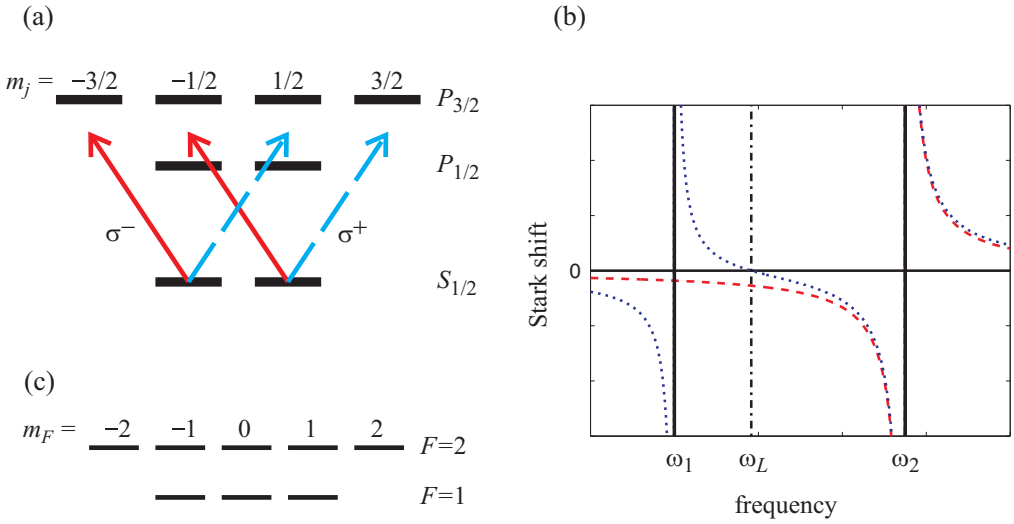

Figure 2.4. (a) Level structure of the alkali atoms ^{23}Na and ^{87}Rb and the (detuned) electric dipole transitions induced by σ^- light (solid arrow) and σ^+ light (dashed arrow). (b) Schematic plot of the resulting ac Stark shifts for σ^+-light. The dashed line gives the shift for the state $|S_{1/2}, m_j = 1/2\rangle$, whereas the dotted line is the sum of the two shifts for state $|S_{1/2}, m_j = -1/2\rangle$. The transition frequencies between the fine structure levels are denoted by ω_1 and ω_2, the critical frequency at which the two Stark shifts for $|S_{1/2}, m_j = -1/2\rangle$ cancel is given by ω_L. (c) Hyperfine structure of the $S_{1/2}$-manifold.

As shown in section 2.1 the strength of the optical potential depends strongly on the dipole moment. By choosing the laser beams accordingly, selection rules can be exploited to tailor the optical potential [44, 130]. A typical level structure of an alkali atom, which corresponds for example to ^{23}Na or ^{87}Rb, is shown in figure 2.4(a). Due to selection rules, the σ^+-light couples the state $|S_{1/2}, m_j = 1/2\rangle$ to $|P_{3/2}, m_j = 3/2\rangle$, and the state $|S_{1/2}, m_j = -1/2\rangle$ to the two states $|P_{1/2}, m_j = 1/2\rangle$ and $|P_{3/2}, m_j = 1/2\rangle$. This means that atoms in state $|S_{1/2}, m_j = -1/2\rangle$ experience two ac Stark shifts. If the laser frequency is chosen such that it lies between the two transition frequencies, the resulting dipole potentials will have opposite signs due to the opposite signs in the respective detuning. Hence there exists a laser frequency ω_L where the two contributions cancel each other, and the atom in state $|S_{1/2}, m_j = -1/2\rangle$ does not experience any potential from σ^+-light. Since transitions to other levels are far detuned their influence can be neglected and atoms in state $|S_{1/2}, m_j = 1/2\rangle$ will experience only one significant ac Stark shift, which leads to a non-vanishing potential. The resulting Stark shifts are depicted in figure 2.4(b). Analogous arguments apply to σ^--light, which yields the same critical frequency ω_L. Hence by choosing the laser frequency as $\omega = \omega_L$, the potentials

for the $m_j = \pm 1/2$ states are purely created by the $\sigma^{\pm}$-contributions of the laser field.

We should note that the above discussion slightly simplified the physics, since the hyperfine structure of the atoms in the $S_{1/2}$-manifold, shown in figure 2.4(c), has not been taken into account. However, by using Clebsch-Gordan coefficients one can easily calculate the respective optical potentials for the hyperfine states [18]. For example, the potential for $|F = 2, m_F = 2\rangle$ is given by $V_{2,2} = V_+(x)$, for $|F = 1, m_F = 1\rangle$ by $V_{1,1} = 3V_+(x)/4 + V_-(x)/4$ and for $|F = 1, m_F = -1\rangle$ by $V_{1,-1} = V_+(x)/4 + 3V_-(x)/4$. Since the contributions of the two polarisations are different for different atomic states it is still possible to shift the atoms state-dependently by changing the polarisation angle ϑ between the two laser beams.

The implementation of state-dependent optical lattices has been successfully demonstrated in experiments [45, 46], where the collisional phase of atoms in different internal states has been used to create entanglement [44]. We illustrate this with the following example. Let us assume two atoms in neighbouring lattice sites $j = 1, 2$, each of which can be in one of the two internal states $|\uparrow\rangle$ or $|\downarrow\rangle$. The lattice may be shifted in such a way that atoms in state $|\uparrow\rangle$ move to the right and atoms in state $|\downarrow\rangle$ to the left. By choosing an angle of $\vartheta = \pi/2$ the wave functions of the atoms overlap if the atom in lattice site 1 is in state $|\uparrow\rangle$ and the atom in site 2 is in state $|\downarrow\rangle$. In this case, due to the interaction between the atoms they will pick up an additional phase φ, which depends on the interaction time, strength, and details of the shifting process [44]. This phase does not occur for the three other cases, which means that after shifting the atoms back again their state evolves to

$$\begin{aligned} |\downarrow\downarrow\rangle &\to |\downarrow\downarrow\rangle \,, & |\downarrow\uparrow\rangle &\to |\downarrow\uparrow\rangle \,, \\ |\uparrow\uparrow\rangle &\to |\uparrow\uparrow\rangle \,, & |\uparrow\downarrow\rangle &\to \mathrm{e}^{\mathrm{i}\varphi} |\uparrow\downarrow\rangle \,. \end{aligned}$$

For $\varphi = \pi$ this gives up to local phases an entangling controlled-phase gate.

Analogous to the discussion above one can show that it is possible to create species-selective optical lattices [131]. The optical potential only affects one atomic species, whereas the other remains unaffected. This allows for the creation of a system that consists of a fermionic or bosonic gas of atoms in an optical lattice, which are submerged into a Bose-Einstein condensate. Such systems are investigated in chapters 4 and 5.

Chapter 3

Publication

Simulating high-temperature superconductivity model Hamiltonians with atoms in optical lattices

Alexander Klein and Dieter Jaksch

Clarendon Laboratory, University of Oxford, Parks Road, Oxford OX1 3PU, United Kingdom

Phys. Rev. A **73**, 053613 (2006)

We investigate the feasibility of simulating different model Hamiltonians used in high-temperature superconductivity. We briefly discuss the most common models and then focus on the simulation of the so-called *t-J-U* Hamiltonian using ultra-cold atoms in optical lattices. For this purpose, previous simulation schemes to realise the spin interaction term J are extended. We especially overcome the condition of a filling factor of exactly one, which otherwise would restrict the phase of the simulated system to a Mott-insulator. Using ultra-cold atoms in optical lattices allows simulation of the discussed models for a very wide range of parameters. The time needed to simulate the Hamiltonian is estimated and the accuracy of the simulation process is numerically investigated for small systems.

3.1 Introduction

Since its discovery, high-temperature superconductivity [132] has attracted much attention on the theoretical as well as on the experimental side. Nevertheless, the mechanisms which lead to this effect are not completely understood [133]. On the theoretical side one encounters the problem that the physics of a very complex many-body system has to be described and calculated. Because quantum effects play a crucial role, the calculation of these systems is a very hard task on a classical computer. Furthermore, it is not certain that the investigated theoretical models accurately describe the macroscopic features of superconducting materials used in experiments. Experimental efforts to test these models have suffered from difficulties in changing the system parameters for a given superconductor. In general, different parameter sets require different types of superconducting material. Due to all these obstacles it is worthwhile searching for a versatile system which can be used to accurately simulate high-temperature superconductor models.

As we will show in this chapter ultra-cold atoms in optical lattices are a very good candidate for simulating high-temperature superconductivity. During the past few years the field of cold atom physics has made tremendous progress and entered the regime of accurately controlled strongly correlated systems. Seminal experiments with bosonic atoms have, e.g., realised the Mott-insulator to superfluid transition and cold controlled collisions between atoms in optical lattices [22, 45, 46, 113]. They found excellent agreement with corresponding theoretical models [17, 44]. For clouds of fermionic atoms superfluidity has been demonstrated by creating vortices [134] and Fermi surfaces of atoms loaded into three-dimensional optical lattices have been measured [135]. Optical lattice systems are also very flexible; a large range of Hamiltonians can be realised and system parameters are easily varied over a wide range by changing external laser parameters [18]. For instance, it has also been proposed to implement effective magnetic fields [25–28, 136, 137], and even the implementation of non-Abelian gauge fields seems to be feasible [138, 139].

We will briefly discuss some of the model Hamiltonians which are used to describe high-temperature superconductive cuprates. We will then focus on the t-J-U Hamiltonian [55], which includes a spin-spin coupling term J additionally to hopping t and on-site interaction U. The simulation of this Hamiltonian can be used for obtaining a deeper understanding of the corresponding model, and also enlarges the parameter space by an additional, freely tunable interaction term J. In analogy to the cuprates we expect this model to show a very rich phase diagram for the atoms in the optical lattice including the appearance of (anti)ferromagnetic phases.

The simulation of the spin-spin interaction part in optical lattices has already been discussed in Refs. [23, 24, 140]. Atoms with two internal states simulate a spin chain and the spin-spin interaction is implemented by state-dependent shifting of the atoms causing controlled atomic collisions. These collisions induce state-dependent phase shifts of the atomic wave function mimicking the spin-spin interaction. However, all of the proposals [23, 24, 140] require a filling of very close to or exactly one atom per lattice site. For superconductors, this corresponds to a Mott-insulating state. In order to extend this method to the simulation of the t-J-U Hamiltonian, we will relax the condition of having exactly one atom in each lattice site. Additional shifts of the atoms will be necessary for simulating the spin interaction term J and we will also show that by choosing appropriate parameters it is possible to implement effectively attractive interaction terms $U < 0$.

The simulation of the time evolution of the whole t-J-U Hamiltonian is performed via a Trotter-Suzuki expansion [140–145] and we will consider the case of temperature $T = 0$ in our calculations. To be able to experimentally observe superconductivity effects using our simulation method the temperature of the optical lattice atoms will have to be lower than $k_{\mathrm{B}}T < 0.02t$ [146], where k_{B} is the Boltzmann constant. Such low temperatures are experimentally difficult to achieve. However, theoretical proposals for fault tolerant loading of fermionic atoms [147]

into the lowest motional band of an optical lattice and phonon assisted side band cooling within this motional band [148, 149] exist. These methods will be realisable with current and near future experimental techniques and enable achievement and control of temperatures sufficiently small for our purpose.

This chapter is organised as follows. In Sec. 3.2 we briefly discuss some of the model Hamiltonians used to describe high-temperature superconductivity in cuprates. In Sec. 3.3 we explain how one of these Hamiltonians, namely the t-J-U model, can be simulated using ultra-cold atoms in optical lattices. The simulation process is numerically tested in Sec. 3.4 and we conclude in Sec. 3.5.

3.2 Model Hamiltonians for high-T_c superconductors

In this section we briefly discuss some of the model Hamiltonians which are used to describe high-temperature superconductors [54, 119, 120]. The most basic microscopic description is given by the Hubbard model

$$\hat{H}_{tU} = -t \sum_{\langle i,j\rangle,\sigma} \hat{c}^\dagger_{i,\sigma}\hat{c}_{j,\sigma} + U \sum_j \hat{n}_{j,\uparrow}\hat{n}_{j,\downarrow}\,. \tag{3.1}$$

The operator $\hat{c}^\dagger_{j,\sigma}$ ($\hat{c}_{j,\sigma}$) creates (annihilates) an electron with spin $\sigma =\uparrow,\downarrow$ in lattice site j and obeys the standard fermionic anticommutation relations, the number operator is denoted by $\hat{n}_{j,\sigma} = \hat{c}^\dagger_{j,\sigma}\hat{c}_{j,\sigma}$. This Hamiltonian describes electrons in the lowest Bloch band tightly bound to the lattice sites formed by the atoms of the solid. The electrons can tunnel from one lattice site to the nearest-neighbour site (indicated by the brackets $\langle i,j\rangle$) with hopping energy t and the repulsive onsite Coulomb interaction is given by U. Due to the Pauli exclusion principle for electrons and the single Bloch band assumption in Hamiltonian Eq. (3.1), there can be a maximum of one electron of each spin state in a single lattice site. Hence no onsite interaction term for electrons in the same spin state is included in the Hamiltonian.

The Hamiltonian Eq. (3.1) describes the behaviour of the electron gas, which is assumed to be confined in two-dimensional (2D) layers. If the lattice sites are all occupied by a single electron the system behaves like a Mott-insulating antiferromagnet. By hole-doping of the cuprate the behaviour of the gas changes considerably and for a critical doping and temperatures below T_c the solid gets superconductive (see, e.g., [146, 150]). In a real superconductor many of these two-dimensional layers are stacked on top of each other. The influence of these layers can be included by a small inter-layer tunnelling strength [151].

Quantum cluster calculations give very strong evidence that the Hubbard Hamiltonian Eq. (3.1) is already a sufficient minimal model to describe the main prop-

erties of the phase diagrams of cuprates [152]. Nevertheless, these calculations suffer from finite size effects. The simulation of this Hamiltonian using ultra-cold fermionic atoms in an optical lattice is straightforward and can overcome this problem for sufficiently large lattices. It requires the loading of the atoms into the lattice and choosing the lattice parameters such that two-dimensional layers are created. Details on which parameter range can be simulated are discussed in Sec. 3.3.1.

However, the Hubbard Hamiltonian Eq. (3.1) does not describe all properties encountered in a superconductor [153]. Other effective model Hamiltonians have been discussed trying to incorporate such experimentally observed effects. For example, it has been suggested [154] to introduce a next-nearest neighbour hopping term

$$\hat{H}_{nn} = -t' \sum_{\langle\langle i,j\rangle\rangle,\sigma} \hat{c}^\dagger_{i,\sigma} \hat{c}_{j,\sigma} \,. \tag{3.2}$$

These terms can be realised in the simulation process by using very shallow optical lattices. In this case, however, the probability to excite atoms into higher Bloch bands increases and off-site interaction terms U_{os} are important. Also, it becomes more difficult to adjust all parameters in this Hamiltonian independently. Therefore, in this chapter, we do not discuss the realisation of this model Hamiltonian any further.

Another effective model is the so-called t-J-U Hamiltonian, which has recently been used in connection with gossamer superconductivity[1] [55, 155]. It is given by

$$\hat{H} = \hat{H}_{tU} + \hat{H}_J \,, \tag{3.3}$$

where

$$\hat{H}_J = J \sum_{\langle i,j\rangle} \hat{\mathbf{S}}_i \cdot \hat{\mathbf{S}}_j \tag{3.4}$$

is the spin interaction Hamiltonian of electrons in neighbouring lattice sites. The spin operator $\hat{\mathbf{S}}_j$ is defined by its components

$$\hat{\mathbf{S}}^w = \frac{1}{2} \sum_{\varsigma,\zeta=\uparrow,\downarrow} \hat{c}^\dagger_\varsigma \sigma^w \hat{c}_\zeta \,, \tag{3.5}$$

where σ^w are Pauli matrices, $w = x, y, z$. For very large interaction strengths U Hamiltonian Eq. (3.3) converges to the so-called t-J model, where double-occupancy of a single lattice site is excluded. This Hamiltonian has also very often been used to describe the behaviour of high-T_c cuprates. In the following sections we will investigate in detail how the t-J-U Hamiltonian can be simulated using atoms in optical lattices. Such simulations can help to understand and test features of the model, and also to investigate a larger parameter space which is

[1] The term "gossamer superconductor" was used by R. B. Laughlin for a superconducting state that is physically equivalent to a dilute gas of bosons and thus highly unstable [155].

likely to exhibit very interesting phase diagrams.

3.3 Simulation of the t-J-U model with atoms in optical lattices

In this section we show how Hamiltonian Eq. (3.3) can be simulated by using ultra-cold atoms in optical lattices. First we explain how to implement the t-U-Hamiltonian and the spin-interaction independently from each other. Then these Hamiltonians are combined to realise the full t-J-U Hamiltonian.

3.3.1 The hopping and interaction terms

The Hamiltonian $\hat{H}_{tU}$, Eq. (3.1), is simulated using a three-dimensional optical lattice where hopping along the z-direction is suppressed by high potential barriers [18]. The lattice is filled with ultra-cold fermionic atoms occupying the lowest motional Bloch band only and moving in planes parallel to the xy-plane. We restrict our considerations to one such 2D layer of the optical lattice. The two spin states of the electrons are represented by two long-living internal states of the atoms, which we denote by $\sigma = \uparrow, \downarrow$. The Hamiltonian, which describes the dynamics of fermionic atoms in the lattice, is given by $\hat{H}_{tU_s}$, cf. Eq. (3.1), with the hopping constant t and the interaction strength U_s. By an appropriate choice of the lattice constants the system parameters t and U_s can be tuned over a wide range [18] and using a Feshbach resonance it is possible to change the s-wave scattering length between the atoms, which gives additional control over the interaction strength U_s.

However, we are not completely free in our choice of the lattice depths. In order to observe the superconducting phase in high-T_c cuprates the temperature has to be lower than the critical temperature T_c, which is for high-temperature superconductors of the order of $0.02t$ [146]. For our system with atoms in an optical lattice we expect the same behaviour. We consider a lattice depth of $5E_\mathrm{R}$ with $E_\mathrm{R} = \hbar^2(2\pi)^2/2m\lambda^2$ the recoil energy, m the mass of the atoms and λ the wave length of the laser producing the lattice potential. In this case the hopping term t is of the order of $0.07E_\mathrm{R}$ and thus the superconducting phase will be observable for temperatures lower than approximately $0.0014E_\mathrm{R}/k_\mathrm{B}$. For the fermionic species ^{6}Li trapped in a lattice with $\lambda = 670$nm this corresponds to a temperature of 5nK. In recent experiments with ^{6}Li temperatures of about 30nK have been reported [134]. The required lower temperatures can be reached for example with phonon side band cooling [147–149].

As an aside we note that in the case of bosonic atoms we have to assume a very high interaction strength $U_{\uparrow\uparrow} = U_{\downarrow\downarrow}$ between two atoms in the same state to realise the above Hamiltonian $\hat{H}_{tU_s}$ and replace anticommutator relations with commutator relations. This interaction has to be much larger than the inter-species

interaction strength $U_{\uparrow\downarrow} = U_s$, the hopping constant t and the spin-spin interaction strength J. In this case all states with two or more identical atoms in the same lattice sites can be discarded. However, a direct mapping to a fermionic system using a Jordan-Wigner transformation is only possible in one spatial dimension [156]. There are proposals for similar mappings in higher dimensions which require the addition of Majorana fermions to the system [157, 158]. Although appealing from a theoretical point of view it is not clear how to realise such systems with atoms in optical lattices. Nevertheless, in the case of bosons the above conditions on the interaction strength lead to a rich phase diagram similar to models discussed in Ref. [24].

3.3.2 Implementation of the spin-spin interaction

In general, the van der Waals interaction between two atoms in neighbouring lattice sites is not sufficient to realise the required ratios of J, t, and U. Lowering the lattice barriers such that there is a significant nearest neighbour interaction also causes problems since in this case it is more likely that higher Bloch bands are occupied. Hence the spin interaction J has to be simulated indirectly. Methods for achieving this have already been detailed in Refs. [23, 24, 140]. These proposals require a filling factor of very close to or exactly one atom per lattice site, which corresponds to half-filling of the electron system and thus a Mott-insulating phase [150]. Therefore, these proposals cannot be used to simulate superconductivity.

In order to circumvent this problem we extend the scheme proposed in Ref. [23]. Let us first consider the one-dimensional spin-spin interaction in z-direction, i.e.,

$$\begin{aligned} \hat{H}_{zz} &= J_z \sum_{\langle i,j \rangle} \hat{S}_i^z \hat{S}_j^z \\ &= \frac{J_z}{4} \sum_{\langle i,j \rangle} \hat{n}_\uparrow^i \hat{n}_\uparrow^j + \hat{n}_\downarrow^i \hat{n}_\downarrow^j - \hat{n}_\uparrow^i \hat{n}_\downarrow^j - \hat{n}_\downarrow^i \hat{n}_\uparrow^j \,. \end{aligned} \tag{3.6}$$

This type of interaction between the atoms is realised by state selectively moving atoms. They are stored in very deep optical lattices such that any hopping is strongly suppressed, i.e., $t = 0$. The atoms in, e.g., state $|\uparrow\rangle$ are shifted and overlapped for a certain time with their neighbouring atoms to the left and to the right in state $|\downarrow\rangle$. The resulting atom-atom interaction leads to the desired phase shift as described in Ref. [44]. For illustration let us assume two lattice sites described by the Fock states $\left|n_\uparrow^1, n_\downarrow^1; n_\uparrow^2, n_\downarrow^2\right\rangle$, where n_σ^j is the number of atoms in state $|\sigma\rangle$ in the jth lattice site. After the above shifting procedure this state evolves to

$$\left|n_\uparrow^1, n_\downarrow^1; n_\uparrow^2, n_\downarrow^2\right\rangle \longrightarrow \exp(\mathrm{i}\chi(n_\downarrow^1 n_\uparrow^2 + n_\uparrow^1 n_\downarrow^2)) \left|n_\uparrow^1, n_\downarrow^1; n_\uparrow^2, n_\downarrow^2\right\rangle \,, \tag{3.7}$$

where χ is the phase acquired during the collision process. This is exactly the action of the last two summands $-\hat{n}_\uparrow^i \hat{n}_\downarrow^j - \hat{n}_\downarrow^i \hat{n}_\uparrow^j$ of Eq. (3.6).

However, this process is not yet sufficient to implement the spin interaction in z-direction. In order to achieve our goal the spin state of the atoms in every second lattice site has to be flipped, i.e., the operation $V_{\text{fl}} = \sigma_1^x \otimes \mathbf{1}_2 \otimes \sigma_3^x \otimes \mathbf{1}_4 \otimes ...$ has to be applied to the atoms. This operation requires addressing each second lattice site, which can be done by using an additional standing wave laser field. The resulting superlattice must have twice the wavelength of the original lattice and its intensity minima need to coincide with every second lattice site of the trapping potential.[2] Thus the energy levels of every second atom are AC-Stark shifted out of resonance such that a microwave or laser-field driving the transition $|\uparrow\rangle \leftrightarrow |\downarrow\rangle$ realises V_{fl}.

By repeating this shifting process after the spin flip operation V_{fl} and flipping the atoms back the state evolves according to

$$\left|n_\uparrow^1, n_\downarrow^1; n_\uparrow^2, n_\downarrow^2\right\rangle \longrightarrow \exp(-\mathrm{i}\chi(n_\downarrow^1 n_\downarrow^2 + n_\uparrow^1 n_\uparrow^2)) \left|n_\uparrow^1, n_\downarrow^1; n_\uparrow^2, n_\downarrow^2\right\rangle , \tag{3.8}$$

where the collision time has to be chosen such that the acquired phase is equal to $-\chi$. The whole process induces dynamics according to Hamiltonian Eq. (3.6), where $\chi = J_z\tau/4\hbar$ and τ is the time for which $\hat{H}_{zz}$ is applied (details on calculating the phases can be found in Appendix 3.A).

The creation of such spin-dependent phases has already been demonstrated experimentally. In Ref. [45] the authors used Rb atoms in an optical lattice with $V_0 = 34E_{\text{R}}$. Excitations of atoms into higher Bloch bands were avoided by using an appropriate time of $\tau_s = 40\mu$s to shift the atoms spin-dependently into the neighbouring lattice sites [46]. After holding the atoms in the shifted position for $\tau_h = 450\mu$s and shifting them back again, collisional phases of $\chi \approx 2\pi$ were achieved.

With being able to implement Hamiltonian Eq. (3.6) it is also possible to realise the Hamiltonians

$$\hat{H}_{xx} = J_x \sum_{\langle i,j\rangle} \hat{S}_i^x \hat{S}_j^x , \tag{3.9}$$

$$\hat{H}_{yy} = J_y \sum_{\langle i,j\rangle} \hat{S}_i^y \hat{S}_j^y . \tag{3.10}$$

We first observe that with suitable laser pulses it is possible to implement the following rotations on single atoms

$$V_y = \exp\left(i\frac{\pi}{4}\sigma^y\right) , \tag{3.11}$$

$$V_x = \exp\left(-i\frac{\pi}{4}\sigma^x\right) . \tag{3.12}$$

By simultaneously applying one of these rotations on all atoms, implementing

[2]The experimental realisation of such a configuration is planned. I. Bloch, private communication (2005).

Hamiltonian Eq. (3.6), and applying the Hermitian conjugate of the same rotation we get the time evolutions [23, 140, 159]

$$V_y^\dagger \exp\left(-\mathrm{i}\hat{H}_{zz}\frac{\tau}{\hbar}\right) V_y = \exp\left(-\mathrm{i}\hat{H}_{xx}\frac{\tau}{\hbar}\right) , \tag{3.13}$$

$$V_x^\dagger \exp\left(-\mathrm{i}\hat{H}_{zz}\frac{\tau}{\hbar}\right) V_x = \exp\left(-\mathrm{i}\hat{H}_{yy}\frac{\tau}{\hbar}\right) . \tag{3.14}$$

The interaction strengths J_x, J_y, and J_z can be tuned independently from each other by the choice of the collisional phase χ during the simulation of the respective Hamiltonian.

3.3.3 Combining the Hamiltonians

We simulate Hamiltonian Eq. (3.3) using the well known Trotter-Suzuki expansion [140–145] described in detail in Appendix 3.B. In this approach, the different parts of the Hamiltonian are simulated for a small time τ separately. For instance, in first order, the decomposition of the t-J-U Hamiltonian reads

$$\begin{aligned}\exp\left(\frac{-\mathrm{i}\hat{H}\,\tau}{\hbar}\right) = &\exp\left(\frac{-\mathrm{i}\hat{H}_{zz}\,\tau}{\hbar}\right) V_x^\dagger \exp\left(\frac{-\mathrm{i}\hat{H}_{zz}\,\tau}{\hbar}\right) V_x \\ &\times V_y^\dagger \exp\left(\frac{-\mathrm{i}\hat{H}_{zz}\,\tau}{\hbar}\right) V_y \exp\left(\frac{-\mathrm{i}\hat{H}_{tU_s}\,\tau}{\hbar}\right) + \mathcal{O}(\tau^2) .\end{aligned} \tag{3.15}$$

The last part $\exp\left(-\mathrm{i}\hat{H}_{tU_s}\,\tau/\hbar\right)$ of this time evolution is simulated by choosing a suitable lattice depth such that the required values of t and U_s are realised. After waiting a time[3] τ the lattice has to be ramped up avoiding any excitation into higher Bloch bands. Then the shifting and flipping processes V_{fl}, as described in the previous section, have to be applied in order to simulate the time evolution of $\hat{H}_{zz}$, $\hat{H}_{yy}$, and $\hat{H}_{xx}$. The latter two require the implementation of the operations V_x and V_y, cf. Eqs. (3.11) and (3.12). By repeating all of these simulation steps m times a time $m\tau$ is simulated with an error $\propto \tau^2 m$. Better accuracies can be achieved by using higher order approximations, see Appendix 3.B.

During the simulation of the spin-spin interaction term two atoms may occupy the same lattice site j. This gives rise to an additional term not considered so far. We illustrate this by considering shifts in x-direction during the simulation of the spin interaction. The atoms will acquire an additional phase (compare Appendix

[3] Alternatively, if the real values t_r and U_r implemented in the lattice are different from the desired values t and U, it is also possible to let the system evolve for a real time τ_r such that $\tau t = \tau_r t_r$ and $\tau U = \tau_r U_r$.

3.A)

$$\phi = K \int_{-\tau_0}^{\tau_0} \mathrm{d}\tau \, \exp\left(-\frac{[x_\uparrow^j(\tau) - x_\downarrow^j(\tau)]^2}{2x_0^2} \right) , \tag{3.16}$$

with K given in Eq. (3.24). This phase corresponds to an (additional) effective interaction term

$$\hat{H}_U^{\text{eff}} = U_{\text{eff}} \sum_j \hat{n}_{j,\uparrow} \hat{n}_{j,\downarrow} , \tag{3.17}$$

where the interaction constant is given by $U_{\text{eff}} = \hbar\phi/\tau$. Note that this effective interaction does not diverge for $\tau \to 0$ as in this case also ϕ goes to zero. This interaction provides an additional opportunity for tuning the simulated interaction constant U. The total interaction for small $U_{\text{eff}} \ll 2\pi\hbar/\tau$ is given by $U = U_s + 3dU_{\text{eff}}$ with d the number of spatial dimensions in which the spin-spin interaction is simulated. Here the factor of 3 in front of the dimension number d arises because the phase ϕ occurs in the simulations of $\hat{H}_{xx}$, $\hat{H}_{yy}$, and $\hat{H}_{zz}$, which are all simulated for the same time τ. By an appropriate choice of U_s and ϕ it is possible to simulate effective interactions that are attractive. For this purpose, the phase ϕ has to be chosen in such a way that it can be written as $\phi = 2\pi + U'_{\text{eff}}\tau/\hbar$ with a small negative U'_{eff} and $2\pi \gg |U'_{\text{eff}}|\tau/\hbar$. The total simulated interaction is then given by $U = U_s + 3dU'_{\text{eff}}$. For not too large U_s this leads to a negative U.[4]

The total time for which the system can be simulated is restricted by the life- and decoherence-time of the ultra-cold atoms in the optical lattice. This is typically on the order of one second [22]. Hence we have to estimate the time which is needed for simulating one time step of Hamiltonian Eq. (3.3). During the shifting process heating of the atoms has to be avoided. Since the lattice is required to be very deep during the atoms are shifted hopping is strongly suppressed. This leads to a flat Bloch band and thus no excitation can take place within the band during the shift. Any heating thus means that atoms are excited into higher Bloch bands. In order to avoid such excitations we require for each shift of atoms in, e.g., state $|\uparrow\rangle$ into the neighbouring lattice site a time larger than the inverse of the lattice site trapping frequency $\omega_t = \sqrt{V_0/E_{\text{R}}}\,\hbar(2\pi)^2/m\lambda^2$, as already demonstrated experimentally in Refs. [45, 46]. Furthermore, the atoms have to be held in the shifted position for a certain time in order to achieve the desired phase. This phase is either χ or $2\pi - \chi$. Thus the average time for one shifting and holding process is given by

$$\tau_{sh} > 2\pi \left(\frac{4}{\omega_t} + \frac{1}{K} \right) . \tag{3.18}$$

The minimal shifting times for varying lattice depths are shown in Fig. 3.1 and are of the order of a few hundred microseconds for Rb or a few tens of microseconds

[4] This method can also be used to simulate negative interaction strengths in Hubbard models in optical lattices. Properly timed periodic raising and lowering of the potential barriers to switch off the hopping terms leads to effective negative onsite interaction strengths.

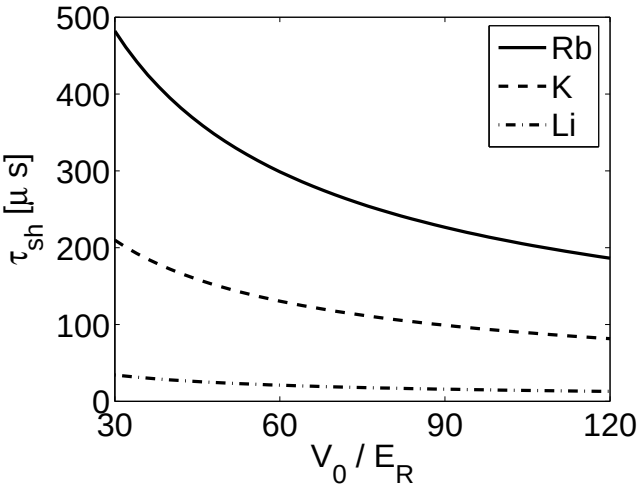

Figure 3.1. Lower bounds for the calculated shifting and holding times τ_{sh} (cf. Eq. (3.18)) for lattices with ^{87}Rb atoms ($\lambda = 826$nm, $a_s = 5.1$nm), ^{40}K atoms ($\lambda = 826$nm, $a_s = 5.5$nm) and ^{6}Li atoms ($\lambda = 670$nm, $a_s = 2.4$nm). The values given in brackets are typical values used for the calculation of τ_{sh}.

for Li. To simulate the time evolution of $\hat{H}_{zz}$ these shifts have to be repeated $2d$ times.

The constraints for the ramping time between the application of the t-U-Hamiltonian and the spin-spin interaction are twofold: The ramping has to be adiabatic on a time scale given by $1/\omega_t$ to avoid excitations into higher Bloch bands and it has to be rapid compared to $\hbar\pi/2t$. This ensures that the system does not evolve for too long with a hopping term t that is different from the desired one or even follows the change in t adiabatically in contrast to the sudden change required by the Trotter-Suzuki expansion. The first constraint has been experimentally tested for Rb atoms [113] and was found to be fulfilled for ramping times longer than 50μs in accordance with theoretical calculations [160]. For typical lattice parameters the hopping time is given by $\hbar\pi/2t = 1$ms and is thus more than one order of magnitude larger than the minimal ramping time required to avoid excitations into higher Bloch bands. Therefore, both constraints can be fulfilled at the same time. Furthermore, the ramping process conserves quasi-momentum, and excitations that do not change the quasi-momentum involve at least two hopping processes. Because the lattice is ramped on a time scale short compared to $\hbar\pi/2t$, excitations within the lowest Bloch band are also strongly suppressed. Together with the time needed to simulate the t-U-Hamiltonian it is thus feasible to simulate several hundreds of Trotter steps m within the lifetime of the atoms in the lattice.

We finally remark that this procedure for simulating the t-J-U Hamiltonian is compatible with the additional simulation of a magnetic field. Various methods for

creating effective magnetic fields at the same time as the hopping and interaction terms in $\hat{H}_{tU}$ were recently proposed [25–28, 136, 137]. Thus it is possible to extend our setup for studying the t-J-U Hamiltonian in external magnetic fields.

3.3.4 Measuring the properties of the atom gas

The properties of the time-evolved state can be probed by measurements of first- and second-order correlation functions as proposed in Ref. [161]. The atoms are released from their trapping potential and imaged after a certain time of flight. Depending on the phase of the atomic gas these images reveal interference patterns; second-order correlation functions give additional information on the phase and the underlying structure of the lattice. Such measurements are similar to the Hanbury Brown and Twiss experiment [162] and have already been performed for bosonic atoms in the Mott-insulating phase [22, 163]. They agree very well with the theoretical predictions [124]. With these techniques it will be possible to check the phase diagrams of the simulated systems and compare them to calculated or measured phase diagrams for different high-temperature superconductors (see, e.g., [146, 150, 164]).

3.4 Numerical simulations

As already mentioned in the introduction the simulation of Hamiltonian Eq. (3.3) is a very hard computational task. Even for a few lattice sites an exact simulation of the system is no longer feasible and one has to use approximations such as mean-field theories or Quantum Monte Carlo calculations. Since we want to compare the results of the simulation of Hamiltonian Eq. (3.3) with exact results we have thus restricted ourselves to the one-dimensional case with a few lattice sites only.

The anti-fidelity of the simulated state compared to a state which is time-evolved using the full Hamiltonian Eq. (3.3) is calculated as follows. Let $\hat{\mathcal{U}}_0(\tau) = \exp(-\mathrm{i}\hat{H}\tau/\hbar)$ be the full time evolution operator, $\hat{\mathcal{U}}(\tau)$ the simulated time evolution, $|\psi\rangle_{\mathrm{in}}$ an input state and $|\psi\rangle = \hat{\mathcal{U}}(\tau)\,|\psi\rangle_{\mathrm{in}}$, $|\psi_0\rangle = \hat{\mathcal{U}}_0(\tau)\,|\psi\rangle_{\mathrm{in}}$. Due to the Cauchy-Schwarz inequality and the properties of the matrix norm we get

$$\begin{aligned} ||\hat{\mathcal{U}}(\tau) - \hat{\mathcal{U}}_0(\tau)||^2 &\geq |(\langle\psi| - \langle\psi_0|)(|\psi\rangle - |\psi_0\rangle)| \\ &= |2 - 2\mathfrak{Re}(\langle\psi|\psi_0\rangle)|\,. \end{aligned} \tag{3.19}$$

Since $|\,\langle\psi|\psi_0\rangle\,| \leq 1$ the rhs of Eq. (3.19) is always positive even without the modulus and we can rearrange

$$|\,\langle\psi|\psi_0\rangle\,| \geq 1 - \frac{1}{2}||\hat{\mathcal{U}}(\tau) - \hat{\mathcal{U}}_0(\tau)||^2\,. \tag{3.20}$$

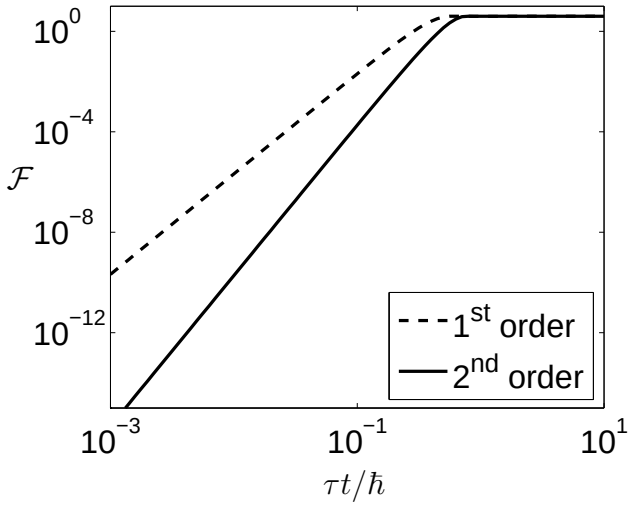

Figure 3.2. Simulation of Hamiltonian Eq. (3.3) using first- and second-order Trotter expansions, cf. Eqs. (3.25) and (3.26). Upper bounds for the anti-fidelity $\mathcal{F}$ are shown. The number of lattice sites is $M = 5$, the parameters for the simulation are $J = 0.3t$, $U_s = 5t$, $U'_{\text{eff}} = -2t$, $m = 1$ leading to $U = -t$.

For $||\hat{\mathcal{U}}(\tau) - \hat{\mathcal{U}}_0(\tau)||^2 \leq 2$ this yields an upper bound for the anti-fidelity $\mathcal{F}$

$$\mathcal{F} = 1 - |\langle\psi|\psi_0\rangle|^2 \leq ||\hat{\mathcal{U}}(\tau) - \hat{\mathcal{U}}_0(\tau)||^2 , \tag{3.21}$$

which can be easily calculated from the time evolution operators.

We have calculated this anti-fidelity $\mathcal{F}$ for several cases. First, we investigate a parameter set which gives a negative (attractive) interaction strength U and compare this to the exact time evolution according to Eq. (3.3). Upper bounds for the corresponding anti-fidelity $\mathcal{F}$ are shown in Fig. 3.2. It has been assumed that no errors such as unprecise creation of the phase shifts χ or excitation of higher Bloch bands occur during the shifting process. For small times the slopes of the curves for the first and second order approximations agree very well with the predictions from first and second order expansions, cf. Eqs. (3.25) and (3.26). Note that the slopes shown are increased by a factor of two since we take the square of the matrix norm in order to calculate the anti-fidelity $\mathcal{F}$. Figure 3.2 shows that for small times the simulation of the time evolution of Hamiltonian Eq. (3.3) agrees very well with the full time evolution but the desired simulation times of order $100\hbar/t$ can only be reliably achieved by repeating this simulation process.

The dependence of the upper bounds of the anti-fidelity $\mathcal{F}$ on the number m of Trotter steps for a fixed time $\tau = 100\hbar/t$ is shown in Fig. 3.3 for values corresponding to typical parameters in high-temperature superconductivity [165].

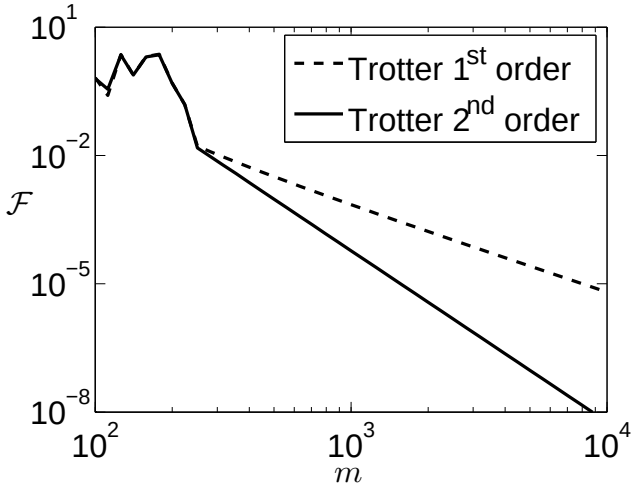

Figure 3.3. Upper bounds for the anti-fidelity $\mathcal{F}$ for first- and second-order Trotter expansions, cf. Eq. (3.28). The simulated time is fixed to $\tau = 100\hbar/t$, the number of lattice sites is $M = 5$. We have used $J = 0.3t$, $U_s = 10t$, and $\phi = 0$.

As expected the fidelity gets better for an increasing number of steps. In second order approximation for $m = 500$ steps the anti-fidelity is already smaller than 10^{-3}. For the same accuracy using the first-order approximation $m = 900$ Trotter steps have to be used. This means in first-order approximation the lattice has to be ramped up and down 900 times and $\hat{H}_{zz}$ has to be simulated 2700 times with 1800 applications of $V_{x,y}$. In second-order each single step is more complicated, but by choosing the simulation process in a judicious way only 500 rampings of the lattice are required. By optimising the process (cf. Appendix 3.B) only 2500 simulations of $\hat{H}_{zz}$ are required with 1500 applications of $V_{x,y}$.

To get an impression on how the anti-fidelity $\mathcal{F}$ scales with the number of lattice sites M we calculated it for different values of lattice sites M in a 1D lattice. The results are shown in Fig. 3.4 for a simulated time of $\tau = 0.01\hbar/t$. They indicate that the anti-fidelity $\mathcal{F}$ does not increase quickly with the number of lattice sites. Therefore, it should be possible to experimentally simulate systems of realistic size.

Since the time evolution of the full Hamiltonian Eq. (3.3) is only simulated approximately in our scheme, the state vector of the atoms after the time evolution will also only approximate the real state. However, we expect errors due to this effect to be small, since the necessary measurements to distinguish the phases involve only first- and second-order correlation functions. The influence of small imperfections of the simulated Hamiltonian on these functions will in general be smaller than the influence on the state vector estimated by the upper bounds of the anti-fidelity $\mathcal{F}$. Thus, the deviations of the simulated phase diagrams is expected

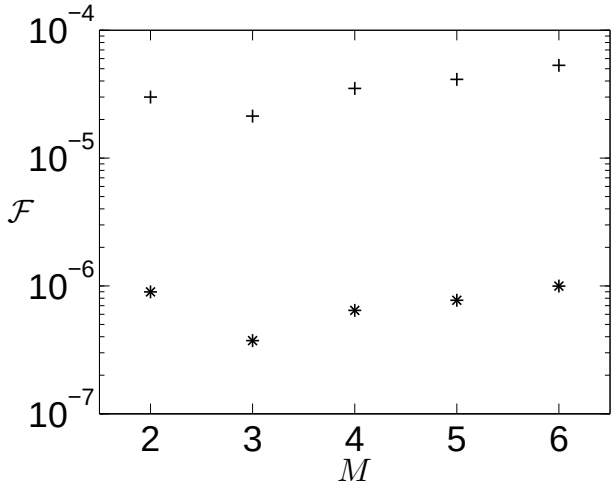

Figure 3.4. Upper bounds for the anti-fidelity $\mathcal{F}$ vs number of lattice sites M for first- (pluses) and second-order (stars) Trotter expansion. The simulated time was $\tau = 0.01\hbar/t$ and we have chosen $J = 0.3t$, $U_s = 10t$ and $\phi = 0$.

to be smaller than implied by the anti-fidelities.

3.5 Conclusion

In the present chapter we have shown that it is feasible to simulate different model Hamiltonians which are used to describe high-temperature superconductive cuprates. The simulation of the most minimal model, the Hubbard model Eq. (3.1), can already be expected to deepen our understanding of the phase diagrams encountered in the cuprates. Since this model does not describe all experimentally measured effects and to enlarge the accessible parameter space, which can be investigated using atoms in optical lattices, we have especially discussed how to simulate the t-J-U Hamiltonian Eq. (3.3), which requires the inclusion of an additional spin-spin interaction term J.

In order to make the simulation possible we have extended earlier proposals to create an effective spin interaction between atoms to the case where the lattice is not fully occupied. We found that near future technology will allow to simulate Hamiltonian Eq. (3.3) for times which are longer than the typical time scales associated with the dynamics of the t-J-U Hamiltonian. Hence the properties of the Hamiltonian can be made visible using our simulation method. We also showed that by an appropriate choice of the lattice parameters and shifting times it is possible to create attractive on-site interactions U. Also, our method is compatible with the simulation of magnetic fields in the lattice.

Furthermore, we simulated the simulation process numerically for small systems and compared the results with exact calculations of the time evolution. For these simulations the results show very good agreement between the simulated and the real time evolution. Anti-fidelities $\mathcal{F} < 10^{-3}$ can be achieved. Because of these results and of the experimental progress we are confident that the proposed method will help to deepen our knowledge and understanding of the *t-J-U* Hamiltonian model.

3.A Calculation of the collisional phases

The exact phase shift due to the shift and interaction process can be calculated analytically [44]. If we assume deep lattice potentials $V_{x,y,z}$, we can approximate the wave functions of the atoms located in one lattice site by Gaussians. For illustration we assume an atom of state $|\uparrow\rangle$ in lattice site j and one of state $|\downarrow\rangle$ in lattice site $j+1$. The shift shall occur in x-direction. Let $x_\uparrow^j(\tau)$, $x_\downarrow^{j+1}(\tau)$ denote the time-dependent x-coordinates of the atoms. Because of the collision process the state of the two atoms will evolve to

$$|1,0;0,1\rangle \to \mathrm{e}^{-\mathrm{i}\chi}\,|1,0;0,1\rangle \tag{3.22}$$

with the collisional phase given by

$$\chi = K\int_{-\tau_0}^{\tau_0}\mathrm{d}\tau\,\exp\left(-\frac{[x_\uparrow^j(\tau)-x_\downarrow^{j+1}(\tau)]^2}{2x_0^2}\right). \tag{3.23}$$

Here we have defined

$$K = \frac{4\pi a_s\hbar}{m}\frac{(\sqrt{2\pi})^3}{\lambda^3}\left(\frac{V_0}{E_\mathrm{R}}\right)^{\frac{3}{4}}, \tag{3.24}$$

where a_s is the s-wave scattering length between the two atoms in states $|\uparrow\rangle$ and $|\downarrow\rangle$, V_0 is the depth of the lattice, $x_0 = \sqrt[4]{E_\mathrm{R}/V_0}\lambda/2\pi$ and $E_\mathrm{R} = \hbar^2(2\pi)^2/m\lambda^2$ is the recoil energy, m the mass of the atoms and λ the wavelength of the lasers creating the optical lattice. The time τ_0 is chosen such that the entire shift process is contained in the time interval from $-\tau_0$ to τ_0. For typical experimental parameters [45] of $V_0 = 34E_\mathrm{R}$ and ^{87}Rb atoms with $a_s = 5.1$nm the prefactor in front of the integral has a value of roughly $K = 19$rad/ms such that after a collisional time of a few hundred microseconds phase shifts of the order of 2π can be achieved. For Li atoms the prefactor has a value of the order of $K = 230$rad/ms and hence only roughly a tenth of the time is necessary to achieve similar phase shifts. The exact phase shifts depend on the details of the shifting process itself, i.e., on the exact form of the functions $x_\sigma^j(\tau)$.

3.B The Trotter-Suzuki expansion

For an arbitrary Hamiltonian $\hat{H}_{\text{arb}} = \sum_{j=1}^{f} \hat{H}_j$ the Trotter-Suzuki expansion [140–145] is found by defining

$$Q_1(x) = \prod_{j=1}^{f} \exp(x\hat{H}_j)\,, \tag{3.25}$$

$$Q_2(x) = \mathrm{e}^{\hat{H}_1 x/2} ... \mathrm{e}^{\hat{H}_{f-1} x/2} \mathrm{e}^{\hat{H}_f x} \mathrm{e}^{\hat{H}_{f-1} x/2} ... \mathrm{e}^{\hat{H}_1 x/2}\,, \tag{3.26}$$

where $x = -i\tau/\hbar$ and τ is the simulation time. The operators $Q_1(x)$ and $Q_2(x)$ are approximations to the time evolution operator of $\hat{H}_{\text{arb}}$ with

$$\exp(\hat{H}_{\text{arb}} x) = Q_1(x) + \mathcal{O}(|x|^2) = Q_2(x) + \mathcal{O}(|x|^3)\,. \tag{3.27}$$

Higher order approximations to the time evolution of $\hat{H}_{\text{arb}}$ exist, but they either require the simulation of negative time, which is difficult for the hopping Hamiltonian $\hat{H}_{tU}$, or they include terms which make the simulation unstable [142]. Therefore, we simulate longer times using a generalised version of the Trotter formula [145] with m simulation steps, reading

$$\exp(\hat{H}_{\text{arb}} x) = \left[Q_j\left(\frac{x}{m}\right)\right]^m + \mathcal{O}\left(\frac{|x|^{j+1}}{m^j}\right)\,. \tag{3.28}$$

When using the second-order approximation Eq. (3.26) in this formula the experimental procedure can be optimised by combining subsequent simulations of $\hat{H}_1$ since $\exp(\hat{H}_1 x/2)\exp(\hat{H}_1 x/2) = \exp(\hat{H}_1 x)$.

Chapter 4

Polaron physics in optical lattices

We investigate the effects of a nearly uniform Bose-Einstein condensate (BEC) on the properties of immersed trapped impurity atoms. Using a weak-coupling expansion in the BEC-impurity interaction strength, we derive a model describing polarons, i.e., impurities dressed by a coherent state of Bogoliubov phonons, and apply it to ultracold bosonic atoms in an optical lattice. We show that stable polaron clusters are formed via a phonon-mediated off-site attraction.[1]

The lack of lattice phonons is a distinguishing feature of optical lattices, i.e., conservative optical potentials formed by counterpropagating laser beams, and contributes to the excellent coherence properties of atoms trapped in them [19]. However, some of the most interesting phenomena in condensed matter physics involve phonons, and thus it is also desirable to introduce them in a controlled way into optical lattices. Recently, it has been shown that immersing an optical lattice into a Bose-Einstein condensate (BEC) leads to interband phonons, which can be used to load and cool atoms to extremely low temperatures [148]. Here, we instead concentrate on the dynamics within the lowest Bloch band of an immersed lattice, and show how intraband phonons lead to the formation of polarons [53, 166]. Polarons aggregate on *adjacent* lattice sites into stable clusters, which are not prone to loss from inelastic collisions. Since this phenomenon is relevant to the physics of conduction in solids, introducing phonons into an optical lattice system may lead to a better understanding of high-temperature superconductivity [53, 167] and charge transport in organic molecules [168]. Additionally, this setup may allow the investigation of the dynamics of classically indistinguishable particles [169].

Experimental progress in trapping and cooling atoms has recently made a large class of interacting many-body quantum systems [20] accessible. For instance, the formation of repulsively bound atom pairs on a single site has been demonstrated

[1] This chapter is based on the publication "Polaron physics in optical lattices", Phys. Rev. A **76**, 011605(R) (2007) by Martin Bruderer, Alexander Klein, Stephen R. Clark and Dieter Jaksch. The chapter emphasises my own contributions to this publication and does not include all of the published results.

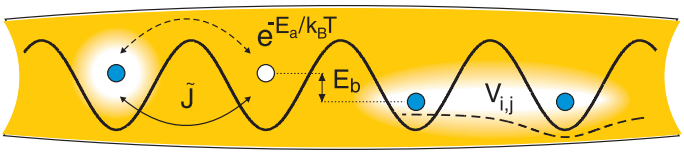

Figure 4.1. A quantum degenerate gas confined to an optical lattice is immersed in a much larger BEC. For increasing BEC temperature T, a crossover from coherent to diffusive hopping, characterised by $\tilde{J}$ and E_a, respectively, can be observed, as shown in [178]. The phonon-induced interaction potential $V_{i,j}$ leads to the formation of off-site polaron clusters, separated by a gap E_b from the continuum of unbound states.

[170], and strongly correlated mixtures of degenerate quantum gases have been realised [33, 34]. In such Bose-Fermi mixtures, rich phase diagrams can be expected, including charge and spin density wave phases [171, 172], pairing of fermions with bosons [173], and a supersolid phase [174]. Here we instead consider one atomic species, denoted as the impurities, confined to a trapping potential, for example an optical lattice, immersed in a nearly uniform BEC, as shown in Fig. 4.1. Based on a weak-coupling expansion in the BEC-impurity interaction strength, we derive a model in terms of polarons, which are composed of impurity atoms dressed by a coherent state of Bogoliubov phonons [53, 166]. The model also includes attractive impurity-impurity interactions mediated by the phonons [175, 176]. An essential requirement for our model is that neither interactions with impurities nor the trapping potential confining the impurities impairs the ability of the surrounding gas to sustain phononlike excitations. The first condition limits the number of impurity atoms [33, 34], whereas the latter requirement can be met by using a species-specific optical lattice potential [131]. Moreover, unlike in the case of self-localised impurities [177], we assume that the one-particle states of the impurities are not modified by the BEC, which can be achieved by sufficiently tight impurity trapping.

Model.—The Hamiltonian of the system is composed of three parts, $\hat{H} = \hat{H}_\chi + \hat{H}_\mathrm{B} + \hat{H}_\mathrm{I}$, where $\hat{H}_\chi$ governs the dynamics of the impurity atoms, which can be either bosonic of fermionic. The BEC Hamiltonian $\hat{H}_\mathrm{B}$ and the density-density interaction Hamiltonian $\hat{H}_\mathrm{I}$ are

$$\hat{H}_\mathrm{B} = \int \mathrm{d}\mathbf{r}\, \hat{\phi}^\dagger(\mathbf{r}) \left[-\frac{\hbar^2\nabla^2}{2m_b} + V_\mathrm{ext}(\mathbf{r}) + \frac{g}{2}\hat{\phi}^\dagger(\mathbf{r})\hat{\phi}(\mathbf{r}) \right] \hat{\phi}(\mathbf{r}) \,,$$

$$\hat{H}_\mathrm{I} = \kappa \int \mathrm{d}\mathbf{r}\, \hat{\chi}^\dagger(\mathbf{r})\hat{\chi}(\mathbf{r})\hat{\phi}^\dagger(\mathbf{r})\hat{\phi}(\mathbf{r}) \,,$$

where $\hat{\chi}(\mathbf{r})$ is the impurity field operator and $\hat{\phi}(\mathbf{r})$ is the condensate atom field operator satisfying the commutation relations $[\hat{\phi}(\mathbf{r}), \hat{\phi}^\dagger(\mathbf{r}')] = \delta(\mathbf{r}-\mathbf{r}')$ and $[\hat{\phi}(\mathbf{r}), \hat{\phi}(\mathbf{r}')] =$

0. The coupling constants $g > 0$ and κ account for the boson-boson and impurity-boson interaction respectively, m_b is the mass of a condensate atom and $V_{\text{ext}}(\mathbf{r})$ a weak external trapping potential. Without yet specifying $\hat{H}_\chi$ we expand $\hat{\chi}(\mathbf{r}) = \sum_\nu \eta_\nu(\mathbf{r})\hat{a}_\nu$, where $\eta_\nu(\mathbf{r})$ are a set of orthogonal mode functions of the impurities and $\hat{a}_\nu$ ($\hat{a}_\nu^\dagger$) the corresponding annihilation (creation) operators, labelled by the quantum numbers ν.

A common approach to find the elementary excitations of the BEC in the presence of impurities is to solve the Gross-Pitaevskii equation (GPE) [104] for the full system, i.e., for $\kappa \neq 0$, and to subsequently quantise small oscillations around the classical ground state. To obtain a quantum description of the impurity dynamics, we instead solve the GPE without taking $\hat{H}_I$ into account, and express the BEC deformations around the impurities as coherent states of Bogoliubov phonons. Specifically, we write $\hat{\phi}(\mathbf{r}) = \phi_0(\mathbf{r}) + \delta\hat{\phi}(\mathbf{r})$, with $\phi_0(\mathbf{r}) = \phi_0^*(\mathbf{r})$ the solution of the GPE for $\kappa = 0$. Provided that the impurity-boson coupling is sufficiently weak, i.e., $|\kappa|/gn_0(\mathbf{r})\xi^D(\mathbf{r}) \ll 1$, with $\xi(\mathbf{r}) = \hbar/\sqrt{m_b g n_0(\mathbf{r})}$ the healing length, $n_0(\mathbf{r}) = \phi_0^2(\mathbf{r})$ and D the number of spatial dimensions, we expect that the deviation of $\hat{\phi}(\mathbf{r})$ from $\phi_0(\mathbf{r})$ is of order κ, i.e., $\langle \delta\hat{\phi}(\mathbf{r})\rangle \propto \kappa$, where $\langle\,\cdot\,\rangle$ stands for the expectation value. We insert $\phi_0(\mathbf{r}) + \delta\hat{\phi}(\mathbf{r})$ into the Hamiltonian $\hat{H}_{\text{B}} + \hat{H}_{\text{I}}$, keep terms up to second order in κ, and obtain the with respect to $\delta\hat{\phi}$ linear term $\kappa \int \mathrm{d}\mathbf{r}\, \hat{\chi}^\dagger(\mathbf{r})\hat{\chi}(\mathbf{r})\phi_0(\mathbf{r})[\delta\hat{\phi}^\dagger(\mathbf{r}) + \delta\hat{\phi}(\mathbf{r})]$, in addition to the standard constant and quadratic terms in $\delta\hat{\phi}(\mathbf{r})$ and $\delta\hat{\phi}^\dagger(\mathbf{r})$, since $\phi_0(\mathbf{r})$ is no longer the ground state of the system.

In order to diagonalise the quadratic terms in $\delta\hat{\phi}(\mathbf{r})$ and $\delta\hat{\phi}^\dagger(\mathbf{r})$, we use the expansion $\delta\hat{\phi}(\mathbf{r}) = \sum_\mu [u_\mu(\mathbf{r})\hat{b}_\mu - v_\mu^*(\mathbf{r})\hat{b}_\mu^\dagger]$, where $u_\mu(\mathbf{r})$ and $v_\mu^*(\mathbf{r})$ are the solutions of the Bogoliubov–de Gennes equations [104] for $\kappa = 0$, and $\hat{b}_\mu$ ($\hat{b}_\mu^\dagger$) are the bosonic Bogoliubov annihilation (creation) operators, labelled by the quantum numbers μ. We assume that the mode functions $\eta_\nu(\mathbf{r})$ are localised on a length scale much smaller than is set by $V_{\text{ext}}(\mathbf{r})$, and that $\int \mathrm{d}\mathbf{r}\, |\eta_\nu(\mathbf{r})|^2 |\eta_\tau(\mathbf{r})|^2 \approx 0$ for $\nu \neq \tau$, i.e., the probability densities $|\eta_\nu(\mathbf{r})|^2$ for different mode functions deviate appreciably from zero only within mutually exclusive spatial regions. In this case $\int \mathrm{d}\mathbf{r}\, \phi_0(\mathbf{r})[u_\mu(\mathbf{r}) - v_\mu(\mathbf{r})]\eta_\nu(\mathbf{r})\eta_\tau^*(\mathbf{r}) \approx 0$ and $\int \mathrm{d}\mathbf{r}\, n_0(\mathbf{r})\eta_\nu(\mathbf{r})\eta_\tau^*(\mathbf{r}) \approx 0$ hold for $\nu \neq \tau$, and hence the nondiagonal impurity-phonon coupling is negligible. The total Hamiltonian can thus be rewritten in the form of a Hubbard-Holstein model [179] $\hat{H} = \hat{H}_\chi + \sum_{\nu,\mu} \hbar\omega_\mu (M_{\nu,\mu}\hat{b}_\mu + M_{\nu,\mu}^*\hat{b}_\mu^\dagger)\hat{n}_\nu + \sum_\nu \bar{E}_\nu\, \hat{n}_\nu + \sum_\mu \hbar\omega_\mu \hat{b}_\mu^\dagger \hat{b}_\mu$, with $\hbar\omega_\mu$ the energies of the Bogoliubov excitations, the number operator $\hat{n}_\nu = \hat{a}_\nu^\dagger \hat{a}_\nu$, the dimensionless matrix elements $M_{\nu,\mu} = (\kappa/\hbar\omega_\mu) \int \mathrm{d}\mathbf{r} \phi_0(\mathbf{r})\, [u_\mu(\mathbf{r}) - v_\mu(\mathbf{r})]\, |\eta_\nu(\mathbf{r})|^2$ and the mean field shift $\bar{E}_\nu = \kappa \int \mathrm{d}\mathbf{r}\, n_0(\mathbf{r}) |\eta_\nu(\mathbf{r})|^2$. We obtain an effective Hamiltonian $\hat{H}_{\text{eff}}$ including corrections to $\phi_0(x)$ of order κ by applying the unitary Lang-Firsov transformation[2] [53, 166] $\hat{H}_{\text{eff}} = \hat{U}\hat{H}\hat{U}^\dagger$, with $\hat{U} = \exp\left[\sum_{\nu,\mu}(M_{\nu,\mu}^*\hat{b}_\mu^\dagger - M_{\nu,\mu}\hat{b}_\mu)\hat{n}_\nu\right]$,

[2]Martin Bruderer had the idea of applying the Lang-Firsov transformation at this point. An alternative way to derive the mediated interaction potential using an exact solution for fixed

which yields

$$\begin{aligned}\hat{H}_{\rm eff} &= \hat{U}\hat{H}_\chi\hat{U}^\dagger + \sum_\nu(\bar{E}_\nu - E_\nu)\hat{n}_\nu - \sum_\nu E_\nu\hat{n}_\nu(\hat{n}_\nu - 1) \\ &\quad -\frac{1}{2}\sum_{\nu\neq\tau} V_{\nu,\tau}\hat{n}_\nu\hat{n}_\tau + \sum_\mu \hbar\omega_\mu\hat{b}_\mu^\dagger\hat{b}_\mu\,. \end{aligned} \tag{4.1}$$

The transformed impurity Hamiltonian $\hat{U}\hat{H}_\chi\hat{U}^\dagger$ is obtained using $\hat{U}\hat{a}_\nu^\dagger\hat{U}^\dagger = \hat{a}_\nu^\dagger\hat{X}_\nu^\dagger$, where $\hat{X}_\nu^\dagger = \exp\left[\sum_\mu(M_{\nu,\mu}^*\hat{b}_\mu^\dagger - M_{\nu,\mu}\hat{b}_\mu)\right]$ is a Glauber displacement operator that creates a coherent phonon cloud, i.e., a BEC deformation, around the impurity. In the limit where the BEC adjusts instantaneously to the impurity configuration, polarons created by $\hat{a}_\nu^\dagger\hat{X}_\nu^\dagger$ are the appropriate quasiparticles, and $\hat{H}_{\rm eff}$ describes a nonretarded interaction with the potential $V_{\nu,\tau} = \sum_\mu \hbar\omega_\mu\left(M_{\nu,\mu}M_{\tau,\mu}^* + M_{\nu,\mu}^*M_{\tau,\mu}\right)$. The polaronic level shift $E_\nu = \sum_\mu \hbar\omega_\mu|M_{\nu,\mu}|^2$ is equal to the characteristic potential energy of an impurity in the deformed BEC.

We now turn to the specific case of bosons loaded into an optical lattice immersed in a homogeneous BEC [148]. In the tight-binding approximation, the impurity dynamics is well described by the Bose-Hubbard model $\hat{H}_\chi = -J\sum_{\langle i,j\rangle}\hat{a}_i^\dagger\hat{a}_j + \frac{1}{2}U\sum_j\hat{n}_j(\hat{n}_j-1) + \mu\sum_j\hat{n}_j$, where μ describes the energy offset, U the on-site interaction strength, and J the hopping matrix element between adjacent sites [17, 18, 20]. The modes of the lattice atoms are Wannier functions $\eta_j(\mathbf{r})$ of the lowest Bloch band localised at site j, and $\langle i,j\rangle$ denotes the sum over nearest neighbours. Noting that $[\hat{U},\hat{n}_j] = 0$, we find

$$\hat{U}\hat{H}_\chi\hat{U}^\dagger = -J\sum_{\langle i,j\rangle}(\hat{X}_i\hat{a}_i)^\dagger\hat{X}_j\hat{a}_j + \frac{U}{2}\sum_j\hat{n}_j(\hat{n}_j-1) + \mu\sum_j\hat{n}_j\,. \tag{4.2}$$

The corresponding matrix elements are given by $M_{j,\mathbf{q}} = \kappa\sqrt{n_0\varepsilon_\mathbf{q}/(\hbar\omega_\mathbf{q})^3}\,f_j(\mathbf{q})$. Here, $f_j(\mathbf{q}) = \Omega^{-1/2}\int{\rm d}\mathbf{r}|\eta_j(\mathbf{r})|^2\exp({\rm i}\mathbf{q}\cdot\mathbf{r})$, with Ω the quantisation volume, $\mathbf{q}$ isthe phonon momentum, $\varepsilon_\mathbf{q} = (\hbar\mathbf{q})^2/2m_b$ the free particle energy, and $\hbar\omega_\mathbf{q} = \sqrt{\varepsilon_\mathbf{q}(\varepsilon_\mathbf{q}+2gn_0)}$ the Bogoliubov dispersion relation. We note that, for $|\mathbf{q}|\ll 1/\xi$, we have $M_{j,\mathbf{q}}\propto f_j(\mathbf{q})/\sqrt{|\mathbf{q}|}$, whereas for $|\mathbf{q}|\gg 1/\xi$, one obtains $M_{j,\mathbf{q}}\propto f_j(\mathbf{q})/\mathbf{q}^2$.

The Hamiltonian $\hat{H}_{\rm eff}$ describes the dynamics of *hopping* polarons according to an extended Hubbard model [20], provided that $c\gg aJ/\hbar$, with $c\sim\sqrt{gn_0/m_b}$ the phonon velocity and a the lattice spacing. We gain qualitative insight into the dependence of $V_{i,j}$ and the constant polaronic level shift $E_\nu\equiv E_p$ on the system parameters by considering a one-dimensional quasi-BEC in the thermodynamic limit. We assume a sufficiently deep lattice to approximate the Wannier functions by Gaussians of width $\sigma\ll\xi$, and find $V_{i,j} = (\kappa^2/\xi g)\,{\rm e}^{-2|i-j|a/\xi}$ and $E_p = \kappa^2/2\xi g$. We note that the interaction between impurities is always attractive. More importantly, for realistic experimental parameters, $\xi\sim a$, and hence the off-site terms $V_{j,j+1}\propto$

impurities or a quantum master equation for non-fixed ones is presented in the next chapter.

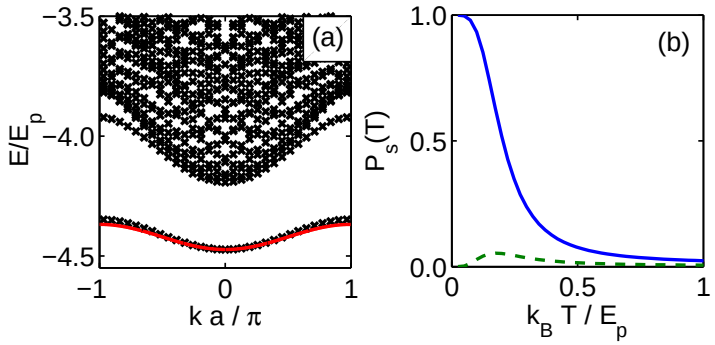

Figure 4.2. (a) Energy spectrum of three polarons in a 1D optical lattice. The solid line shows the lowest energy band $E_3(k)$ characterising off-site three-polaron clusters. The lattice (wavelength $\lambda = 790$nm, $M = 31$ sites, periodic boundary conditions) contains ^{133}Cs atoms with $\tilde{J} = 7.5\times10^{-3}E_R$, $U = 50E_p$, and $\kappa/E_R\lambda = 1.05 \times 10^{-1}$. The BEC consists of ^{87}Rb atoms with $n_0 = 5 \times 10^6\,\mathrm{m}^{-1}$ and $g/E_R\lambda = 4.5 \times 10^{-2}$. (b) Probability of finding a three-polaron cluster (solid line) or a two-polaron cluster (dashed line) versus temperature. The parameters are $g/E_R\lambda = 6.5 \times 10^{-2}$, $\kappa/E_R\lambda = 1.32 \times 10^{-1}$, $U = 2.2E_p$, $M = 27$, and the rest as for (a).

$\mathrm{e}^{-2a/\xi}$ are non-negligible. This interaction potential is a direct consequence of the local deformation of the BEC around each impurity, as shown in Fig. 4.1. For a set of static impurities at positions $x_j = aj$, the overall deformation of the BEC density to order κ is given by $n(x) = n_0 + \sum_j \langle \hat{X}_j \hat{b}^\dagger_{\mathbf{q}} \hat{b}_{\mathbf{q}} \hat{X}^\dagger_j \rangle = n_0 - (\kappa/g\xi) \sum_j \mathrm{e}^{-2|x-x_j|/\xi}$.

In the following, we consider coherent dynamics at small BEC temperatures $k_B T \ll E_p$, where incoherent phonon scattering is highly suppressed. Provided that $\zeta = J/E_p \ll 1$, we can apply the so-called strong-coupling theory [167], and treat the hopping term in Eq. (4.2) as a perturbation. Including terms of first order in ζ, we obtain the impurity Hamiltonian

$$\hat{H}^{(1)} = -\tilde{J} \sum_{\langle i,j \rangle} \hat{a}^\dagger_i \hat{a}_j + \frac{1}{2}\tilde{U} \sum_j \hat{n}_j(\hat{n}_j - 1) + \tilde{\mu} \sum_j \hat{n}_j - \frac{1}{2} \sum_{i \neq j} V_{i,j}\, \hat{n}_i \hat{n}_j \,, \qquad (4.3)$$

with $\tilde{\mu} = \mu + \kappa n_0 - E_p$, $\tilde{U} = U - 2E_p$, and $\tilde{J} = J \langle\!\langle \hat{X}^\dagger_i \hat{X}_j \rangle\!\rangle$. Here $\langle\!\langle \cdot \rangle\!\rangle$ denotes the average over the thermal phonon distribution and i, j are nearest neighbours. We find $\langle\!\langle \hat{X}^\dagger_i \hat{X}_j \rangle\!\rangle = \exp\big\{ -\sum_{\mathbf{q}\neq 0} |M_{0,\mathbf{q}}|^2 [1 - \cos(\mathbf{q}\cdot\mathbf{a})](2N_{\mathbf{q}} + 1) \big\}$, with $\mathbf{a}$ the position vector connecting two nearest neighbour sites and $N_{\mathbf{q}} = (\mathrm{e}^{\hbar\omega_{\mathbf{q}}/k_B T} - 1)^{-1}$. Thus, the hopping bandwidth decreases exponentially with increasing coupling constant κ and temperature T.

Polaron Clusters.—We now discuss the formation of polaron clusters for $k_B T \lesssim E_p$, based on Hamiltonian $\hat{H}^{(1)}$ in Eq. (4.3), and assume that the bosonic impurities

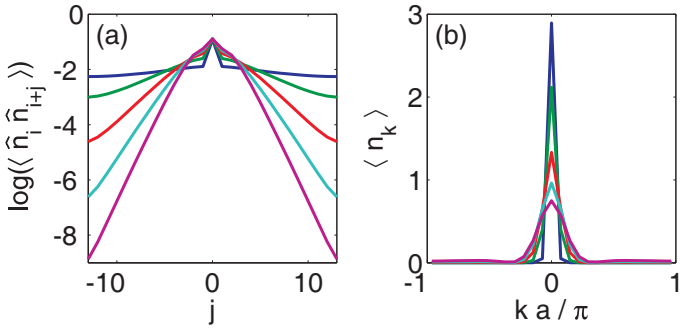

Figure 4.3. (a) Density-density correlation in a system of three polarons indicating the formation of off-site three-polaron clusters. (b) Corresponding momentum distribution $\langle n_k \rangle$. $\kappa/E_R\lambda = \{\,4.0,\, 6.1,\, 8.1,\, 10.1,\, 12.1\,\} \times 10^{-2}$ where a higher value corresponds to a more localised correlation in (a) and a more spread distribution in (b). The other parameters are $g/E_R\lambda = 6.5 \times 10^{-2}$, $M = 27$, $U = 3E_p$, and the rest as in Fig. 4.2(a).

are in thermal equilibrium with the BEC. At these temperatures $V_{i,j}$, and $\tilde{J}$ are well approximated by their $T = 0$ values. We consider the limit $\tilde{U} \gg V_{j,j+1}$, $\tilde{U} \gg \tilde{J}$, and adiabatically eliminate configurations with multiply occupied sites. Keeping only nearest neighbour interactions, we obtain approximate expressions for the binding energy $E_b(s) \approx (s-1)V_{j,j+1}$ of a cluster of s polarons located in adjacent sites and the lowest energy band $E_k(s) \approx -E_b(s) - 2\tilde{J}^s(V_{j,j+1})^{1-s}\cos(ka)$ [180], with k the quasimomentum. This band approximation is in good agreement with the results from exact diagonalisation of $\hat{H}^{(1)}$ using the full interaction potential $V_{i,j}$, as shown for three polarons in Fig. 4.2(a).

This model predicts a decreasing average cluster size with increasing temperature. For a small system with $N = 3$ polarons, we calculate the probability of finding a three-polaron cluster $P_3 = \sum_\nu \langle n_\nu \rangle$, where the sum is taken over all states with energies $\varepsilon_\nu < E_g(2) + E_g(1)$, $E_g(N)$ is the ground state energy of an N-polaron cluster, and the occupation probabilities are given by the Boltzmann law $\langle n_\nu \rangle \propto \exp(-\varepsilon_\nu/k_BT)$. Analogously, we determine the probability P_2 of finding a two-polaron cluster or bipolaron. The results are shown in Fig. 4.2(b). The probability of having a three-polaron cluster goes down with increasing temperature and for $T = E_p/k_B \approx 18$nK is essentially zero for the parameters chosen. For this three-polaron cluster, three-particle loss is negligible due to the on-site repulsion U. Decreasing the value of U gives a significantly increased P_2 compared to the values shown in Fig. 4.2(b).

The clustering of polarons leads to their mutual exponential localisation. This is illustrated by the density-density correlations $\langle \hat{n}_i \hat{n}_{i+j} \rangle$ for the three-polaron cluster in Fig. 4.3(a). With increasing attractive interaction $V_{i,j}$, the mutual localisation

gets stronger, leading to an increased broadening of the momentum distribution, as shown in Fig. 4.3(b). This allows polaron clusters to be identified in time of flight experiments. We note that the transition from a superfluid to a Mott insulator also leads to broadening of the momentum distribution as, e.g., observed in [33, 34]. However, using Bragg spectroscopy [170] would allow the unambiguous distinction of boson clustering from this transition.

Conclusion.—We have demonstrated that the dynamics of bosonic impurities immersed in a BEC is accurately described in terms of polarons. The phonons induce off-site interactions, which lead to the formation of stable clusters that are not affected by loss due to inelastic collisions. Using the techniques introduced in this chapter, qualitatively similar phenomena can also be shown to occur for fermionic impurities. In either case these effects can be controlled by external parameters and lie within the reach of current experimental techniques.

Chapter 5

Publication

Dynamics, dephasing and clustering of impurity atoms in Bose-Einstein condensates[1]

Alexander Klein[a,b], Martin Bruderer[a], Stephen R. Clark[a,c], and Dieter Jaksch[a,b]

[a] *Clarendon Laboratory, University of Oxford, Parks Road, Oxford OX1 3PU, United Kingdom*
[b] *Keble College, Parks Road, Oxford OX1 3PG, United Kingdom*
[c] *Trinity College, Broad Street, Oxford OX1 3BH, United Kingdom*

New J. Phys. **9**, 411 (2007)

We investigate the influence of a Bose-Einstein condensate (BEC) on the properties of immersed impurity atoms, which are trapped in an optical lattice. Assuming a weak coupling of the impurity atoms to the BEC, we derive a quantum master equation for the lattice system. In the special case of fixed impurities with two internal states the atoms represent a quantum register and the quantum master equation reproduces the exact evolution of the qubits. We characterise the qubit dephasing which is caused by the interspecies coupling and show that the effect of sub- and superdecoherence is observable for realistic experimental parameters. Furthermore, the BEC phonons mediate an attractive interaction between the impurities, which has an important impact on their spatial distribution. If the lattice atoms are allowed to move, there occurs a sharp transition with the impurities aggregating in a macroscopic cluster at experimentally achievable temperatures. We also investigate the impact of the BEC on the transport properties of the impurity atoms and show that a crossover from coherent to diffusive behaviour occurs with increasing interaction strength.

5.1 Introduction

Ultracold atoms in optical lattices have attracted considerable interest during the last few years. Theoretical investigations showed that ultracold atoms in optical lattices can be used for mimicking a wide range of models encountered in condensed

[1] Apart from the results shown in figure 5.8, the work presented in this chapter is my contribution, the co-authors were discussion partners.

matter physics [20]. These models include the Hubbard Hamiltonian [17, 18], spin-spin interactions [23, 24], high-temperature superconductivity [181, 182], effective magnetic fields [25–28, 136, 137], even with non-abelian gauge potentials [138, 139], and the fractional quantum Hall effect [26, 183], to name but a few. Experimental efforts have led to an unprecedented control over the properties of optical lattice systems [19], including such milestones as the Mott insulator to superfluid transition [22, 113], investigations of Bose-Fermi [33, 34] as well as Bose-Bose mixtures [184], vortex pinning [185], the creation of repulsively bound atom pairs [170], and cold controlled collisions between atoms in optical lattices [45, 46]. Especially for the latter experiments the absence of lattice phonons and thus the suppression of decoherence mechanisms was crucial. However, when mimicking the behaviour of electrons in crystals this lack of phonons might lead to an oversimplification of the underlying model and it is desirable to introduce phonons in a controlled manner into the optical lattice system.

One way of achieving this goal is to immerse the optical lattice system into a Bose-Einstein condensate (BEC). Experiments where both atom species are trapped by the optical lattice are common and decoherence effects in such systems have already been observed [33, 34]. Furthermore, these Bose-Fermi mixtures promise rich phase diagrams including charge and spin density wave phases [171, 172], pairing of fermions with bosons [173] and a supersolid phase [174]. We, however, focus on the case where only one species is trapped by the optical lattice. This can be achieved by a suitable choice of the laser wavelengths and atomic species such that the BEC is not affected by the optical lattice [131]. The lattice atoms interact with the condensate via density-density interaction, which can be described by Bogoliubov phonons coupling to the impurities. Earlier studies on such systems have shown that this coupling can be exploited to cool the lattice atoms to extremely low temperatures [148, 149], which are otherwise very difficult to achieve. In Ref. [178], the present authors have derived a model in which lattice atoms dressed by a coherent state of Bogoliubov phonons constitute polarons [166]. The model exhibits an attractive interaction potential between the lattice atoms [175, 176] and allows a generalised master equation to be deduced which shows that the system exhibits a crossover from coherent to diffusive dynamics.

Instead, in this chapter we concentrate on describing the lattice atoms by a quantum master equation (QME), which is derived in Sec. 5.3. In contrast to the generalised master equation, which only describes the density distribution of the atoms, the QME also allows the investigation of the off-diagonal density matrix elements. Furthermore, both equations operate in complementary parameter regimes, which widens the scope of physics that can be investigated. We show in Sec. 5.4 that for the case of fixed impurities the system can be solved exactly and after tracing out the BEC degrees of freedom the QME reproduces this exact solution. Due to the coupling to the phonons the lattice atoms experience dephasing, which can be used to demonstrate the effects of sub- and superdecoherence [186] and to

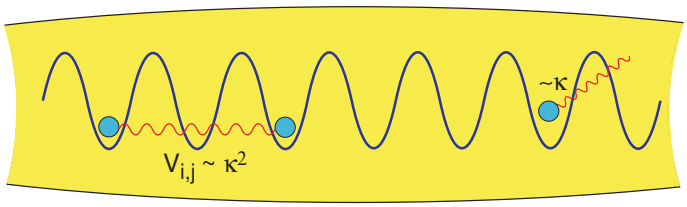

Figure 5.1. An ultracold quantum gas trapped in an optical lattice is immersed in a much larger BEC. The impurities interact with the BEC via the coupling constant κ and can excite Bogoliubov phonons (right). These lead to dephasing effects. By exchanging phonons an off-site interaction $V_{i,j}$ is mediated between the lattice atoms (left).

probe spatial properties of the BEC analogous to Ref. [187]. We also investigate the severe effect this decoherence has if the atoms in the lattice are used as a quantum register. In Sec. 5.5 we show that the attractive interaction mediated between the lattice atoms leads to the formation of atom clusters, which should be observable for typical experimental parameter regimes. This effect is reminiscent of the clustering of ad-atoms on crystal surfaces [188]. The influence of the phonon coupling on the transport properties of the lattice atoms is investigated in Sec. 5.6. We show that the crossover from coherent to diffusive transport, which was observed in Ref. [178], can also be described by the QME. In contrast to the treatment in Ref. [178], the QME in addition gives access to the off-diagonal elements of the density operator. We also show the limitations of the QME by applying it to a tilted lattice system and comparing the results to a near-exact numerical solution for the time evolution.

5.2 Model

The system under consideration is composed of a BEC and an ultracold gas of impurity atoms trapped in an optical lattice giving a setup like that shown in Fig. 5.1. The impurities can be either bosonic or fermionic atoms. For most of the results derived in this chapter the statistics of the lattice atoms is unimportant, but for concreteness we will assume bosonic impurities in the following. The dynamics of the whole system is governed by the Hamiltonian $\hat{H} = \hat{H}_\mathrm{L} + \hat{H}_\mathrm{B} + \hat{H}_\mathrm{I}$, where

$$\hat{H}_\mathrm{B} = \int \mathrm{d}\mathbf{r}\, \hat{\phi}^\dagger(\mathbf{r}) \left[-\frac{\hbar^2 \nabla^2}{2m_b} + V_\mathrm{ext}(\mathbf{r}) + \frac{g}{2} \hat{\phi}^\dagger(\mathbf{r}) \hat{\phi}(\mathbf{r}) \right] \hat{\phi}(\mathbf{r}) \tag{5.1}$$

describes the BEC, with $\hat{\phi}^\dagger$ the condensate field operator, m_b the mass of the BEC atoms, $V_\mathrm{ext}(\mathbf{r})$ an external potential confining the BEC, and $g > 0$ the coupling constant between the BEC atoms. Here, we have assumed that the optical lattice

potential does not affect the BEC atoms, which can be achieved by choosing the laser wavelengths and atom species accordingly [131]. The atoms in the optical lattice, which are distinguishable from the atoms in the BEC, are described by the Hamiltonian $\hat{H}_{\mathrm{L}}$, whereas the interaction between the two sub-systems is given by

$$\hat{H}_{\mathrm{I}} = \kappa \int \mathrm{d}\mathbf{r}\, \hat{\chi}^{\dagger}(\mathbf{r})\hat{\chi}(\mathbf{r})\hat{\phi}^{\dagger}(\mathbf{r})\hat{\phi}(\mathbf{r})\,. \tag{5.2}$$

Here, $\hat{\chi}^{\dagger}$ is the field operator of the lattice atoms, and κ is the density-density coupling constant between the BEC and the impurities. It was shown in Ref. [178] that in the tight-binding limit and under the condition $|\kappa|/gn_0\xi^D \ll 1$ (where D is the dimensionality of the system, n_0 the density of the BEC in the trap centre, and $\xi = \hbar/\sqrt{m_b g n_0}$ the healing length) the total Hamiltonian reduces to a Hubbard-Holstein model, given by

$$\hat{H}_{\mathrm{L}} = -J\sum_{\langle i,j\rangle} \hat{a}_j^{\dagger}\hat{a}_i + \frac{U}{2}\sum_i \hat{n}_i(\hat{n}_i - 1) + \mu\sum_i \hat{n}_i\,, \tag{5.3}$$

$$\hat{H}_{\mathrm{I}} = {\sum_{\nu}}' \sum_j \hbar\omega_\nu \left[M_{j,\nu}\hat{b}_\nu + M^*_{j,\nu}\hat{b}^{\dagger}_\nu\right]\hat{n}_j\,, \tag{5.4}$$

$$\hat{H}_{\mathrm{B}} = {\sum_{\nu}}' \hbar\omega_\nu \hat{b}^{\dagger}_\nu\hat{b}_\nu\,. \tag{5.5}$$

Here, the prime at the sum indicates that zero energy modes have been excluded, $\hat{b}^{\dagger}_\nu$ creates a Bogoliubov phonon in mode ν with energy $\hbar\omega_\nu$, $\hat{a}^{\dagger}_j$ creates a lattice atom in site j, $\hat{n}_j = \hat{a}^{\dagger}_j\hat{a}_j$ is the number operator on site j, J describes the hopping of the impurities, U is their on-site interaction, and the coupling between the phonons and the lattice atoms is given by

$$F_{j,\nu} = \hbar\omega_\nu M_{j,\nu} = \kappa\int \mathrm{d}\mathbf{r}\,\phi_0(\mathbf{r})\left[u_\nu(\mathbf{r}) - v_\nu(\mathbf{r})\right]|\eta_j(\mathbf{r})|^2\,. \tag{5.6}$$

In this equation, η_j is a Wannier function describing an atom in lattice site j, ϕ_0 is the solution of the Gross-Pitaevskii equation and u_ν and v_ν solve the Bogoliubov-de Gennes equations, see also Ref. [104].

For the case of a homogenous condensate, which we consider in the remainder of the chapter, the condensate wave function is given by $\phi_0 = \sqrt{n_0}$ and the solutions of the Bogoliubov-de Gennes equations yield $u_{\mathbf{q}}(\mathbf{r}) - v_{\mathbf{q}}(\mathbf{r}) = \sqrt{\varepsilon_{\mathbf{q}}/\hbar\omega_{\mathbf{q}}}\exp(\mathrm{i}\mathbf{k}\cdot\mathbf{r})/\sqrt{\Omega}$, see also Eq. (2.26). Here, $\mathbf{q}$ is the phonon quasi-momentum, Ω the quantisation volume, $\varepsilon_{\mathbf{q}} = (\hbar\mathbf{q})^2/2m_b$ the free particle energy, and $\hbar\omega_{\mathbf{q}} = \sqrt{\varepsilon_{\mathbf{q}}(\varepsilon_{\mathbf{q}} + 2gn_0)}$ the Bogoliubov dispersion relation. This gives

$$F_{j,\mathbf{q}} = \kappa\sqrt{\frac{n_0\varepsilon_{\mathbf{q}}}{\hbar\omega_{\mathbf{q}}}}\, f_j(\mathbf{q})\,, \tag{5.7}$$

with $f_j(\mathbf{q}) = \Omega^{-1/2} \int \mathrm{d}\mathbf{r} |\eta_j(\mathbf{r})|^2 \exp(\mathrm{i}\mathbf{q}\cdot\mathbf{r})$. The latter integral can in general not be solved analytically. However, for sufficiently deep lattices [91], the Wannier functions can be approximated by Gaussians, yielding

$$f_j(\mathbf{q}) = \frac{\mathrm{e}^{\mathrm{i}\mathbf{q}\cdot\mathbf{r}_j}}{\sqrt{\Omega}} \exp\left(-\frac{1}{4}\sum_{l=1}^{D} q_l^2 x_0^2\right), \tag{5.8}$$

with $x_0 = \sqrt{\hbar/m_b\omega_\mathrm{t}}$, where ω_t is the trapping frequency of a harmonic trap approximating the lattice potential at a given lattice site.

An experimental realisation of this setup is achievable with present techniques as follows. The creation of Rb condensates with 10^6 atoms has been demonstrated leading to the desired BEC densities of about $10^{20}/\mathrm{m}^3$ in three dimensions, see for instance [189]. By choosing a sufficiently flat trapping potential of a few Hz the BEC can be assumed to be homogenous to a good approximation in the centre of the trap, extending over a few micrometers. Furthermore, in references [33, 34] a mixture of Rb and K atoms has been created and trapped in a three-dimensional optical lattice, where several tens of thousands of lattice sites have been occupied. The filling for the K atoms ranged between 0 and 1 atoms per lattice site, whereas the filling of the Rb atoms could exceed 5 atoms per site in the centre of the trap. Although in these experiments both atom species were trapped by the optical lattice, techniques to trap only one of the two species, for example K, have been studied extensively in reference [131]. Applying these techniques leaves the Rb atoms virtually unaffected and enables the creation of a nearly homogenous BEC.

5.3 The quantum master equation

In order to investigate the behaviour of the impurity atoms we derive a Quantum Master Equation (QME) for the lattice system by tracing out the surrounding BEC. The details are given in appendix 5.A. Here we note that the main condition of deriving the QME is that the sound velocity of the condensate, $c \sim \sqrt{gn_0/m_b}$, is larger than the typical hopping speed of the atoms, i.e., $c \gg Ja/\hbar$, where $a = \lambda/2$ is the distance between two lattice sites. With this assumption we get

$$\begin{aligned}\mathrm{i}\hbar\partial_t\hat{\varrho}_L(t) = &\left[\hat{H}_g(t)\,,\ \hat{\varrho}_L(t)\right] \\ &- \frac{\mathrm{i}}{\hbar}\sum_{\mathbf{q}}{}'\sum_{l,l'}\frac{\sin(\omega_\mathbf{q}t)}{\omega_\mathbf{q}}\left(\hat{n}_l\hat{n}_{l'}\hat{\varrho}_L(t) + \hat{\varrho}_L(t)\hat{n}_l\hat{n}_{l'} - 2\hat{n}_{l'}\hat{\varrho}_L(t)\hat{n}_l\right) \\ &\quad\times\left(F_{\mathbf{q},l}F^*_{\mathbf{q},l'} + N_\mathbf{q}(T)(F_{\mathbf{q},l}F^*_{\mathbf{q},l'} + F^*_{\mathbf{q},l}F_{\mathbf{q},l'})\right).\end{aligned} \tag{5.9}$$

Here, $N_\mathbf{q}(T) = 1/(\exp(\hbar\omega_\mathbf{q}/k_\mathrm{B}T) - 1)$ is the number of thermal phonons at temperature T, and $\hat{\varrho}_\mathrm{L}(t) = \mathrm{Tr}_\mathrm{B}\hat{\varrho}(t)$, where Tr_B denotes the trace over the condensate.

Furthermore, the Hamiltonian

$$\hat{H}_g(t) = \hat{H}_L - \sum_{\mathbf{q}}{}' \sum_{l,l'} \frac{1-\cos(\omega_{\mathbf{q}} t)}{2\hbar\omega_{\mathbf{q}}} (F_{\mathbf{q},l} F^*_{\mathbf{q},l'} + F^*_{\mathbf{q},l} F_{\mathbf{q},l'}) \hat{n}_l(t) \hat{n}_{l'}(t) \tag{5.10}$$

describes the coherent evolution of the lattice atoms, most notably an off-site interaction that is mediated by the phonons of the BEC. The interaction term includes a transient behaviour described by the cosine functions, which accounts for suddenly turning on the interaction between lattice atoms and BEC. The sum over all these cosine functions vanishes in the limit $t \to \infty$.

The Born approximation used in deriving the QME is valid if the perturbation caused by the BEC is small compared to the typical energy scales given by the lattice system. If only the hopping term is important for the lattice atoms, this energy scale is determined by J. The energy scale of the perturbation is given by the so-called polaron energy $E_p = \sum'_{\mathbf{q}} (F_{\mathbf{q},l} F^*_{\mathbf{q},l} + F^*_{\mathbf{q},l} F_{\mathbf{q},l})/2\hbar\omega_{\mathbf{q}} \sim \kappa^2/g\xi^D$, which leads to the condition $J \gg E_p$, known as the weak coupling regime. This parameter regime is complementary to the one considered in Ref. [178] (see also chapter 4). There, the opposite limit was investigated, namely the strong coupling regime, where the polaron energy is larger than the hopping of the atoms. As we will show in the following section, the condition $J \gg E_p$ is not required for the case of $J = 0$, where an analytical solution of the dynamics of the whole system can be derived. After tracing out the BEC degrees of freedom this solution agrees with the one given by the QME.

5.4 Fixed impurities and the Quantum Register

For very deep optical lattices the hopping constant J is essentially zero and the impurities cannot leave their site. If there is a maximum of one atom in each lattice site, the setup can be used as a quantum register [190]. The lattice atoms represent qubits on which single qubit rotations can be implemented via external laser pulses. For the manipulation of the atoms single site addressability is necessary, which may be achieved by using infrared lattices [41], by leaving empty sites between the atoms [39, 40], by exploiting the properties of marker atoms [36], or by additional external fields [37, 38]. An entangling two-qubit gate can be implemented by using the interaction which is mediated by the condensate [176]. For this it is necessary to turn the interaction on and off, which can be done by using different internal states of the lattice atoms, some of which couple to the BEC, and others that do not couple. However, due to the coupling to the BEC the qubits also experience dephasing, which will be investigated in this section.

5.4.1 Analytical solution of the time evolution

We first calculate the time evolution of the atoms subject to the BEC coupling. For easier notation we focus on the case where the lattice atoms have only one internal state and we assume that there is a maximum of one atom per lattice site. In the regime were our model introduced in section 5.2 is valid, i.e. $|\kappa|/gn_0\xi^D \ll 1$, and for $J = 0$, the Hamiltonian of the whole system simplifies to $\hat{H}_0 = \hat{H}_\mathrm{B} + \hat{H}_\mathrm{I}$, where $\hat{H}_\mathrm{I}$ is given in Eq. (5.4) and $\hat{H}_\mathrm{B}$ in Eq. (5.5). The time evolution $\hat{U}(t) = \exp(-\mathrm{i}\hat{H}_0 t/\hbar)$ of this Hamiltonian is solved analytically. We first note that $\hat{U}(t) = \prod'_{\mathbf{q}} \hat{U}_{\mathbf{q}}(t)$ with

$$\hat{U}_{\mathbf{q}}(t) = \exp\left[-\mathrm{i}\left(\hbar\omega_{\mathbf{q}}\hat{b}^\dagger_{\mathbf{q}}\hat{b}_{\mathbf{q}} + \sum_l \hat{n}_l(F_{l,\mathbf{q}}\hat{b}_{\mathbf{q}} + F^*_{l,\mathbf{q}}\hat{b}^\dagger_{\mathbf{q}})\right)\frac{t}{\hbar}\right]. \tag{5.11}$$

This operator can be decomposed using the methods described in Ref. [191], yielding

$$\begin{aligned}\hat{U}_{\mathbf{q}}(t) = \exp\left[-\mathrm{i}\omega_{\mathbf{q}}\hat{b}^\dagger_{\mathbf{q}}\hat{b}_{\mathbf{q}}t\right]\exp\left[\sum_l \hat{n}_l(\tilde{F}_{l,\mathbf{q}}\hat{b}_{\mathbf{q}} - \tilde{F}^*_{l,\mathbf{q}}\hat{b}^\dagger_{\mathbf{q}})\right] \\ \times \exp\left[\frac{\mathrm{i}(\omega_{\mathbf{q}}t - \sin(\omega_{\mathbf{q}}t))}{2\hbar^2\omega^2_{\mathbf{q}}}\sum_{l,l'}\hat{n}_l\hat{n}_{l'}(F_{l,\mathbf{q}}F^*_{l',\mathbf{q}} + F^*_{l,\mathbf{q}}F_{l',\mathbf{q}})\right].\end{aligned} \tag{5.12}$$

Here, we have defined $\tilde{F}_{l,\mathbf{q}} = F_{l,\mathbf{q}}\left[-\mathrm{i}\sin(\omega_{\mathbf{q}}t) - (1-\cos(\omega_{\mathbf{q}}t))\right]/\hbar\omega_{\mathbf{q}}$. The last term in Eq. (5.12) describes the off-site interaction between two atoms confined in lattice sites l and l', which is mediated by a phonon with quasi-momentum $\mathbf{q}$. The total interaction potential is derived by adding all phonon contributions together. For $t \to \infty$, the oscillations caused by the sine function cancel each other and the off-site interaction potential is given by[2]

$$V_{l,l'} = \sum_{\mathbf{q}}{}' \frac{F_{l,\mathbf{q}}F^*_{l',\mathbf{q}} + F^*_{l,\mathbf{q}}F_{l',\mathbf{q}}}{2\hbar\omega_{\mathbf{q}}}. \tag{5.13}$$

This interaction potential was already found earlier [176, 178], however, the exact solution in addition reveals the transient behaviour after suddenly turning on the interaction, which is described by the sine functions.

The coupling to the BEC leads to dephasing of the lattice atoms as gets apparent after tracing out the condensate degrees of freedom. There are in essence two different types of dephasing. One can be observed when a lattice atom is driven into a superposition of two different states that couple differently to the condensate. This situation has been discussed in reference [187]. The other type

[2]For later convenience, we define this $V_{l,l'}$ in such a way that the interaction term in the Hamiltonian is given by $-\sum_{l,l'} V_{l,l'}\hat{n}_l\hat{n}_{l'}$.

of dephasing is given when comparing the phase of two atoms in different lattice sites. We illustrate this effect of dephasing by calculating the correlation function $\langle \hat{a}_\gamma^\dagger \hat{a}_\beta \rangle = \mathrm{Tr}\left[\hat{a}_\gamma^\dagger \hat{a}_\beta \hat{\varrho}(t)\right] = \mathrm{Tr}\left[\hat{U}^\dagger(t)\hat{a}_\gamma^\dagger \hat{U}(t)\hat{U}^\dagger(t)\hat{a}_\beta \hat{U}(t)\hat{\varrho}(0)\right]$. A combination of the two dephasing effects is discussed in section 5.4.2.

If we choose the same initial conditions as in appendix 5.A, namely $\hat{\varrho}(0) = \hat{\varrho}_\mathrm{L}(0) \otimes \hat{\varrho}_\mathrm{B}(0)$ and $\hat{\varrho}_\mathrm{B}(0)$ describes a thermal state of the BEC, we get

$$\begin{aligned}\langle \hat{a}_\gamma^\dagger \hat{a}_\beta \rangle = \; & \mathrm{Tr}_\mathrm{L}\left[\exp\left(\tfrac{\mathrm{i}}{\hbar}\int_0^t \hat{H}_g(s)\,\mathrm{d}s\right)\tilde{a}_\gamma^\dagger(0)\tilde{a}_\beta(0)\exp\left(-\tfrac{\mathrm{i}}{\hbar}\int_0^t \hat{H}_g(s)\,\mathrm{d}s\right)\tilde{\varrho}_L(0)\right]\times \\ & \exp\left(-{\sum_{\mathbf{q}}}' \tfrac{1}{\hbar^2\omega_\mathbf{q}^2}|F_{\beta,\mathbf{q}} - F_{\gamma,\mathbf{q}}|^2(1-\cos(\omega_\mathbf{q}t))(2N_\mathbf{q}(T)+1)\right). \quad (5.14)\end{aligned}$$

Here, Tr_L denotes the trace over the lattice system, $\hat{H}_g$ was introduced in Eq. (5.10), and we made use of the identity $\mathrm{Tr}_\mathrm{B}\left[\exp(\alpha_\mathbf{q}\hat{b}_\mathbf{q}^\dagger - \alpha_\mathbf{q}^*\hat{b}_\mathbf{q})\hat{\varrho}_\mathrm{B}\right] = \exp[-|\alpha_\mathbf{q}|^2(2N_\mathbf{q}(T)+1)/2]$ for thermally distributed $\hat{\varrho}_\mathrm{B}$ and some complex number $\alpha_\mathbf{q}$ [192]. The first part of Eq. (5.14) describes the correlations between lattice sites γ and β which are induced by the dynamics of the lattice atoms. In our case, their time evolution only contributes a phase term. The second part describes the dephasing which is caused by the coupling to the BEC atoms. Let us denote the dephasing term by Γ. In the thermodynamic limit of the Bogoliubov modes we can replace the sum by an integral and get

$$\begin{aligned}\Gamma &\geq \exp\left(-{\sum_{\mathbf{q}}}' \frac{8d_\mathbf{q}}{(\hbar\omega_\mathbf{q})^2}(2N_\mathbf{q}(T)+1)\right) \\ &\approx \exp\left(-\int \mathrm{d}^D\mathbf{k}\,\frac{8\kappa^2}{(2\pi)^D g^2 n_0 \xi^D}\frac{\exp(-\mathbf{k}^2x_0^2/2\xi^2)}{k\sqrt{k^2+2}^3}(2N_\mathbf{k}(T)+1)\right) =: \Gamma_{\min}\,,\end{aligned} \quad (5.15)$$

where $d_\mathbf{q} = \kappa^2 n_0 \varepsilon_\mathbf{q}\exp(-\mathbf{q}^2x_0^2/2)/\Omega\hbar\omega_\mathbf{q}$, $F_{\mathbf{q},j} = \sqrt{d_\mathbf{q}}\exp(\mathrm{i}\mathbf{q}\mathbf{r}_j)$, and D is the number of spatial dimensions. For zero temperature, $D = 3$, and $\xi \gg x_0$ the integral can be approximated by neglecting the exponential function which gives $\Gamma(T=0) \geq \exp(-4\kappa^2/\sqrt{2}\pi^2 g^2 n_0 \xi^3)$, whereas for sufficiently high finite temperature $k_\mathrm{B}T \gg gn_0$ we find $\Gamma \geq \exp(-\kappa^2 k_\mathrm{B}T/\sqrt{2}\pi g^3 n_0^2 \xi^3)$. In both cases the factor Γ describing the dephasing fulfils $\Gamma > \varsigma > 0$ for a suitable real number ς. This is independent of time or of the distance between the two atoms, which is different from the one-dimensional case, where numerical calculations show that Γ decays to 0 in the thermodynamic limit for $t \to \infty$ as well as for $|r_\gamma - r_\beta| \to \infty$, indicating that no correlations survive.

Interestingly, the solution of the QME introduced in Sec. 5.3 gives the same correlation functions, which also holds for the time evolution of the operators $\hat{a}_j$ after tracing out the condensate. This is due to the fact that the interaction commutes with the lattice Hamiltonian for $J = 0$ and that the BEC is initially in a Gaussian, namely a thermal, state [193]. Hence, for the case $J = 0$ the QME

describes the lattice atoms exactly after the trace over the BEC is taken. For $J \neq 0$ the interaction Hamiltonian and the one describing the lattice atoms do no longer commute, and the QME is only valid for a large hopping with $J \gg E_p$.

5.4.2 Sub- and superdecoherence and probing the BEC

It has been predicted in Ref. [186] that decoherence effects caused by a qubit-bath coupling can be enhanced (superdecoherence) or suppressed (subdecoherence) for certain cases.[3] Here we show that these effects are indeed observable in a BEC for realistic experimental parameters. The effect can moreover be used in order to probe such BEC properties as the temperature with different sensitivity, similar to the method introduced in Ref. [187].

Let us assume that the atoms have two internal states $|0\rangle$ and $|1\rangle$ which couple to the BEC with different coupling constants $\kappa_0 = 0$, $\kappa_1 = \kappa$. This case can be easily generalised to a non-zero κ_0. The different coupling strengths can for example be realised in a $^{40}\mathrm{K}-^{87}\mathrm{Rb}$ mixture. The positions of the Feshbach resonances for the scattering with the rubidium atoms depends on the fine structure levels $|F, m_F\rangle$ of the potassium atoms [194]. By choosing the external magnetic field close to one Feshbach resonance considerable differences between the scattering lengths and hence the coupling constants for different internal states can be achieved, and it is even possible to tune one scattering length to zero.

Initially, the total state of the two atoms is described by the density matrix $\hat{\varrho}_{\mathbf{2}}(0) = \sum_{ijkl=0,1} \varrho_{ijkl}(0) \, |ij\rangle \langle kl|$. After evolving for a certain time t and tracing out the BEC the density matrix changes to $\hat{\varrho}_{\mathbf{2}}(t) = \hat{U}_{\mathrm{coh}} \sum_{ijkl=0,1} \overline{\varrho}_{ijkl}(t) \, |ij\rangle \langle kl| \, \hat{U}_{\mathrm{coh}}^{\dagger}$, where $\hat{U}_{\mathrm{coh}}$ describes the coherent evolution of the atoms induced by the off-site interaction term, which for our case only changes the phase of the matrix elements, but not their absolute value. The elements $\overline{\varrho}_{ijkl}(t)$ are given by $\overline{\varrho}_{ijkl}(t) = \varrho_{ijkl}(0)$ if $i = k$ and $j = l$, $\overline{\varrho}_{ijkl}(t) = \Gamma_0 \varrho_{ijkl}(0)$ if $i + j + k + l$ is an odd number, $\overline{\varrho}_{ijkl}(t) = \Gamma_- \varrho_{ijkl}(0)$ for ϱ_{0110} and ϱ_{1001} and $\overline{\varrho}_{ijkl}(t) = \Gamma_+ \varrho_{ijkl}(0)$ for ϱ_{1100} and ϱ_{0011}. The functions $\Gamma_{+,0,-}$ are calculated analogously to the dephasing term Γ in Sec. 5.4.1 and are given by

$$\Gamma_0 = \exp\left(- {\sum_{\mathbf{q}}}' d_{\mathbf{q}} \frac{1 - \cos(\omega_{\mathbf{q}} t)}{(\hbar^2 \omega_{\mathbf{q}})^2} (2N_{\mathbf{q}}(T) + 1) \right) , \tag{5.16}$$

$$\Gamma_- = \exp\left(- {\sum_{\mathbf{q}}}' d_{\mathbf{q}} [2 - 2\cos(\mathbf{q}(\mathbf{r}_\gamma - \mathbf{r}_\beta))] \frac{1 - \cos(\omega_{\mathbf{q}} t)}{(\hbar^2 \omega_{\mathbf{q}})^2} (2N_{\mathbf{q}}(T) + 1) \right) , \tag{5.17}$$

$$\Gamma_+ = \exp\left(- {\sum_{\mathbf{q}}}' d_{\mathbf{q}} [2 + 2\cos(\mathbf{q}(\mathbf{r}_\gamma - \mathbf{r}_\beta))] \frac{1 - \cos(\omega_{\mathbf{q}} t)}{(\hbar^2 \omega_{\mathbf{q}})^2} (2N_{\mathbf{q}}(T) + 1) \right) , \tag{5.18}$$

[3] In our case it would be more appropriate to speak of sub- and superdephasing. We will however stick to the conventions introduced in Ref. [186].

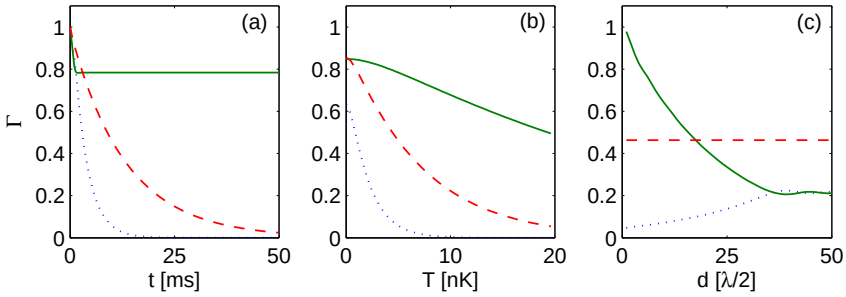

Figure 5.2. The different behaviour of the dephasing functions Γ_- (solid line), Γ_0 (dashed line) and Γ_+ (dotted line) versus (a) time, (b) temperature, and (c) distance d of the lattice atoms. Two ^{133}Cs atoms were assumed in an optical lattice with wavelength $\lambda = 790$nm and a depth of $V_0 = 40E_\mathrm{R}$, where $E_\mathrm{R} = (2\pi\hbar)^2/2m_l\lambda^2$. The one-dimensional BEC consists of ^{87}Rb atoms with a linear number density of 5×10^6/m. The couplings are given by $g = 4.5 \times 10^{-2} E_\mathrm{R}\lambda$ and $\kappa = 3.5 \times 10^{-2} E_\mathrm{R}\lambda$. In (a), a temperature of $T = 5$nK and a distance of $d = 5\lambda/2$ were chosen, in (b) the same distance and a time of $t = 10$ms, in (c) $T = 5$nK and $t = 10$ms. For recent experiments of RbCs-mixtures, see Refs. [195, 196].

where $\mathbf{r}_\gamma$ and $\mathbf{r}_\beta$ denote the positions of the two atoms. Although the overall structure of these three decoherence terms looks very similar they behave quite differently. Let us for the moment assume that only such momenta $\mathbf{q}$ contribute considerably to the sum for which the condition $\mathbf{q}(\mathbf{r}_\gamma - \mathbf{r}_\beta) \ll 1$ holds. This is typically the case for a temperature of $T \approx 0$ and the atoms trapped in two neighbouring lattice sites. Then, $\Gamma_- \approx 1$, which means that the decoherence for an initial state $|\psi\rangle = (|10\rangle \pm |01\rangle)/\sqrt{2}$ is strongly suppressed, because the fluctuations of the condensate happen on a length scale which is too large to resolve the distance between the two atoms. In contrast, the decay of the off-diagonal elements of the initial state $|\psi\rangle = (|11\rangle \pm |00\rangle)/\sqrt{2}$ is enhanced. These effects of sub- and superdecoherence have been predicted in Ref. [186] for a general type of qubit-environment coupling and are similar to the Dicke effect [197] well known in quantum optics. However, in our case it is not the decay rate of the excited state which is suppressed or enhanced. Instead, only the off-diagonal elements of the density matrix are affected leaving the occupation numbers unchanged.

As depicted in Fig. 5.2, these effects can indeed be observed for realistic experimental parameters. Figure 5.2(a) shows the time dependence of the three functions. Γ_- reaches its stationary state very quickly, whereas the two other functions drop exponentially to zero. The temperature dependence is shown in Fig. 5.2(b). Since for higher temperatures phonons with shorter wavelengths become more important, the condition $\mathbf{q}(\mathbf{r}_\gamma - \mathbf{r}_\beta) \ll 1$ is no longer fulfilled and Γ_- decreases, however considerably slower than Γ_+. The condition is also violated when the distance between

the two atoms is increased, as shown in Fig. 5.2(c). Interestingly, the function Γ_+ shows exactly the opposite behaviour: With increasing distance, the value of the function increases as well, until it reaches the same value as Γ_-.

5.4.3 Implications for the quantum register

The dephasing investigated in the previous section has severe implications on the performance of a quantum register. In order to store the information two internal states $|0'\rangle$ and $|1'\rangle$ of the lattice atoms are needed, and we assume that these states do not couple to the BEC, in which case there is also no decoherence caused by the condensate coupling. However, the BEC can be used to perform a two-qubit gate between two atoms submerged into it as detailed in Ref. [176]. In short, if an atom is in state, say, $|1'\rangle$, it will be driven by a laser pulse to a state $|1\rangle$ which couples to the condensate, whereas the state $|0'\rangle$ is either unaffected or driven to a state $|0\rangle$ which does not couple to the BEC. If both atoms involved are in state $|1\rangle$ they can exchange BEC phonons which causes an additional energy shift. In the previous section, this evolution was described by the unitary $\hat{U}_{\mathrm{coh}}$, and by appropriately chosen laser pulses this operator results in a controlled-phase gate. However, due to the coupling the atoms also get entangled with the BEC, which results in dephasing after tracing out the condensate.

The influence of the dephasing on the density matrix $\hat{\varrho}_{\mathbf{2}}$ is suitably expressed by using Kraus operators E_j. The super-operator Λ giving the effect of the dephasing (excluding the controlled-phase gate) can be expressed as

$$\Lambda(\hat{\varrho}_{\mathbf{2}}) = \sum_{j=1}^{d^2} E_j \hat{\varrho}_{\mathbf{2}} E_j^\dagger \,, \tag{5.19}$$

where d is the dimensionality of the quantum system, here $d = 4$ for two qubits. Since the dephasing Λ commutes with the controlled-phase operation, the effect of the noisy gate is described by $\Lambda_g(\hat{\varrho}_{\mathbf{2}}) = \hat{U}_{cZ}\Lambda(\hat{\varrho}_{\mathbf{2}})\hat{U}_{cZ}^\dagger = \Lambda(\hat{U}_{cZ}\hat{\varrho}_{\mathbf{2}}\hat{U}_{cZ}^\dagger)$. The Kraus operators for Λ are given in appendix 5.B, where we also show how the average fidelity $\langle F\rangle$ of the noisy gate can be calculated using the explicit form of these operators. We find

$$\langle F\rangle = \frac{1}{10}(4 + 4\Gamma_0 + \Gamma_- + \Gamma_+) \,. \tag{5.20}$$

From the definition of the dephasing terms it is evident that the fidelity is worse for higher interactions κ between the BEC and the lattice atoms. On the other hand, a lower interaction κ means a lower interaction strength between the two atoms and hence it takes a longer time to perform the gate. In the three-dimensional case, by choosing an arbitrary low interaction strength κ, the average gate fidelity can be brought arbitrarily close to 1, however the time to perform the gate gets arbitrarily long as well. Since there also exist other decoherence mechanisms in

cold atom systems, this will eventually decrease the performance of the setup.

For concreteness, we consider the three-dimensional case where two ^{133}Cs atoms are placed in two neighbouring lattice sites with wavelength $\lambda = 790$nm. They are surrounded by a ^{23}Na BEC with a number density of $(5 \times 10^6)^3/\mathrm{m}^3$ and an interaction strength of $g = 1.5 \times 10^{-2} E_\mathrm{R} \lambda^3$. Here, $E_\mathrm{R} = (2\pi\hbar)^2/2m_l\lambda^2$ is the recoil energy, with m_l the mass of the lattice atoms and λ the wave length of the laser creating the lattice. The interspecies coupling is given by $\kappa = 1.1 \times 10^{-2} E_\mathrm{R}\lambda^3$. In the thermodynamic limit, for $i \neq j$ and $\xi \gg x_0$ the mediated interaction is $V_{i,j} = \kappa^2 \xi \exp(-\sqrt{2}|i-j|a/\xi)/\pi g \xi^3 |i-j|a$, where a is the distance between two neighbouring lattice sites. This leads to the (minimal) gate time $t_g = \hbar\pi/V_{1,2} =$ 40ms [176], where the gate fidelity is given by $\langle F \rangle = 0.99$. For getting the last result, we used the approximations $\Gamma_x \geq \exp(-c_x \kappa^2/\sqrt{2}\pi^2 g^2 n_0 \xi^3)$, which hold in the thermodynamic limit, $T = 0$, $\xi \gg x_0$, and where $c_0 = 1$, $c_- = 2$, and $c_+ = 4$.

For the case of two or one spatial dimensions, the interaction is in general larger and thus the expected gate times shorter. However, the fidelities decrease much faster than for three dimensions, and all of our numerical tests showed that for the same gate times the three-dimensional fidelities were always better than the ones achieved in lower dimensions. Although this restricts the applicability of this setup for quantum information purposes, the scheme can still be used for probing the interaction strength which is mediated by the condensate, simply by measuring the phase differences for varying interaction times.

5.5 Clustering of the lattice atoms

If the lattice is not uniformly filled with atoms but the filling ranges somewhere between zero and one atom per lattice site, the mediated interaction has an important impact on the spatial distribution of the atoms. For low enough temperatures, it will lead to atom clusters. To observe the clustering of the atoms we have to allow for a weak hopping $J \ll |V_{1,2}|, |U|$,[4] because otherwise the atom distribution remains stationary. We can assume that the perturbation due to the hopping does not change the interaction potential $V_{i,j}$ derived from the exact solution, which is in agreement with our earlier findings [178]. The hopping energy can furthermore be neglected compared to the interaction potential, such that the weak hopping leads only to a re-arrangement of the atoms, which is similar to the treatment of ad-atoms on crystal surfaces [188]. The Hamiltonian for this situation is given by

$$\hat{H}_\mathrm{cl} = \frac{U}{2} \sum_j \hat{n}_j(\hat{n}_j - 1) - \sum_{i,j} V_{i,j} \hat{n}_i \hat{n}_j \,. \tag{5.21}$$

[4] In the assumed homogeneous setup the value $V_{1,2}$ corresponds to the mediated interaction between two nearest neighbours and $V_{1,1}$ to the mediated on-site interaction.

The mediated on-site interaction $V_{1,1}$, which in our case is always attractive, cf. equation (5.13), might overcompensate the on-site interaction U, i.e., $U+V_{1,1} < 0$. If this happens, all the atoms can aggregate in a single lattice site, which will inevitably lead to three-body losses. We therefore assume that the repulsive on-site interaction U is large enough such that states with more than one atom in a single lattice site can be neglected, i.e., $U + V_{1,1} \gg J$. For the parameters used below (see captions of Figs. 5.3 and 5.4) the mediated on-site interaction is given by $V_{1,1} = -0.03E_\mathrm{R}$ in one dimension and $V_{1,1} = -0.08E_\mathrm{R}$ in two. Since we require a deep lattice for the hopping J to be small, a sufficiently high U can easily be achieved. For a reasonably deep lattice of $15E_\mathrm{R}$ and perpendicular confinement of $35E_\mathrm{R}$, the interaction strength is on the order of $U \approx 0.4E_\mathrm{R}$ for a one-dimensional lattice and $U \approx 0.3E_\mathrm{R}$ for two dimensions and thus sufficiently high to overcome the induced on-site attractive interaction. The repulsive interaction strength corresponds to a temperature of $U/k_\mathrm{B} = 150\mathrm{nK}$ in one dimension ($U/k_\mathrm{B} = 130\mathrm{nK}$ in two dimensions), such that neglecting states with more than one atom per lattice site is well-justified for the temperature regime considered, see below. With these assumptions, the ground state for the lattice system consists of a cluster where all the atoms are located in neighbouring lattice sites. We note that this also holds if the lattice is loaded with spin-polarised fermions, in which case the Pauli exclusion principle ensures that there is never more than one atom in each lattice site. The restriction to a maximum of one atom per lattice site and ignoring interactions beyond nearest neighbours makes it also possible to map the system to an Ising model by using the correspondence $\hat{n}_j = (1 + \hat{s}_j)/2$, which gives

$$\hat{H}_\mathrm{cl} = -\frac{V_{1,2}}{4} \sum_{\langle i,j \rangle} \hat{s}_i \hat{s}_j - V_{1,2} \sum_j \hat{s}_j \,, \tag{5.22}$$

where a constant term has been neglected. We will make use of this correspondence shortly when we compare our results to analytical ones found for the Ising model in two dimensions.

In an experiment, the lattice atoms will have a finite temperature T, which leads to a breaking up of the ground state into smaller clusters, reflecting the increased average energy. It is therefore important to investigate at which temperatures the clustering can be observed. To this end, we simulated the lattice system using the well-established Metropolis algorithm [198, 199], which is often used in the simulation of classical lattice spin and lattice gas models when the kinetic energy can be neglected compared to the interaction energies. For a one-dimensional lattice, the averaged number of clusters[5] for different temperatures is shown in Fig. 5.3(a). For temperatures above $T = 7\mathrm{nK}$ the number of clusters does not change very much with the temperature and roughly 110 clusters exist, which shows that most of the atoms do not have nearest neighbours. A drastic reduction

[5]Note that a single atom without nearest neighbours is also considered to constitute a cluster.

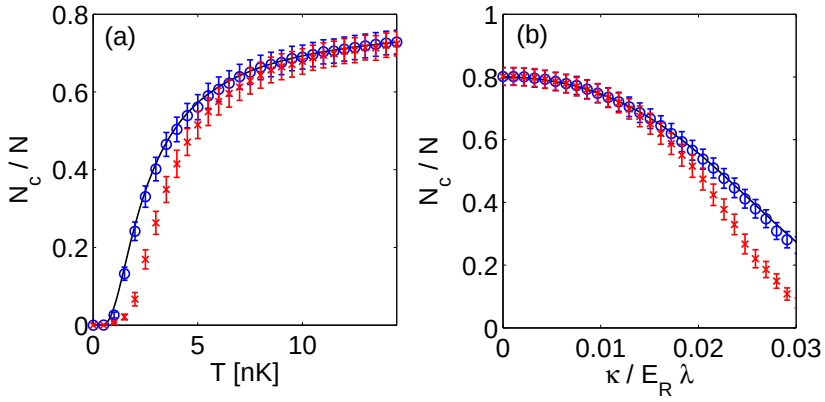

Figure 5.3. Normalised cluster number N_c/N versus (a) temperature of the one-dimensional lattice gas and (b) coupling to the BEC. The solid line shows the analytical estimate given in Eq. (5.23), results from numerical calculations only taking the nearest neighbour interaction into account are marked by 'o' and numerical results including the full interaction potential are marked by 'x'. The algorithm was run for 10^8 steps after which an equilibrium state is reached. Then, another 5×10^7 steps were done and after every 1000 steps the number of clusters was calculated. Error bars show one standard deviation derived from averaging over those results. The lattice with wavelength $\lambda = 790$nm consists of $M = 800$ lattice sites filled with $N = 160$ ^{41}K atoms. The surrounding BEC was assumed to consist of ^{87}Rb atoms with a linear number density of $n = 5 \times 10^6$/m and a coupling $g/E_R\lambda = 1.1 \times 10^{-2}$. In (a), the interspecies coupling is given by $\kappa/E_R\lambda = 2.5 \times 10^{-2}$, whereas in (b) the temperature is fixed to $T = 3$nK. Periodic boundary conditions were assumed.

of the cluster number only occurs for $T < 7$nK, such that the number of clusters finally reaches $N_c = 1$ for $T \approx 0$. A method to achieve such low temperatures of below 7 nK has been proposed, where the surrounding BEC is first used for dark-state cooling [148, 149].

The numerical data in Fig. 5.3 is compared to an analytical result derived in the thermodynamic limit, where the number of lattice sites M goes to infinity whilst keeping the filling fraction N/M constant, and only taking nearest-neighbour interactions into account [200]. In this case, the normalised number of clusters N_c/N is given by

$$\frac{N_c}{N} = \frac{M}{N} \frac{\sqrt{1 + 4(M-N)N\left[\exp(2|V_{1,2}|/k_B T) - 1\right]/M^2} - 1}{2[\exp(2|V_{1,2}|/k_B T) - 1]}, \tag{5.23}$$

where k_B is Boltzmann's constant. Our calculations show that the numerical results taking only the nearest neighbour term of the interaction into account is in

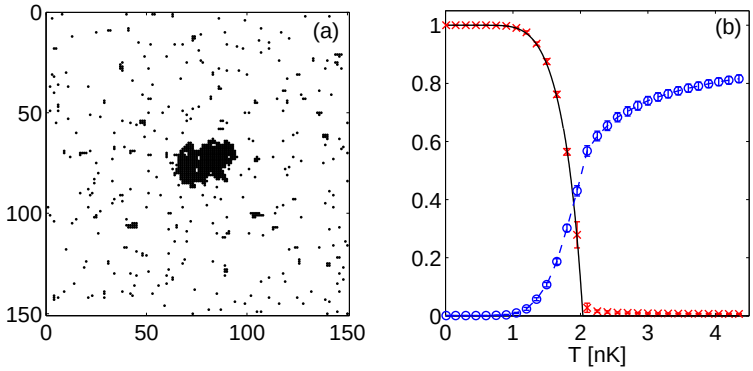

Figure 5.4. (a) Distribution of the atoms in a homogenous two-dimensional lattice with periodic boundary conditions and a temperature of $T = 1.8$nK. A macroscopic island is clearly visible. (b) Normalised size of the largest cluster N_I/N versus temperature of the lattice gas for a two-dimensional system (marked by 'x') and normalised number of clusters N_c/N (marked by 'o'). The solid line shows the analytical expression given in Eq. (5.24), the dashed line is a guide to the eye. Error bars show one standard deviation derived from averaging over several runs. The lattice with wavelength $\lambda = 790$nm consists of $M = 150 \times 150$ lattice sites filled with 900 ^{41}K atoms. The surrounding BEC was assumed to consist of ^{87}Rb atoms with a number density of $n = 25 \times 10^{12}/\mathrm{m}^2$ and a coupling $g/E_\mathrm{R}\lambda^2 = 5.1 \times 10^{-3}$. The interspecies coupling is given by $\kappa/E_\mathrm{R}\lambda^2 = 1.87 \times 10^{-2}$.

excellent agreement with the result for the thermodynamic limit. We furthermore observe that the number of clusters for the full interaction potential is for low temperatures considerably smaller than for the truncated one, which indicates that the interaction terms beyond nearest neighbours make the clusters more stable. This gets also apparent when the temperature is fixed and the number of clusters is calculated for different coupling strengths κ, as shown in Fig. 5.3(b). For small κ the interaction beyond nearest neighbours is still quite weak and does not change the number of clusters significantly, whereas for stronger coupling κ, interaction terms beyond nearest neighbours are considerable, reflected in a smaller number of clusters or, equivalently, in a larger average cluster size.

The situation gets more interesting if we consider a two-dimensional lattice. For $T \approx 0$, the atoms aggregate in an "island" and for increasing temperature parts of this island break away, see Fig. 5.4(a). We have calculated the size of the largest cluster (i.e. the number N_I of atoms constituting the island) numerically, only taking nearest neighbour interactions into account. This will give a lower bound for the temperature below which the formation of the island can be observed. The results are shown in Fig. 5.4(b). For very low temperatures, all the atoms are contained in a single cluster. This largest cluster gets smaller with increasing temperature

and shows a pronounced transition at a temperature of $T \approx 2$nK, above which the system mainly consists out of many small clusters. It has been shown in Ref. [201], that the normalised size N_I/N of the island in the thermodynamic limit and only taking nearest neighbour interactions into accout behaves as

$$\frac{N_I}{N} = \frac{(1+N_0)(N_0-N_r)}{2N_0(1-N_r)}\,. \tag{5.24}$$

Here, $N_0 = \{1-[\sinh(2J_\mathrm{s}/k_\mathrm{B}T)]^{-4}\}^{1/8}$, and $J_\mathrm{s} = |V_{1,2}|/4$. For this formula to be valid we further require a filling of $N/M \leq 1/2$, such that $N_r = 1-2N/M \geq 0$, and above the transition temperature T_I where N_I/M hits zero for the first time, the function has to be set to zero, since for this temperature the normalised size of the largest island vanishes in the thermodynamic limit. Our Monte-Carlo results are in excellent agreement with Eq. (5.24), deviations above the transition temperature are due to finite size effects. We note that a higher transition temperature T_I can be achieved by increasing the interaction strength $V_{i,j}$ or by loading more atoms into the lattice. We find $k_\mathrm{B}T_I = 2J_\mathrm{s}/\mathrm{arsinh}\left[1/\sqrt[4]{1-N_r^8}\right]$, which yields for the chosen values (see caption of Fig. 5.4) and $N_r \to 0$ a value of $T_I = 2.34$nK.

We note that for a ground state where the atoms are anticlustered, for example a density wave state, a repulsive off-site interaction would be necessary. For identical atoms in the lattice this can not be achieved with our setup, since the mediated interaction between the atoms is always attractive irrespective of the sign of the interspecies interaction κ.

5.6 Transport properties of the impurity atoms

In this section, we use the QME to investigate the behaviour of the lattice system for a hopping $J \gg E_p$. In general, an analytical solution of the QME is no longer possible, and the dynamics has to be calculated numerically. Let us consider the simple case of one atom initially localised in a single lattice site. With vanishing coupling to the condensate, the atom will spread across the lattice coherently in a wavelike motion, as shown in Fig. 5.5(a). The interference fringes between the two wave fronts are clearly visible. The coherent nature of the evolution is also reflected in the density matrix, where all off-diagonal elements have their maximum possible value, compare Fig. 5.5(b). The situation changes when the coupling to the condensate is increased, as shown in Fig. 5.5(c). The wave-fronts still exist, however the region in between no longer exhibits clear interference patterns, which are washed out instead. This implies that the coherent nature of the evolution is impaired, which is also supported by the density matrix, see Fig. 5.5(d). The off-diagonal elements are clearly suppressed, which confirms the incoherent character.

The motion of the atom in the lattice can be explained by the coexistence of

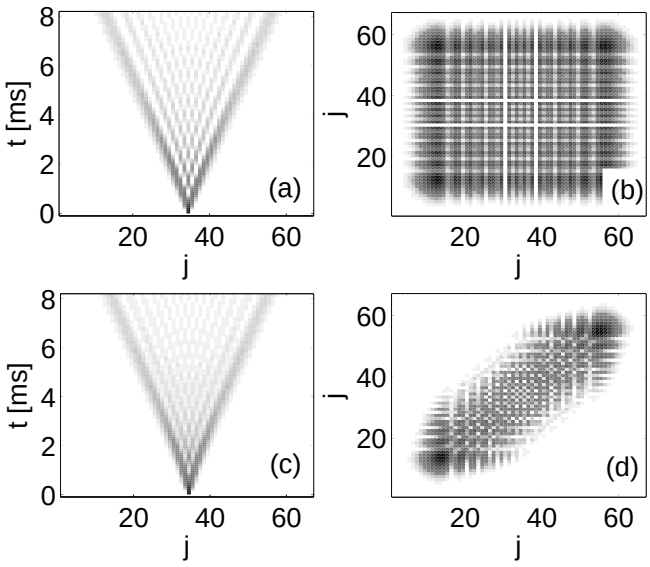

Figure 5.5. (a) and (c) time evolution of the atom density. (b) and (d) graphical representation of the absolute values of the density matrix for the final time step $t = 8.2$ms shown in (a) and (c). A darker colour corresponds to a higher density in (a) and (c) or a higher absolute value of the matrix elements in (b) and (d). For the examples shown we have assumed a ^{41}K atom in an optical lattice with wave length $\lambda = 790$nm, and a hopping of $J = 0.03E_{\mathrm{R}}$. The BEC consists of ^{87}Rb atoms with a density of $n_0 = 5 \times 10^6/\mathrm{m}$ and a coupling of $g/E_{\mathrm{R}}\lambda = 1.1 \times 10^{-2}$. The temperature is given by $T = 100$nK. The interspecies coupling for case (a) and (b) was assumed to be $\kappa = 0$, whereas for (c) and (d) it was $\kappa/E_{\mathrm{R}}\lambda = 1.94 \times 10^{-2}$. For recent experiments on these mixtures, see Refs. [184, 202].

wavelike, coherent evolution responsible for the two wave-fronts, and a diffusive, incoherent evolution. The diffusive motion stems from the decay of the off-site elements in the density matrix, which destroys the memory of the atom and causes it to perform a random walk, leading to the washing out of the interference effects between the two wave fronts. To investigate the time evolution more quantitatively, we calculate the standard deviation σ_{d} of the atom density distribution at a time t, given by $\sigma_{\mathrm{d}} = \sum_j p_j (j - j_0)^2$, where j labels the lattice sites, p_j is the probability of finding the atom at lattice site j, and j_0 is the initial lattice site of the atom at $t = 0$. Figure 5.6(a) shows that for an increasing coupling to the condensate this standard deviation σ_{d} decreases. This stems from the fact that the hopping is reduced due to the coupling between the lattice atoms and the phonons of the BEC, which has also been observed in Ref. [178].

Taking one standard deviation to either side of j_0 defines a suitable interval I between the two wave fronts to investigate the diffusive character of the mo-

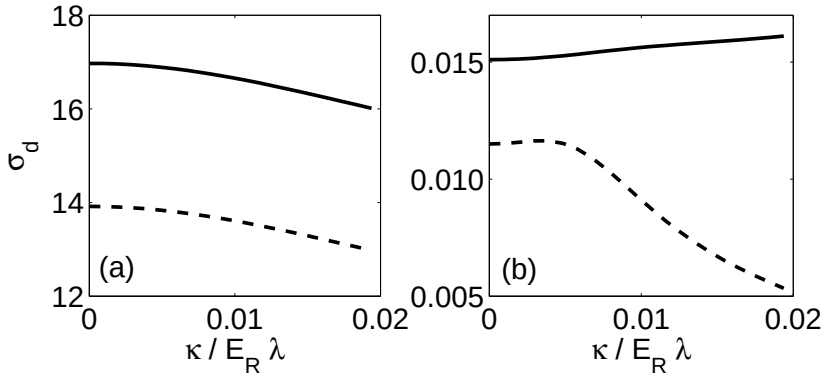

Figure 5.6. (a) Standard deviation of the density distribution after an evolution time of $t = 6.7$ms (dashed line) and $t = 8.2$ms (solid line). (b) Average density $\bar{p}$ (solid line) and standard deviation p_d (dashed line). Apart from the interspecies coupling κ, all the parameters are as in Fig. 5.5.

tion. For this interval, we calculate the average atom density $\bar{p} = \sum_{j\in I} p_j/2\sigma_\mathrm{d}$ and the standard deviation of the density distribution $p_\mathrm{d} = \sum_{j\in I}(p_j - \bar{p})^2/2\sigma_\mathrm{d}$. For the coherent case, we expect that this standard deviation is on the order of the average density $\bar{p}$ due to the interference patterns, whereas for the incoherent case the standard deviation should be much lower than the average density due to the more homogenous spread of the atom between the two wave fronts. These expectations are confirmed by our findings shown in Fig. 5.6(b). We observe that the average density between the two wave fronts $\bar{p}$ moderately increases with increasing interspecies coupling. The standard deviation of this density p_d stays first approximately constant with increasing κ, indicating a regime where the evolution can still be considered to be coherent, but then for $\kappa > 5 \times 10^{-3} E_\mathrm{R}\lambda$ drops off considerably, caused by the increased loss of coherence.

The QME describes the lattice atoms well as long as only dephasing has to be taken into account and energy exchange with the BEC can be neglected. This is consistent with the approximations we have used to derive the QME: It was assumed that $Ja/\hbar \ll c$, which means that the atoms move slower than the critical velocity of the BEC. Then, according to the Landau criterion for superfluidity, no energy exchange is possible with a single phonon process, and higher order phonon processes are not included into the QME.

This gets especially apparent when we try to describe the decay of Bloch oscillations with the QME. Let us assume a Stark potential $\hat{H}_s = K\sum_j j\hat{n}_j$ is applied to the one-dimensional optical lattice. For one particle initially located in a single lattice site and not coupling to the BEC, we expect breathing oscillations with frequency $\omega_B = K/\hbar$ and width $4J_a|\sin(\omega_B t/2)|/K$ [203]. This is shown in Fig. 5.7(a). When the atom couples to the BEC, it can dissipate energy into the condensate

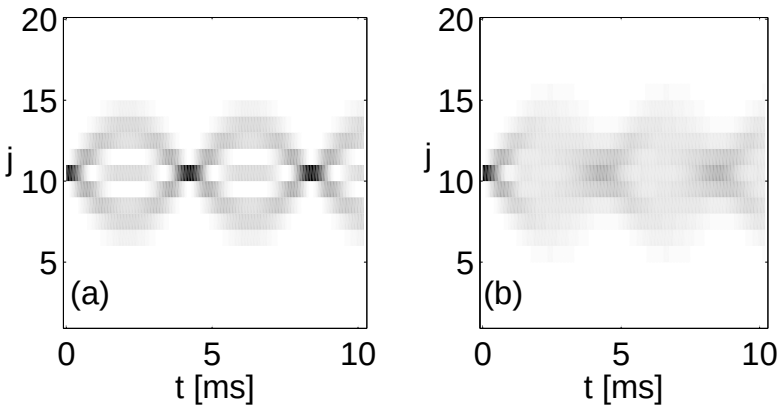

Figure 5.7. Bloch oscillations in an optical lattice submerged into a BEC of ^{87}Rb atoms with a density of $n_0 = 5 \times 10^6/\mathrm{m}$, a coupling of $g/E_\mathrm{R}\lambda = 1.1 \times 10^{-2}$ and a temperature of $T = 75\mathrm{nK}$. The ^{41}K atom is trapped in a lattice with wavelength $\lambda = 790\mathrm{nm}$ and has a hopping rate of $J = 0.03E_\mathrm{R}$. The strength of the Stark potential is given by $K/\hbar = 1.5\mathrm{kHz}$. The interspecies coupling is given by (a) $\kappa = 0$ and (b) $\kappa/E_\mathrm{R}\lambda = 1.6 \times 10^{-2}$.

modes and one expects that the atom can "fall down" the tilted lattice, causing a net current. When using the QME to describe the dynamics this is, however, not the case. Instead, the Bloch oscillations only get washed out, but the mean position of the atom remains unchanged, as shown in Fig. 5.7(b). This is in agreement with our expectations and with other attempts to describe the system with a simple master equation approach [204]. An alternative way based on a generalised master equation, which includes the coupling of phonons to the hopping term, has been devised to describe the occurrence of an atomic net current. Details are given in reference [205].

Another way to observe the net current is given by solving the complete dynamics of the atom and the surrounding BEC numerically. For this, the BEC has to be discretised, which is equivalent to assuming that it is trapped in an optical lattice with appropriately chosen hopping and interaction constants [206]. The Hamiltonian describing the system is then given by

$$\hat{H} = \hat{H}_\mathrm{L} - J_b \sum_{\langle i,j \rangle} \hat{\beta}_i^\dagger \hat{\beta}_j + \frac{U_b}{2} \sum_j \hat{\beta}_j^\dagger \hat{\beta}_j^\dagger \hat{\beta}_j \hat{\beta}_j + U_i \sum_j \hat{\beta}_j^\dagger \hat{\beta}_j \hat{a}_j^\dagger \hat{a}_j \,, \tag{5.25}$$

with $\hat{\beta}_j^\dagger$ ($\hat{\beta}_j$) an operator that creates (annihilates) a boson in lattice site j, U_b the on-site interaction strength and J_b the hopping matrix element of the BEC atoms, and U_i the interspecies interaction strength. The time evolution of this Hamiltonian including the BEC and a single atom in the lattice is performed numerically by using the time evolving block decimation (TEBD) algorithm [8, 160, 207]. The

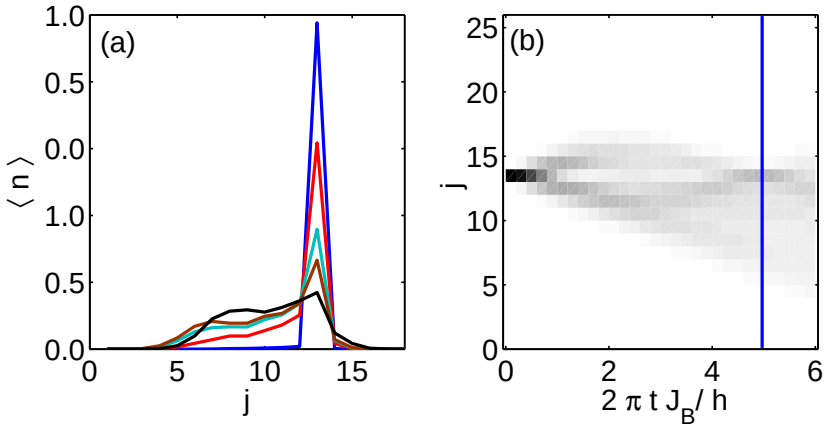

Figure 5.8. (a) Decay of Bloch oscillations and occurrence of a net current. Shown are the density distributions of one atom initially localised in lattice site 13 after a time evolution of $t = 2\pi/\omega_B$ for different interaction strengths ranging from $U_i = \{0.1; 0.5; 0.8; 1; 2\}J_b$ (top to bottom line in lattice site 13). The dynamics of the lattice atom and the BEC consisting of 25 atoms was calculated in an optical lattice with 25 lattice sites using the TEBD algorithm. We used $J_a = J_b$, $U_b = 0.5J_b$, $K = 1.25J_b$, $T = 0$. (b) Time evolution of the density distribution for one lattice atom with $U_i = J_b$. The coexistence of Bloch oscillations and a current is visible. The vertical line indicates the time where the densities of (a) are taken.

resulting density distribution of the lattice atom initially placed in a single lattice site and evolved for one Bloch period is shown in Fig. 5.8(a). For a weak interaction strength $U_i \ll J_b$ the surrounding BEC atoms hardly affect the dynamics of the lattice atom and after one cycle it ends up in its original lattice site again. For increased interaction the lattice atom is able to dissipate more and more energy to the BEC and to drift towards lattice sites with a lower potential energy, which leads to a net current. This is illustrated in Fig. 5.8(b), where a competition between Bloch oscillation and net current is clearly visible. The current can be measured either directly or after a time of flight expansion of the lattice atoms as detailed in Ref. [208].

5.7 Conclusion

In the present chapter we have investigated the behaviour of an optical lattice system immersed into a BEC. To this end, we have derived a quantum master equation which describes the time evolution of the lattice atoms. For the case of fixed impurities, the lattice system represents a quantum register and the internal states of the atoms represent the states of the qubit. We have derived an exact

solution for this system, which is reproduced by the QME. We found that an interaction between the lattice atoms is mediated by the condensate and that the coupling to the phonon modes of the BEC causes a dephasing of the lattice atoms, i.e., of the qubits they represent. This dephasing can be used to probe the properties of the BEC with different sensitivity.

The interaction between the lattice atoms leads to a clustering process at low enough temperatures. In contrast to on-site clusters, which are prone to three-body losses, the clustering in our case is caused by the off-site interaction terms. We have simulated the clustering process using the Metropolis algorithm and compared our results with analytical ones originally found for spin systems or ad-atoms on a crystal surface. Our findings indicate that for realistic experimental parameters the clustering process occurs at temperatures of about 5nK and is observable with near-future experimental techniques.

We also investigated the transport properties of the lattice atoms subject to the BEC coupling. We found that the lattice atoms undergo a crossover from coherent to incoherent evolution when the interaction to the condensate is increased. This process is indicated by a washing out of the typical interference fringes in the density distribution and by vanishing off-diagonal elements in the one-particle density matrix. However, due to the approximations necessary to derive the QME, it does not include dissipation of energy to the BEC. This process is a vital effect to describe the decay of Bloch oscillations in a tilted lattice. More work is necessary to include this effect into a master equation description.

5.A Derivation of the QME

The details of deriving the QME are given in this appendix. Our starting point is the Liouville-von Neumann equation for the total density operator $\hat{\varrho}(t)$,

$$\mathrm{i}\hbar\partial_t\hat{\varrho}(t) = [\hat{H}, \hat{\varrho}(t)]\,. \tag{5.26}$$

For a general operator $\hat{O}$ in the Schrödinger picture we define the corresponding operator $\tilde{O}(t)$ in the interaction picture by

$$\tilde{O}(t) = \mathrm{e}^{\mathrm{i}(\hat{H}_B+\hat{H}_L)t/\hbar}\,\hat{O}\,\mathrm{e}^{-\mathrm{i}(\hat{H}_B+\hat{H}_L)t/\hbar}\,. \tag{5.27}$$

With this, the Liouville-von Neumann equation changes to

$$\mathrm{i}\hbar\partial_t\tilde{\varrho}(t) = [\tilde{H}_I(t), \tilde{\varrho}(t)]\,. \tag{5.28}$$

If there was no interaction between the lattice atoms and the BEC before a time $t_0 = 0$, it is reasonable to assume that the density operator at time t_0 is described by $\hat{\varrho}(0) = \hat{\varrho}_\mathrm{L}(0)\otimes\hat{\varrho}_\mathrm{B}(0)$, i.e., at time t_0 there are no correlations present between the

BEC and the lattice atoms. Here, $\hat{\varrho}_{\mathrm{L}}(0)$ and $\hat{\varrho}_{\mathrm{B}}(0)$ are the initial density operators of the lattice system and the BEC, respectively. We furthermore assume that at t_0 the BEC is in a thermal state with temperature T. Integrating the Liouville-von Neumann equation, substituting it into itself and using the definition of $\tilde{H}_I(t)$, we find after applying the Born approximation and taking the trace over the BEC variables [192]

$$\begin{aligned}\partial_t \tilde{\varrho}_L(t) = \; -\tfrac{1}{\hbar^2}\int_0^t \mathrm{d}t' \; {\sum_{\mathbf{q}}}' \sum_{l,l'} \{[\tilde{n}_l(t)\tilde{n}_{l'}(t')\tilde{\varrho}_L(t') - \tilde{n}_{l'}(t')\tilde{\varrho}_L(t')\tilde{n}_l(t)] C_{\mathbf{q},l,l'}(t-t') \\ + [\tilde{\varrho}_L(t')\tilde{n}_{l'}(t')\tilde{n}_l(t) - \tilde{n}_l(t)\tilde{\varrho}_L(t')\tilde{n}_{l'}(t')] C^*_{\mathbf{q},l,l'}(t-t')\}\,, \quad (5.29)\end{aligned}$$

with

$$C_{\mathbf{q},l,l'}(t-t') = F_{\mathbf{q},l}F^*_{\mathbf{q},l'}(1+N_{\mathbf{q}}(T))\,\mathrm{e}^{-\mathrm{i}\omega_{\mathbf{q}}(t-t')} + F^*_{\mathbf{q},l}F_{\mathbf{q},l'}N_{\mathbf{q}}(T)\,\mathrm{e}^{\mathrm{i}\omega_{\mathbf{q}}(t-t')}\,. \quad (5.30)$$

Under the assumption that the sound velocity of the condensate, $c \sim \sqrt{gn_0/m_b}$, is larger than the typical hopping speed of the atoms, $c \gg Ja/\hbar$, the dynamics of the BEC is much faster than the typical dynamics of the lattice atoms. This means that the BEC reacts almost instantaneously and without memory effects to changes caused by the lattice atoms and we are allowed to perform the Markov-approximation by replacing $\tilde{\varrho}_L(t') \to \tilde{\varrho}_L(t)$ and $\tilde{n}_l(t') \to \tilde{n}_l(t)$. After calculating the time integral and transforming back into the Schrödinger picture we finally arrive at Eq. (5.9).

5.B Kraus operators for the two-qubit dephasing

Here, we give explicit formulas for the Kraus operators describing the operator Λ given by $\Lambda(\hat{\varrho}_{\mathbf{2}}) = \hat{U}^\dagger_{cZ}\Lambda_g(\hat{\varrho}_{\mathbf{2}})\hat{U}_{cZ}$. We find

$$E_1 = \sqrt{(1+2\Gamma_0+\Gamma_+)/4}\,\mathbf{1}_4\,, \quad (5.31)$$

$$E_2 = \sqrt{(1-2\Gamma_0+\Gamma_+)/4}\,\sigma_z\otimes\sigma_z\,, \quad (5.32)$$

$$E_3 = \sqrt{(1-\Gamma_-)/4}\,\sigma_z\otimes\mathbf{1}_2\,, \quad (5.33)$$

$$E_4 = \sqrt{(1-\Gamma_-)/4}\,\mathbf{1}_2\otimes\sigma_z\,, \quad (5.34)$$

$$E_5 = \sqrt{(\Gamma_--\Gamma_+)/4}\,\mathrm{diag}(-1,1,1,1)\,, \quad (5.35)$$

$$E_6 = \sqrt{(\Gamma_--\Gamma_+)/4}\,\mathrm{diag}(1,1,1,-1)\,, \quad (5.36)$$

and all other Kraus operators are zero. Here, $\mathbf{1}_n$ is the $n\times n$ unit matrix, σ_z is the Pauli z matrix, and diag is a diagonal matrix with the entries on the diagonal given as the argument.

With the knowledge of the Kraus operators the average fidelity $\langle F\rangle$ of the gate

is calculated as follows. We first note that the fidelity F of the noisy operation Λ_g with respect to the perfect (i.e., noise-free) operation $\hat{U}_{cZ}$ on a special input state $|\psi\rangle$ is defined by

$$F(\psi) = \langle\psi|\, \hat{U}_{cZ}^{\dagger}\, \Lambda_g\{|\psi\rangle\,\langle\psi|\}\, \hat{U}_{cZ}\, |\psi\rangle\ . \tag{5.37}$$

By taking the average over all possible input states the overall performance of the gate operation can be estimated. It has been shown [209, 210] that the average fidelity is given by

$$\langle F\rangle = \int_{S^{2d-2}} F(\psi)\,\mathrm{d}\psi = \frac{1}{d(d+1)}\left(\sum_{j=1}^{d^2} |\mathrm{Tr}(E_j)|^2 + d\right)\ , \tag{5.38}$$

where the integral is taken over the unit sphere S^{2d-2} embedded in $(2d-1)$-dimensional real space, which is isomorphic to the d-dimensional complex space after eliminating a global phase, and $\mathrm{d}\psi$ is the normalised measure over the sphere, also know as Haar measure. With this formula and the explicit form of the Kraus operators the calculation of the average fidelity Eq. (5.20) is straight forward.

We note that the Kraus operators for a coupling to independent reservoirs are given by replacing $\Gamma_- = \Gamma_+ = (\Gamma_0)^2$. This gives an average fidelity of $\langle F_{\mathrm{ind}}\rangle = (2+2\Gamma_0+(\Gamma_0)^2)/5$. Hence the coupling to the BEC reservoir is worse than the one to independent reservoirs if $\Gamma_+ + \Gamma_- < 2(\Gamma_0)^2$.

Chapter 6

Quantum repeaters and decoherence-free subspaces

In this chapter, we review some preliminaries which are useful for the following chapter on the robust implementation of quantum repeaters. We will first show why it is important to devise a new kind of cryptographic scheme, namely quantum cryptography [2, 211], and what measures would have to be taken to enable a communication scheme over large distances [47–49]. We will then briefly discuss why storing qubits in single atoms leads to loss of quantum information and how this problem can be circumvented by using decoherence-free subspaces [56–59].

6.1 Quantum cryptography

Since people started to exchange information by sending messages it was also their desire to keep this information secret so that only the intended recipient can read the message. Cryptography has developed from using simple code words via shifting the letters of the alphabet to the asymmetric RSA method [211–213]. In this section, we show that the implementation of a new type of cryptography, called quantum key distribution, seems advisable if secret communication were to be ensured in the future. We will then present some of the main protocols of quantum cryptography. Since these proposals only allow for a secure communication over a short distance we also briefly discuss an extension of these protocols, namely the quantum repeater.

6.1.1 The need for quantum cryptography

Nowadays, many people send personal data via the internet, for example to purchase goods and services or to communicate with other people. Often, the exchanged data consists of sensitive information such as credit card or insurance numbers which should not be disclosed to third parties. It is therefore important that this data is securely encrypted before it is sent via the internet. Currently, this is widely achieved using an asymmetric RSA protocol [211–213]. Asymmetric means that one party A makes an encryption key k_e publicly available to everyone

who wants to communicate with A. For decrypting the encoded message, A uses a decryption key k_d, which is only known to A. In principle, the decryption key can be deduced from the encryption key by prime factorising a large number. The security of the RSA protocol is hence based on the *believe* that it is a mathematically hard task to find the prime factors of a large number. Here, "hard" means that the effort in terms of time or resources scales exponentially with the length of the number. Up to now, the best known classical algorithm to perform the factorisation of a large number is the general number field sieve which scales as $\mathcal{O}(\exp(cn^{1/3}(\log n)^{2/3}))$, where n is the number of decimal digits and $c \approx 1.9$ is a constant [214, 215]. It is, however, not proven that this algorithm is optimal, and it is possible that there exist better, yet unknown classical algorithms to perform the task. To give an insight into the complexity of the problem we note that in 2005 a special number known as RSA-640, consisting of 640 binary digits, was factorised. The task took approximately 30 2.2GHz-Opteron-CPU years, which was equivalent to 5 months since the factorisation was performed on a multi-processor cluster.[1] With the current algorithms and computers, it is deemed to be extremely hard to factorise a number with 1024 binary digits, often used for encryption nowadays, and factorising any number with more than 2048 binary digits is deemed to be infeasible in the foreseeable future. Hence, a classical algorithm which could perform the factorisation task in a significantly shorter, polynomial time would lead to a collapse of the current asymmetric cryptographic systems.

But even if there were no better classical algorithm, it has been shown by P. Shor that a quantum algorithm can do better [16]. By making use of quantum computation, the algorithm is able to accomplish the factorisation task with an effort of $\mathcal{O}(n^2(\log n)(\log\log n))$, where n is the number of digits. Thus Shor's algorithm is exponentially faster than the best present-known classical algorithm. This especially means if a quantum computer with a sufficient number of qubits was available the factorisation task would be an easy problem and the RSA encryption scheme would no longer be secure. So far, quantum computation has only been accomplished for a very small number of qubits. For example, the number 15 has been factorised using a 7 qubit NMR technique [217]. However, this technique exhibits a poor scaling behaviour, that means it is difficult to devise NMR molecules with a large number of qubits. Other methods, such as ion traps [218, 219], Josephson junctions [220], quantum dots in solids [221, 222], or cold atoms [219] have been developed to circumvent this problem, but they currently still suffer from uncontrolled interactions with their environment, inducing decoherence. This decoherence leads

[1] Factorising this number was part of the RSA-challenge. The RSA company announced prizes for the factorisation of certain numbers known as the RSA numbers in order to "prove" the security of the RSA method. Although the challenge run for about 10 years, no-one managed to factorise any of the numbers with more than 700 binary digits. For more information see `http://www.rsa.com/rsalabs/node.asp?id=2092` . For earlier developments of the challenge see also [216].

to an unwanted loss of quantum information which eventually makes the successful application of quantum algorithms impossible. Even though, with the current state of the art, it will be a long time before quantum computers with a reasonable number of qubits can be implemented, it is advisable to devise cryptographic methods which are able to overcome the problems involved with RSA.

One provably secure way of encrypting a message is given by the application of a so-called Vernam cipher, also known as a one time pad [2]. The idea of this cipher is as follows. Assume the message m is a string of bits. The key k then consists of a random string of bits which is as long as the message m. The bits of m and k are bitwise added modulus 2 yielding the encrypted message e. The receiver of the message e can decrypt this message by simply bitwise adding the key k to e (modulus 2), thereby restoring the original message m. The important point is that the key k is only known to the sender and the receiver, but not to any other party. If the secrecy of the sufficiently random key is ensured and it is only used once, this method is proven to be secure. It is a purely classical way of encryption and easily implemented with today's technology. The only problem remaining is the distribution of the key k.

In the following, we will discuss two protocols which are used for quantum key distribution. However, they do not allow for the authentication of the communicating parties. This makes them vulnerable to man-in-the-middle attacks [223], where a third party interrupts the communication channel of the two communicating parties and pretends to be one of the two parties. There exist proposals of how this problem can be overcome, such as quantum digital signatures [224] or using a (shorter) pre-established key [223, 225]. Since these methods are not important for the presented protocols and the problems discussed in the following chapters, we will not go into more detail and refer the reader to the literature [211, 226].

6.1.2 Quantum cryptography protocols

In this section we will briefly discuss two protocols for securely generating and distributing a key for a one time pad. Due to this the methods should rather be called "quantum key distribution protocols" since quantum mechanics is only required to ensure the security of the key, but "quantum cryptography protocols" is also an established expression. Both methods are based on discrete quantum variables such as qubits, in contrast to schemes which are based on continuous variable quantum communication [227, 228]. The security of all these schemes is ensured by the fact that quantum mechanical states in general cannot be copied without disturbing them. This is also known as the no-cloning theorem [229, 230].

The first method we discuss is the BB84 protocol, named after C. Bennett and G. Brassard [231] and the year of publication. Let us call the two communicating parties Alice and Bob. Alice sends single photon pulses for example through an optical fibre to Bob. For the preparation of the photon, she uses two sets of orthog-

onal bases, for example horizontally and vertically polarised light for the first basis set and circular polarised σ^+ and σ^- light for the second. She chooses randomly first a basis set and then one of the two possible polarisations. Bob also randomly chooses one of the two basis sets for measuring the polarisation of the arriving photon. Only if he uses the same basis as Alice will the measurement result tell with certainty in which state Alice has prepared the photon. Otherwise, the two outcomes of the measurement are equally likely and he cannot gather any information about the polarisation chosen by Alice. After a sufficient number of runs Alice and Bob publicly[2] announce which basis they have used to prepare/measure the qubit. Only if the two basis sets agree do they then keep the results of the preparation/measurement, otherwise they discard them. The results are then assigned bit values, for example 0 for horizontally and σ^+-polarised light and 1 for vertically and σ^--polarised light. This bit sequence then constitutes their so called sifted key for the Vernam cipher, and provided that all measurements and the channel are perfect Alice's and Bob's keys are identical. The secrecy of the key is ensured by the no-cloning theorem [2]. A possible eavesdropper, commonly called Eve, is not able to perfectly copy the quantum state of the single photon or to manipulate it without the chance of being detected. Hence Eve can only gather partial information on the key. If the quality of the channel is known to Alice and Bob and sufficiently high, they can estimate the information Eve has won on the key by comparing some of their key bits. If their bit sequences are the same, the probability that an eavesdropper is present is practically zero and they can assume that their key is secure. If the result of their comparison is completely random, i.e. the qubits in the two sequences agree only with a probability of 50%, their key is useless. Provided that the errors were not caused by noise in the channel, the eavesdropper has successfully prevented the exchange of a secure key by intercepting the qubits and Alice and Bob have to start the protocol again. If Eve has only intercepted some of the qubits and her information is below a certain threshold, by sacrificing some of the key bits Alice and Bob can use privacy amplification algorithms known from classical communication in order to decrease Eve's information below any desired level [232].

An alternative protocol, which is also proven to be secure, is the one proposed by A. Ekert [233]. An EPR pair [234] such as $\phi_+ = (|0,0\rangle + |1,1\rangle)/\sqrt{2}$ is created by a common source and one of the two qubits is sent to Alice, the other one to Bob. The entanglement of the EPR pair leads to the fact that when Alice and Bob make measurements of their qubit in the same basis, their results are perfectly correlated, but it is impossible to gain any information on the outcome of the other party's measurement when two orthogonal bases are used. Thus Alice and Bob perform measurements in randomly chosen, orthogonal bases and afterwards announce which basis they have used. If the bases agree, they can deduce the

[2]Here, publicly means via a non-encrypted channel, which might be overheard by an eavesdropper.

measurement result of the other party, since the two qubits were entangled, and convert them to a key bit sequence analogous to the BB84 protocol. Otherwise, they do not use the result for the key, but still keep the results of the measurements. When an eavesdropper Eve tries to gain information on the key she will disturb the entangled qubits. Alice and Bob can check this by testing Bell's inequality [235]. They randomly choose some of their measurement results, including those where the bases did not agree, and check whether they fulfill the inequality. Depending on the outcome they can trust their key since no eavesdropper was present, use privacy amplification to reduce Eve's information, or discard their key if Eve has gained too much information. In the latter case, they have to start the protocol from the beginning.

A successful implementation of quantum key distribution protocols has been demonstrated in several experiments [236–239]. For example, a recent experimental implementation of the Ekert protocol (also known as the EPR protocol) under real-world conditions has been carried out in Vienna [239]. The two communicating parties were based in a Viennese bank and in the city hall, both connected by a 1.45km long, commercial optical telecom fibre installed in the sewage system. The EPR source, hosted by Alice and realised by parametric down-conversion, was able to produce 8200 entangled photon pairs per second. The choice of the measurement basis for the photons was done by beam splitters and hence intrinsically random. For the creation of a sifted key of the length of about 245000 bits the experiment run for 18 minutes. During this time, Alice's detectors registered more than 12.8 million counts. The big difference is mainly due to losses in the optical fibre, but also due to imperfections of the detectors and discarding of bits during sifting the key. After error correction and privacy amplification there were about 79500 bits left for the final secure key. The corresponding average key distribution rate was about 76 bits/second.

6.1.3 The quantum repeater

The schemes introduced in the previous section work well as long as the distance between the two communicating parties is not too large, which means on the order of a few kilometers. For larger distances on the order of several hundred kilometers and above, one has to fight an essential problem. The qubits are transmitted by single photon pulses through optical fibres. In these optical fibres, the photons will eventually be absorbed if the distance between Alice and Bob is increased, making it impossible to exchange a secret key. Alternatives have been proposed such as free-space protocols, where the photons are sent through the atmosphere or even to satellites. However, experimental implementations so far suffered from loss of photons in the atmosphere, from straylight and from the fact that instead of single photon sources, weak laser pulses were used, opening more opportunities for an eavesdropper and compromising the security of the scheme [240–242].

Another way for allowing a larger distance between the two communicating parties is given by using quantum repeaters [47–49]. The communication channel between Alice and Bob is divided into shorter sections, each of which is short enough to ensure the near-lossless exchange of single photon pulses. Between those sections, there are quantum repeater nodes which consist of a quantum memory capable of storing several qubits (the exact number depends on the details of the implementation scheme). By sending single photon pulses from one repeater node to another, qubits in neighbouring nodes are entangled. For simplicity only assume one node. Let us define the Bell states $|\phi_\pm\rangle = (|00\rangle \pm |11\rangle)/\sqrt{2}$ and $|\psi_\pm\rangle = (|01\rangle \pm |10\rangle)/\sqrt{2}$. By exchanging photons Alice's qubit is entangled with one qubit of the node creating the Bell state, say, $|\phi_+\rangle$, and the other qubit of the node is entangled with Bob's qubit, yielding the total state

$$|\psi\rangle = |\phi_+\rangle_{A,N_1} |\phi_+\rangle_{N_2,B} \ , \tag{6.1}$$

where the index A denotes Alice's qubit, B Bob's and N_j the j-th qubit of the repeater node. It is easy to see that this state can be rewritten as

$$\begin{aligned} |\psi\rangle = \frac{1}{2} \Big(& |\phi_+\rangle_{A,B} |\phi_+\rangle_{N_1,N_2} + |\phi_-\rangle_{A,B} |\phi_-\rangle_{N_1,N_2} \\ & + |\psi_+\rangle_{A,B} |\psi_+\rangle_{N_1,N_2} + |\psi_-\rangle_{A,B} |\psi_-\rangle_{N_1,N_2} \Big) \ . \end{aligned} \tag{6.2}$$

This means after performing a Bell measurement on the two qubits in the repeater node, the remaining two qubits shared by Alice and Bob will end up in one of the four possible Bell states, which can be transformed to the desired Bell state $|\phi_+\rangle_{A,B}$ by local operations. This procedure is known as entanglement swapping [243] and is closely related to quantum teleportation [244]. For more than one node the process is iterated in a straightforward manner. The entangled pair which is shared by Alice and Bob is then used as in the original Ekert protocol.

Since imperfections during the creation of the entangled pairs and the entanglement swapping are unavoidable, the fidelity of the entangled states is decreased, which eventually would make a successful implementation of the entanglement swapping and the Ekert protocol impossible. This can be overcome by using entanglement purification methods [47, 245, 246]. Additional pairs of (sufficiently) entangled qubits are produced and they are sacrificed in order to increase the entanglement of other pairs. More details on the whole scheme can be found in chapter 7.2.

6.2 Decoherence and decoherence-free subspaces

In contrast to ordinary bits, which are typically stored as a macroscopic (and hence classical) current or in the magnetisation of a macroscopic part of a solid, qubits

are stored in small quantum systems such as single atoms, ions, nuclear spins or photons. Especially atoms, ions, and nuclear spins, couple to external electric and magnetic fields [2], which change the energy levels of the respective system or even lead to spontaneous decay of an excited level. This has a destructive influence on the information stored in the system which needs to be circumvented. The earliest proposals to handle this problem are active error correction codes [247–249]. One logical qubit is encoded in several physical qubits thereby introducing redundancy. Depending on the specific error correction code used, certain errors can be detected and corrected by applying suitable gates. However, a large overhead of qubits and operations is needed to implement these schemes. An alternative route is given by suppressing the errors using decoherence-free subspaces (DFSs), also known as passive quantum error correction [56–59]. Here, the quantum information is encoded in a part of the Hilbert space which does not couple to the kind of noise which has been identified to be the dominant one. In the following, we will demonstrate the benefit of DFSs using the example of dephasing noise.

Let us for concreteness assume the quantum information is stored in two internal levels of an atom. The Hamiltonian of this two-level atom might be represented by

$$\hat{H}_a = \frac{1}{2}\hbar\omega\sigma_z\,, \tag{6.3}$$

where $\hbar\omega$ is the energy difference between the two atomic levels and σ_z the Pauli spin operator in z direction. The atom (or qubit) is described by the density matrix

$$\hat{\varrho}(t) = \begin{pmatrix} \varrho_{11}(t) & \varrho_{12}(t) \\ \varrho_{12}^*(t) & \varrho_{22}(t) \end{pmatrix}. \tag{6.4}$$

The two internal states of the atom are normally chosen such that they are metastable and hence the decay of the excited state can be neglected. The coupling of the atom to randomly varying magnetic or electric fields causes dephasing which is described by the quantum master equation [250, 251]

$$\partial_t\hat{\varrho}(t) = -\frac{\mathrm{i}}{\hbar}\left[\hat{H}_a, \hat{\varrho}(t)\right] + \frac{\gamma}{2}\big(\sigma_z\hat{\varrho}(t)\sigma_z - \hat{\varrho}(t)\big)\,, \tag{6.5}$$

where γ is the dephasing constant. The solution of this master equation in the interaction picture gives

$$\hat{\varrho}(t) = \begin{pmatrix} \varrho_{11}(0) & \varrho_{12}(0)\exp(-\gamma t) \\ \varrho_{12}^*(0)\exp(-\gamma t) & \varrho_{22}(0) \end{pmatrix}. \tag{6.6}$$

This means that the off-diagonal elements, describing the coherence of the qubit, get damped. For the completely dephased state where the off-diagonal elements are zero, the atom is no longer in a superposition of the two internal states, but in a statistical mixture, which is useless for most quantum information purposes [2].

One way of suppressing this kind of noise is to use decoherence-free subspaces (DFSs). For atoms the relevant source of noise are magnetic or electric stray fields, which are homogenous over several micrometers and do not depend on the exact position of the atom [252–255]. The Hamiltonian describing this homogenous kind of noise is then given by

$$\hat{H}_{\text{int}} = \sum_j B_x \sigma_x^j + B_y \sigma_y^j + B_z \sigma_z^j \,, \tag{6.7}$$

where j labels the atoms. The quantities B_x and B_y represent a decay or an excitation of the upper level of the atom. Since typically metastable states are used to represent the qubits, these processes are strongly suppressed, and only dephasing given by a non-zero B_z is the predominant source of noise, which has been confirmed by experiments [252–255]. For this case with $B_x = B_y = 0$, the information can be protected in a DFS making use of two atoms. The logical qubits are for example encoded as

$$|0\rangle_{\text{L}} = \frac{1}{2}(|10\rangle + |01\rangle) \,, \qquad |1\rangle_{\text{L}} = \frac{1}{2}(|10\rangle - |01\rangle) \,. \tag{6.8}$$

The z component of the total spin has always a value of zero, which means that the noise Hamiltonian has no effect on the logical qubits, $\hat{H}_{\text{int}} |0\rangle_{\text{L}} = \hat{H}_{\text{int}} |1\rangle_{\text{L}} = 0$. As a consequence, the time evolution of the logical qubits is still unitary after tracing out the field degrees of freedom. No dephasing occurs and hence the logical qubits are protected from this kind of noise. The usefulness of DFSs to protect qubits from dephasing has been impressively demonstrated in a recent experiment [255], where the dephasing time of a qubit encoded in a DFS using $^9\text{Be}^+$ ions could be extended to about 7s. In chapter 7 we will show how a decoherence-free subspace which is immune against all homogenous noise can be implemented by using atoms in optical lattices, and how to combine them with quantum repeaters.

Chapter 7

Publication

Robust implementations of quantum repeaters[1]

Alexander Klein, Uwe Dorner, Carolina Moura Alves, and Dieter Jaksch

Clarendon Laboratory, University of Oxford, Parks Road, Oxford OX1 3PU, United Kingdom

Phys. Rev. A **73**, 012332 (2006)

We show how to efficiently exploit decoherence free subspaces (DFSs), which are immune to collective noise, for realising quantum repeaters with long lived quantum memories. Our setup consists of an assembly of simple modules and we show how to implement them in systems of cold, neutral atoms in arrays of dipole traps. We develop methods for realising robust gate operations on qubits encoded in a DFS using collisional interactions between the atoms. We also give a detailed analysis of the performance and stability of all required gate operations and emphasise that all modules can be realised with current or near future experimental technology.

7.1 Introduction

One of the major obstacles in the realisation of quantum information processors (QIP) is decoherence, caused by the unwanted interaction of the system with its environment. Even the feasibility of simple special purpose quantum devices, such as quantum repeaters, is significantly affected by the presence of decoherence, and a special precaution to counteract the resulting loss of quantum information has to be taken. A number of concepts have been developed to fight decoherence and increase the reliability of QIP including active error correction [247–249] and fault tolerant quantum computing [256]. Aside from this it was shown that, dependent on the type of interaction processes between the qubits and their environment, subspaces of the system's Hilbert space can exist which are immune to decoherence processes induced by this interaction [56–59]. These decoherence free subspaces are a method of passive error correction or error prevention, and can significantly increase the lifetime of quantum information and reliability of QIP as already demonstrated

[1] Section 7.2.1 has been contributed by Uwe Dorner.

with ion traps, NMR and optical methods [252, 255, 257–262]. However, this robustness makes states within the decoherence free subspace (DFS) difficult to manipulate via controlled operations and, in general, complicated interactions with a DFS are necessary for realising universal QIP [59].

A particularly promising application of DFSs are quantum repeaters [47, 49], which require very long quantum information storage times but only a limited set of quantum manipulations. In this chapter we show that the quantum operations necessary for a quantum repeater can be realised on DFS qubits with nearest neighbour hopping [263, 264] and interactions with ancilla qubits [265] only, thus circumventing the difficulties usually associated with the use of DFSs [59]. Quantum repeaters are used to distribute maximally entangled pairs of qubits over long distances, which is a necessary prerequisite for important applications such as quantum cryptography [233] and quantum teleportation [266]. They are thus considered one of the most important near future special purpose QIP.

The basic idea of a quantum repeater is to divide the transmission line into segments with a length of the order of the attenuation length of the channel. On each segment entangled particle pairs are created and by applying entanglement swapping [243] and purification protocols [47, 245, 246] entangled pairs of larger distances are produced. By repeating these steps a distant pair of qubits with high entanglement fidelity is obtained. Entanglement purification, distillation, and concentration have been realised in a number of seminal experiments [267–270] using photonic states for encoding the qubits. Techniques for converting flying photonic qubits into atomic ones by means of cavity-enhanced interactions [271, 272] or the use of atomic ensembles [273, 274] have been proposed. Very recently, a demonstration of long distance entanglement of massive particles has been achieved [275].

Here we develop a proposal for a quantum repeater with DFS quantum memory using the entanglement purification scheme introduced in [47, 48] (also known as the "Innsbruck protocol"). During the purification procedure the entanglement of a primary pair of qubits is increased by sacrificing auxiliary entangled qubit pairs. The entanglement fidelity of the final entangled qubit pair does not converge to 1, but to a value which depends on the fidelity of the initial primary pair and on the constant fidelity of the auxiliary pairs. However, the scheme [47, 48] is favourable from a pragmatic point of view, since it requires fewer physical resources than the purification schemes used in [245, 246, 276]. On the other hand, the protocol [47, 48] takes longer and thus quantum information has to be stored reliably for the whole duration of the protocol. We overcome this apparent disadvantage by the usage of DFS qubits of four neutral atoms, which form the key elements of our DFS quantum repeater.

Our scheme is based on current and near future technology and is motivated by the extraordinary progress of the field of cold, neutral atoms in dipole traps over the past few years both on the theoretical [107, 219, 277, 278] and on the experimental [279, 280] side. Atomic quantum registers have been realised in arrays of

microlenses [281, 282] and by exploiting the superfluid to Mott-Insulator transition in optical lattices [17, 108, 283], single and many atoms have been manipulated coherently [284, 285], atoms stored in standing waves have been transported over macroscopic distances using conveyor belt techniques [42, 43, 286, 287], and multipartite entangled states of atoms were created [285, 288]. Furthermore, extremely versatile technologies such as optical tweezers and holographic traps that are controlled by liquid crystal spatial light modulators [289–291] are currently developed. They allow for essentially arbitrary designs of optical potentials.

We will show that a DFS quantum repeater can be assembled from modules which only require rotations of the logical DFS qubits around the x and z axes by angles π and $\pi/2$, and a controlled phase (CPHASE) gate where an ancilla atom acts as the control qubit. The single qubit rotations will be realised by selectively lowering potential barriers between atoms and the system will not leave the DFS during these gates. The ancilla qubit, which is required to interact with a DFS qubit for realising the CPHASE gate, will not be decoherence free. However, we will show that its influence on the DFS memory is sufficiently small to allow for gate fidelities better than 98.7%. Furthermore, we will show that our scheme allows for deviations of the system parameters of a few percent without significantly affecting the gate fidelities.

This chapter is structured as follows: In Sec. 7.2 we will briefly summarise the repeater protocol and show how DFSs can be embedded into this scheme. The goal of this section is to show which resources are needed for the implementation of the quantum repeater. In Sec. 7.3 we propose methods of how the operations of Sec. 7.2 can be physically realised with cold, neutral atoms in arrays of dipole traps. The results are summarised in Sec. 7.4.

7.2 Quantum Repeaters with decoherence free subspaces

In the following we will describe the purification and repeater protocol of Refs. [47, 48] and extend it by using a DFS. The basic steps of the purification scheme are illustrated in Fig. 7.1. Only one quantum channel (represented by the lines with an arrow) and two DFS qubits (represented by the solid circles) are needed. The goal is to share a high fidelity Bell state between A and B which is done by transmission of "one-half" of a maximally entangled flying qubit pair (open circles in Fig. 7.1(i)). In general, the flying qubit (e.g., a photon) is not directly sent from A to B since the present available transmission quantum channels (particularly optical fibres) degrade the entanglement of the flying qubit pair exponentially with the distance between the nodes. Thus, if the channel is too long, the minimum fidelity required for the successful application of the purification protocol ($F_{\min}$) is not achieved. To overcome this problem a sufficiently high number of intermediate nodes between A

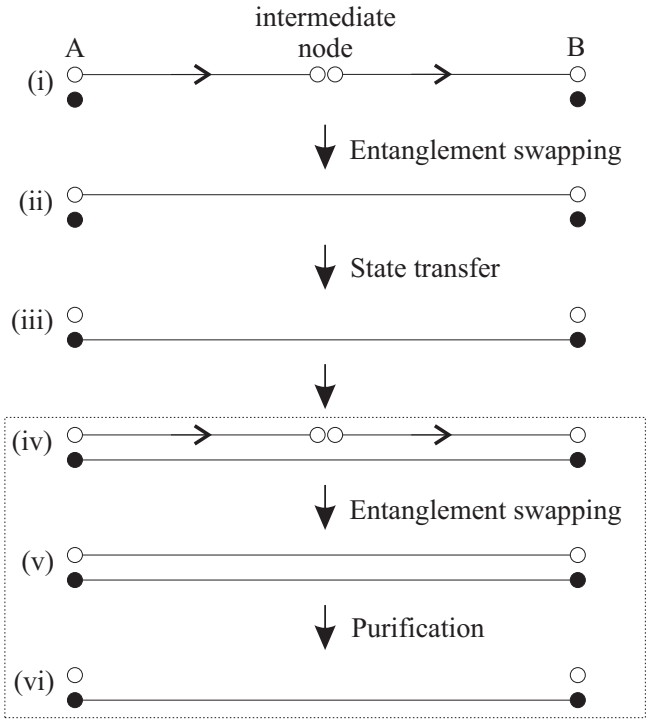

Figure 7.1. Illustration of the entanglement purification scheme. Pairs of entangled flying qubits (open circles) are created via entanglement swapping. These pairs are then used to purify an entangled pair of DFS qubits (solid circles; see text). The framed steps (iv)-(vi) are repeated until a desired entanglement fidelity is achieved.

and B is introduced, such that the distance between two nodes is of the order of the optical fibre's attenuation length [48]. Entangled flying qubit pairs are prepared at each of the intermediate nodes and transmitted to the next node. In Fig. 7.1 this is illustrated for the example of one intermediate node. After this, entanglement swapping [243] at all intermediate nodes is performed, which yields a partially entangled pair of flying qubits between A and B, and its state is transferred to a DFS qubit pair (step (ii)). Finally, as in (i) and (ii), auxiliary entangled qubit pairs are generated, which are sacrificed in order to increase the entanglement of the DFS qubit pair (step (iv)-(vi)). Steps (iv)-(vi) are repeated until a desired degree of entanglement is obtained for the DFS qubit pair.

However, a straightforward extension of this scheme in order to connect arbitrary separated points A and B is not possible since the distance between the intermediate nodes has to be chosen such that the fidelity of the final pair is not lower than $F_{\min}$. This is, in general, not possible if the distance between A and B is too large. Therefore, a quantum repeater concept by means of a nested purification scheme was proposed [47, 48], which uses the above purification protocol to create

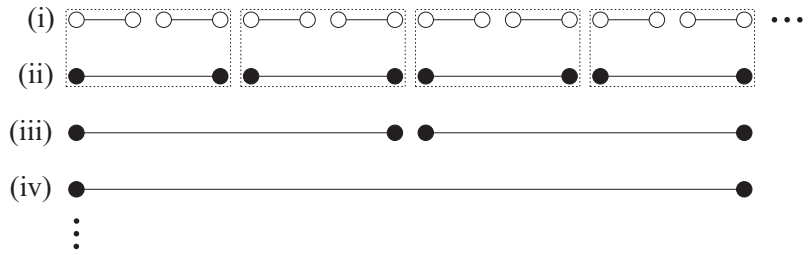

Figure 7.2. The quantum repeater scheme. The dashed boxes indicate the subroutine shown in Fig. 7.1. The created entangled DFS qubit pairs are used to purify further DFS qubit pairs (in line (iii)). The resulting pairs are then used to purify the pairs of line (iv) and so on.

a number of entangled DFS qubit pairs that are then used to purify a lower number of additional DFS pairs with greater distance. These pairs are then again used to purify an even lower number of pairs, etc., until merely one entangled pair is left. This procedure is illustrated in Fig. 7.2: The boxes stretching over lines (i) and (ii) represent the purification protocol of Fig. 7.1. The entangled pairs of line (ii) are then used to purify the pairs in line (iii) in the same way as in Fig. 7.1 except that the flying qubits have to be replaced by DFS qubits, i.e., entanglement swapping between DFS qubits, a state transfer between DFS qubits (to initialise the pairs in line (iii) and (iv)) and purification by using entangled DFS pairs have to be performed. The diagram shown in Fig. 7.2 can be extended in horizontal and vertical directions such that an arbitrary distance between the final pair can be achieved. It was shown that the number of (DFS) qubits necessary for the scheme increases merely logarithmically with the distance of the final entangled pair [47, 48].

In summary, the purification procedure shown in Fig. 7.1 can be realised by assembling the following modules: (0) The creation of pairs of flying qubits and performing entanglement swapping between them, (1) the realisation of two DFS qubits, (2) the transfer of the state of the flying qubits to the DFS qubits, and (3) the actual purification of the entangled DFS qubit pair. Additionally, for the nested purification protocol, i.e., for the full implementation of the quantum repeater, we have to (4) perform entanglement swapping between neighbouring DFS qubits, (5) we need a state transfer between DFS qubits (analogously to module (2)), and (6) we must perform entanglement purification using two DFS qubit pairs. Module (0) can be implemented using standard quantum optical methods as demonstrated in [292–296]. It does not involve DFS qubits and will thus not be discussed further in this chapter.

In the following we will show how each of the remaining modules can be realised. For the operations using ancilla qubits and thus leaving the DFS we then calculate the achievable fidelities.

7.2.1 Realisation of the repeater modules

7.2.1.1 Module 1: Decoherence free memory and single qubit rotations

The main sources of decoherence in systems of cold atoms are fluctuations of the optical potential and external electromagnetic (stray-)fields [297]. These sources are homogeneous across the region of the physical qubits and the interaction with them thus only depends on their internal states. The Hamiltonian describing the situation is given by

$$H_I = \sum_i \sigma_i^x B_x + \sigma_i^y B_y + \sigma_i^z B_z \,. \tag{7.1}$$

Here, i labels the physical qubits, $\mathbf{B} = (B_x, B_y, B_z)$ describes the fields and fluctuations, and the σ_i are Pauli matrices acting on the ith physical qubit.

The corresponding decoherence free subspace is spanned by the states with total zero angular momentum, and the lowest number of physical qubits giving a twofold degenerate DFS is 4. The DFS qubit is then represented by [59, 298]

$$\begin{aligned} |0\rangle_L &= \frac{1}{2}(|01\rangle - |10\rangle) \otimes (|01\rangle - |10\rangle)\,, \\ |1\rangle_L &= \frac{1}{2\sqrt{3}}(2\,|1100\rangle + 2\,|0011\rangle - (|01\rangle + |10\rangle)^{\otimes 2})\,, \end{aligned} \tag{7.2}$$

where $|ijkl\rangle = |i\rangle_1 |j\rangle_2 |k\rangle_3 |l\rangle_4$ with $i, j, k, l = 0, 1$ describes the computational basis states of the four physical qubits. Each of the four physical qubits is represented by two internal states of an atom, which is trapped in an array of dipole traps, for example, an optical lattice. By the method described in Sec. 7.3.1 the system is prepared in the logical state $|0\rangle_L$ and in Sec. 7.3.2 it is shown that by tuning the system parameters appropriately we can implement the Hamiltonians H_X and H_Z with

$$H_X = X_L = \frac{1}{\sqrt{3}}(V_{12} + 2V_{23})\,, \tag{7.3}$$

$$H_Z = Z_L = -V_{12}\,, \tag{7.4}$$

where X_L (Z_L) is the X-gate (Z-gate) for the logical qubit and V_{ij} are permutations of the physical qubits i and j. Note that the logical Z-gate can also be represented as $Z_L = -V_{34}$. Since the DFS defined by Eq. (7.2) is invariant under permutations of the physical qubits [59], the time evolution of the system generates rotations

$$R_L^x(\theta) = \mathrm{e}^{-\mathrm{i}\frac{\theta}{2}X_L}\,, \tag{7.5}$$

$$R_L^z(\theta) = \mathrm{e}^{-\mathrm{i}\frac{\theta}{2}Z_L} \tag{7.6}$$

without ever leaving the DFS, where $\theta = 2t$ and t is the time necessary for performing the rotations. The index L indicates that these are operations on the logical

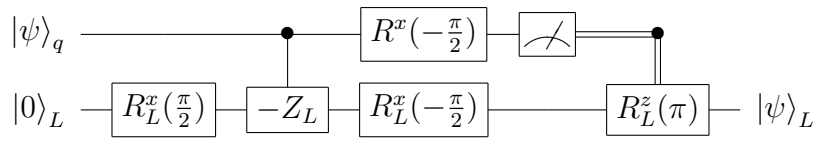

Figure 7.3. Quantum circuit for the state transfer of the auxiliary qubit to the DFS qubit.

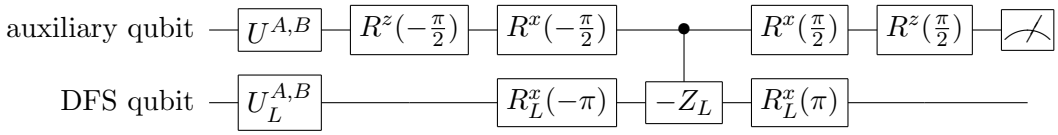

Figure 7.4. Quantum circuit for entanglement purification. The procedure is performed on both sides, A and B.

qubit; in the following we will also use this notation for operations on physical qubits, where we omit the index L.

Although it is not required in the repeater protocol, we can thus perform arbitrary rotations of the logical qubit (and hence we can prepare arbitrary states in the DFS) since every two level unitary operator can be decomposed in R^x_L and R^z_L [2].

7.2.1.2 Module 2: State transfer between flying and DFS qubit

The quantum circuit for the state transfer of the flying qubit to the logical qubit is shown in Fig. 7.3. The state of the flying qubit is denoted as $|\psi\rangle_q = \alpha\,|0\rangle_q + \beta\,|1\rangle_q$. As described in Sec. 7.3 the state of the flying qubit (a photon) is first transferred to an appropriate internal state of an auxiliary atom. The state of this atom then controls the interaction between physical qubits 3 and 4 leading to a controlled SWAP operation between these atoms. Since $Z_L = -V_{34}$, a controlled SWAP operation of the physical qubits 3 and 4 leads to a controlled $(-Z_L)$ (CPHASE) gate on the logical qubit. As can be seen from Fig. 7.3, apart from rotations given in Eqs. (7.5) and (7.6), we need to perform a rotation $R^x(-\pi/2)$ and a measurement of the control atom, which can be done by standard techniques such as laser induced Rabi oscillations and state selective laser excitations. Eventually, the state of the atom is transferred to the logical qubit, i.e., $|\psi\rangle_L = \alpha\,|0\rangle_L + \beta\,|1\rangle_L$.

7.2.1.3 Module 3: Entanglement purification

The local operations required for entanglement purification are shown in Fig. 7.4. This circuit corresponds to the scheme proposed in [246], but here it is expressed in terms of operations that we can implement in our setup. The circuit has to be

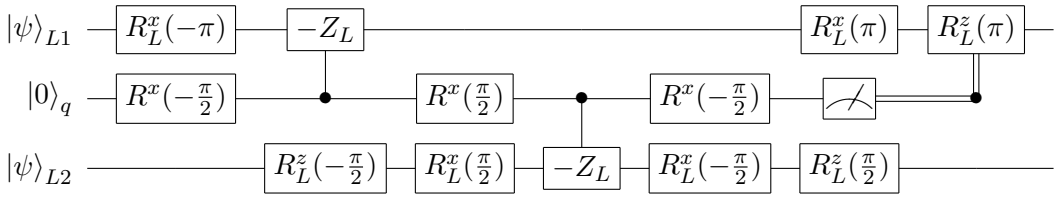

Figure 7.5. Quantum circuit for a CNOT operation between two logical qubits.

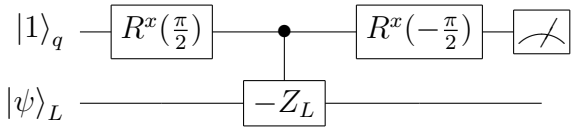

Figure 7.6. Measurement of the logical qubit.

applied on both ends of the transmission line A and B, where

$$U_L^A = \left(U_L^B\right)^\dagger = R_L^x(\pi/2)\,. \tag{7.7}$$

As in subsection 7.2.1.2, the auxiliary qubit is again an atom that controls a phase operation on the logical qubit. If the outcome of the measurements at A and B coincide we end up with an entangled DFS qubit pair of higher fidelity. If they do not coincide the purification procedure has to be repeated.

7.2.1.4 Module 4: Entanglement swapping between DFS qubits

Entanglement swapping between neighbouring DFS qubit pairs can be done by a Bell measurement and subsequent local operations $R_L^x(\pi/2)$ and $R_L^z(\pi/2)$ that are controlled by the outcome of the measurement [48]. The Bell measurement can be decomposed in a controlled not (CNOT) gate, a Hadamard gate, and a measurement in the computational basis. The Hadamard gate can be replaced by, e.g., the sequence $R_L^z(\pi/2)R_L^x(\pi/2)R_L^z(\pi/2)$.

The implementation of a decoherence free CNOT operation is relatively complicated including lengthy sequences of two-particle interactions with pairwise individual tuning [59]. Thus, we use as before an ancilla atom to mediate the interaction between different DFS qubits. A possible quantum circuit for a CNOT gate between DFS qubits is shown in Fig. 7.5. The middle line in the circuit represents the ancilla qubit. The shown circuit uses only gates that we can implement in our scheme and leads to a CNOT gate with the upper DFS qubit as the control qubit. We will discuss in Sec. 7.2.2 how the decoherence of the auxiliary atom influences the fidelity of this operation.

For the measurement of the DFS qubit we use the same ancilla as for the CNOT gate. The corresponding circuit is shown in Fig. 7.6. The final measurement of the

ancilla is equivalent to a measurement of the DFS qubit.

7.2.1.5 Modules 5 and 6: State transfer between DFS qubits and entanglement purification using pairs of DFS qubits

The state transfer of one DFS qubit to another can be done analogously to Fig. 7.3, where $|\psi\rangle_q$ has to be replaced by $|\psi\rangle_L$. The necessary CPHASE gate between DFS qubits can be constructed similarly to the CNOT gate: We merely have to omit the single qubit rotations in the last line of Fig. 7.5. Also the entanglement purification scheme of Fig. 7.4 can be adapted in this way. Again, the auxiliary qubit is replaced by a DFS qubit and the CPHASE (or CNOT) gate is realised as described above.

7.2.2 Operation time and decoherence

Some of the above operations require the use of a single auxiliary qubit that is not decoherence free. Entangling this qubit with the DFS qubits will therefore lower the overall fidelity of the corresponding gate operations on the DFS qubits. The auxiliary qubit is represented in our scheme by two long-lived internal states of an atom and thus the major experimentally expected decoherence mechanism is dephasing [299]. This process is described by the master equation

$$\partial_t \varrho_{\text{aux}} = -\frac{\mathrm{i}}{\hbar}[\hat{H}, \varrho_{\text{aux}}] + \frac{\gamma}{2}\left(\sigma_z \varrho_{\text{aux}} \sigma_z - \varrho_{\text{aux}}\right) , \tag{7.8}$$

where ϱ_{aux} is the density matrix of the auxiliary atom, $\hat{H}$ is the Hamiltonian of the system, $1/\gamma$ characterises the decoherence time, and σ_z is a Pauli matrix. Decoherence of the DFS qubits is not taken into account here.

A quantitative measure of the operation fidelity is derived from Ref. [2]. A distance measure of two density matrices ϱ, σ is given by

$$f(\varrho, \sigma) = \left(\mathrm{Tr}\sqrt{\sqrt{\sigma}\varrho\sqrt{\sigma}}\right)^2 , \tag{7.9}$$

where, in contrast to [2], we use the squared trace. This measure has the advantage that if ϱ and σ represent pure states, it corresponds to a probability, namely the absolute square of the overlap of the two states. In the theoretical framework of this chapter, it furthermore allows for an easy calculation of the encountered fidelities, for example by making use of the chaining property [2]. The operation- (or gate-) fidelity can be derived from Eq. (7.9): Let $\mathcal{E}$ be a quantum operation describing a quantum circuit where decoherence is taken into account, and $\mathcal{E}_0$ the same operation without decoherence. We define the operation fidelity by

$$F(\mathcal{E}_0, \mathcal{E}) = \min_{\varrho} f(\mathcal{E}_0(\varrho), \mathcal{E}(\varrho)) , \tag{7.10}$$

where it is sufficient to minimise over pure input states ϱ [2].

Let us first consider the state transfer from the atom to the DFS qubit (Fig. 7.3). To minimise decoherence effects, the $R_L^x(\pi/2)$ and $R_L^x(-\pi/2)$ gates are applied before the auxiliary atom interacts with the DFS qubit and after the measurement, respectively. In addition, we neglect decoherence during the $R^x(-\pi/2)$ rotation since the time to perform such a gate on one atom is, in general, much smaller than the expected decoherence time $1/\gamma$, see Sec. 7.3.4. Thus, decoherence occurs mainly during the CPHASE gate. We examined the dynamics of the system during the application of the CPHASE gate by solving Eq. (7.8) analytically. The resulting gate fidelity for the CPHASE operation is given by

$$F_{\mathrm{CPHASE}}(\mathcal{E}_0, \mathcal{E}) = \frac{1 + \mathrm{e}^{-\gamma t}}{2} \geq 1 - \frac{\gamma t}{2}\,. \tag{7.11}$$

As will be discussed in Sec. 7.3.4, this behaviour is sufficient to ensure a working repeater scheme.

Note that, since unitary operations do not change the fidelity of the circuits [2], all operations which only involve one CPHASE gate have the same fidelity given in Eq. (7.11). This includes particularly the operations shown in Figs. 7.4 and 7.6.

In a similar way we calculated the fidelity of the CNOT gate between the two DFS qubits (Fig. 7.5). Again, all $R_L^{(x,z)}$ gates are applied before the auxiliary atom interacts with the DFS qubit and after the measurement, respectively. During these periods the auxiliary atom is not entangled with either DFS qubit and thus its decoherence has no influence on them. Furthermore, we assume again that decoherence during the $R^{(x,z)}$ rotations can be neglected. The gate fidelity of the CNOT operation is then given by

$$F_{\mathrm{CNOT}}(\mathcal{E}_0, \mathcal{E}) = \left(\frac{1 + \mathrm{e}^{-\gamma t}}{2}\right)^2 \geq 1 - \gamma t\,, \tag{7.12}$$

where t is the time which is needed to perform *one* CPHASE gate. Since the two DFS qubits are not entangled before the CNOT gate is applied it is sufficient to use only pure, unentangled states for the minimisation [2]. The fidelity for a CPHASE gate between two DFS qubits is the same as for the CNOT gate because they differ only by unitary operations. As in the case of the CPHASE gate, the decay of the CNOT fidelity is slow enough to ensure a working quantum repeater, see Sec. 7.3.4.

The fidelity of the state transfer between two DFS qubits described in Sec. 7.2.1.5 can also be calculated by explicitly solving the time evolution. The state transfer fidelity F_{ST} is given by

$$F_{\mathrm{ST}}(\mathcal{E}_0, \mathcal{E}) = \frac{1}{4}\left(1 + \mathrm{e}^{-2\gamma t}\right)\left(1 + \mathrm{e}^{-\gamma t}\right) \geq 1 - \frac{3}{2}\gamma t\,. \tag{7.13}$$

The fidelity of the entanglement purification using pairs of DFS qubits, see

Sec. 7.2.1.5, is calculated using the chaining property for fidelity measures [2]. Assuming that the two DFS qubits on one side A or B are not entangled with each other we find as a lower bound

$$F_{\mathrm{EP}}(\mathcal{E}_0, \mathcal{E}) \geq 1 - \left(\frac{3}{2} + \sqrt{2}\right) \gamma t \,. \tag{7.14}$$

In both formulas, Eqs. (7.13) and (7.14), the time t is again the time needed for performing *one* CPHASE gate. As we will show in Sec 7.3.4 all of these infidelities are small for typical experimental decoherence times.

In summary, we have shown in this section that the DFS quantum repeater can be divided into simple modules, which require (apart from single qubit rotations and measurements of an ancilla atom which can be realised by standard methods) merely the operations $R_L^x(\pm\frac{\pi}{2})$, $R_L^x(\pm\pi)$, $R_L^z(\pm\frac{\pi}{2})$, $R_L^z(\pi)$, and a CPHASE gate on a DFS qubit with the ancilla atom as control qubit. In the following section we proceed by describing how these basic operations can be implemented in systems of trapped neutral atoms.

7.3 Physical implementation in arrays of dipole traps

The physical system we consider for the implementation of a DFS qubit is a one-dimensional chain of four atoms in an array of optical dipole traps, e.g., an optical lattice [277] with one atom per site. Each of the atoms has two long-lived internal states a and b, which encode a physical qubit $\hat{a}^\dagger |\mathrm{vac}\rangle \equiv |0\rangle$, $\hat{b}^\dagger |\mathrm{vac}\rangle \equiv |1\rangle$. In Fig. 7.7 two DFS qubits are schematically shown. The thick, diagonal line represents an optical conveyor belt [42] storing the auxiliary atom. This atom can be transported to the DFS strings where it occupies an empty site between the third and the fourth atom, which is necessary for the CPHASE operations described in Sec. 7.2. Aside from this, the auxiliary atom is needed for the state transfer of the flying qubit to the DFS qubit: The flying qubits in our repeater scheme are represented by entangled photon pairs. After a photon arrives at a repeater node its state is transferred to the auxiliary atom, e.g., by a cavity-enhanced interaction [271, 272]. The atom is then moved to the DFS qubit and the operation shown in Fig. 7.3 is performed. In order to implement the rotations on the DFS qubits we also have to be able to selectively lower lattice barriers between certain lattice sites. This can be done by using suitable superlattices or by applying single laser pulses as described in [263]. The addressability of single atoms is only required for the initialisation of the register, cf. Sec. 7.3.1.

The general Hamiltonian for a one-dimensional atom chain for M lattice sites

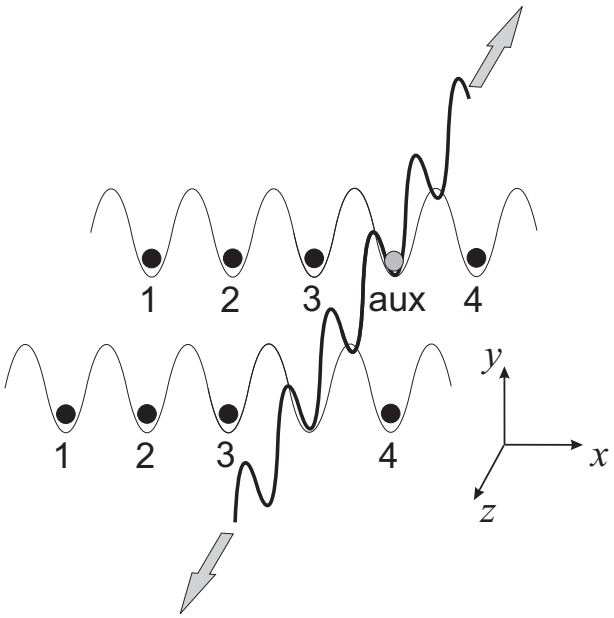

Figure 7.7. Schematic picture of a repeater node. The four register atoms per qubit (black circles) are stored in a one-dimensional array of dipole traps, e.g., an optical lattice. Between the third and fourth atom there is a free lattice site in which the auxiliary atom (grey) can be moved, e.g., via an optical conveyor belt.

(without auxiliary atom) is given by [17]

$$\begin{aligned}\hat{H} = &\sum_{j=1}^{M-1}\left(-J_j^{(a)}\hat{a}_j^\dagger\hat{a}_{j+1} - J_j^{(b)}\hat{b}_j^\dagger\hat{b}_{j+1} + \text{h.c.}\right)\\ &+\sum_{j=1}^{M}\left(\frac{U_a}{2}\hat{a}_j^\dagger\hat{a}_j^\dagger\hat{a}_j\hat{a}_j + \frac{U_b}{2}\hat{b}_j^\dagger\hat{b}_j^\dagger\hat{b}_j\hat{b}_j + U_{ab}\hat{a}_j^\dagger\hat{a}_j\hat{b}_j^\dagger\hat{b}_j\right),\end{aligned} \tag{7.15}$$

where $J_j^{(\alpha)}$ are state dependent hopping matrix elements from site j to site $j+1$ and $U_{a,b}$, U_{ab} are state dependent on-site interaction strengths. We should mention that for the rotations R_{L}^x and R_{L}^z and for the CPHASE gate the hopping constants for both kinds of atoms are required to be the same, $J_j^{(a)} = J_j^{(b)}$, as well as $U_a = U_b = U_{ab}$, cf. also Appendix 7.A. Apart from the initialisation of the register we need $M = 5$ lattice sites.

In the following subsections we will show how the register can be prepared in state $|0\rangle_{\mathrm{L}}$ and how the rotations $R_{\mathrm{L}}^{(x,z)}$ and the CPHASE gate can be implemented. These three ingredients are sufficient to realise the repeater protocol.

7.3.1 Initialisation of state $|0\rangle_{\mathrm{L}}$

The preparation of state $|0\rangle_{\mathrm{L}}$ requires the creation of a pair of singlet states $(|01\rangle - |10\rangle)/\sqrt{2}$. These states are decoupled from global operations but can be realised by local operations and by selectively lowering the potential barriers between neighbouring atoms. Starting from the product state $|0110\rangle$, the potential barrier between the first and second atom and between the third and fourth atom are lowered, e.g. via a superlattice potential. This generates two double well type potentials. The parameters of the Hamiltonian Eq. (7.15) are then given by

$$J_2 = 0,\ J_{1,3}^{(a)} = J_{1,3}^{(b)} = J,\ U_a = U_b = U_{ab} = U\,. \tag{7.16}$$

Assuming that J/U is sufficiently small (see also Sec. 7.3.2), states with two atoms in one site can be adiabatically eliminated leading to an effective Hamiltonian [24] of the form

$$H_{\mathrm{ini}} = -\frac{J^2}{U}(\sigma_1^x\sigma_2^x + \sigma_1^y\sigma_2^y + \sigma_1^z\sigma_2^z + \sigma_3^x\sigma_4^x + \sigma_3^y\sigma_4^y + \sigma_3^z\sigma_4^z)\,. \tag{7.17}$$

Turning this Hamiltonian on for a time $t = \pi\hbar U/8J^2$ we obtain the state $(|01\rangle + \mathrm{i}\,|10\rangle) \otimes (|10\rangle + \mathrm{i}\,|01\rangle)/2$. Finally, a local operation on the first and fourth physical qubit of the form $\exp(-\mathrm{i}\pi\sigma_1^z/4)$ and $\exp(-\mathrm{i}\pi\sigma_4^z/4)$, respectively, yields the desired product of singlet states. Alternatively, methods proposed in [300] can be used to realise the state $(|01\rangle + |10\rangle) \otimes (|10\rangle + |01\rangle)/2$. Local single qubit rotations of the first and fourth qubit can be used to bring this state into the desired from. If laser addressing of single physical qubits in adjacent lattice sites is not possible we can move the first and the fourth atom into their neighbouring, free sites (and back again) by lowering the corresponding potential barriers.

In order to write information into the register we require a free lattice site between the third and fourth atom. Hence, in a last step the fourth atom is moved into the fifth lattice site by lowering the potential barrier between the fourth and fifth site.

7.3.2 Rotations of the logical qubit

In this section we analytically investigate how to implement the rotations R_{L}^x and R_{L}^z in the two limiting cases of a very high interaction between the register atoms and a vanishing interaction. The system is simulated numerically to check our results.

7.3.2.1 Analytical treatment

The Hamiltonian H_Z is, apart from a sign, equivalent to a swap of the first two atoms V_{12} [see Eq. (7.4)]. If we assume high potential barriers between the second,

the third, and the fourth atom, i.e., $J_2^{(a,b)} = J_3^{(a,b)} = 0$, such that these atoms form a separate, decoupled system, we only have to describe the dynamics of the first and the second atom. If we further assume that $U_{a,b}, U_{ab}$ are much larger than the hopping terms $J_j^{(a,b)}$, we can adiabatically eliminate all states with more than one atom in a lattice site. By choosing the parameters according to

$$J_1^{(a)} = J_1^{(b)} = J, \tag{7.18}$$

$$U_a = U_b = U_{ab} = U, \tag{7.19}$$

we arrive at the effective Hamiltonian

$$\begin{aligned} H_Z &= -\frac{J^2}{U}\left(\sigma_1^x\sigma_2^x + \sigma_1^y\sigma_2^y + \sigma_1^z\sigma_2^z + \mathbf{1}_{12}\right) \\ &= -\frac{2J^2}{U}V_{12} = \frac{2J^2}{U}Z_{\mathrm{L}}\,, \end{aligned} \tag{7.20}$$

where we omitted a constant term. The time evolution of the system then generates the rotation

$$R_{\mathrm{L}}^z(\theta) = \exp\left(-\mathrm{i}\frac{\theta}{2}Z_{\mathrm{L}}\right)\,, \tag{7.21}$$

where $\theta = 4J^2t/U\hbar$. Hence, the time for an $R_{\mathrm{L}}^z(\pi)$-rotation is given by $t = \pi U\hbar/4J^2$. As an example we consider Na atoms in an optical lattice with a wavelength of $\lambda = 514$nm. The height of the transverse potential barriers are assumed to be $V_y = V_z = 50E_{\mathrm{R}}$, which is in the range of today's experiments [280]. Here, $E_{\mathrm{R}} = \hbar^2(2\pi)^2/2m\lambda^2$ is the recoil energy and m is the mass of the atoms. If we increase the s-wave scattering length by a factor of 5 using a Feshbach resonance and choose $V_x = 7.7E_{\mathrm{R}}$ between the first and second lattice site we get a ratio $U/J = 75$, which is well in the regime where the adiabatic elimination is valid, as will be discussed in more detail below. Note that for these parameters the assumptions for the validity of the Bose-Hubbard Hamiltonian Eq. (7.15) are fulfilled. The hopping term is then calculated to be $J = 0.033E_{\mathrm{R}}$, which results in an operation time of $t = 8.7$ms for the $R_{\mathrm{L}}^z(\pi)$-rotation. We emphasise that we never leave the DFS during the rotation and it is expected that this time is much shorter than the decoherence time of the DFS qubit.

Nevertheless, the time for an $R_{\mathrm{L}}^z(\pi)$-rotation can be made considerably shorter by tuning the interaction between the register atoms to zero (e.g., via a Feshbach resonance). As we show in Appendix 7.B, the qubits still remain in the DFS for all times. In this interaction-free case, the exact dynamics of the two atom system (i.e., without adiabatic elimination) results after a time $t = \pi\hbar/2J$ in the mapping

$$|\alpha,\beta\rangle_{12} \rightarrow -\,|\beta,\alpha\rangle_{12}\;,\; \alpha,\beta = 0,1\,. \tag{7.22}$$

Up to a global phase this is equivalent to an $R_{\mathrm{L}}^z(\pi)$-rotation on the logical qubits.

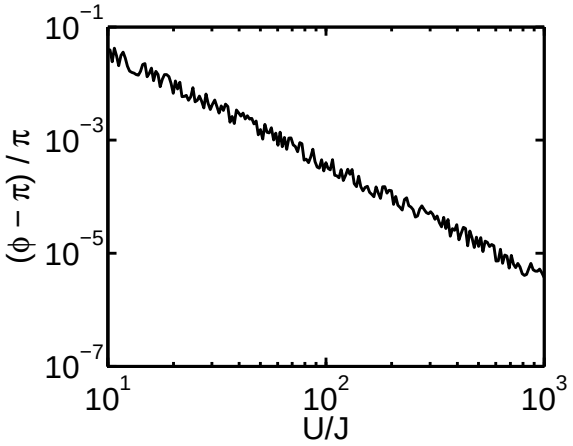

Figure 7.8. Numerical studies of the phase difference ϕ between states $|0\rangle_{\mathrm{L}}$ and $|1\rangle_{\mathrm{L}}$ after applying the rotation $R^z_{\mathrm{L}}(\pi)$ versus the ratio U/J calculated with the full Hamiltonian Eq. (7.15) and the parameters Eqs. (7.18) and (7.19) given by adiabatic elimination.

The time needed for a lattice as above is $t = 0.23$ms. The disadvantage of this scheme is that only rotations with a phase of π can be performed.

According to Eq. (7.3) the implementation of H_X involves three atoms. In the same spirit as for the Z_{L}-gate we require that the potential barrier between the third and fourth lattice site is high, i.e., $J_3^{(a,b)} = 0$. By choosing the remaining parameters as

$$J_2^{(a)} = \sqrt{2}J_1^{(a)} = \sqrt{2}J_1^{(b)} = J_2^{(b)} \equiv \sqrt{2}J\,, \tag{7.23}$$

$$U_a = U_b = U_{ab} = U\,, \tag{7.24}$$

and requiring that $J/U \ll 1$, we again adiabatically eliminate all states with more than one atom in one well. A detailed calculation is given in Appendix 7.A. The resulting Hamiltonian on the logical qubits is then given by

$$H_X = -\frac{2\sqrt{3}J^2}{U}X_{\mathrm{L}}\,, \tag{7.25}$$

where we omitted a constant term. This Hamiltonian generates a rotation

$$R^x_{\mathrm{L}}(\theta) = \exp\left(-\mathrm{i}\frac{\theta}{2}X_{\mathrm{L}}\right)\,, \tag{7.26}$$

where $\theta = -4\sqrt{3}J^2t/U\hbar$. Taking the numbers of the above example, the time required for an $R^x_{\mathrm{L}}(-\pi)$ rotation is $t = 5.0$ms.

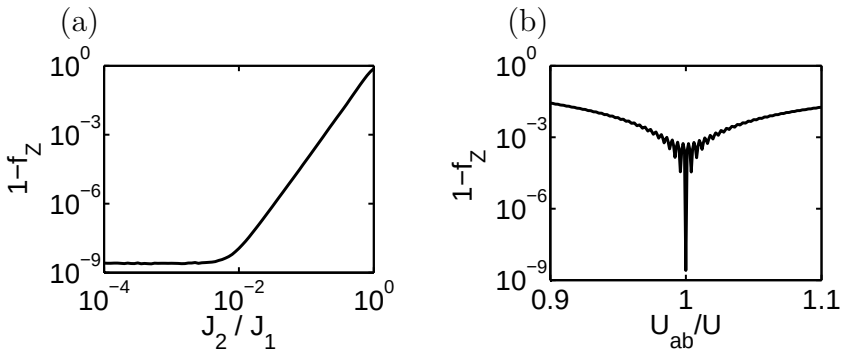

Figure 7.9. Fidelity Eq. (7.27) for the rotation $R^z_{\mathrm{L}}(\pi)$. In (a) the hopping term between the second and third atom is detuned, in (b) the interaction between register atoms of kind a and b. The other parameters are (a) $U_{a,b} = U_{ab} = 100J_1$, (b) $U_{a,b} = U = 100J$.

7.3.2.2 Numerical simulation

To test the validity of the adiabatic elimination we simulated the system numerically. For R^z_{L}-rotations the parameters of the exact Hamiltonian Eq. (7.15) are chosen according to Eqs. (7.18)-(7.19). We numerically calculated the fidelity of the DFS qubit remaining in its state during an R^z_{L}-rotation,

$$f_Z \equiv |\, \langle l|_{\mathrm{L}} \exp(-\mathrm{i}H_Z t/\hbar)\, |l\rangle_{\mathrm{L}}\, |^2\,, \tag{7.27}$$

with $l = 0, 1$. For $U/J = 75$ it turns out that the infidelity $1 - f_Z$ is smaller than 3×10^{-3} for $l = 1$ and smaller than 10^{-9} for $l = 0$ during the whole duration of an $R^z_{\mathrm{L}}(2\pi)$-rotation.

Since this fidelity does not take the phase difference ϕ between states $|0\rangle_{\mathrm{L}}$ and $|1\rangle_{\mathrm{L}}$ into account, ϕ was calculated as well. In Fig. 7.8 the phase difference is shown for the rotation $R^z_{\mathrm{L}}(\pi)$. As expected, for increasing ratios U/J the phase difference gets closer to π. For $U/J \approx 75$ the inaccuracy of the achieved phase is already smaller than 10^{-3}, which shows that the adiabatic elimination is well justified.

From an experimental point of view it is also important to know what happens when some of the parameters are detuned. Some results are shown in Fig. 7.9. The error due to the nonvanishing hopping between the second and third lattice site J_2 is negligible as long as $J_2 < 10^{-2}J_1$. Because of this we have completely neglected the influence of the fourth register atom, which is not involved in these rotations. For a detuned interaction coefficient U_{ab} the infidelity changes quite quickly if U_{ab}/U differs from 1, but still remains smaller than 10^{-3} as long as the detuning is less than 2%.

The fidelity Eq. (7.27) and the phase difference ϕ between the logical qubit for the faster scheme of a $R^z_{\mathrm{L}}(\pi)$-rotation for small, residual interactions U/J (in the

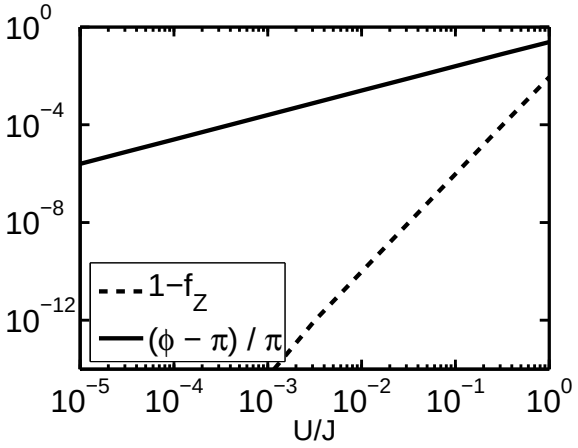

Figure 7.10. Numerical studies for a fast rotation with no or only weak interaction between the atoms. The fidelity Eq. (7.27) of the rotation $R^z_{\mathrm{L}}(\pi)$ and the phase difference between the two logical qubits after this rotation versus the ratio U/J is calculated with the full Hamiltonian Eq. (7.15). The accuracy of the gate gets better with a smaller interaction U between the atoms. Note that here no adiabatic elimination has been used.

ideal case this interaction is vanishing) are shown in Fig. 7.10. For this case the inaccuracy of the gate decreases with decreasing U/J and is smaller than 2×10^{-3} for $U/J \approx 10^{-2}$. The error calculated according to Eq. (7.27) is orders of magnitudes smaller than the phase inaccuracy.

The simulations of the R^x_{L}-rotations lead to similar numbers. The fidelity of this process, determined by

$$f_X \equiv |\, \langle 0|_{\mathrm{L}} \exp(-\mathrm{i}H_X t/\hbar)\, |1\rangle_{\mathrm{L}}\, |^2, \tag{7.28}$$

is shown in Fig. 7.11 depending on the ratio U/J. As can be seen from this figure, the infidelity $1 - f_X$ decreases with increasing ratio of U/J and for $U/J \approx 75$ the infidelity is smaller than 10^{-3}. Any infidelities caused by a change of the relative phases between the two logical states are orders of magnitudes smaller and do not play any role.

Figure 7.12 shows the results of numerical simulations if various system parameters are detuned. For the case of a nonideal hopping the deviation should be smaller than 1.5% to yield infidelities smaller than 3×10^{-3}. A slight detuning in the interaction strength is less critical, but should nevertheless be smaller than 4% to achieve small errors.

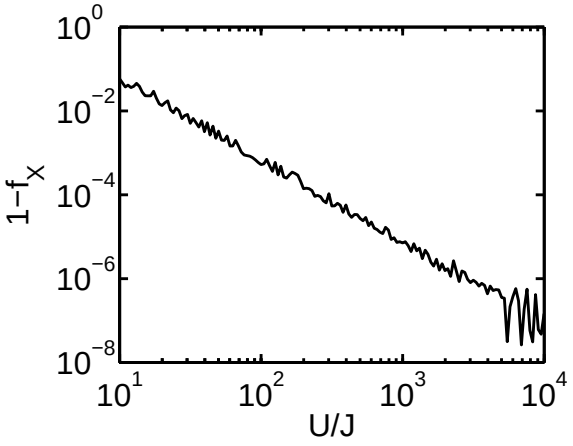

Figure 7.11. Numerical studies of the fidelity Eq. (7.28) of the rotation $R^x_{\mathrm{L}}(\pi)$ versus the ratio U/J calculated with the full Hamiltonian Eq. (7.15) and the parameters Eqs. (7.23) and (7.24) given by adiabatic elimination.

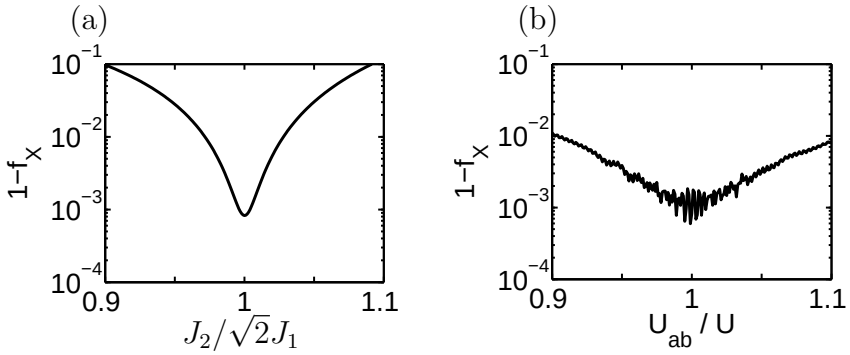

Figure 7.12. Fidelity Eq. (7.28) for the rotation $R^x_{\mathrm{L}}(\pi)$. In (a) the hopping term between the second and third atom is detuned, in (b) the interaction between register atoms of kind a and b. The other parameters are (a) $U_{a,b} = U_{ab} = 100J_1$, (b) $U_{a,b} = U = 100J$.

7.3.3 Controlled phase gate

The CPHASE gate can be realised by a controlled swap operation between the third and the fourth atom since, as mentioned in Sec. 7.2.1.1, $Z_{\mathrm{L}} = -V_{34}$. We assume that the potential barriers between the first, second, and third atom of the DFS qubit are high enough to ignore the dynamics of the first two atoms. The auxiliary atom is assumed to be distinguishable from the DFS atoms and is confined in a sufficiently deep lattice such that it always remains at its site. If the auxiliary atom is moved to the free site of the DFS string (cf. Fig. 7.7) and if a

register atom tunnels into the site of the auxiliary they interact with each other according to the Hamiltonian

$$\hat{H}_{\mathrm{CPHASE}} = \hat{H} + \sum_{\sigma=0,1} U_\sigma^q \hat{a}_4^\dagger \hat{a}_4 \hat{q}_\sigma^\dagger \hat{q}_\sigma + U_\sigma^q \hat{b}_4^\dagger \hat{b}_4 \hat{q}_\sigma^\dagger \hat{q}_\sigma \,, \tag{7.29}$$

where $\hat{H}$ is the Hamiltonian given by Eq. (7.15), $\hat{q}_\sigma$ is the state-dependent annihilation operator of the auxiliary atom with q its internal state, and U_σ^q the interaction strength which is independent of the internal state of the DFS atoms. If the interaction U_0^q for state $|0\rangle_q$ of the auxiliary atom is very large compared to the hopping strength, the third or fourth register atoms cannot enter the lattice site of the auxiliary atom and hence they will remain in their sites. Numerical tests show that during the gate operation this still holds for an interaction strength of $U_0^q/J \approx 100$, where J is the hopping term of the register atoms. Under these circumstances the probability of finding the register in its original state is larger than $1 - 10^{-3}$. If the auxiliary atom is in the state $|1\rangle_q$ and $U_1^q = 0$, the existence of the auxiliary atom can be ignored and we only need to solve the dynamics of two register atoms in three lattice sites. A similar scheme has been discussed in [301, 302], where an electromagnetically induced transparency-like configuration was used to control the interaction strength. We will investigate in the following the two limiting cases of very large and vanishing interaction strength between the register atoms.

7.3.3.1 Large interaction between the register atoms

For the case of large U/J we calculate the fidelities of the swap operation,

$$f_{01} = |\langle 0\sigma 1|\,\mathcal{U}(t)\,|1\sigma 0\rangle|^2 \,, \tag{7.30}$$

$$f_{00} = f_{11} = |\langle 0\sigma 0|\,\mathcal{U}(t)\,|0\sigma 0\rangle|^2 \tag{7.31}$$

numerically, where t is the numerically obtained time for the CPHASE gate and $\mathcal{U}(t) = \exp(-\mathrm{i}\hat{H}_{\mathrm{CPHASE}} t/\hbar)$ is the time evolution operator corresponding to Hamiltonian Eq. (7.29). The states $|\alpha\sigma\beta\rangle\,,\ \alpha,\beta = 0,1$ denote the states of the third and the fourth DFS atom, $|\alpha\rangle$ and $|\beta\rangle$, and $|\sigma = 1\rangle$ is the internal state of the auxiliary atom, located in between the two DFS atoms. We choose $J^{(a,b)} = J$ and $U_{a,b} = U_{ab} = U$.

In Fig. 7.13a the fidelities Eqs. (7.30) and (7.31) are shown for a small but nonvanishing interaction U_1^q between the auxiliary atom and the register atoms for a ratio $U/J = 100$. As can be seen the infidelities are smaller than 10^{-3} as long as the interaction fulfills $U_1^q/J < 0.05$. A further numerical observation is that the value of f_{00} (f_{01}) for very small U_1^q/J gets smaller with increasing U/J.

The fidelities Eqs. (7.30) and (7.31) do not take into account the occurrence of

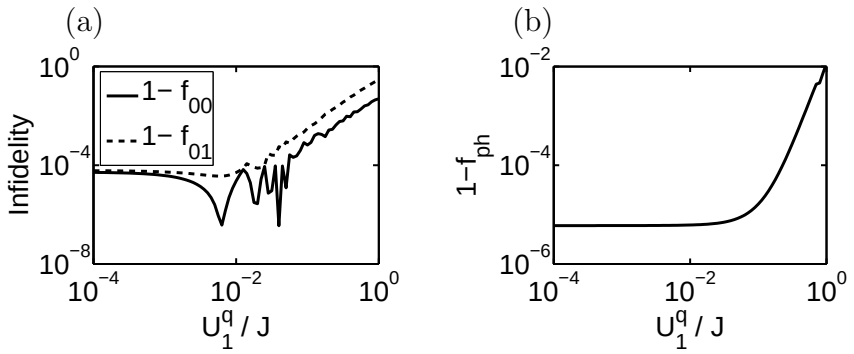

Figure 7.13. (a) Numerical results for the fidelities Eqs. (7.30) and (7.31), where the auxiliary atom has a nonvanishing rest interaction with the register atoms. (b) Numerical results for the fidelity Eq. (7.35) due to the phase difference, where the auxiliary atom has a nonvanishing rest interaction with the register atoms. In both cases we took for the register atoms $U/J = 100$.

phases. In general, the dynamics of the system will yield a phase,

$$|\alpha\sigma\beta\rangle \rightarrow \mathrm{e}^{\mathrm{i}\varphi_{\alpha\beta}} |\beta\sigma\alpha\rangle \tag{7.32}$$

with $\alpha, \beta = 0, 1$. Since the interactions U_σ^q do not depend on the state of the DFS atoms we have $\varphi_{01} = \varphi_{10}$ and $\varphi_{00} = \varphi_{11}$, and a nonvanishing U_1^q leads to the behaviour

$$\mathcal{U}(t) |0\rangle_{\mathrm{L}} = \mathrm{e}^{\mathrm{i}\varphi_{10}} |0\rangle_{\mathrm{L}} \,, \tag{7.33}$$

$$\mathcal{U}(t) |1\rangle_{\mathrm{L}} = \mathrm{e}^{\mathrm{i}\varphi_{10}} \frac{1}{2\sqrt{3}} [2(|1100\rangle + |0011\rangle) - \mathrm{e}^{\mathrm{i}\varphi}(|01\rangle + |10\rangle)^{\otimes 2}] \tag{7.34}$$

of the four DFS atoms, i.e., to the presence of a nonzero phase $\varphi \equiv \varphi_{00} - \varphi_{10}$. Thus the state $\mathcal{U}(t) |1\rangle_{\mathrm{L}}$ is not entirely contained in the DFS anymore. To study this error we define the fidelity

$$f_{\mathrm{ph}} = |\, \langle 1|_{\mathrm{L}} \mathcal{U}(t) |1\rangle_{\mathrm{L}} \,|^2 = \frac{5 + 4\cos\varphi}{9} \,, \tag{7.35}$$

which is shown in Fig. 7.13b depending on U_1^q/J. The infidelity $1 - f_{\mathrm{ph}}$ is typically one order of magnitude smaller than the infidelities shown in Fig. 7.13a.

The time that is needed to perform the swap gate has been calculated numerically. For a ratio of $U/J = 75$ and the same lattice parameters as for the R_{L}^z-rotations we get $t = 11.4$ms.

Numerical tests show that for the same ratio $U/J = 75$ the probability of finding the qubit outside the DFS is smaller than 5×10^{-4} during the whole gate operation

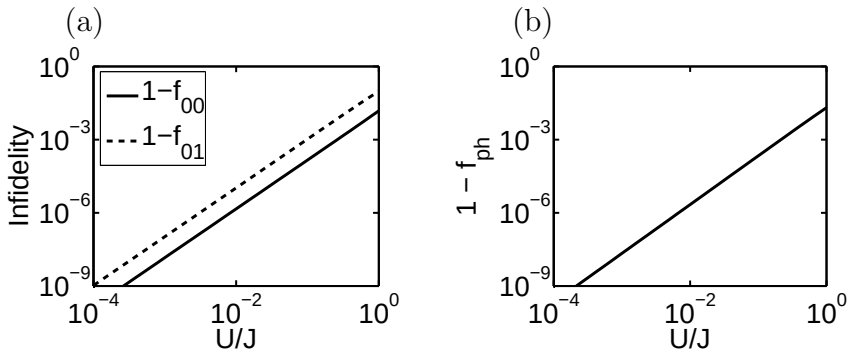

Figure 7.14. (a) Fidelity after evolving the state for a time $t = \pi\hbar/\sqrt{2}J$ for the case of noninteracting register atoms. (b) Fidelity Eq. (7.35) of state $|1\rangle_{\mathrm{L}}$ after the time evolution, where a perfect fidelity of the atom swap operation has been assumed and the error is only due to the phase difference, see text.

time.

7.3.3.2 No interaction between DFS atoms

A substantially shorter gate time can be achieved for the case of a vanishing interaction between the DFS atoms. In Appendix 7.B it is shown that the qubits still remain in the DFS during the gate operation. By analytically solving the time evolution of the Hamiltonian it can be shown (see also Appendix 7.B) that after a time $t = \pi\hbar/\sqrt{2}J$ the dynamics yields the mapping

$$|\alpha\sigma\beta\rangle \rightarrow |\beta\sigma\alpha\rangle \ , \alpha, \beta = 0, 1, \ \sigma = 1 \, , \tag{7.36}$$

which is a swap operation between the third and the fourth DFS atom and thus a CPHASE gate. For the same lattice potential as earlier with $V_x = 7.7E_{\mathrm{R}}$ the gate time is given by $t = 0.33$ms.

The results of numerical tests for a small rest interaction between the register atoms are shown in Fig. 7.14. Figure 7.14a shows the infidelities derived from Eqs. (7.30) and (7.31) and Fig. 7.14b shows the infidelity derived from Eq. (7.35), all depending on U/J. The fidelities are better than $1 - 10^{-3}$ for interactions $U/J < 0.05$. The results of numerical simulations for a nonvanishing rest interaction between the DFS atoms and a state $|1\rangle_q$ of the auxiliary atom yield an infidelity smaller that 3×10^{-3} for $U_1^q/J \leq 0.05$.

In conclusion, a reliable CPHASE gate can be implemented in both cases. If the auxiliary atom is in the state $|1\rangle_q$ and thus a swap of register atoms 3 and 4 should occur, the interaction U_1^q between the auxiliary atom and the register atoms is required to be smaller than $0.05J$. If the auxiliary atom is in the state $|0\rangle_q$ no

swap should occur. This holds during the gate interaction time for an interaction U_0^q larger than approximately $100J$. The difference of more than three orders of magnitude in the interaction can be achieved either by using a Feshbach resonance or by using an electromagnetically induced transparency scheme as in [301].

7.3.4 Gate times and decoherence

Recent experiments have demonstrated that the decoherence time of quantum information stored in DFSs can be increased by several orders of magnitudes compared to unprotected qubits. In the case of ion traps decoherence times of more than 7s have been reported [255] and although the DFS scheme in this experiment was different from ours we expect a similar improvement in the reliability of our quantum memory. The required storage time is found by adding the single qubit and CPHASE gate times calculated in previous sections. According to these the state transfer from the auxiliary atom to the DFS takes 11ms, neglecting the time that is needed to implement the rotation and measurement of the auxiliary atom. The entanglement purification module described in Fig. 7.4 takes 26ms, the CNOT operation of Fig. 7.5 takes 28ms. The necessary readout process of the DFS qubits takes 11ms. In comparison to these times the additional operations in steps (i), (ii), and (iii) of Fig. 7.1 are expected to contribute a negligible amount of extra time to the overall scheme [271, 272, 292–296]. All these times are very short compared to the expected decoherence time of the DFS qubit. Since the system remains in the DFS during the entire single qubit operations we conclude that decoherence of the DFS qubits plays only a minor role.

However, in the modules which involve a CPHASE gate between the auxiliary qubit and a DFS qubit the decoherence of the auxiliary atom has to be taken into account since, in general, it gets entangled with the DFS qubit thus lowering the overall fidelity. As discussed in Sec. 7.2.2 the fidelity for, e.g., the CNOT gate is better than $1 - \gamma t$, where γ is the inverse decoherence time and t is the time to perform a CPHASE gate. In our fastest example (without interaction between register atoms) a CPHASE gate takes approximately 0.33ms. In Ref. [297] decoherence times of 146ms for ~ 50 Cs atoms stored in a red-detuned standing wave have been reported. In the experiment presented in Ref. [43] the influence of a moving conveyor belt is investigated. It is found that the transport procedure decreases the coherence time by approximately a factor of 2. This would still be long enough for our purposes. For the entanglement purification module, which has the worst fidelity of all our models, the influence of the auxiliary atom leads to a fidelity of better than 98.7%. For the other modules the fidelity due to decoherence of the auxiliary atom is better than 99%. Using a blue-detuned trap could give further considerable increase of the decoherence time. Aside from this, it should be emphasised that all these times have been measured for many atoms in a trap. In the case of single atoms longer decoherence times can be expected. Thus, the

influence of the auxiliary atom on the modules described in Sec. 7.2.1 is small and only slightly decreases their fidelity.

7.4 Conclusion

In this chapter we developed a scheme for the robust implementation of a quantum repeater. The qubits at the repeater nodes are encoded in a DFS, which increases the decoherence time of the quantum memory considerably and thus improves the reliability of the scheme. We showed that the quantum repeater can be divided into simple modules whose implementation only requires a small number of different quantum gate operations. The single qubit gates can be realised by selectively lowering potential barriers between the atoms without ever leaving the DFS. Controlled operations are mediated by a single auxiliary qubit, which is not decoherence free. However, the influence of this qubit on the gate fidelities was thoroughly investigated and shown to be sufficiently small as not to significantly affect the quality of the repeater scheme.

Furthermore, we presented proposals for implementing the DFS qubits and all necessary operations in systems of neutral atoms trapped in arrays of optical dipole traps. The times for implementing these gates were calculated and shown to be much smaller than the expected decoherence time of the DFS qubits. Numerical examinations have shown that the achieved gate fidelities can be better than 98.7% and that the gate operations are stable against possible, small deviations of the system parameters.

Our scheme is extendable to general purpose quantum computing with DFS qubits, since the elementary one-qubit rotations R^x_{L}, R^z_{L} and a two-qubit gate, which together form a universal set of gates, can be realised. However, during the CPHASE gate the DFS is left. This effect is very small for our quantum repeater scheme and the influence of leaving the DFS in other applications as well as the scalability of the scheme is the subject of further investigations.

Recent experiments have demonstrated that it is possible to implement and control quantum registers with a few atoms in optical lattices [35] or dipole trap arrays [282] and that the decoherence times of the auxiliary atom are long enough to ensure a successful operation of our scheme [43, 297]. The experimental combination of atom registers and optical conveyor belts is also planned [35]. Hence we are confident that the presented scheme can be implemented with current and near future experimental techniques.

7.A Adiabatic elimination for the X_{L}-gate

The derivation of Hamiltonian H_X, Eq. (7.25), is given in more detail. The starting point is the Hamiltonian Eq. (7.15) for three atoms in three lattice sites. Since the

number of atoms in state a and b is conserved the states decouple in two subspaces where the first one contains only states with one atom in state a and two atoms in state b and the other one contains two atoms in state a and one atom in state b. The states with three atoms in the same internal state do not occur in our system. For simplicity we only consider the second subset, the results for the other subset can be derived in the same way.

Let Q be the projection operator on all states with more than one atom in a lattice site, $P = \mathbf{1} - Q$. The Hamiltonian after adiabatic elimination in first order perturbation theory is given by

$$\hat{H}_{\text{eff}} = \lim_{\varepsilon \to 0} P\hat{H}P - P\hat{H}Q(Q\hat{H}Q + \varepsilon\mathbf{1})^{-1}Q\hat{H}P\,. \tag{7.37}$$

The inversion of $Q\hat{H}Q + \varepsilon\mathbf{1}$ was calculated up to first order in the perturbation parameter J/U since in this treatment higher orders of J/U are neglected anyway. In the basis $\{|100\rangle, |010\rangle, |001\rangle\}$ the adiabatically eliminated Hamiltonian has the form

$$\hat{H}_{\text{eff}} = \begin{pmatrix} f_1 & g_1 & 0 \\ g_1 & f_2 & g_2 \\ 0 & g_2 & f_3 \end{pmatrix} \tag{7.38}$$

with

$$f_1 = -\frac{U_a\left((J_1^{(a)})^2 + (J_1^{(b)})^2\right) + 4U_{ab}(J_2^{(a)})^2}{U_a U_{ab}}\,, \tag{7.39}$$

$$f_2 = -\frac{(J_1^{(a)})^2 + (J_2^{(a)})^2 + (J_1^{(b)})^2 + (J_2^{(b)})^2}{U_{ab}}\,, \tag{7.40}$$

$$f_3 = -\frac{U_a\left((J_2^{(a)})^2 + (J_2^{(b)})^2\right) + 4U_{ab}(J_1^{(a)})^2}{U_a U_{ab}}\,, \tag{7.41}$$

$$g_1 = -2\frac{J_1^{(a)} J_1^{(b)}}{U_{ab}}\,, \qquad g_2 = -2\frac{J_2^{(a)} J_2^{(b)}}{U_{ab}}\,. \tag{7.42}$$

The action of this Hamiltonian on the logical qubits can be written in the form

$$\hat{H}_{\text{eff}}\,|0\rangle_{\text{L}} = u\,|0\rangle_{\text{L}} + v\,|1\rangle_{\text{L}}\,, \tag{7.43}$$

$$\hat{H}_{\text{eff}}\,|1\rangle_{\text{L}} = u\,|1\rangle_{\text{L}} + v\,|0\rangle_{\text{L}}\,. \tag{7.44}$$

Solving the corresponding equations for u and v one finds

$$u = f_2\,, \qquad v = \frac{\sqrt{3}}{2}g_2\,, \tag{7.45}$$

$$f_1 = f_2 + 2g_1\,, \qquad g_2 = 2g_1\,, \qquad f_3 = f_2 + g_1\,. \tag{7.46}$$

Because of the symmetry between the states with two atoms in state a and one in state b and vice versa the only physical solution for these equations is given by Eqs. (7.23) - (7.25).

7.B Qubits remain in the DFS

In this appendix we show that the DFS qubits remain decoherence free in the case without any interaction between the physical qubits, which is relevant for the fast $R^z_{\rm L}(\pi)$ rotation and the CPHASE gate. Since in this case there can be more than one atom in a lattice site we introduce Fock states $|n^1_a, n^1_b; n^2_a, n^2_b; ...; n^5_a, n^5_b\rangle$, where n^j_a (n^j_b) is the number of atoms in mode a (b) in lattice site $j = 1, ..., 5$, respectively.

The fast $R^z_{\rm L}(\pi)$ rotation can be performed by setting $U_{a,b} = U_{ab} = 0$, $J_2^{(a,b)} = J_3^{(a,b)} = J_4^{(a,b)} = 0$. In this case the corresponding time evolution operator $U(t) = \exp(-{\rm i}\hat{H}t/\hbar)$, where $\hat{H}$ is given by Eq. (7.15), can be calculated analytically and we get

$$U(t)\,|0\rangle_{\rm L} = |0\rangle_{\rm L}\ , \tag{7.47}$$

for all t and thus the system never leaves the DFS if it is in state $|0\rangle_{\rm L}$. The state $|1\rangle_{\rm L}$ evolves as

$$\begin{aligned} U(t)\,|1\rangle_{\rm L} &= \cos\left(\frac{2Jt}{\hbar}\right)|1\rangle_{\rm L} \\ &+ \frac{\rm i}{2\sqrt{3}}\sin\left(\frac{2Jt}{\hbar}\right)\Big\{\frac{2}{\sqrt{2}}\left[|0,2;0,0\rangle + |0,0;0,2\rangle\right]\otimes|1,0;0,0;1,0\rangle \\ &+ \frac{2}{\sqrt{2}}\left[|2,0;0,0\rangle + |0,0;2,0\rangle\right]\otimes|0,1;0,0;0,1\rangle \\ &- \left[|1,1;0,0\rangle + |0,0;1,1\rangle\right]\otimes\left[|1,0;0,0;0,1\rangle + |0,1;0,0;1,0\rangle\right]\Big\}. \end{aligned} \tag{7.48}$$

Clearly, the first term $\cos(2Jt/\hbar)\,|1\rangle_{\rm L}$ remains in the DFS. In order to see that this is also true for the second part we rewrite the states in first quantisation. Let $|\alpha\beta\rangle_A$ denote a state where the first atom is in state $|\alpha\rangle$ and the second one in state $|\beta\rangle$, independent in which lattice site they are stored. Due to symmetrisation we get

$$\frac{1}{\sqrt{2}}\left[|1,1;0,0\rangle + |0,0;1,1\rangle\right] \to \frac{1}{\sqrt{2}}\left[|01\rangle_A + |10\rangle_A\right]\ , \tag{7.49}$$

$$\frac{1}{\sqrt{2}}\left[|2,0;0,0\rangle + |0,0;2,0\rangle\right] \rightarrow |00\rangle_A \ , \tag{7.50}$$

$$\frac{1}{\sqrt{2}}\left[|0,2;0,0\rangle + |0,0;0,2\rangle\right] \rightarrow |11\rangle_A \ . \tag{7.51}$$

By rewriting Eq. (7.48) we get

$$\begin{aligned} U(t)\,|1\rangle_{\mathrm{L}} = \cos\left(\frac{2Jt}{\hbar}\right)|1\rangle_{\mathrm{L}} + \frac{\mathrm{i}}{2\sqrt{3}}\sin\left(\frac{2Jt}{\hbar}\right)\{2\,|11\rangle_A \otimes |00\rangle_A + 2\,|00\rangle_A \otimes |11\rangle_A \\ - \left[|01\rangle_A + |10\rangle_A\right] \otimes \left[|01\rangle_A + |10\rangle_A\right]\} \ . \end{aligned} \tag{7.52}$$

The part proportional to the sine function is again decoherence free, because it is just the state $|1\rangle_{\mathrm{L}}$.

The case of the CPHASE gate is more complicated because the atoms can hop into an additional lattice site. The time evolution of state $|1\rangle_{\mathrm{L}}$ is given by

$$\begin{aligned} U(t)\,|1\rangle_{\mathrm{L}} = {} & \left[|1,0;1,0\rangle + |0,1;0,1\rangle\right] \otimes \\ & \left\{\frac{1}{4}\left(3+\cos\left(\frac{2\sqrt{2}Jt}{\hbar}\right)\right)\left[|0,1;0,0;1,0\rangle + |1,0;0,0;0,1\rangle\right]\right. \\ & + \frac{\mathrm{i}}{2\sqrt{2}}\sin\left(\frac{2\sqrt{2}Jt}{\hbar}\right)\left[|0,0;0,1;1,0\rangle + \right. \\ & \qquad \left.|0,0;1,0;0,1\rangle + |0,1;1,0;0,0\rangle + |1,0;0,1;0,0\rangle\right] \\ & \left. - \frac{1}{2}\sin^2\left(\frac{\sqrt{2}Jt}{\hbar}\right)\left[|1,1;0,0;0,0\rangle + 2\,|0,0;1,1;0,0\rangle + |0,0;0,0;1,1\rangle\right]\right\} \\ & + |0,1;0,1\rangle \otimes \left\{\frac{1}{4}\left(3+\cos\left(\frac{2\sqrt{2}Jt}{\hbar}\right)\right)|1,0;0,0;1,0\rangle\right. \\ & + \frac{\mathrm{i}}{2\sqrt{2}}\sin\left(\frac{2\sqrt{2}Jt}{\hbar}\right)\left[|1,0;1,0;0,0\rangle + |0,0;1,0;1,0\rangle\right] \\ & \left. - \frac{1}{2\sqrt{2}}\sin^2\left(\frac{\sqrt{2}Jt}{\hbar}\right)\left[|2,0;0,0;0,0\rangle + 2\,|0,0;2,0;0,0\rangle + |0,0;0,0;2,0\rangle\right]\right\} \\ & + |1,0;1,0\rangle \otimes \left\{\frac{1}{4}\left(3+\cos\left(\frac{2\sqrt{2}Jt}{\hbar}\right)\right)|0,1;0,0;0,1\rangle\right. \\ & + \frac{\mathrm{i}}{2\sqrt{2}}\sin\left(\frac{2\sqrt{2}Jt}{\hbar}\right)\left[|0,1;0,1;0,0\rangle + |0,0;0,1;0,1\rangle\right] \\ & \left. - \frac{1}{2\sqrt{2}}\sin^2\left(\frac{\sqrt{2}Jt}{\hbar}\right)\left[|0,2;0,0;0,0\rangle + 2\,|0,0;0,2;0,0\rangle + |0,0;0,0;0,2\rangle\right]\right\} \ . \end{aligned} \tag{7.53}$$

For $|0\rangle_{\mathrm{L}}$ we get

$$\begin{aligned} U(t)\,|0\rangle_{\mathrm{L}} = {} & [|1,0;0,1\rangle - |0,1;1,0\rangle] \\ & \otimes \left\{ \cos\left(\frac{\sqrt{2}Jt}{\hbar}\right) [|1,0;0,0;0,1\rangle - |0,1;0,0;1,0\rangle] + \frac{\mathrm{i}}{\sqrt{2}} \sin\left(\frac{\sqrt{2}Jt}{\hbar}\right) \right. \\ & \left. [|1,0;0,1;0,0\rangle - |0,1;1,0;0,0\rangle + |0,0;1,0;0,1\rangle - |0,0;0,1;1,0\rangle] \right\}. \end{aligned} \tag{7.54}$$

Making analogous substitutions as above we see that these qubits are again decoherence free at all times.

Chapter 8

Publication

A quantum repeater based on decoherence free subspaces[1]

Uwe Dorner, Alexander Klein, and Dieter Jaksch

Clarendon Laboratory, University of Oxford, Parks Road, Oxford OX1 3PU, United Kingdom

Quant. Inf. Comp. **8**, 468 (2008).

We study a quantum repeater which is based on decoherence free quantum gates recently proposed by Klein *et al.* [Phys. Rev. A, **73**, 012332 (2006)]. A number of operations on the decoherence free subspace in this scheme makes use of an ancilla qubit, which undergoes dephasing and thus introduces decoherence to the system. We examine how this decoherence affects entanglement swapping and purification as well as the performance of a quantum repeater. We compare the decoherence free quantum repeater with a quantum repeater based on qubits that are subject to decoherence and show that it outperforms the latter when decoherence due to long waiting times of conventional qubits becomes significant. Thus, a quantum repeater based on decoherence free subspaces is a possibility to greatly improve quantum communication over long or even intercontinental distances.

8.1 Introduction

Quantum communication is one of the experimentally most advanced areas of quantum information processing and promises to yield commercial applications in the near future [211]. In addition to free space quantum communication, current setups mainly use photon transmission in optical fibres and the distances over which quantum cryptography is possible so far are in the range of up to about 100km [303]. However, quantum communication over longer distances is primarily limited by photon loss, which grows exponentially with the length of the fibre. A possible solution of this problem is the use of quantum repeaters [47, 49] to distribute maximally entangled pairs of qubits over long distances. These pairs can then be used

[1]Uwe Dorner took the leading role in writing the paper and is thus the first author. The results were found in close collaboration, where analytical expressions were mainly found by me and numerical implementations were mainly done by Dr Dorner.

for entanglement based quantum communication by teleporting [266] quantum information from one party to the other. The basic idea of a quantum repeater is to divide the transmission line into shorter segments with a length of the order of the attenuation length of the fibre. On each segment entangled particle pairs are created and by applying entanglement swapping [243] and purification protocols [47, 245, 246] entangled pairs of larger distances are produced. Successive application of these steps according to a nested repeater protocol [47] creates a distant qubit pair with high entanglement fidelity.

During the purification process the entanglement fidelity of a pair of qubits is successively increased by sacrificing auxiliary entangled pairs. In the present chapter we will use a purification protocol known as "entanglement pumping" [48]. From a practical point of view the use of entanglement pumping is favourable compared to other purification schemes [245, 246, 276] since it requires significantly fewer qubits and thus might be easier to implement. However, the decrease of physical resources comes at the cost of long operation times of the repeater during which quantum information has to be stored. These waiting times grow quickly with the distance of the two parties who desire to share an entangled state and if they are too long the stored quantum information will decohere to such a degree that the quantum repeater can not be successfully operated anymore. This problem was recently addressed by Hartmann *et al.* [50] (see also [304]), who examined the limitations of a quantum repeater (in terms of maximal distance) depending on the noise strength. A number of modifications of the repeater protocol have been proposed and it was shown that the maximal distance might be increased by an order of magnitude at the cost of a reasonable overhead of resources. Unlimited distances are only possible with the help of quantum error correction. However, this imposes very stringent error thresholds, which seem out of reach with present technology.

In this chapter we pursue the different and conceptually more straightforward strategy of improving the quality of the quantum memories at the repeater nodes. We study a repeater architecture based on a scheme recently proposed by Klein *et al.* [305], which relies on the concept of decoherence free subspaces (DFSs) [56–59]. DFSs are a method of passive error correction or error prevention and can significantly increase the lifetime of quantum information and reliability of quantum computing as already demonstrated in a number of experiments [252–255, 257–262]. In Ref. [305] a logical qubit at a repeater node is represented by two states of a decoherence free subspace of a Hilbert space consisting of four atomic qubits. The logical qubits are immune to collective noise thus greatly improving the lifetime of stored quantum information. However, gate operations become more complicated and slower than operations on "bare", unprotected atomic qubits. In fact the two qubit operation proposed in [305] is not decoherence free since an unprotected auxiliary qubit is used to mediate between two logical DFS qubits. In the present chapter we examine how this noise affects the performance of the quantum repeater

network and show that it is possible to create entangled pairs of high fidelity over intercontinental distances. We compare the results to a repeater based on unprotected qubits, i.e., qubits that are subject to decoherence, and show that it outperforms the latter when decoherence due to long waiting times becomes significant. Although we consider only the special case of a quantum repeater, we emphasise that the methods we employ are generally applicable to arbitrary quantum networks.

This chapter is organised as follows. In Sec. 8.2 we briefly review the quantum repeater protocol. In Sec. 8.3 we present the error model we use for quantum repeaters based on unprotected qubits and DFS qubits. In the same section we furthermore describe the quantum circuits necessary to implement the repeater. In Sec. 8.4 we present the results of simulations for both repeater setups. Finally we conclude in Sec. 8.5.

8.2 The quantum repeater

In this chapter we use the nested repeater protocol developed in [47, 48], which consists of a combination of entanglement purification and entanglement swapping. The goal is to create a highly entangled pair between two parties, say, A and B, which might be attempted by transmitting a photon through a fibre. However, unwanted noise will decrease the entanglement fidelity of the qubit pair monotonously with the distance between A and B. The fidelity can be increased again by applying purification procedures, in which additional entangled pairs between A and B are created and sacrificed in order to distill an entangled pair with high fidelity. However, if the distance between A and B is too large, the entanglement fidelity of the pairs can drop below a minimum value $f_{\min}$, which is required by the purification protocol to increase the entanglement fidelity [48]. To overcome this problem, a number of intermediate nodes N_i with sufficiently small distances l_0 are introduced between A and B, and entangled qubit pairs are prepared between each of the intermediate nodes such that the entanglement fidelity of each pair is greater than $f_{\min}$. These pairs can be purified and connected via entanglement swapping to create an entangled pair of larger distance. For the setup used in this chapter we consider purification via "entanglement pumping" [48], which requires considerably less qubits than other schemes [245, 246, 276] and is thus preferable from a practical point of view.

The principle of the nested repeater protocol is illustrated by the example shown in Fig. 8.1: Each bullet represents a qubit and the lines between them indicate entanglement. On repeater level 1 (indicated by the dashed box on the top left) two entangled qubit pairs between nodes A and N_1 and between nodes N_1 and N_2 are created in line (i). The two qubits at node N_1 are then connected via entanglement swapping, creating an entangled pair of qubits with larger distance,

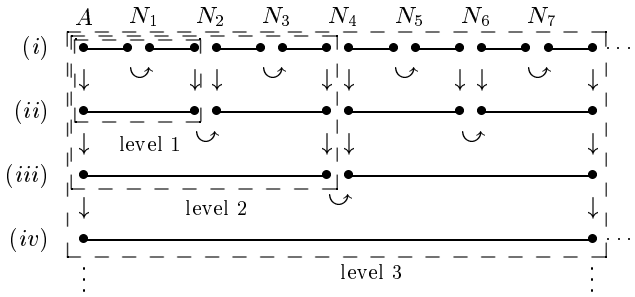

Figure 8.1. Illustration of the nested repeater protocol. For explanation see text.

indicated by the curved arrow. Within the schematic of Fig. 8.1 the state of this qubit pair is then transfered by a quantum operation to the qubit pair in line (ii). We then generate further entangled pairs in line (i), which are used to purify the pair in line (ii), indicated by vertical arrows. Given that l_0 is the distance between the nodes, the final pair will have a distance $2l_0$. Repeater level 2 consists of two adjacent level 1 repeaters, both of which create an entangled pair of distance $2l_0$ on line (ii). These two pairs are then connected, the resulting pair is transfered to line (iii) and subsequently produced pairs are used to purify the pair in line (iii), which has now a distance $4l_0$. Repeater level 3 is constructed in the same way: We use two level 2 repeaters which successively generate pairs in line (iii). After connecting them the resulting pair is transfered to line (iv), and subsequently produced pairs are used to purify the pair with distance $8l_0$ in line (iv). In this example the distance between the entangled qubits is doubled with each further repeater level. In general, the number of entanglement swapping steps on each repeater level can vary from level to level and is adapted to the specific physical situation. The distance between entangled qubits on repeater level n is then given by

$$S_n \equiv l_0 \prod_{j=1}^{n} (L_j + 1) \tag{8.1}$$

for $n \geq 1$ and $S_0 = l_0$. The quantity L_j is the number of connections on level j immediately before the final qubit pair of this level is purified, i.e. in the example shown in Fig. 8.1 we have $L_1 = L_2 = L_3 = 1$. Thus, L_j is generally different from the total number of connections necessary to operate a level j repeater.

We note that in basically all quantum communication schemes flying qubits are represented by photons. For our setup we assume that the states of these photons are first transferred to stationary qubits (atoms) creating an entangled pair with entanglement fidelity f_0, which might be lower than the entanglement fidelity of the photon pair. We use this fidelity f_0 as the starting fidelity in all our discussions. We also note that the state transfer described above is not necessary if we do an

appropriate relabelling of the qubits. However, for reasons given in Sec. 8.4 we assume that this transfer is done via a quantum operation.

8.3 Error models

8.3.1 Error model for unprotected qubits

The error model we use in this chapter is motivated by realisations of quantum information processing with single atoms stored in tight traps [253, 254, 305]. In this scenario, qubits can be represented by two metastable states of atoms. The lifetime of these states is typically on the order of several minutes or longer, such that their spontaneous decay can be neglected [252–255, 297]. The major source of decoherence is then given by dephasing, represented by the σ_z-Pauli operator. Unitary single qubit operations necessary to manipulate the qubits can be realised by laser pulses and static magnetic or electric fields. It is thus easily possible to implement Hamiltonians which are proportional to Pauli operators such that the time evolution of the system corresponds to rotations around the x, y, and z axis of the Bloch sphere. For two qubit operations various schemes have been developed [219]. Here, we consider two qubit operations caused by an Ising interaction, which can be realised via the collisional interaction between neutral atoms stored in optical traps [285, 288].

8.3.1.1 Single qubit gates and measurements

We assume that the major source of noise is dephasing so that the time evolution of the system state ρ whilst applying a gate described by H_α^i on qubit i is determined by the master equation ($\hbar = 1$)

$$\dot{\rho} = -\mathrm{i}[H_\alpha^i, \rho] + \frac{\gamma}{2}(\sigma_z^i \rho \sigma_z^i - \rho)\,. \tag{8.2}$$

Here,

$$H_\alpha^i = \Omega_\alpha \sigma_\alpha^i, \tag{8.3}$$

where σ_α^i are the Pauli operators with $\alpha = 0, x, y, z$. In the case of $\alpha = 0$ we set $\sigma_0^i = \mathbf{1}$ so that the above master equation also describes the dephasing of a quantum channel or memory. For simplicity we furthermore assume that Ω_α is real and non-negative. For vanishing noise (i.e., $\gamma = 0$) the ith qubit undergoes a rotation around the x, y or z axis

$$\rho \to R_\alpha^i(\theta) \rho R_\alpha^i(\theta)^\dagger \quad \text{with} \quad R_\alpha^i(\theta) \equiv \mathrm{e}^{-\mathrm{i}\frac{\theta}{2}\sigma_\alpha^i}, \tag{8.4}$$

where the rotation angle is given by $\theta = 2\Omega_\alpha t$.

In the presence of dephasing (i.e., $\gamma \neq 0$) the solutions of Eq. (8.2) can be described by quantum operations $\mathcal{E}^i_\alpha$,

$$\rho \to \mathcal{E}^i_\alpha(\theta)[\rho] = \sum_k E^i_{\alpha,k} \rho \left(E^i_{\alpha,k}\right)^\dagger . \tag{8.5}$$

For $\alpha = 0$, i.e., if the commutator in Eq. (8.2) vanishes, the evolution of the density operator is given by

$$\rho \to \mathcal{E}^i_0(\gamma t)[\rho] = p_1(\gamma t)\rho + p_2(\gamma t)\sigma^i_z \rho \sigma^i_z, \tag{8.6}$$

where

$$p_1(\gamma t) = \frac{1}{2}\left(1 + \mathrm{e}^{-\gamma t}\right), \quad p_2(\gamma t) = \frac{1}{2}\left(1 - \mathrm{e}^{-\gamma t}\right). \tag{8.7}$$

Note that for $\alpha = z$ the noise operator σ^i_z commutes with H^i_z so that

$$\mathcal{E}^i_z(\theta)[\rho] = \mathcal{E}^i_0(\gamma t)[R_z(\theta)\rho R_z(\theta)^\dagger] = R_z(\theta)\mathcal{E}^i_0(\gamma t)[\rho]R_z(\theta)^\dagger, \tag{8.8}$$

i.e., the process can be replaced by a perfect rotation followed by noise in the channel, or vice versa. In the remainder of the present chapter we omit the superscript i whenever it is clear from the context (e.g. in quantum circuits) on which qubit the operation is acting on.

Non-ideal measurements are described in this chapter by the positive operator valued measure [48]

$$P_0 = \eta \left|0\right\rangle \left\langle 0\right| + (1-\eta)\left|1\right\rangle \left\langle 1\right| \tag{8.9}$$

$$P_1 = \eta \left|1\right\rangle \left\langle 1\right| + (1-\eta)\left|0\right\rangle \left\langle 0\right| \tag{8.10}$$

with $0 \leq \eta \leq 1$. The parameter η is the probability to obtain the correct result if a measurement is done in the $\{\left|0\right\rangle, \left|1\right\rangle\}$-basis.

8.3.1.2 Two qubit gates

We consider two qubit operations mediated by an Ising interaction. The dynamics of the system can thus be described by a master equation of the form

$$\dot{\rho} = -\mathrm{i}[\Omega_{zz}\sigma^i_z\sigma^j_z, \rho] + \frac{\gamma}{2}(\sigma^i_z\rho\sigma^i_z - \rho) + \frac{\gamma}{2}(\sigma^j_z\rho\sigma^j_z - \rho), \tag{8.11}$$

where we assume that the noise on qubit i and j is uncorrelated. Since the Ising Hamiltonian commutes with the noise operators σ^i_z, the time evolution is simply given by

$$\rho \to \mathcal{E}^{ij}_{zz}(\xi)[\rho] = \mathcal{E}^i_0(\gamma t)[\mathcal{E}^j_0(\gamma t)[\mathrm{e}^{-\mathrm{i}\frac{\xi}{2}\sigma^i_z\sigma^j_z}\rho\mathrm{e}^{\mathrm{i}\frac{\xi}{2}\sigma^i_z\sigma^j_z}]], \tag{8.12}$$

where $\xi = 2\Omega_{zz}t$. The order of the three distinct operations in the above equation is arbitrary. This means that $\mathcal{E}_{zz}^{ij}$ can, for example, be described by a perfect operation followed by dephasing in the quantum channels. An application of this

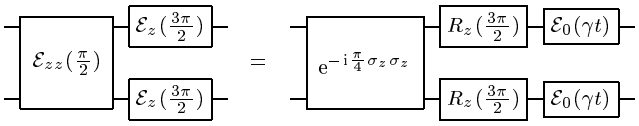

Figure 8.2. Controlled-Z operation, $\mathcal{Z}_{\downarrow}^{AA}$, on two unprotected qubits. The left circuit can be replaced by an effective circuit consisting of ideal gates followed by noise in the quantum channels. The time t is given by $t = \pi/4\Omega_{zz} + 3\pi/4\Omega_z$, which is the time needed to perform the noiseless gates.

fact is illustrated in Fig. 8.2, which shows the realisation of a noisy controlled-Z gate on two qubits. In the following figures we denote this gate as $\mathcal{Z}_{\downarrow}^{AA}$, the superscript indicating that the gate is acting on two unprotected (atomic) qubits. The subscript defines control and target qubit, i.e., in quantum circuits the arrowhead points to the target qubit. Strictly speaking this is not necessary since this gate is symmetric under qubit exchange. However, in later sections we use a similar notation for controlled-$(-Z)$ gates which are not symmetric.

8.3.1.3 Building blocks of the quantum repeater with unprotected qubits

As indicated in Sec. 8.2, three basic modules are needed to run the quantum repeater. In particular, these are the transfer of a state from one qubit to another one, entanglement swapping, and entanglement purification. In Figs. 8.3-8.5 we show possible implementations of these three blocks according to the error models and gate operations described in Secs. 8.3.1.1 and 8.3.1.2. In our simulations qubits that are measured are immediately removed from the system by tracing them out. The removal of a qubit is indicated by a Tr-symbol in the corresponding quantum circuits unless we perform measurements that classically control further operations. Furthermore, we assume for simplicity that $\Omega \equiv \Omega_x = \Omega_y = \Omega_z$.

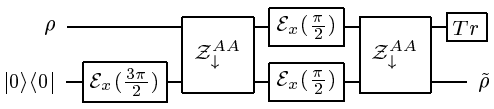

Figure 8.3. State transfer between two unprotected qubits. In the noiseless case the output state $\tilde{\rho}$ would be equal to the input state ρ.

Clearly, the partitioning of the three blocks into elementary gate operations is not unique and in the presence of noise different architectures can lead to different

fidelities. In our simulations we compared various possibilities, and the realisations shown in this article are the ones which led to the best results for the error models and corresponding error parameters we use, see Sec. 8.4. Moreover, in the case of a quantum repeater based on unprotected qubits, which is used for communication over long distances, the dominant source of noise is due to long waiting times during classical communications (see below and Ref. [50]) and the specific partitioning of the blocks becomes less important.

Apart from noise during gate operations, the quantum circuits shown in this section also include noise which is due to waiting times of qubits. Whenever it is unavoidable that a qubit has to wait until an operation on another qubit is finished or until a classical signal arrives it undergoes dephasing $\mathcal{E}_0$. Fig. 8.4 shows entanglement swapping between two entangled pairs $A-C_1$ and C_2-B of qubits. The goal is to teleport the state of qubit C_1 to qubit B by using the entanglement of the pair C_2-B. In a noiseless version of this circuit qubit A would be simply represented by a straight line, which is disconnected from the remaining qubits, and undergoes no operations (and thus it would normally be omitted in the circuit). However, in the presence of noise, it has to wait until the whole procedure is finished and undergoes dephasing during this time. On repeater level n we have to wait a time $t_{\mathrm{w}} = S_{n-1}/c$, where c is the speed of light, until the classical signal resulting from the measurement of qubits C_1 and C_2 arrives at qubit B. For large distances between qubits C_1, C_2 and B, i.e. on higher repeater levels, this waiting times will be quite long. For instance, taking $S_{n-1} = 1000$km yields a waiting time $t_{\mathrm{w}} \approx 3$ms, which is considerably larger than gate operation times of atomic qubits that are typically in the μs regime, see for instance [285, 306]. Realisations solely based on solid state systems such as electron spins in quantum dots would have even shorter gate operation times [307]. However, in the case of a quantum repeater this is of no advantage since in solid state systems coherence times are typically shorter than in atomic systems where it can exceed 100ms [43, 297]. Since the waiting times during classical communication necessary for entanglement swapping are independent of the implementation, solid state realisations would be less suitable.

If more than two qubit pairs are to be connected we can use a simultaneous entanglement swapping scheme. For example three entangled qubit pairs $A-C_1$, C_2-C_3 and C_4-B, can be transformed into one entangled qubit pair $A-B$ by teleporting the state of qubit C_2 to qubit A (using the entanglement of $A-C_1$) and by teleporting the state of qubit C_3 to qubit B (using the entanglement of C_4-B) at the same time. In general, a sequence of qubit pairs $A-C_1$, C_2-C_3, $\ldots$, $C_{2L_n}-B$ with L_n even can be transformed into a single entangled qubit pair $A-B$ by simultaneously teleporting the state of qubit C_{L_n} to C_{L_n-2} and the state of qubit C_{L_n+1} to C_{L_n+3} before C_{L_n-2} is teleported to C_{L_n-4} and C_{L_n+3} to C_{L_n+5} and so on. If L_n is odd we start by teleporting C_{L_n-1} to C_{L_n-3} and C_{L_n} to C_{L_n+2} before C_{L_n-3} is teleported to C_{L_n-5} and C_{L_n+2} to C_{L_n+4} and so on. This leads to two remaining entangled qubit pairs $A-C_{2L_n-1}$ and $C_{2L_n}-B$ which can be connected

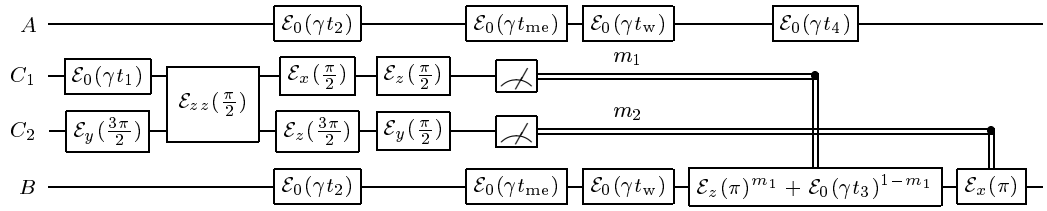

Figure 8.4. Entanglement swapping of qubit pairs $A - C_1$ and $C_2 - B$. The state of qubit C_1 is teleported to qubit B by using the entanglement of qubit pair $C_2 - B$ yielding an entangled pair $A - B$. The waiting times are given by $t_1 = 3\pi/4\Omega$, $t_2 = 5\pi/4\Omega + \pi/4\Omega_{zz}$ and $t_3 = \pi/2\Omega$. The value of t_4 depends on the outcome of the measurement of qubit C_2, given by $m_2 = 0, 1$. In particular we have $t_4 = \pi/\Omega$ if $m_2 = 1$ and $t_4 = \pi/2\Omega$ if $m_2 = 0$. The time $t_{\rm me}$ corresponds to the time necessary to perform a measurement and $t_{\rm w} = S_{n-1}/c$ is the classical communication time between qubits $C_{1,2}$ and qubit B where S_{n-1} is the distance between $C_{1,2}$ and B on repeater level n.

to a single pair $A - B$ via the procedure shown in Fig. 8.4. In total this method takes a time $\lceil L_n/2 \rceil (t_{\rm sw} + S_{n-1}/c)$ where $t_{\rm sw}$ is the time of the operation shown in Fig. 8.4 minus the classical communication time $t_{\rm w}$ and $\lceil . \rceil$ is the ceiling function.

Fig. 8.5 shows the quantum circuit for an entanglement purification step of a qubit pair. The circuit corresponds to the scheme proposed by Deutsch *et al.* [246], but here it is expressed in terms of operations which correspond to our gate and error model. We start with two entangled pairs $A_1 - B_1$ and $A_2 - B_2$ and sacrifice the pair $A_1 - B_1$ in order to get—whenever we obtain a coincidence in the measurements—a new pair $A_2' - B_2'$, which can have a higher entanglement fidelity than the pair $A_2 - B_2$. Whether the fidelity increases depends on the noise strength and the fidelity of the input pairs and will be discussed in Sec. 8.4. If we do not get coinciding measurement results the procedure fails and has to be repeated with a new set of pairs. The measurement result has to be classically exchanged between node A (the location of qubits $A_{1,2}$) and node B (the location of qubits $B_{1,2}$), which are a macroscopic distance apart from each other. This is indicated by the double wire connecting the two measurements in Fig. 8.5. The classical communication time is given by $t_{\rm w} = S_n/c$ and will thus be, as in the case of entanglement swapping, quite large on higher repeater levels leading to a significant dephasing of qubit A_2' and B_2'.

In addition to the already discussed waiting times during entanglement swapping and purification there will be further waiting times for entangled qubits during the repeater protocol: After an entangled pair on repeater level n is created we have to wait a certain time until a second pair is available that we can use for a purification step. In the following, we derive a lower bound for these waiting times.

On the lowest repeater level photons are sent to the repeater nodes and their

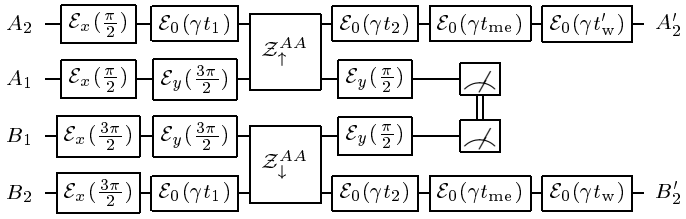

Figure 8.5. Quantum circuit for an entanglement purification step. The waiting times are given by $t_1 = 3t_2 = 3\pi/4\Omega$, $t_{\rm w} = S_n/c$, where S_n is the distance between the qubits $A_{1,2}$ and $B_{1,2}$ on repeater level n, $t_{\rm me}$ is the time required to perform a measurement and $t'_{\rm w} = t_{\rm w} + \pi/2\Omega$.

state is transfered to atomic qubits. The travelling time of the photons can be omitted since they can be triggered such that they arrive at the nodes just in time before a transfer is possible. After the transfer, which consumes a time t_0, entanglement swapping is performed L_1 times taking a total time $t'_0 = t_0 + \lceil L_1/2 \rceil (t_{\rm sw} + S_0/c)$, where we take $t_{\rm sw} = 9\pi/4\Omega + \pi/4\Omega_{zz} + t_{\rm me}$. The resulting state is then transfered to another qubit pair in a time $t_{\rm tr} = 5\pi/2\Omega + \pi/2\Omega_{zz}$. Only after this transfer is complete, it is possible to transfer photonic states to atomic qubits again and connect them. These pairs are then used to purify the pair previously generated, which takes a time $t_{\rm pur} = 5\pi/2\Omega + \pi/4\Omega_{zz} + t_{\rm me}$ for the operations and measurements, and a time S_1/c for the classical communication of the measurement outcome. During this communication, we can already start creating a subsequent pair necessary for purification, such that the second purification step can be started after a delay $t_{\rm pur} + \max(t'_0, S_1/c)$. The purification is performed K_1 times and thus the minimum time it takes to create a pair on repeater level 1 is given by

$$t_1 = t_{\rm tr} + t'_0 + K_1 \left[t_{\rm pur} + \max\left(t'_0\,,\, S_1/c\right) \right] . \tag{8.13}$$

During this process, the pairs on level 1 might have to wait until subsequent pairs for purification are created. After each purification step, this additional waiting time is given by $t_{\rm aw} = \max(0, t'_0 - S_1/c)$.

On higher levels, the minimum additional waiting time can be estimated as follows. In order to create a pair on level $n \geq 2$ one has to create $\prod_{m=2}^{n}(K_m + 1)$ times the pairs on level 1, which takes at least a time

$$t_n = t_1 \prod_{m=2}^{n} (K_m + 1). \tag{8.14}$$

However, while the pairs created on level $n-1$ are used to purify the pairs on level n, we can already start to prepare the pairs on level $n-2$, $n-3$, an so on. Hence, the minimum time the pairs on level n have to wait for the completion of the pairs

on level $n-1$ is given by

$$t_{n-1}^{\mathrm{c}} = \max\left\{0\,,\, t_{n-1} - \sum_{l=1}^{n-2} t_l\right\} \tag{8.15}$$

for $n \geq 2$ and $t_0^c = t_0$. The minimum additional waiting time after each purification and transfer step on level n is then given by

$$t_{\mathrm{aw}} = \max\left\{0\,,\, \lceil L_n/2\rceil(t_{\mathrm{sw}} + S_{n-1}/c) + t_{n-1}^{\mathrm{c}} - S_n/c\right\} \tag{8.16}$$

and

$$\tilde{t}_{\mathrm{aw}} = \lceil L_n/2\rceil(t_{\mathrm{sw}} + S_{n-1}/c) + t_{n-1}^{\mathrm{c}}\,, \tag{8.17}$$

respectively. Note that in Eq. (8.16) the waiting time $t_{\mathrm{w}} = S_n/c$ has been subtracted from the additional waiting time t_{aw}, since it is already included in the purification scheme, see Fig. 8.5.

Equation (8.14) can be used to estimate the operation time for the quantum repeater. It provides only a lower bound since it gives the time if the operation of the repeater was successful "in one go", i.e., if all involved purification steps have been successful. However, the probability for this to happen is extremely small [50] and most likely one would operate the repeater in a different way, such that on each repeater level one would wait until the corresponding purification steps are successful, which introduces further waiting times.

8.3.2 Error model for DFS qubits

The setup we consider for an experimental implementation of the repeater nodes utilises single atoms stored in neighbouring dipole traps, such as the wells of an optical lattice [305]. Recent experiments [252–255, 297] showed that for this case the coupling of the qubits to their environment, for example caused by electric or magnetic stray fields, can be considered to be homogeneous, that means identical for all qubits. Thus it is possible to extend the lifetime of the stored information considerably by encoding it in a DFS, which protects the qubits from homogeneous noise. In the next subsection, we briefly discuss two possible DFSs which we consider in this chapter. The first DFS scheme, which was used in Ref. [305], encodes a logical qubit in four two-level atoms in such a way that it is protected against arbitrary kinds of homogeneous noise [59]. The second DFS scheme employs only two atoms, and is therefore easier to realise, but protects the encoded quantum information only against homogeneous dephasing. However, this is sufficient for a lot of implementations, as has already been demonstrated in experiments [252–255]. For both cases we present how the single and two qubit gates necessary for implementing the repeater protocol can be performed and which limitations occur.

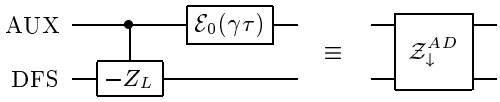

Figure 8.6. Noisy controlled-$(-Z)$ operation, $\mathcal{Z}_{\downarrow}^{AD}$, between an auxiliary qubit and a DFS qubit. In reality the dephasing takes place during the gate operation. In simulations it can be applied before or after the controlled-$(-Z)$ operation.

8.3.2.1 Single qubit gates, two qubit gates and measurements of DFS qubits

The two logical states of a DFS qubit are represented by two states of a system consisting of four two-level atoms, which are stored in an array of dipole traps,

$$\begin{aligned} |0\rangle_{\mathrm{DFS}} &= \frac{1}{2}(|01\rangle - |10\rangle) \otimes (|01\rangle - |10\rangle)\,, \\ |1\rangle_{\mathrm{DFS}} &= \frac{1}{2\sqrt{3}}(2\,|1100\rangle + 2\,|0011\rangle - (|01\rangle + |10\rangle)^{\otimes 2})\,, \end{aligned} \tag{8.18}$$

where $|ijkl\rangle = |i\rangle_1 |j\rangle_2 |k\rangle_3 |l\rangle_4$ with $i, j, k, l = 0, 1$ are the basis states of the four-atom system. This subspace does not couple to collective noise corresponding to fluctuating fields of the form

$$H_I = \sum_{i=1}^{4} \sigma_i^x B_x + \sigma_i^y B_y + \sigma_i^z B_z\,. \tag{8.19}$$

As a consequence, the subspace is immune to all kinds of homogeneous noise. So far the DFS in equation (8.18) has not been implemented using an atomic system. There are, however, experimental realisations of a DFS which protects qubits against homogeneous dephasing [252–255] using the simpler DFS described below. It has been demonstrated that the coherence time of quantum information stored in such a DFS is ultimately limited by the lifetime of the excited atomic level with respect to spontaneous decay [253, 254]. The lifetime of ground state hyperfine levels with respect to spontaneous decay is extremely long, in fact times exceeding 10 minutes have been observed [255]. We can therefore neglect uncorrelated spontaneous emission and assume that quantum information is stored without loss in the DFS.

It was shown in [305] that single qubit rotations $R_x(\theta)$ and $R_z(\theta)$ can be done without leaving the decoherence free subspace and thus we assume that these operations are performed without any error. In contrast to this it was shown that a feasible implementation of a two qubit gate can be achieved by applying a controlled-$(-Z)$ operation, which involves the use of an unprotected auxiliary

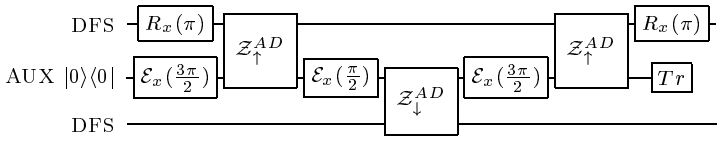

Figure 8.7. Implementation of a controlled-$(-Z)$ operation, $\mathcal{Z}^{DD}_{\downarrow}$, between two DFS qubits.

atom. The five atoms are then subject to collective noise of the form $H_I + \sigma^x_{\mathrm{AUX}} B_x + \sigma^y_{\mathrm{AUX}} B_y + \sigma^z_{\mathrm{AUX}} B_z$ and the action of this operator on a state $|\psi\rangle_{\mathrm{DFS}} |\phi\rangle_{\mathrm{AUX}}$ is given by $|\psi\rangle_{\mathrm{DFS}} |\phi\rangle_{\mathrm{AUX}} \rightarrow |\psi\rangle_{\mathrm{DFS}} (\sigma^x_{\mathrm{AUX}} B_x + \sigma^y_{\mathrm{AUX}} B_y + \sigma^z_{\mathrm{AUX}} B_z) |\phi\rangle_{\mathrm{AUX}}$. Hence, we can assume that the noise acts independently on the auxiliary atom. We further restrict our considerations to dephasing noise $B_z \sigma^z_{\mathrm{AUX}}$. The dynamics of the auxiliary atom is thus described by the model detailed in Sec. 8.3.1. Since the noise operation (dephasing of the auxiliary atom) and the controlled-$(-Z)$ operation commute, the combined operation can be represented by an effective operation as shown in Fig. 8.6, where τ is the time needed to perform the controlled-$(-Z)$ gate. In the following figures we denote this gate as $\mathcal{Z}^{AD}_{\downarrow}$, the arrow again defining control and target qubit. Since τ is relatively large ($\sim 1\,\mathrm{ms}$) we expect decoherence caused by the auxiliary atom to be the major limiting factor in our setup, because the long waiting times of the qubits during classical communication between the repeater nodes do not play any role for the DFS qubits.

Although Ref. [305] concentrates on a DFS given by Eq. (8.18), we point out that in the case where only collective dephasing (i.e. $B_x = B_y = 0$) is the relevant source of noise a DFS consisting of two atoms is sufficient. In this case, the logical states are

$$\begin{aligned} |0\rangle_{\mathrm{DFS}} &= \frac{1}{\sqrt{2}}(|01\rangle + |10\rangle)\,, \\ |1\rangle_{\mathrm{DFS}} &= \frac{1}{\sqrt{2}}(|01\rangle - |10\rangle)\,. \end{aligned} \tag{8.20}$$

The controlled-$(-Z)$ operation between an auxiliary (atomic) qubit and a DFS qubit as well as rotations $R_z(\theta)$ can be done in exactly the same way as described in Ref. [305] (omitting two of the four atoms) with the same fidelities and operation times. Rotations $R_x(\theta)$ can be performed using a laser to induce a rotation around the $z-$axis of the Bloch sphere of, e.g., the first atom constituting the DFS. As in the case of the four-qubit DFS, these operations can be done without leaving the DFS and noise is mainly introduced by the auxiliary atom. Hence, all methods and results presented in this chapter are also valid for the DFS spanned by the states given in Eq. (8.20).

The operation depicted in Fig. 8.6 can be used to implement controlled op-

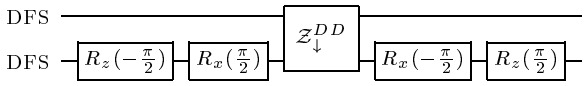

Figure 8.8. Quantum circuit for a controlled-not operation, $\mathcal{X}_{\downarrow}^{DD}$, between two logical qubits.

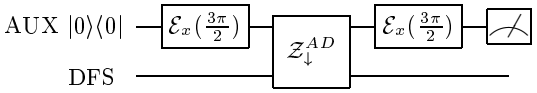

Figure 8.9. Measurement of a DFS qubit.

erations between two DFS qubits by using an auxiliary qubit. Fig. 8.7 shows a possibility to implement a controlled-$(-Z)$ gate between two DFS qubits. The single qubit operations and the measurement of the auxiliary qubit are the same as in Sec. 8.3.1. The controlled-$(-Z)$ operation can then be used to generate a controlled-not between two DFS qubits as shown in Fig. 8.8. Analogously to our previous notation, these are denoted in the following figures as $\mathcal{Z}_{\downarrow}^{DD}$ and $\mathcal{X}_{\downarrow}^{DD}$.

In order to measure the state of a DFS qubit we again make use of an auxiliary qubit. The corresponding circuit is shown in Fig. 8.9. The measurement of the auxiliary qubit is equivalent to a measurement of the DFS qubit.

8.3.2.2 Building blocks of the quantum repeater using DFS qubits

The basic modules necessary to implement a quantum repeater involving DFS qubits are shown in Figs. 8.10-8.12. In the case of state transfer shown in Fig. 8.10 we need two procedures, namely a transfer from an auxiliary qubit to a DFS qubit and a transfer of the state from one DFS qubit to another one. In contrast to the state transfer between two DFS qubits (and also between two unprotected qubits, see Fig. 8.3), which can theoretically be avoided, the transfer between auxiliary (atomic) qubit and DFS qubit is necessary on the lowest level of the quantum repeater. This is required since we assume that the state of the flying qubit (typically a photon) is first transferred to an atom, see Sec. 8.2 and Ref. [305], and not directly to a DFS qubit. The circuit shown in Fig. 8.10a includes a dephasing operation, which accounts for the fact that the first qubit has to wait until the $R_x(-\pi/2)$ gate on the second qubit is finished. This operation is relatively slow ($\sim 2.5\,\mathrm{ms}$) [305] and is thus much slower than typical single qubit gates on atomic (auxiliary) qubits. However, since the $\mathcal{E}_0$ operation commutes with the $\mathcal{Z}_{\downarrow}^{AD}$ operation, this noise has no effect on the outcome of the state transfer.

The quantum circuit for entanglement swapping with DFS qubits is shown in Fig. 8.11. The principle is the same as described in Sec. 8.3.1.3: The state of qubit C_1 is teleported to qubit B using the entanglement of the pair $C_2 - B$. Since quantum information can be stored in the DFS without losses, waiting times during

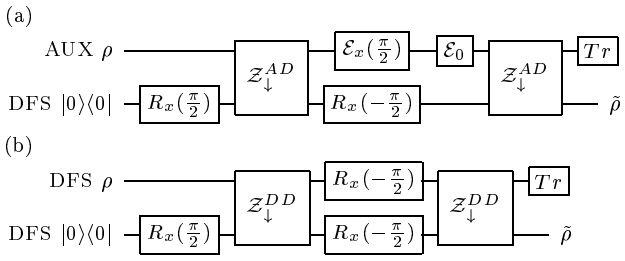

Figure 8.10. Quantum circuits for the transfer of (a) the state of an atomic qubit to a DFS qubit and (b) the sate of a DFS qubit to a DFS qubit. The operation $\mathcal{E}_0$ shown in (a) has no effect on the outcome of the state transfer, see text. In the noiseless case the output state $\tilde{\rho}$ would be equal to the input state ρ.

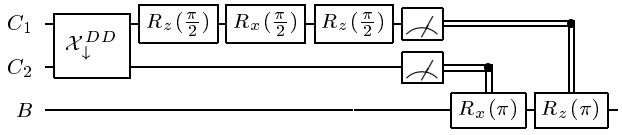

Figure 8.11. Quantum circuit for entanglement swapping involving only DFS qubits. The shown circuit corresponds to the standard protocol of teleporting the state of qubit C_1 to qubit B.

classical communications do not have any effect if they do not exceed the coherence time of the DFS qubit (see above). Thus qubit A is omitted in this circuit since it would be simply represented by a straight line.

Figure 8.12 shows the quantum circuit for entanglement purification of (a) a pair of auxiliary qubits $A_1 - B_1$ and a pair of DFS qubits $A_2 - B_2$, and (b) two pairs of DFS qubits $A_1 - B_1$ and $A_2 - B_2$. The major difference to the corresponding case of unprotected qubits (Fig. 8.5) is again that the waiting times during classical communication do not have any effect if they are shorter than the coherence time of the DFS qubit.

8.4 Results of simulations

In this section, we present results of simulations of the full nested purification protocol. For a better understanding we first concentrate on its main components, namely entanglement swapping and entanglement purification, as well as state transfer. As indicated in Sec. 8.2 the state transfer is theoretically not necessary, however it turns out that its inclusion into the repeater protocol does not reduce the final entanglement fidelity significantly. Therefore, we include the state transfer into the repeater protocol since in an experimental implementation it might be

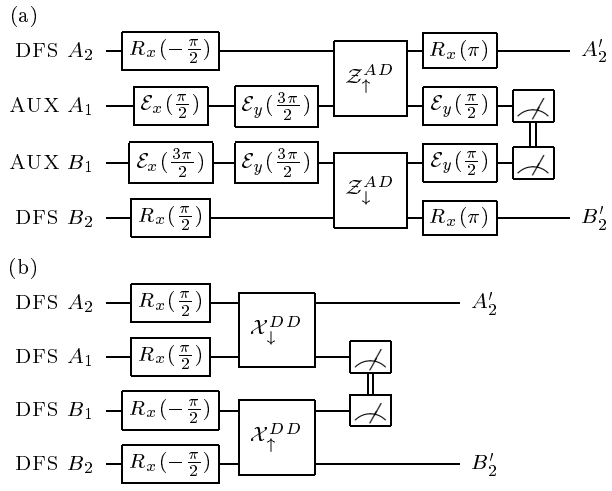

Figure 8.12. Quantum circuit for an entanglement purification step between (a) pairs of auxiliary and DFS qubits and (b) two pairs of DFS qubits.

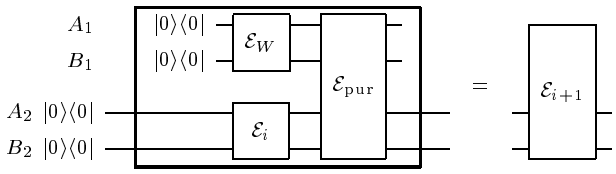

Figure 8.13. Illustration of the numerical method taking entanglement purification with Werner states as an example. The operation in the big box can be combined via process tomography to a single operation $\mathcal{E}_{i+1}$ given by a set of Kraus operators. Initially we have $\mathcal{E}_0 = \mathcal{E}_W$. The method is repeated n times corresponding to n entanglement pumping processes. For more details see text.

easier to do so.

We assume that the initial states are either Werner states

$$\rho_W = f_0 \left|\Phi_+\right\rangle \left\langle\Phi_+\right| + \frac{1-f_0}{3}(\left|\Phi_-\right\rangle \left\langle\Phi_-\right| + \left|\Psi_+\right\rangle \left\langle\Psi_+\right| + \left|\Psi_-\right\rangle \left\langle\Psi_-\right|) \tag{8.21}$$

or binary (mixture) states

$$\rho_B = f_0 \left|\Phi_+\right\rangle \left\langle\Phi_+\right| + (1-f_0) \left|\Phi_-\right\rangle \left\langle\Phi_-\right| , \tag{8.22}$$

where

$$\left|\Phi_\pm\right\rangle = \frac{1}{\sqrt{2}}(\left|00\right\rangle \pm \left|11\right\rangle) , \qquad \left|\Psi_\pm\right\rangle = \frac{1}{\sqrt{2}}(\left|01\right\rangle \pm \left|10\right\rangle) . \tag{8.23}$$

The entanglement fidelity of a state ρ is defined as

$$f = \langle \Phi_+ | \, \rho \, | \Phi_+ \rangle \ . \tag{8.24}$$

In order to simulate the repeater and its constituents we developed a program with a modular structure, i.e., it allows the simulation of a quantum circuit by successively applying subroutines with mixed states as input. Each of these subroutines corresponds to a quantum operation (gates and measurements), which is represented by a Kraus decomposition. Furthermore, we extensively use the fact that a quantum network can be combined into one effective quantum operation, the Kraus operators of which can be calculated by using the quantum process tomography algorithm [2].

We illustrate this method in more detail for the example of entanglement purification with Werner states as shown in Fig. 8.13. The aim is to purify a qubit pair $A_2 - B_2$ via entanglement pumping using Werner states. The operation $\mathcal{E}_W$ creates a Werner state out of the input state $|00\rangle \langle 00|$ and the operation $\mathcal{E}_{pur}$ corresponds to the actual entanglement purification circuit, for example as shown in Fig. 8.5. The operation $\mathcal{E}_i$ is set initially to $\mathcal{E}_0 = \mathcal{E}_W$. The circuit shown in Fig. 8.13 then leads to an output state which corresponds to the state after one entanglement pumping process. All the operations inside the large box in Fig. 8.13 can be combined to one effective quantum operation $\mathcal{E}_1$, which acts on two qubits and which can be determined via process tomography. The operation $\mathcal{E}_1$ is then used instead of $\mathcal{E}_0$ in a repetition of these steps and so forth. After n iterations we get an effective operation $\mathcal{E}_n$ which, when applied to the input state $|00\rangle \langle 00|$, creates a state that we would get after n entanglement pumping steps. By replacing the quantum operations inside the large box in Fig. 8.13 appropriately, we applied this method also to state transfer and entanglement swapping, since in all cases all but two qubits are measured at the end of the operation, i.e., also transfer and swapping can be represented by an effective operation with two input and two output qubits. Ultimately, the combination of state transfer, entanglement swapping, and purification makes it possible to calculate an effective quantum operation for the whole repeater, which transforms a given input state (e.g. $|00\rangle \langle 00|$) into the final state of the repeater.

For the examples shown in this section we set $\Omega = \Omega_x = \Omega_y = \Omega_z = 2\pi \times 50\text{kHz}$, which means we assume that a 2π-rotation around the x, y, z axes can be done in 10μs. The two particle interaction strength of Eq. (8.11) is set to $\Omega_{zz} = 0.1\Omega$, i.e., the controlled-Z gate described in Fig. 8.2 takes 32.5μs. Furthermore, we assume an operation time for the controlled-$(-Z)$ operation between an auxiliary qubit and a DFS qubit (see Fig. 8.6) of $\tau = 1\text{ms}$, which corresponds to the gate operation times calculated in Ref. [305]. The measurement time is set to $t_{\text{me}} = 10\mu$s and the measurement error is assumed to be $1 - \eta = 0.01$ unless otherwise stated.

Figure 8.14 shows the fidelity of the state of an entangled particle pair after it

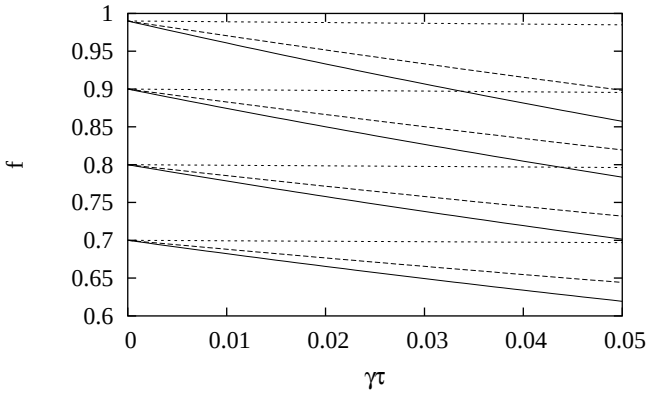

Figure 8.14. Fidelities after transfer of the state of a qubit pair depending on the noise parameter γ ($\tau = 1$ms). The initial states are Werner states with fidelities $f_0 = 0.7, 0.8, 0.9, 0.99$ (bottom to top). Dotted lines correspond to the transfer of auxiliary (unprotected) qubits (cf. Fig. 8.3), dashed lines correspond to a transfer from auxiliary to DFS qubits (cf. Fig. 8.10a) and solid lines correspond to the transfer of DFS qubits (cf. Fig. 8.10b).

was transfered to another qubit pair versus γ by means of the circuits described in the previous section. The initial states are Werner states. The corresponding plot for binary states (not shown) is very similar and deviates from Fig. 8.14 appreciably only for small fidelities. Assuming a coherence time of $1/\gamma = 100$ms, the initial fidelity is reduced by $\sim 0.1\%$ in the case of a transfer between auxiliary qubits, by $\sim 1-2\%$ for a transfer from auxiliary to DFS qubits and by $\sim 2-3\%$ in the case of a transfer between DFS qubits.

The fidelities after connecting $L+1$ entangled qubit pairs (i.e., after L connection processes) via entanglement swapping are shown in Fig. 8.15. In these examples we assumed that there are initially $L+1$ qubit pairs of fidelity f_0 and distance l_0 in a Werner state (Fig. 8.15a) or in a binary state (Fig. 8.15b), which are connected according to the method described in Sec. 8.3.1.3. This implies that the ith entangled pair with $i = 1, 2, \ldots, L+1$ has to wait an additional time $\max\{0, |\lceil (L+1)/2 \rceil - i| - 1\}(l_0/c + t_{\rm sw})$, until the connection process starts for this pair. The final pair has then a distance of $(L+1)l_0$.

As can be seen from these plots, entanglement swapping with partially entangled states leads to a significant loss of fidelity, in fact it has been shown that the fidelity decreases exponentially in the noiseless case [50]. The effect of noisy gate operations and waiting times becomes less important for small fidelities. For example, starting with two Werner pairs of fidelity 80% we lose about 15% fidelity by connecting them. For short distances a swapping procedure using unprotected qubits performs generally better than one with DFS qubits due to the long gate operation times in the decoherence-free case. However, for distances l_0 larger than about 1000km entanglement swapping with DFS qubits becomes advantageous.

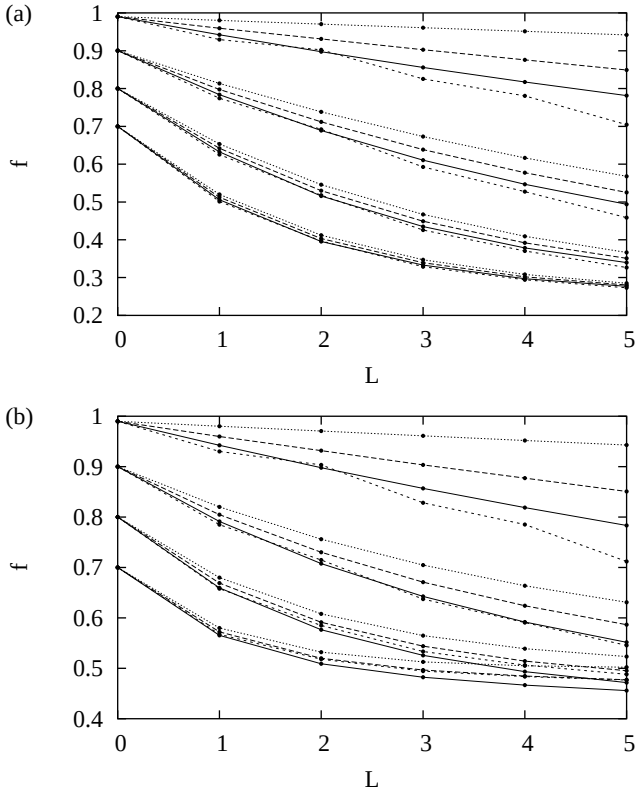

Figure 8.15. Fidelities depending on the number of connection processes L for $\gamma = 1/100$ms. The qubit pairs are initially (a) in Werner states and (b) in binary states with fidelities $f_0 = 0.7, 0.8, 0.9, 0.99$ (bottom to top). The solid lines correspond to DFS qubits, and the short dashed and long dashed lines correspond to auxiliary (unprotected) qubit pairs with distances of $l_0 = 1000$km and $l_0 = 10$km, respectively. The dotted line corresponds to the noiseless case, i.e., $\gamma = 0$, $\eta = 1$.

The effect of entanglement purification (using entanglement pumping) of an entangled qubit pair, which has initially the fidelity f_0, is shown in Fig. 8.16 and Fig. 8.17. In particular, we calculated the maximally reachable fidelity $f_{\max}$ after a large number of successful purification steps depending on f_0, which is also the fidelity of the successively provided additional pairs used for entanglement pumping. In Figs. 8.16 and 8.17 the initial pair and the additional pairs are Werner states and binary states, respectively. Whenever the curves are above the bold diagonal line we gain fidelity, otherwise the fidelity is decreased during the process. These figures illustrate again that the DFS scheme becomes better than the scheme based on unprotected qubits at a distance of $l_0 \approx 500$km. For $\gamma = 1/25$ms and a distance of $l_0 = 1000$km (lowest short dashed line in Fig. 8.16b) purification would not be possible at all for unprotected qubits. Moreover, binary states perform generally better than Werner states [48]. Also shown in these figures are the maximal fideli-

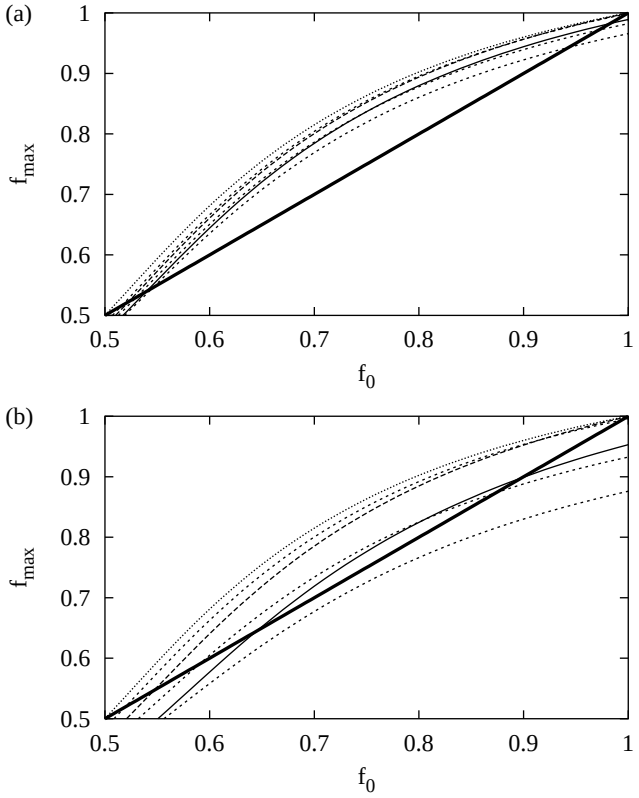

Figure 8.16. Maximal fidelity obtainable via entanglement purification using Werner states versus initial fidelity f_0, which is also the fidelity of the successively generated entangled pairs, for (a) $\gamma = 1/100$ms and (b) $\gamma = 1/25$ms. The bold, diagonal lines aid to read off whether entanglement is gained or lost, see text. The thin, solid lines correspond to purification using DFS qubits, and the short dashed lines correspond to purification using unprotected qubits for $l_0 = 10$km, 500km, 1000km (top to bottom). The long dashed line was obtained by purifying a DFS qubit pair with an auxiliary (unprotected) qubit pair. As a reference we also plotted the corresponding result for the noiseless case (dotted lines).

ties for purification between an auxiliary qubit and a DFS qubit (long dashed lines), which is needed on the first level of the DFS repeater, compare Fig. 8.12a. Note that in this case the maximally reachable fidelity, i.e., the point where the curves intersect the diagonal line in the upper right corner of the plots, is very close to one even for small coherence times $1/\gamma$. The points where the curves intersect the bold diagonal line in the lower left corner correspond to the purification threshold below which no purification is possible.

As described in Sec. 8.2, the quantum repeater protocol we use in this chapter is a nested arrangement of entanglement purification and entanglement swapping. The DFS repeater suffers from long gate operation times, which particularly affects

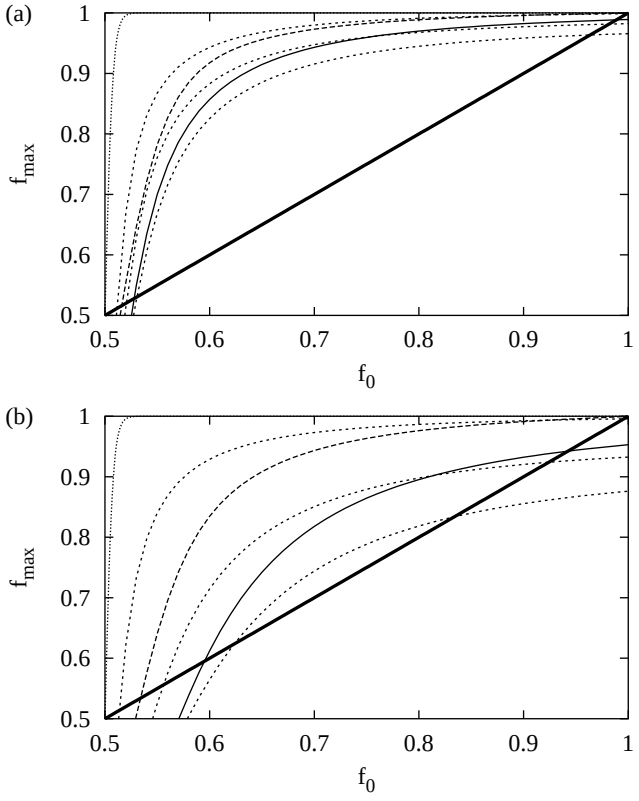

Figure 8.17. Same as in Fig. 8.16 but using binary states instead of Werner states.

the noisy two qubit gate. Quantum gates based on unprotected qubits are significantly faster, however, due to long waiting times during the repeater protocol in the case of long distances, the involved memory qubits are strongly prone to decoherence. In Fig. 8.18 we show an example which compares these two cases. We calculated the fidelity of the entangled pair generated by a quantum repeater with n levels. On each level we perform 5 purification steps and perform one connection (i.e., $L_j = 1$) except for the first level where no connection is done (i.e., $L_1 = 0$). For the repeater based on unprotected qubits we assume $t_0 = 10\mu$s. The distance of the generated entangled pair on level n scales like $S_n = 2^{n-1}l_0$. If we take for example $l_0 = 10$km and $n = 12$, we get a distance of 20480km. Clearly, we do not suggest that the distance over which entangled pairs can be distributed with the DFS quantum repeater is unlimited. The DFS we use protects only against noise given by Eq. (8.19) and is for example not immune to fluctuating inhomogeneous fields. Therefore, the "decoherence free" subspace ultimately has a finite coherence time which, however, can be very long (see Sec. 8.3.2.1). In particular, we expect it to exceed the time necessary to generate an entangled pair on an intercontinental distance, which is on the order of tens of seconds [48]. As can be seen from Fig. 8.18,

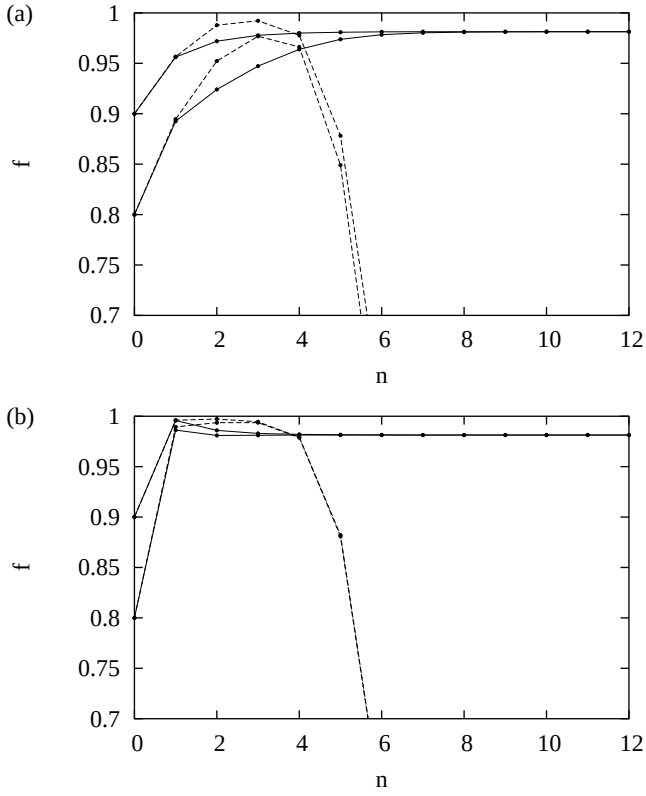

Figure 8.18. Fidelity f of an entangled pair created by a quantum repeater using (a) Werner states and (b) binary states on the lowest level depending on the repeater level n. The solid lines correspond to a DFS repeater and the dashed lines to a repeater based on unprotected qubits. The fidelities of the initially created pairs are $f_0 = 0.8, 0.9$ (bottom to top), $l_0 = 10$km and $\gamma = 1/100$ms. For further parameters see text.

the DFS repeater outperforms the repeater based on unprotected qubits already on repeater level 4 which corresponds to 80km in the above example. The final fidelity of the entangled pairs produced by the DFS repeater is $f = 98.1\%$. The waiting times, which are relevant for the repeater based on unprotected qubits, are calculated according to Eqs. (8.16) and (8.17), i.e., they represent a lower bound. We emphasise here that the strategy (i.e., the choice of the L_j, the number of purification steps on a repeater level, the distance l_0 of the initially created pairs etc.) used in this example might not be the most optimal one. A systematic approach to this problem, albeit with a different error model, can be found in [50]. However, it was found in this reference that even with an optimised strategy and reasonable errors intercontinental distances can not be reached by a repeater using entanglement pumping. Therefore, a number of alterations to the repeater protocol have been proposed to increase the distance [50]. Our results show that improving the quantum memory by employing a decoherence free subspace (and not changing the

repeater protocol) gives an alternative method to reach intercontinental distances.

8.5 Conclusions

In the present chapter we described in detail the implementation of a quantum repeater based on DFS quantum memories, i.e., the qubits at the repeater nodes are represented by two states of a DFS consisting of four physical qubits, which can be manipulated as proposed in Ref. [305]. We showed that the distribution of entangled pairs over long distances is possible with our setup. We simulated the DFS repeater as well as a repeater based on unprotected qubits using realistic parameters, and demonstrated that the DFS scheme outperforms the scheme based on unprotected qubits if waiting times due to classical communication become too large. The implementation of a repeater based on a reliable memory, even in the case of slow and faulty gate operations as in the example we considered, would thus offer the possibility for long distance quantum communication.

In future work one might enhance the performance of the quantum repeater even further by conceiving hybrid architectures, which combine the advantages of fast schemes based on unprotected qubits and schemes involving DFS qubits. For example, one could use the DFS qubits merely as a memory and quantum information is processed with unprotected qubits. The memory could be accessed via state transfer mechanisms as it is discussed in the present chapter acting as an interface between memory and processing qubits. Fast gate operations would then be performed on and between unprotected qubits. A further option along the lines of these ideas is based on the observation that the maximally reachable fidelity $f_{\max}$ of purification of a DFS qubit pair with unprotected qubit pairs is larger than purification using only DFS qubit pairs (see long dashed lines in Figs. 8.16 and 8.17): On the final repeater level(s) we could therefore transfer the state of the DFS qubit pair to an unprotected qubit pair and use this in turn to purify another DFS qubit pair. If the loss in fidelity induced by the state transfer is not too high the results presented in Figs. 8.16 and 8.17 suggest that this could lead to final fidelities exceeding those obtained from using exclusively DFS qubits on higher repeater levels.

Chapter 9

Conclusion

In this thesis we have shown how a system of ultracold atoms in an optical lattice can be used for special purpose quantum simulations. The proposed methods make use of recent experimental developments in this field such as spin-dependent optical lattices [44–46], the implementation of superlattices [308, 309], and mixtures of degenerate quantum gases [33, 34].

Specifically, we have shown that it is possible to implement model Hamiltonians known from high-temperature superconductivity by using atoms in spin-dependent optical lattices. The crucial point of the implementation is the spin-spin interaction, which is realised by inducing state-dependent collisional phases as already demonstrated in experiments [45, 46]. This interaction is combined with the usual Hubbard Hamiltonian by employing a Trotter-Suzuki expansion. We have compared the fidelity of this expansion to an exact calculation of the Hamiltonian and found that reliable results can be expected. The whole scheme can be implemented with current experimental techniques and opens the way to explore high-temperature superconductivity model Hamiltonians in a novel manner.

We have also shown that the effect of phonons, which are always present in a solid crystal, can be mimicked in a cold atom setup by immersing an optical lattice system into a Bose-Einstein condensate (BEC). The atoms in the lattice are then accurately described in terms of polarons and behave similarly to electrons in a solid. For this system, we derived a generalised and a quantum master equation which both describe the system for different parameter regimes. We were able to observe a crossover in the transport properties from a coherent, wavelike dynamics to a non-coherent, diffusive one. Investigations with the quantum master equation and exact solutions of the system showed that depending on the internal state of the atoms and their distance, effects such as sub- and superdecoherence can be observed [186]. These have to be taken into account when the setup is to be used as a quantum register. We have also investigated the interactions of the lattice atoms mediated by the BEC and showed that a clustering of the atoms occurs for experimentally realistic parameters.

Moreover, we used the optical lattice setup in order to combine the ideas of decoherence-free subspaces and quantum repeaters. A logical qubit is encoded into several atoms such that decoherence is suppressed. During single-qubit rotations

the logical qubit never leaves the DFS, and only the two-qubit gate has to be implemented by using an additional auxiliary atom, which is subject to dephasing. Although this atom induces decoherence into the system, the quantum repeater scheme can still be operated reliably.

The setup we have proposed is specially designed for a quantum repeater, where only a few qubits have to be considered. However, the setup might be extended to more qubits and even to a universal computing device. Several questions arise regarding how this extension can be done. A suitable architecture has to be used to accommodate all the necessary qubits, and ways have to be found to manipulate the qubits individually. Furthermore, if more qubits are involved it is not absolutely clear whether the influence of the decoherence caused by the auxiliary atom can still be suppressed. It would also be interesting to combine the ideas of decoherence-free subspaces with mirror-inverting spin chains [310–312]. Here, we could extend our previous work on the influence of noise on the properties of these spin chains [60] and find means for making them more robust.

Our work on atoms in optical lattices submerged into Bose-Einstein condensates has already received interest in other, recent publications. In reference [184], the authors experimentally produced a Bose-Bose mixture and used some of our results to interpret their findings, especially the reduction of hopping. In reference [313], a system of atoms trapped in a self-assembled dipolar lattice was investigated. This system is qualitatively similar to ours, and the authors also observe a dressing of the atoms with phonons and an induced off-site interaction. As experiments become more and more sophisticated, we hope that our setup will be implemented in the near future. This will lead to the need of a more rigorous theoretical analysis of this system. Especially finite-size effects and the presence of weak trapping potentials, which are unavoidable in experiments, have been neglected in our analysis and should be investigated. Furthermore, the combination of having phonons in an optical lattice with other techniques, such as effective magnetic fields or the incorporation of spin-spin interactions as described in chapter 3, might open the door to a deeper understanding of the effects which take place in a solid crystal.

Bibliography

[1] Gordon E. Moore. Cramming more components onto integrated circuits. *Electronics* **38**(8) April (1965).

[2] M. A. Nielsen and I. L. Chuang. *Quantum Computation and Quantum Information*. Cambridge University Press, Cambridge, (2000).

[3] Steven R. White. Density matrix formulation for quantum renormalization groups. *Phys. Rev. Lett.* **69**, 2863 (1992).

[4] Steven R. White and David A. Huse. Numerical renormalization-group study of low-lying eigenstates of the antiferromagnetic $S = 1$ Heisenberg chain. *Phys. Rev. B* **48**, 3844 (1993).

[5] Kenneth G. Wilson. The renormalization group: Critical phenomena and the Kondo problem. *Rev. Mod. Phys.* **47**, 773 (1975).

[6] U. Schollwöck. The density-matrix renormalization group. *Rev. Mod. Phys.* **77**, 259 (2005).

[7] G. Vidal. Efficient classical simulation of slightly entangled quantum computations. *Phys. Rev. Lett.* **91**, 147902 (2003).

[8] G. Vidal. Efficient simulation of one-dimensional quantum many-body systems. *Phys. Rev. Lett.* **93**, 040502 (2004).

[9] G. Vidal. Classical simulation of infinite-size quantum lattice systems in one spatial dimension. *Phys. Rev. Lett.* **98**, 070201 (2007).

[10] Richard P. Feynman. Simulating physics with computers. *Int. J. Theor. Phys.* **21**, 467 (1982).

[11] A. M. Turing. On computable numbers, with an application to the Entscheidungsproblem. *Proc. Lond. Math. Soc. 2* **42**, 230 (1936).

[12] David Deutsch. Quantum theory, the Church-Turing principle and the universal quantum computer. *Proc. R. Soc. London A* **400**, 97 (1985).

[13] R. Cleve, A. Ekert, C. Macchiavello, and M. Mosca. Quantum algorithms revisited. *Proc. R. Soc. A* **454**, 339 (1998).

[14] Lov K. Grover. Quantum mechanics helps in searching for a needle in a haystack. *Phys. Rev. Lett.* **79**, 325 (1997).

[15] David Deutsch and Richard Jozsa. Rapid solution of problems by quantum computation. *Proc. R. Soc. London A* **439**, 553 (1992).

[16] P. W. Shor. Algorithms for quantum computation: Discrete logarithms and factoring. In *Proceedings, 35th Annual Symposium on Foundations of Computer Science, Santa Fe, NM,* S. Goldwasser, editor, p. 124. IEEE Computer Society Press, (1994).

[17] D. Jaksch, C. Bruder, J. I. Cirac, C. W. Gardiner, and P. Zoller. Cold bosonic atoms in optical lattices. *Phys. Rev. Lett.* **81**, 3108 (1998).

[18] D. Jaksch and P. Zoller. The cold atom Hubbard toolbox. *Ann. Phys. (NY)* **315**, 52 (2005).

[19] Immanuel Bloch. Ultracold quantum gases in optical lattices. *Nat. Phys.* **1**, 23 (2005).

[20] Maciej Lewenstein, Anna Sanpera, Veronica Ahufinger, Bogdan Damski, Aditi Sen, and Ujjwal Sen. Ultracold atomic gases in optical lattices: Mimicking condensed matter physics and beyond. *Advances in Physics* **56**, 243 (2007).

[21] Matthew P. A. Fisher, Peter B. Weichman, G. Grinstein, and Daniel S. Fisher. Boson localization and the superfluid-insulator transition. *Phys. Rev. B* **40**, 546 (1989).

[22] M. Greiner, O. Mandel, T. Esslinger, T. W. Hänsch, and I. Bloch. Quantum phase transition from a superfluid to a Mott insulator in a gas of ultracold atoms. *Nature (London)* **415**, 39 (2002).

[23] Anders Sørensen and Klaus Mølmer. Spin-spin interaction and spin squeezing in an optical lattice. *Phys. Rev. Lett.* **83**, 2274 (1999).

[24] L.-M. Duan, E. Demler, and M. D. Lukin. Controlling spin exchange interactions of ultracold atoms in optical lattices. *Phys. Rev. Lett.* **91**, 090402 (2003).

[25] Dieter Jaksch and Peter Zoller. Creation of effective magnetic fields in optical lattices: The Hofstadter butterfly for cold neutral atoms. *New J. Phys.* **5**, 56 (2003).

[26] Anders S. Sørensen, Eugene Demler, and Mikhail D. Lukin. Fractional quantum Hall states of atoms in optical lattices. *Phys. Rev. Lett.* **94**, 086803 (2005).

[27] G. Juzeliūnas and P. Öhberg. Slow light in degenerate Fermi gases. *Phys. Rev. Lett.* **93**, 033602 (2004).

[28] G. Juzeliūnas, P. Öhberg, J. Ruseckas, and A. Klein. Effective magnetic fields in degenerate atomic gases induced by light beams with orbital angular momenta. *Phys. Rev. A* **71**, 053614 (2005).

[29] T. Rom, Th. Best, D. van Oosten, U. Schneider, S. Fölling, B. Paredes, and I. Bloch. Free fermion antibunching in a degenerate atomic Fermi gas released from an optical lattice. *Nature (London)* **444**, 733 (2006).

[30] F. Bloch. Über die Quantenmechanik der Elektronen in Kristallgittern. *Z. Phys.* **52**, 555 (1928).

[31] B. P. Anderson and M. A. Kasevich. Macroscopic quantum interference from atomic tunnel arrays. *Science* **282**, 1686 (1998).

[32] O. Morsch, J. H. Müller, M. Cristiani, D. Ciampini, and E. Arimondo. Bloch oscillations and mean-field effects of Bose-Einstein condensates in 1D optical lattices. *Phys. Rev. Lett.* **87**, 140402 (2001).

[33] Kenneth Günter, Thilo Stöferle, Henning Moritz, Michael Köhl, and Tilman Esslinger. Bose-Fermi mixtures in a three-dimensional optical lattice. *Phys. Rev. Lett.* **96**, 180402 (2006).

[34] S. Ospelkaus, C. Ospelkaus, O. Wille, M. Succo, P. Ernst, K. Sengstock, and K. Bongs. Localization of bosonic atoms by fermionic impurities in a three-dimensional optical lattice. *Phys. Rev. Lett.* **96**, 180403 (2006).

[35] D. Schrader, I. Dotsenko, M. Khudaverdyan, Y. Miroshnychenko, A. Rauschenbeutel, and D. Meschede. Neutral atom quantum register. *Phys. Rev. Lett.* **93**, 150501 (2004).

[36] T. Calarco, U. Dorner, P. S. Julienne, C. J. Williams, and P. Zoller. Quantum computations with atoms in optical lattices: Marker qubits and molecular interactions. *Phys. Rev. A* **70**, 012306 (2004).

[37] Chuanwei Zhang, S. L. Rolston, and S. Das Sarma. Manipulation of single neutral atoms in optical lattices. *Phys. Rev. A* **74**, 042316 (2006).

[38] Alexey V. Gorshkov, Liang Jiang, Markus Greiner, Peter Zoller, and Mikhail D. Lukin. Coherent quantum optical control with sub-wavelength resolution. *arXiv:0706.3879v1 [quant-ph]* (2007).

[39] Y. Miroshnychenko, Wolfgang Alt, Igor Dotsenko, Leonid Förster, Mkrtych Khudaverdyan, Dieter Meschede, Dominik Schrader, and Arno Rauschenbeutel. An atom-sorting machine. *Nature (London)* **442**, 151 (2006).

[40] Y. Miroshnychenko, Wolfgang Alt, Igor Dotsenko, Leonid Förster, Mkrtych Khudaverdyan, Arno Rauschenbeutel, and Dieter Meschede. Precision preparation of strings of trapped neutral atoms. *New J. Phys.* **8**, 191 (2006).

[41] R. Scheunemann, F. S. Cataliotti, T. W. Hänsch, and M. Weitz. Resolving and addressing atoms in individual sites of a Co_2-laser optical lattice. *Phys. Rev. A* **62**, 051801(R) (2000).

[42] S. Kuhr, W. Alt, D. Schrader, M. Müller, V. Gomer, and D. Meschede. Deterministic delivery of a single atom. *Science* **293**, 278 (2001).

[43] S. Kuhr, W. Alt, D. Schrader, I. Dotsenko, Y. Miroshnychenko, W. Rosenfeld, M. Khudaverdyan, V. Gomer, A. Rauschenbeutel, and D. Meschede. Coherence properties and quantum state transportation in an optical conveyor belt. *Phys. Rev. Lett.* **91**, 213002 (2003).

[44] D. Jaksch, H.-J. Briegel, J. I. Cirac, C. W. Gardiner, and P. Zoller. Entanglement of atoms via cold controlled collisions. *Phys. Rev. Lett.* **82**, 1975 (1999).

[45] O. Mandel, M. Greiner, A. Widera, T. Rom, T. W. Hänsch, and I. Bloch. Controlled collisions for multi-particle entanglement of optically trapped atoms. *Nature (London)* **425**, 937 (2003).

[46] Olaf Mandel, Markus Greiner, Artur Widera, Tim Rom, Theodor W. Hänsch, and Immanuel Bloch. Coherent transport of neutral atoms in spin-dependent optical lattice potentials. *Phys. Rev. Lett.* **91**, 010407 (2003).

[47] H.-J. Briegel, W. Dür, J. I. Cirac, and P. Zoller. Quantum repeaters: The role of imperfect local operations in quantum communication. *Phys. Rev. Lett.* **81**, 5932 (1998).

[48] W. Dür, H.-J. Briegel, J. I. Cirac, and P. Zoller. Quantum repeaters based on entanglement purification. *Phys. Rev. A* **59**, 169 (1999).

[49] L.-M. Duan, M. D. Lukin, J. I. Cirac, and P. Zoller. Long-distance quantum communication with atomic ensembles and linear optics. *Nature (London)* **414**, 413 (2001).

[50] L. Hartmann, B. Kraus, H.-J. Briegel, and W. Dür. Role of memory errors in quantum repeaters. *Phys. Rev. A* **75**, 032310 (2007).

[51] Charles Kittel. *Introduction to Solid State Physics*. John Wiley and Sons, New York, seventh edition, (1996).

[52] Neil W. Ashcroft and N. David Mermin. *Solid State Physics*. Thomson Learning, (1976).

[53] A. S. Alexandrov and N. F. Mott. Bipolarons. *Rep. Prog. Phys.* **57**, 1197 (1994).

[54] F. C. Zhang and T. M. Rice. Effective Hamiltonian for the superconducting Cu oxides. *Phys. Rev. B* **37**, R3759 (1988).

[55] F. C. Zhang. Gossamer superconductor, Mott insulator, and resonating valence bond state in correlated electron systems. *Phys. Rev. Lett.* **90**, 207002 (2003).

[56] P. Zanardi and M. Rasetti. Noiseless quantum codes. *Phys. Rev. Lett.* **79**, 3306 (1997).

[57] L.-M. Duan and G.-C. Guo. Reducing decoherence in quantum-computer memory with all quantum bits coupling to the same environment. *Phys. Rev. A* **57**, 737 (1998).

[58] D. A. Lidar, I. L. Chuang, and K. B. Whaley. Decoherence-free subspaces for quantum computation. *Phys. Rev. Lett.* **81**, 2594 (1998).

[59] D. Bacon, J. Kempe, D. A. Lidar, , and K. B. Whaley. Universal fault-tolerant quantum computation on decoherence-free subspaces. *Phys. Rev. Lett.* **85**, 1758 (2000).

[60] Stephen R Clark, Alexander Klein, Martin Bruderer, and Dieter Jaksch. Graph state generation with noisy mirror-inverting spin chains. *New J. Phys.* **9**, 202 (2007).

[61] Alexander Klein, Dieter Jaksch, Yanzhi Zhang, and Weizhu Bao. Dynamics of vortices in weakly interacting Bose-Einstein condensates. *Phys. Rev. A* **76**, 043602 (2007).

[62] T. W. Hänsch and A. L. Schawlow. Cooling of gases by laser radiation. *Opt. Commun.* **13**, 68 (1975).

[63] William D. Phillips and Harold Metcalf. Laser deceleration of an atomic beam. *Phys. Rev. Lett.* **48**, 596 (1982).

[64] John V. Prodan, William D. Phillips, and Harold Metcalf. Laser production of a very slow monoenergetic atomic beam. *Phys. Rev. Lett.* **49**, 1149 (1982).

[65] John Prodan, Alan Migdall, William D. Phillips, Ivan So, Harold Metcalf, and Jean Dalibard. Stopping atoms with laser light. *Phys. Rev. Lett.* **54**, 992 (1985).

[66] Steven Chu, L. Hollberg, J. E. Bjorkholm, Alex Cable, and A. Ashkin. Three-dimensional viscous confinement and cooling of atoms by resonance radiation pressure. *Phys. Rev. Lett.* **55**, 48 (1985).

[67] M. H. Anderson, J. R. Ensher, M. R. Matthews, C. E. Wieman, and E. A. Cornell. Observation of Bose-Einstein condensation in a dilute atomic vapor. *Science* **269**, 198 (1995).

[68] K. B. Davis, M. O. Mewes, M. R. Andrews, N. J. van Druten, D. S. Durfee, D. M. Kurn, and W. Ketterle. Bose-Einstein condensation in a gas of sodium atoms. *Phys. Rev. Lett.* **75**, 3969 (1995).

[69] Y. Castin. Bose-Einstein condensates in atomic gases. In *Les Houches Session LXXII, Coherent atomic matter waves,* R. Kaiser, editor. Springer (2000).

[70] N. N. Bogoliubov. *J. Phys. USSR* **11**, 23 (1947).

[71] R. Ozeri, N. Katz, J. Steinhauer, and N. Davidson. Colloquium: Bulk Bogoliubov excitations in a Bose-Einstein condensate. *Rev. Mod. Phys.* **77**, 187 (2005).

[72] C. J. Foot. *Atomic Physics.* Oxford University Press, Oxford, first edition, (2005).

[73] W. Ertmer, R. Blatt, J. L. Hall, and M. Zhu. Laser manipulation of atomic beam velocities: Demonstration of stopped atoms and velocity reversal. *Phys. Rev. Lett.* **54**, 996 (1985).

[74] J. Dalibard and C. Cohen-Tannoudji. Laser cooling below the Doppler limit by polarization gradients: simple theoretical models. *J. Optical Soc. Amer. B* **6**, 2023 (1989).

[75] Marlan O. Scully and M. Suhail Zubairy. *Quantum Optics.* Cambridge University Press, Cambridge, first edition, (1997).

[76] Stephen M. Barnett and Paul M. Radmore. *Methods in Theoretical Quantum Optics.* Oxford University Press, Oxford, first edition, (1997).

[77] Per-Olov Löwdin. Studies in perturbation theory. IV. Solution of eigenvalue problem by projection operator formalism. *J. Math. Phys.* **3**, 969 (1962).

[78] C. Cohen-Tannoudji, J. Dupont-Roc, and G. Grynberg. *Atom-Photon Interactions.* John Wiley and Sons, New York, (1998).

[79] A. Einstein. Quantentheorie des einatomigen, idealen Gases. Zweite Abhandlung. *Sitzungsber. preuss. Akad. Wiss.* **3** (1925).

[80] S. N. Bose. Plancks Gesetz und Lichtquantenhypothese. *Z. Phys.* **26**, 178 (1924).

[81] J. Allen and A. Misener. Flow of liquid helium II. *Nature (London)* **141**, 75 (1938).

[82] F. London. The λ-phenomenon of liquid helium and the Bose-Einstein degeneracy. *Nature* **141**, 643 (1938).

[83] F. London. On the Bose-Einstein condensation. *Phys. Rev.* **54**, 947 (1938).

[84] Oliver Penrose and Lars Onsager. Bose-Einstein condensation and liquid helium. *Phys. Rev.* **104**, 576 (1956).

[85] K. Huang. *Statistical Mechanics*. Wiley, New York, (1987).

[86] C. J. Pethick and H. Smith. *Bose-Einstein Condensation in Dilute Gases*. Cambridge University Press, Cambridge, first edition, (2002).

[87] John L. Bohn, James P. Burke Jr., Chris H. Greene, H. Wang, P. L. Gould, and W. C. Stwalley. Collisional properties of ultracold potassium: Consequences for degenerate Bose and Fermi gases. *Phys. Rev. A* **59**, 3660 (1999).

[88] Thorsten Köhler, Krzysztof Góral, and Paul S. Julienne. Production of cold molecules via magnetically tunable Feshbach resonances. *Rev. Mod. Phys.* **78**, 1311 (2006).

[89] Herman Feshbach. Unified theory of nuclear reactions. *Ann. Phys. (NY)* **5**, 357 (1958).

[90] Herman Feshbach. A unified theory of nuclear reactions. II. *Ann. Phys. (NY)* **19**, 287 (1962).

[91] Immanuel Bloch, Jean Dalibard, and Wilhelm Zwerger. Many-body physics with ultracold gases. *arXiv:0704.3011v1* (2007).

[92] S. Inouye, M. R. Andrews, J. Stenger, H.-J. Miesner, D. M. Stamper-Kurn, and W. Ketterle. Observation of Feshbach resonances in a Bose Einstein condensate. *Nature (London)* **392**, 151 (1998).

[93] T. Bourdel, L. Khaykovich, J. Cubizolles, J. Zhang, F. Chevy, M. Teichmann, L. Tarruell, S. J. J. M. F. Kokkelmans, and C. Salomon. Experimental study of the BEC-BCS crossover region in Lithium 6. *Phys. Rev. Lett.* **93**, 050401 (2004).

[94] S. Jochim, M. Bartenstein, A. Altmeyer, G. Hendl, S. Riedl, C. Chin, J. Hecker Denschlag, and R. Grimm. Bose-Einstein condensation of molecules. *Science* **302**, 2101 (2003).

[95] M. W. Zwierlein, C. A. Stan, C. H. Schunck, S. M. F. Raupach, S. Gupta, Z. Hadzibabic, and W. Ketterle. Observation of Bose-Einstein condensation of molecules. *Phys. Rev. Lett.* **91**, 250401 (2003).

[96] M. Bartenstein, A. Altmeyer, S. Riedl, S. Jochim, C. Chin, J. Hecker Denschlag, and R. Grimm. Collective excitations of a degenerate gas at the BEC-BCS crossover. *Phys. Rev. Lett.* **92**, 203201 (2004).

[97] Anthony J. Leggett. Bose-Einstein condensation in the alkali gases: Some fundamental concepts. *Rev. Mod. Phys.* **73**, 307 (2001).

[98] C. W. Gardiner. Particle-number-conserving Bogoliubov method which demonstrates the validity of the time-dependent Gross-Pitaevskii equation for a highly condensed Bose gas. *Phys. Rev. A* **56**, 1414 (1997).

[99] Y. Castin and R Dum. Low-temperature Bose-Einstein condensates in time-dependent traps: Beyond the $U(1)$ symmetry-breaking approach. *Phys. Rev. A* **57**, 3008 (1998).

[100] L. P. Pitaevskii. *Sov. Phys. JETP* **13**, 451 (1961).

[101] E. P. Gross. Hydrodynamics of a superfluid condensate. *J. Math. Phys.* **4**, 195 (1963).

[102] E. H. Lieb, R. Seiringer, and J. Yngvason. Bosons in a trap: A rigorous derivation of the Gross-Pitaevskii energy functional. *Phys. Rev. A* **61**, 043602 (2000).

[103] P. R. de Gennes. *Superconductivity of Metals and Alloys.* Benjamin, New York, first edition, (1966).

[104] P. Öhberg, E. L. Surkov, I. Tittonen, S. Stenholm, M. Wilkens, and G. V. Shlyapnikov. Low-energy elementary excitations of a trapped Bose-condensed gas. *Phys. Rev. A* **56**, R3346 (1997).

[105] R. P. Feynman. Atomic theory of liquid Helium near absolute zero. *Phys. Rev.* **91**, 1301 (1953).

[106] K. I. Petsas, A. B. Coates, and G. Grynberg. Crystallography of optical lattices. *Phys. Rev. A* **50**, 5173 (1994).

[107] L. Santos, M. A. Baranov, J. I. Cirac, H.-U. Everts, H. Fehrmann, and M. Lewenstein. Atomic quantum gases in Kagomé lattices. *Phys. Rev. Lett.* **93**, 030601 (2004).

[108] Thilo Stöferle, Henning Moritz, Christian Schori, Michael Köhl, and Tilman Esslinger. Transition from a strongly interacting 1D superfluid to a Mott insulator. *Phys. Rev. Lett.* **92**, 130403 (2004).

[109] Christoph Maschler and Helmut Ritsch. Cold atom dynamics in a quantum optical lattice potential. *Phys. Rev. Lett.* **95**, 260401 (2005).

[110] B. Vaucher, S. R. Clark, U. Dorner, and D. Jaksch. Fast initialization of a high-fidelity quantum register using optical superlattices. *New J. Phys.* **9**, 221 (2007).

[111] L. Guidoni, C. Triché, P. Verkerk, and G. Grynberg. Quasiperiodic optical lattices. *Phys. Rev. Lett.* **79**, 3363 (1997).

[112] Andrew John Daley. *Manipulation and Simulation of Cold Atoms in Optical Lattices*. PhD thesis, Leopold-Franzens-Universität Innsbruck, (2005).

[113] M. Greiner, O. Mandel, T. W. Hänsch, and I. Bloch. Collapse and revival of the matter wave field of a Bose-Einstein condensate. *Nature (London)* **419**, 51 (2002).

[114] H. P. Büchler, G. Blatter, and W. Zwerger. Commensurate-incommensurate transition of cold atoms in an optical lattice. *Phys. Rev. Lett.* **90**, 130401 (2003).

[115] W. Kohn. Analytic properties of Bloch waves and Wannier functions. *Phys. Rev.* **115**, 809 (1959).

[116] J. Hubbard. Electron correlations in narrow energy bands. *Proc. R. Soc. A* **276**, 238 (1963).

[117] J. Hubbard. Electron correlations in narrow energy bands. II. The degenerate band case. *Proc. R. Soc. A* **277**, 237 (1964).

[118] T. K. Kopeć. Coulomb repulsion, phase stiffnesses, and doping-induced superconductivity from the Mott insulator in the $t-t'-U-J$ model of high-T_c cuprates. *Phys. Rev. B* **70**, 054518 (2004).

[119] P. W. Anderson. The resonating Valence Bond State in La_2CuO_4 and superconductivity. *Science* **235**, 1196 (1987).

[120] J. E. Hirsch. Attractive interaction and pairing in Fermion systems with strong on-site repulsion. *Phys. Rev. Lett.* **54**, 1317 (1985).

[121] D. Finotello, K. A. Gillis, A. Wong, and M. H. W. Chan. Sharp heat-capacity signature at the superfluid transition of Helium films in porous glasses. *Phys. Rev. Lett.* **61**, 1954 (1988).

[122] J. K. Freericks and H. Monien. Strong-coupling expansions for the pure and disordered Bose-Hubbard model. *Phys. Rev. B* **53**, 2691 (1996).

[123] N. Elstner and H. Monien. Dynamics and thermodynamics of the Bose-Hubbard model. *Phys. Rev. B* **59**, 12184 (1999).

[124] D. van Oosten, P. van der Straten, and H. T. C. Stoof. Quantum phases in optical lattices. *Phys. Rev. A* **63**, 053601 (2001).

[125] K. Sheshadri, H. R. Krishnamurthy, R. Pandit, and T. V. Ramakrishnan. Superfluid and insulating phases in an interacting-Boson model: Mean-field theory and the RPA. *Europhys. Lett.* **22**, 257 (1993).

[126] L. D. Landau and E. M. Lifshitz. *Quantum Mechanics*. Pergamon Press, London, first edition, (1958).

[127] Till D. Kühner, Steven R. White, and H. Monien. One-dimensional Bose-Hubbard model with nearest-neighbor interaction. *Phys. Rev. B* **61**, 12474 (2000).

[128] W. M. C. Foulkes, L. Mitas, R. J. Needs, and G. Rajagopal. Quantum Monte Carlo simulations of solids. *Rev. Mod. Phys.* **73**, 33 (2001).

[129] G. G. Batrouni, V. Rousseau, R. T. Scalettar, M. Rigol, A. Muramatsu, P. J. H. Denteneer, and M. Troyer. Mott domains of bosons confined on optical lattices. *Phys. Rev. Lett.* **89**, 117203 (2002).

[130] Gavin K. Brennen, Carlton M. Caves, Poul S. Jessen, and Ivan H. Deutsch. Quantum logic gates in optical lattices. *Phys. Rev. Lett.* **82**, 1060 (1999).

[131] L. J. LeBlanc and J. H. Thywissen. Species-specific optical lattices. *Phys. Rev. A* **75**, 053612 (2007).

[132] J. G. Bednorz and K. A. Müller. Possible high-T_c superconductivity in the Ba-La-Cu-O system. *Z. Phys. B* **64**, 189 (1986).

[133] D. N. Basov and T. Timusk. Electrodynamics of high-T_c superconductors. *Rev. Mod. Phys.* **77**, 721 (2005).

[134] M. W. Zwierlein, J. R. Abo-Shaeer, A. Schirotzek, C. H. Schunck, and W. Ketterle. Vortices and superfluidity in a strongly interacting Fermi gas. *Nature (London)* **435**, 1047 (2005).

[135] Michael Köhl, Henning Moritz, Thilo Stöferle, Kenneth Günter, and Tilman Esslinger. Fermionic atoms in a three dimensional optical lattice: Observing Fermi surfaces, dynamics and interactions. *Phys. Rev. Lett.* **94**, 080403 (2005).

[136] G. Juzeliūnas, J. Ruseckas, P. Öhberg, and M. Fleischhauer. Light induced effective magnetic fields for ultra-cold atoms in planar geometries. *Phys. Rev. A* **73**, 025602 (2006).

[137] Erich J. Mueller. Artificial electromagnetism for neutral atoms: Escher staircase and Laughlin liquids. *Phys. Rev. A* **70**, 041603(R) (2004).

[138] K. Osterloh, M. Baig, L. Santos, P. Zoller, and M. Lewenstein. Cold atoms in non-abelian gauge potentials: From the Hofstadter moth to lattice gauge theory. *Phys. Rev. Lett.* **95**, 010403 (2005).

[139] J. Ruseckas, G. Juzeliūnas, P. Öhberg, and M. Fleischhauer. Non-abelian gauge potentials for ultracold atoms with degenerate dark states. *Phys. Rev. Lett.* **95**, 010404 (2005).

[140] E. Jané, G. Vidal, W. Dür, P. Zoller, and J. I. Cirac. Simulation of quantum dynamics with quantum optical systems. *Quant. Inform. Comput.* **3**, 15 (2003).

[141] H. F. Trotter. On the product of semi-groups of operators. *Proceedings of the American Mathematical Society* **10**, 545 (1959).

[142] Masuo Suzuki. Fractal decomposition of exponential operators with applications to many-body theories and Monte Carlo simulations. *Physics Letters A* **146**, 319 (1990).

[143] Masuo Suzuki. General theory of fractal path integrals with applications to many-body theories and statistical physics. *J. Math. Phys.* **32**, 400 (1991).

[144] Masuo Suzuki and Takashi Yamauchi. Convergence of unitary and complex decompositions of exponential operators. *J. Math. Phys.* **34**, 4892 (1993).

[145] Masuo Suzuki. Convergence of general decompositions of exponential operators. *Commun. Math. Phys.* **163**, 491 (1994).

[146] E. Dagotto. Correlated electrons in high-temperature superconductors. *Rev. Mod. Phys.* **66**, 763 (1994).

[147] A. Griessner, A. J. Daley, D. Jaksch, and P. Zoller. Fault-tolerant dissipative preparation of atomic quantum registers with fermions. *Phys. Rev. A* **72**, 032332 (2005).

[148] A. Griessner, A. J. Daley, S. R. Clark, D. Jaksch, and P. Zoller. Dark-state cooling of atoms by superfluid immersion. *Phys. Rev. Lett.* **97**, 220403 (2006).

[149] A. Griessner, A. J. Daley, S. R. Clark, D. Jaksch, and P. Zoller. Dissipative dynamics of atomic Hubbard models coupled to a phonon bath: dark state cooling of atoms within a Bloch band of an optical lattice. *New J. Phys.* **9**, 44 (2007).

[150] Andrea Damascelli, Zahid Hussain, and Zhi-Xun Shen. Angle-resolved photoemission studies of the cuprate superconductors. *Rev. Mod. Phys.* **75**, 473 (2003).

[151] P. W. Anderson. *The theory of superconductivity in the high-T_c cuprates.* Princeton University Press, Princeton, (1997).

[152] Thomas Maier, Mark Jarrell, Thomas Pruschke, and Matthias H. Hettler. Quantum cluster theories. *Rev. Mod. Phys.* **77**, 1027 (2005).

[153] Henk Eskes and Robert Eder. Hubbard model versus t-J model: The one-particle spectrum. *Phys. Rev. B* **54**, R14226 (1996).

[154] A. Nazarenko, K. J. E. Vos, S. Haas, E. Dagotto, and R. J. Gooding. Photoemission spectra of $Sr_2CuO_2Cl_2$: A theoretical analysis. *Phys. Rev. B* **51**, R8676 (1995).

[155] R. Laughlin. Gossamer superconductivity. *cond-mat/0209269* (2002).

[156] B. Paredes and J. I. Cirac. From Cooper pairs to Luttinger liquids with bosonic atoms in optical lattices. *Phys. Rev. Lett.* **90**, 150402 (2003).

[157] R. C. Ball. Fermions without fermion fields. *Phys. Rev. Lett.* **95**, 176407 (2005).

[158] F. Verstraete and J. I. Cirac. Mapping local Hamiltonians of fermions to local Hamiltonians of spins. *J. Stat. Mech.* **0509**, P09012 (2005).

[159] D. Jaksch, J. I. Cirac, and P. Zoller. Dynamically turning off interactions in a two-component condensate. *Phys. Rev. A* **65**, 033625 (2002).

[160] S. R. Clark and D. Jaksch. Dynamics of the superfluid to Mott-insulator transition in one dimension. *Phys. Rev. A* **70**, 043612 (2004).

[161] E. Altman, E. Demler, and M. D. Lukin. Probing many-body states of ultracold atoms via noise correlations. *Phys. Rev. A* **70**, 013603 (2004).

[162] R. Hanbury Brown and R. Q. Twiss. Correlation between photons in two coherent beams of light. *Nature* **177**, 27 (1956).

[163] S. Fölling, F. Gerbier, A. Widera, O. Mandel, T. Gericke, and I. Bloch. Spatial quantum noise interferometry in expanding ultracold atom clouds. *Nature* **434**, 481 (2005).

[164] Xiao-Gang Wen and Patrik A. Lee. Theory of underdoped cuprates. *Phys. Rev. Lett.* **76**, 503 (1996).

[165] V. I. Anisimov, M. A. Korotin, I. A. Nekrasov, Z. V. Pchelkina, and S. Sorella. First principles electronic model for high-temperature superconductivity. *Phys. Rev. B* **66**, 100502(R) (2002).

[166] Gerald D. Mahan. *Many-Particle Physics.* Kluwer Academic, New York, third edition, (2000).

[167] A. S. Alexandrov, J. Ranninger, and S. Robaszkiewicz. Bipolaronic superconductivity: Thermodynamics, magnetic properties, and possibility of existence in real substances. *Phys. Rev. B* **33**, 4526 (1986).

[168] Paul T. Henderson, Denise Jones, Gregory Hampikian, Yongzhi Kan, and Gary B. Schuster. Long-distance charge transport in duplex DNA: The phonon-assisted polaron-like hopping mechanism. *Proc. Natl. Acad. Sci. USA* **96**, 8353 (1999).

[169] Daniel Gottesman. Quantum statistics with classical particles. *cond-mat/0511207* (2005).

[170] K. Winkler, G. Thalhammer, F. Lang, R. Grimm, J. Hecker Denschlag, A. J. Daley, A. Kantian, H. P. Büchler, and P. Zoller. Repulsively bound atom pairs in an optical lattice. *Nature (London)* **441**, 853 (2006).

[171] L. Mathey, D.-W. Wang, W. Hofstetter, M. D. Lukin, and Eugene Demler. Luttinger liquid of polarons in one-dimensional boson-fermion mixtures. *Phys. Rev. Lett.* **93**, 120404 (2004).

[172] E. Pazy and A. Vardi. Holstein model and Peierls instability in one-dimensional boson-fermion lattice gases. *Phys. Rev. A* **72**, 033609 (2005).

[173] M. Lewenstein, L. Santos, M. A. Baranov, and H. Fehrmann. Atomic Bose-Fermi mixtures in an optical lattice. *Phys. Rev. Lett.* **92**, 050401 (2004).

[174] H. P. Büchler and G. Blatter. Supersolid versus phase separation in atomic Bose-Fermi mixtures. *Phys. Rev. Lett.* **91**, 130404 (2003).

[175] J. Bardeen, G. Baym, and D. Pines. Effective interaction of He^3 atoms in dilute solutions of He^3 in He^4 at low temperature. *Phys. Rev.* **156**, 207 (1967).

[176] Alexander Klein and Michael Fleischhauer. Interaction of impurity atoms in Bose-Einstein condensates. *Phys. Rev. A* **71**, 033605 (2005).

[177] K. Sacha and E. Timmermans. Self-localized impurities embedded in a one-dimensional Bose-Einstein condensate and their quantum fluctuations. *Phys. Rev. A* **73**, 063604 (2006).

[178] M. Bruderer, A. Klein, S. R. Clark, and D. Jaksch. Polaron physics in optical lattices. *Phys. Rev. A* **76**, 011605(R) (2007).

[179] T. Holstein. Studies of polaron motion, Part II. The "small" polaron. *Annals of Physics (NY)* **8**, 343 (1959).

[180] A. C. Scott, J. C. Eilbeck, and H. Gilhøj. Quantum lattice solitons. *Physica D* **78**, 194 (1994).

[181] W. Hofstetter, J. I. Cirac, P. Zoller, E. Demler, and M. D. Lukin. High-temperature superfluidity of fermionic atoms in optical lattices. *Phys. Rev. Lett.* **89**, 220407 (2002).

[182] A. Klein and D. Jaksch. Simulating high-temperature superconductivity model Hamiltonians with atoms in optical lattices. *Phys. Rev. A* **73**, 053613 (2006).

[183] R.N. Palmer and D. Jaksch. High field fractional quantum Hall effect in optical lattices. *Phys. Rev. Lett.* **96**, 180407 (2006).

[184] J. Catani, L. De Sarlo, G. Barontini, and F. Minardi M. Inguscio. Degenerate Bose-Bose mixture in a 3D optical lattice. *arXiv:0706.2781v1* (2007).

[185] S. Tung, V. Schweikhard, and E. A. Cornell. Observation of vortex pinning in Bose-Einstein condensates. *Phys. Rev. Lett.* **97**, 240402 (2006).

[186] G. Massimo Palma, Kalle-Antti Suominen, and Artur K. Ekert. Quantum computers and dissipation. *Proc. R. Soc. Lond. A* **452**, 567 (1996).

[187] Martin Bruderer and Dieter Jaksch. Probing BEC phase fluctuations with atomic quantum dots. *New J. Phys.* **8**, 87 (2006).

[188] Pablo Jensen. Growth of nanostructures by cluster deposition: Experiments and simple models. *Rev. Mod. Phys.* **71**, 1695 (1999).

[189] M. Theis, G. Thalhammer, K. Winkler, M. Hellwig, G. Ruff, R. Grimm, and J. Hecker Denschlag. Tuning the scattering length with an optically induced Feshbach resonance. *Phys. Rev. Lett.* **93**, 123001 (2004).

[190] D. Schrader, I. Dotsenko, M. Khudaverdyan, Y. Miroshnychenko, A. Rauschenbeutel, and D. Meschede. Neutral atom quantum register. *Phys. Rev. Lett.* **93**, 150501 (2004).

[191] James Wei and Edward Norman. Lie algebraic solution of linear differential equations. *J. Math. Phys.* **4**, 575 (1963).

[192] H.-P. Breuer and F. Petruccione. *The theory of open quantum systems.* Oxford University Press, Oxford, (2002).

[193] Roland Doll, David Zueco, Martijn Wubs, Sigmund Kohler, and Peter Hänggi. On the conundrum of deriving exact solutions from approximate master equations. *Chem. Phys. accepted, arXiv:0707.3938v1* (2007).

[194] Francesca Ferlaino, Chiara D'Errico, Giacomo Roati, Matteo Zaccanti, Massimo Inguscio, Giovanni Modugno, and Andrea Simoni. Feshbach spectroscopy of a K-Rb atomic mixture. *Phys. Rev. A* **73**, 040702 (2006).

[195] E. Tiesinga, M. Anderlini, and E. Arimondo. Determination of the scattering length of the $a\ ^3\Sigma^+$ potential of ^{87}RbCs. *Phys. Rev. A* **75**, 022707 (2007).

[196] M. Anderlini, E. Courtade, M. Cristiani, D. Cossart, D. Ciampini, C. Sias, O. Morsch, and E. Arimondo. Sympathetic cooling and collisional properties of a Rb-Cs mixture. *Phys. Rev. A* **71**, 061401(R) (2005).

[197] R. H. Dicke. Coherence in spontanous radiation processes. *Phys. Rev.* **93**, 99 (1954).

[198] Nicholas Metropolis, Arianna W. Rosenbluth, Marshall N. Rosenbluth, Augusta H. Teller, and Edward Teller. Equation of state calculations by fast computing mashines. *J. Chem. Phys.* **21**, 1087 (1953).

[199] K. Binder, editor. *Monte Carlo Methods in Statistical Physics.* Springer Verlag, Berlin, second edition, (1986).

[200] M. B. Yilmaz and Frank M. Zimmermann. Exact cluster size distribution in the one-dimensional Ising model. *Phys. Rev. E* **71**, 026127 (2005).

[201] M. Pleimling and W. Selke. Droplets in the coexistence region of the two-dimensional Ising model. *J. Phys. A: Math. Gen.* **33**, L199 (2000).

[202] G. Modugno, M. Modugno, F. Riboli, G. Roati, and M. Inguscio. Two atomic species superfluid. *Phys. Rev. Lett.* **89**, 190404 (2002).

[203] T. Hartmann, F. Keck, H. J. Korsch, and S. Mossmann. Dynamics of Bloch oscillations. *New J. Phys.* **6**, 2 (2004).

[204] Alexey V. Ponomarev, Javier Madroñero, Andrey R. Kolovsky, and Andreas Buchleitner. Atomic current across an optical lattice. *Phys. Rev. Lett.* **96**, 050404 (2006).

[205] M. Bruderer, A. Klein, S. R. Clark, and D. Jaksch. Transport of strong-coupling polarons in optical lattices. *arXiv:0710.4493v1* (2007).

[206] B. Schmidt, L. I. Plimak, and M. Fleischhauer. Stochastic simulation of a finite-temperature one-dimensional Bose gas: From the Bogoliubov to the Tonks-Girardeau regime. *Phys. Rev. A* **71**, 041601 (2005).

[207] F. Verstraete, J. J. García-Ripoll, and J. I. Cirac. Matrix product density operators: Simulation of finite-temperature and dissipative systems. *Phys. Rev. Lett.* **93**, 207204 (2004).

[208] T. Schulte, S. Drenkelforth, G. Kleine Büning, W. Ertmer, J. Arlt, M. Lewenstein, and L. Santos. Dynamics of Bloch oscillations in disordered lattice potentials. *arXiv:0707.3131v1* (2007).

[209] Christoph Dankert. Efficient simulation of random quantum states and operators. *quant-ph/0512217* (2005).

[210] Line Hjortshøj Pedersen, Klaus Mølmer, and Niels Martin Møller. Fidelity of quantum operations. *Phys. Lett. A* **367**, 47 (2007).

[211] N. Gisin, G. Ribordy, W. Tittel, and H. Zbinden. Quantum cryptography. *Rev. Mod. Phys.* **74**, 145 (2002).

[212] W. Diffie and M. E. Hellman. New directions in cryptography. *IEEE Trans. Inf. Theory* **IT-22**, 644 (1976).

[213] R. L. Rivest, A. Shamir, and L. M. Adleman. A method of obtaining digital signatures and public-key cryptosystems. *Commun. ACM* **21**, 120 (1978).

[214] Carl Pomerance. A tale of two sieves. *Notices of the AMS* **43**, 1473 (1996).

[215] D. Coppersmith. Modifications to the number field sieve. *J. Cryptology* **6**, 169 (1993).

[216] Günter M. Ziegler. The great prime number record races. *Notices of the AMS* **51**, 414 (2004).

[217] Lieven M. K. Vandersypen, Matthias Steffen, Gregory Breyta, Costantino S. Yannoni, Mark H. Sherwood, and Isaac L. Chuang. Experimental realization of Shor's quantum factoring algorithm using nuclear magnetic resonance. *Nature (London)* **414**, 883 (2001).

[218] J. I. Cirac and P. Zoller. Quantum computations with cold trapped ions. *Phys. Rev. Lett.* **74**, 4091 (1995).

[219] J. I. Cirac and P. Zoller. New frontiers in quantum information with atoms and ions. *Phys. Today* **57**(3), 38 (2004).

[220] Yuriy Makhlin, Gerd Schön, and Alexander Shnirman. Quantum-state engineering with Josephson-junction devices. *Rev. Mod. Phys.* **73**, 357 (2001).

[221] Daniel Loss and David P. DiVincenzo. Quantum computation with quantum dots. *Phys. Rev. A* **57**, 120 (1998).

[222] Guido Burkard, Daniel Loss, and David P. DiVincenzo. Coupled quantum dots as quantum gates. *Phys. Rev. B* **59**, 2070 (1999).

[223] Norbert Lütkenhaus. Estimates for practical quantum cryptography. *Phys. Rev. A* **59**, 3301 (1999).

[224] Daniel Gottesman and Isaac Chuang. Quantum digital signatures. *quant-ph/0105032v2* (2001).

[225] Howard Barnum, Claude Crepeau, Daniel Gottesman, Adam Smith, and Alain Tapp. Authentication of quantum messages. In *The 43rd Annual IEEE Symposium on Foundations of Computer Science (FOCS'02)*, 449, (2002).

[226] Kenneth G. Paterson, Fred Piper, and Rüdiger Schack. Why quantum cryptography? *quant-ph/0406147v1* (2004).

[227] Lev Vaidman. Teleportation of quantum states. *Phys. Rev. A* **49**, 1473 (1994).

[228] S. L. Braunstein and P. van Loock. Quantum information with continuous variables. *Rev. Mod. Phys.* **77**, 513 (2005).

[229] W. K. Wootters and W. H. Zurek. A single quantum cannot be cloned. *Nature (London)* **299**, 802 (1982).

[230] D. Dieks. Communication by EPR devices. *Phys. Lett. A* **92**, 271 (1982).

[231] C. H. Bennett and G. Brassard. Quantum cryptography: Public key distribution and coin tossing. In *Proceeding of IEEE International Conference on Computers, Systems and Signal Processing*, p. 175. IEEE, (1984).

[232] C. H. Bennett, G. Brassard, C. Crépeau, and U. M. Maurer. Generalized privacy amplification. *IEEE Trans. Inf. Theory* **41**, 1915 (1995).

[233] A. K. Ekert. Quantum cryptography based on Bell's theorem. *Phys. Rev. Lett.* **67**, 661 (1991).

[234] A. Einstein, B. Podolsky, and N. Rosen. Can quantum-mechanical description of physical reality be considered complete? *Phys. Rev.* **47**, 777 (1935).

[235] J. S. Bell. On the Einstein-Podolsky-Rosen paradox. *Physics* **1**, 195 (1965).

[236] A. Muller, J. Breguet, and N. Gisin. Experimental demonstration of quantum cryptography using polarized photons in optical fiber over more than 1 km. *Europhys. Lett.* **23**, 383 (1993).

[237] A. Muller, H. Zbinden, and N. Gisin. Quantum cryptography over 23 km in installed under-lake telecom fibre. *Europhys. Lett.* **33**, 335 (1996).

[238] P. Townsend, J. Rarity, and P. Tapster. Enhanced single photon fringe visibility in a 10 km-long prototype quantum cryptography channel. *Electron. Lett.* **29**, 1291 (1993).

[239] A. Poppe, A. Fedrizzi, R. Ursin, H. Böhm, T. Lörunser, O. Maurhardt, M. Peev, M. Suda, C. Kurtsiefer, H. Weinfurter, T. Jennewein, and A. Zeilinger. Practical quantum key distribution with polarization entangled photons. *Optics Express* **12**, 3865 (2004).

[240] C. Kurtsiefer, P. Zarda, M. Halder, H. Weinfurter, P. M. Gorman, P. R. Tapster, and J. G. Rarity. Quantum cryptography: A step towards global key distribution. *Nature (London)* **419**, 450 (2002).

[241] Richard J Hughes, Jane E Nordholt, Derek Derkacs, and Charles G Peterson. Practical free-space quantum key distribution over 10 km in daylight and at night. *New J. Phys.* **4**, 43 (2002).

[242] Tobias Schmitt-Manderbach, Henning Weier, Martin Fürst, Rupert Ursin, Felix Tiefenbacher, Thomas Scheidl, Josep Perdigues, Zoran Sodnik, Christian Kurtsiefer, John G. Rarity, Anton Zeilinger, and Harald Weinfurter. Experimental demonstration of free-space decoy-state quantum key distribution over 144 km. *Phys. Rev. Lett.* **98**, 010504 (2007).

[243] M. Żukowski, A. Zeilinger, M. A. Horne, and A. K. Ekert. "Event-ready-detectors" Bell experiment via entanglement swapping. *Phys. Rev. Lett.* **71**, 4287 (1993).

[244] Charles H. Bennett, Gilles Brassard, Claude Crépeau, Richard Jozsa, Asher Peres, and William K. Wootters. Teleporting an unknown quantum state via dual classical and Einstein-Podolsky-Rosen channels. *Phys. Rev. Lett.* **70**, 1895 (1993).

[245] C. H. Bennett, G. Brassard, S. Popescu, B. Schumacher, J. A. Smolin, and W. K. Wootters. Purification of noisy entanglement and faithful teleportation via noisy channels. *Phys. Rev. Lett.* **76**, 722 (1996).

[246] D. Deutsch, A. Ekert, Richard Jozsa, C. Macchiavello, S. Popescu, and A. Sanpera. Quantum privacy amplification and the security of quantum cryptography over noisy channels. *Phys. Rev. Lett.* **77**, 2818 (1996).

[247] P. W. Shor. Scheme for reducing decoherence in quantum computer memory. *Phys. Rev. A* **52**, R2493 (1995).

[248] A. M. Steane. Error correcting codes in quantum theory. *Phys. Rev. Lett.* **77**, 793 (1996).

[249] A. Ekert and Ch. Macchiavello. Quantum error correction for communication. *Phys. Rev. Lett.* **77**, 2585 (1996).

[250] S. F. Huelga, C. Macchiavello, T. Pellizzari, A. K. Ekert, M. B. Plenio, and J. I. Cirac. Improvement of frequency standards with quantum entanglement. *Phys. Rev. Lett.* **79**, 3865 Nov (1997).

[251] C. W. Gardiner. *Quantum Noise.* Springer-Verlag, Berlin, first edition, (1991).

[252] D. Kielpinski, V. Meyer, M. A. Rowe, C. A. Sackett, W. M. Itano, C. Monroe, and D. J. Wineland. A decoherence-free quantum memory using trapped ions. *Science* **291**, 1013 (2001).

[253] C. F. Roos, G. P. T. Lancaster, M. Riebe, H. Häffner, W. Hänsel, S. Gulde, C. Becher, J. Eschner, F. Schmidt-Kaler, and R. Blatt. Bell states of atoms with ultralong lifetimes and their tomographic state analysis. *Phys. Rev. Lett.* **92**, 220402 (2004).

[254] C. F. Roos, M. Chwalla, K. Kim, M. Riebe, and R. Blatt. Designer atoms for quantum metrology. *Nature (London)* **443**, 316 (2006).

[255] C. Langer, R. Ozeri, J. D. Jost, J. Chiaverini, B. DeMarco, A. Ben-Kish, R. B. Blakestad, J. Britton, D. B. Hume, W. M. Itano, D. Leibfried, R. Reichle, T. Rosenband, T. Schaetz, P. O. Schmidt, and D. J. Wineland. Long-lived qubit memory using atomic ions. *Phys. Rev. Lett.* **95**, 060502 (2005).

[256] E. Knill, R. Laflamme, and W. H. Zurek. Resilient quantum computation. *Science* **279**, 342 (1998).

[257] E. M. Fortunato, L. Viola, J. Hodges, G. Teklemariam, and D. G. Cory. Implementation of universal control on a decoherence-free qubit. *New J. Phys.* **4**, 5 (2002).

[258] J. E. Ollerenshaw, D. A. Lidar, and L. E. Kay. Magnetic resonance realization of decoherence-free quantum computation. *Phys. Rev. Lett.* **91**, 217904 (2003).

[259] L. Viola, E. M. Fortunato, M. A. Phys. Rev. Avia, E. Knill, R. Laflamme, and D. G. Cory. Experimental realization of noiseless subsystems for quantum information processing. *Science* **293**, 2059 (2001).

[260] P. G. Kwiat, A. J. Berglund, J. B. Altepeter, and A. G. White. Experimental verification of decoherence-free subspaces. *Science* **290**, 498 (2000).

[261] M. Mohseni, J. S. Lundeen, K. J. Resch, and A. M. Steinberg. Experimental application of decoherence-free subspaces in an optical quantum-computing algorithm. *Phys. Rev. Lett.* **91**, 187903 (2003).

[262] M. Bourennane, M. Eibl, S. Gaertner, C. Kurtsiefer, A. Cabello, and Harald Weinfurter. Decoherence-free quantum information processing with four-photon entangled states. *Phys. Rev. Lett.* **92**, 107901 (2004).

[263] J. K. Pachos and P. L. Knight. Quantum computation with a one-dimensional optical lattice. *Phys. Rev. Lett.* **91**, 107902 (2003).

[264] T. Calarco, E. A. Hinds, D. Jaksch, J. Schmiedmayer, J. I. Cirac, and P. Zoller. Quantum gates with neutral atoms: Controlling collisional interactions in time-dependent traps. *Phys. Rev. A* **61**, 022304 (2000).

[265] T. Calarco, U. Dorner, P. Julienne, C. Williams, and P. Zoller. Quantum computations with atoms in optical lattices: Marker qubits and molecular interactions. *Phys. Rev. A* **70**, 012306 (2004).

[266] C. H. Bennett, G. Brassard, C. Crépeau, R. Jozsa, A. Peres, and W. K. Wootters. Teleporting an unknown quantum state via dual classical and einstein-podolsky-rosen channels. *Phys. Rev. Lett.* **70**, 1895 (1993).

[267] J.-W. Pan, S. Gasparoni, R. Ursin, G. Weihs, and A. Zeilinger. Experimental entanglement purification of arbitrary unknown states. *Nature (London)* **423**, 417 (2003).

[268] T. Yamamoto, M. Koashi, S. K.Özdemir, and N. Imoto. Experimental extraction of an entangled photon pair from two identically decohered pairs. *Nature (London)* **421**, 343 (2003).

[269] P. G. Kwiat, S. Barraza-Lopez, A. Stefanov, and N. Gisin. Experimental entanglement distillation and 'hidden' non-locality. *Nature (London)* **409**, 1014 (2001).

[270] Z. Zhao, T. Yang, Y.-A. Chen, A.-N. Zhang, and J.-W. Pan. Experimental realization of entanglement concentration and a quantum repeater. *Phys. Rev. Lett.* **90**, 207901 (2003).

[271] J. I. Cirac, P. Zoller, H. J. Kimble, and H. Mabuchi. Quantum state transfer and entanglement distribution among distant nodes in a quantum network. *Phys. Rev. Lett.* **78**, 3221 (1997).

[272] S. J. van Enk, J. I. Cirac, and P. Zoller. Ideal quantum communication over noisy channels: A quantum optical implementation. *Phys. Rev. Lett.* **78**, 4293 (1997).

[273] M. Fleischhauer and M. D. Lukin. Dark-state polaritons in electromagnetically induced transparency. *Phys. Rev. Lett.* **84**, 5094 (2000).

[274] D. F. Phillips, A. Fleischhauer, A. Mair, R. L. Walsworth, and M. D. Lukin. Storage of light in atomic vapor. *Phys. Rev. Lett.* **86**, 783 (2001).

[275] D. N. Matsukevich, T. Chaneliere, S. D. Jenkins, S.-Y. Lan, T.A.B. Kennedy, and A. Kuzmich. Entanglement of remote atomic qubits. *quant-ph/0511012* (2005).

[276] C. H. Bennett, D. P. DiVincenzo, J. A. Smolin, and W. K. Wootters. Mixed-state entanglement and quantum error correction. *Phys. Rev. A* **54**, 3824 (1996).

[277] D. Jaksch, C. Bruder, J. I. Cirac, C. W. Gardiner, and P. Zoller. Cold bosonic atoms in optical lattices. *Phys. Rev. Lett.* **81**, 3108 (1998).

[278] For a review see D. Jaksch and P. Zoller. The cold atom hubbard toolbox. *Ann. Phys. (NY)* **315**, 52 (2005).

[279] B. Darquié, M. P. A. Jones, J. Dingjan, J. Beugnon, S. Bergamini, Y. Sortais, G. Messin, A. Browaeys, and P. Grangier. Controlled single-photon emission from a single trapped two-level atom. *Science* **454**, 2005 (309).

[280] S. Fölling, F. Gerbier, A. Widera, O. Mandel, T. Gericke, and I. Bloch. Spatial quantum noise interferometry in expanding ultracold atom clouds. *Nature* **434**, 481 (2005).

[281] R. Dumke, T. Müther, M. Volk, W. Ertmer, and G. Birkl. Interferometer-type structures for guided atoms. *Phys. Rev. Lett.* **89**, 220402 (2002).

[282] R. Dumke, M. Volk, T. Müther, F. B. J. Buchkremer, G. Birkl, and W. Ertmer. Micro-optical realization of arrays of selectively addressable dipole traps: A scalable configuration for quantum computation with atomic qubits. *Phys. Rev. Lett.* **89**, 097903 (2002).

[283] M. Greiner, O. Mandel, T. Esslinger, T. W. Hänsch, and I. Bloch. Quantum phase transition from a superfluid to a mott insulator in a gas of ultracold atoms. *Nature (London)* **415**, 39 (2002).

[284] A. Widera, O. Mandel, M. Greiner, S. Kreim, T. W. Hänsch, and I. Bloch. Entanglement interferometry for precision measurement of atomic scattering properties. *Phys. Rev. Lett.* **92**, 160406 (2004).

[285] O. Mandel, M. Greiner, A. Widera, T. Tom, T. W. Hänsch, and I. Bloch. Controlled collisions for multi-particle entanglement of optically trapped atoms. *Nature (London)* **425**, 937 (2003).

[286] S. Nußmann, M. Hijlkema, B. Weber, F. Rohde, G. Rempe, and A. Kuhn. Submicron positioning of single atoms in a microcavity. *Phys. Rev. Lett.* **95**, 173602 (2005).

[287] J. A. Sauer, K. M. Fortier, M. S. Chang, C. D. Hamley, and M. S. Chapman. Cavity qed with optically transported atoms. *Phys. Rev. A* **69**, 051804(R) (2004).

[288] D. Jaksch, H.-J. Briegel, J. I. Cirac, C. W. Gardiner, and P. Zoller. Entanglement of atoms via cold controlled collisions. *Phys. Rev. Lett.* **82**, 1975–1978 (1999).

[289] D. G. Grier. A revolution in optical manipulation. *Nature (London)* **424**, 810 (2003).

[290] S. Bergamini, B. Darquié, M. Jones, L. Jacubowiez, A. Browaeys, and P. Grangier. Holographic generation of microtrap arrays for single atoms. *J. Opt. Soc. Am. B* **21**, 1889 (2004).

[291] U. Dorner, T. Calarco, P. Zoller, A. Browaeys, and P. Grangier. Quantum logic via optimal control in holographic dipole traps. *J. Opt. B* **7**, S341–S346 (2005).

[292] J.-W. Pan, D. Bouwmeester, H. Weinfurter, and A. Zeilinger. Experimental entanglement swapping: Entangling photons that never interacted. *Phys. Rev. Lett.* **80**, 3891 (1998).

[293] T. Jennewein, G. Weihs, J.-W. Pan, and A. Zeilinger. Experimental nonlocality proof of quantum teleportation and entanglement swapping. *Phys. Rev. Lett.* **88**, 017903 (2002).

[294] F. Sciarrino, E. Lombardi, G. Milani, and F. De Martini. Delayed-choice entanglement swapping with vacuum-one-photon quantum states. *Phys. Rev. A* **66**, 024309 (2002).

[295] N. Takei, H. Yonezawa, T. Aoki, and A. Furusawa. High-fidelity teleportation beyond the no-cloning limit and entanglement swapping for continuous variables. *Phys. Rev. Lett.* **94**, 220502 (2005).

[296] H. de Riedmatten, I. Marcikic, J. A. W. van Houwelingen, W. Tittel, H. Zbinden, and N. Gisin. Long-distance entanglement swapping with photons from separated sources. *Phys. Rev. A* **71**, 050302(R) (2005).

[297] S. Kuhr, W. Alt, D. Schrader, I. Dotsenko, Y. Miroshnychenko, A. Rauschenbeutel, and D. Meschede. Analysis of dephasing mechanisms in a standing-wave dipole trap. *Phys. Rev. A* **72**, 023406 (2005).

[298] J. Kempe, D. Bacon, D. A. Lidar, and K. B. Whaley. Theory of decoherence-free fault-tolerant universal quantum computation. *Phys. Rev. A* **63**, 042307 (2001).

[299] G. Palma, K. Suominen, and A. Ekert. Quantum computers and dissipation. *Proc. R. Soc. A* **452**, 567 (1996).

[300] U. Dorner, P. Fedichev, D. Jaksch, M. Lewenstein, and P. Zoller. Entangling strings of neutral atoms in 1d atomic pipeline structures. *Phys. Rev. Lett.* **91**, 073601 (2003).

[301] A. Micheli, A. J. Daley, D. Jaksch, and P. Zoller. Single atom transistor in a 1d optical lattice. *Phys. Rev. Lett.* **93**, 140408 (2004).

[302] A. J. Daley, S. R. Clark, D. Jaksch, and P. Zoller. Numerical analysis of coherent many-body currents in a single atom transistor. *Phys. Rev. A* **72**, 043618 (2005).

[303] A. V. Sergienko, editor. *Quantum Communications and Cryptography*. Taylor and Francis, New York, (2006).

[304] O. A. Collins, S. D. Jenkins, A. Kuzmich, and T. A. B. Kennedy. Multiplexed memory-insensitive quantum repeaters. *Phys. Rev. Lett.* **98**, 060502 (2007).

[305] Alexander Klein, Uwe Dorner, Carolina Moura Alves, and Dieter Jaksch. Robust implementations of quantum repeaters. *Phys. Rev. A* **73**, 012332 (2006).

[306] M. Riebe, K. Kim, P. Schindler, T. Monz, P. O. Schmidt, T. K. Körber, H. Häffner W. Hänsel, C. F. Roos, and R. Blatt. Process tomography of ion trap quantum gates. *Phys. Rev. Lett.* **97**, 220407 (2006).

[307] G. Burkard. Theory of solid state quantum information processing. *arXiv:cond-mat/0409626v2* (2004).

[308] J. Sebby-Strabley, M. Anderlini, P. S. Jessen, and J. V. Porto. Lattice of double wells for manipulating pairs of cold atoms. *Phys. Rev. A* **73**, 033605 (2006).

[309] S. Peil, J. V. Porto, B. Laburthe Tolra, J. M. Obrecht, B. E. King, M. Subbotin, S. L. Rolston, and W. D. Phillips. Patterned loading of a Bose-Einstein condensate into an optical lattice. *Phys. Rev. A* **67**, 051603(R) (2003).

[310] Matthias Christandl, Nilanjana Datta, Artur Ekert, and Andrew J. Landahl. Perfect state transfer in quantum spin networks. *Phys. Rev. Lett.* **92**, 187902 (2004).

[311] Matthias Christandl, Nilanjana Datta, Tony C. Dorlas, Artur Ekert, Alastair Kay, and Andrew J. Landahl. Perfect transfer of arbitrary states in quantum spin networks. *Phys. Rev. A* **71**, 032312 (2005).

[312] Man-Hong Yung and Sougato Bose. Perfect state transfer, effective gates, and entanglement generation in engineered bosonic and fermionic networks. *Phys. Rev. A* **71**, 032310 (2005).

[313] G. Pupillo, A. Griessner, A. Micheli, M. Ortner, D.-W. Wang, and P. Zoller. Cold atoms and molecules in self-assembled dipolar lattices. *Phys. Rev. Lett. accepted, arXiv:0709.1825v1* (2007).